Durham E-Theses

Infrared Structure of Dijet Production at the LHC

STEVEN CHRISTIAN WELLS

How to cite:

WELLS, STEVEN CHRISTIAN (2013) *Infrared Structure of Dijet Production at the LHC*. Doctoral thesis, Durham University.

Use policy

Infrared Structure of Dijet Production at the LHC

Steven Christian Wells

A Thesis presented for the degree of
Doctor of Philosophy
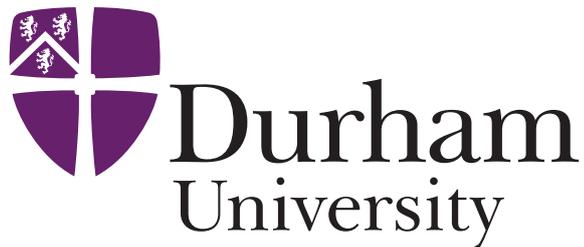
Institute for Particle Physics Phenomenology
Department of Physics
University of Durham
England

August 2013

For Mum, Dad and Christian.

Infrared Structure of Dijet Production at the LHC

Steven Christian Wells

Submitted for the degree of Doctor of Philosophy

August 2013

Abstract

Higher order corrections to QCD scattering processes are crucial for phenomenological analyses in hadronic collider environments such as the LHC. In this thesis we consider the infrared divergent structures emerging from Next-to-Next-to-Leading Order (NNLO) perturbative QCD predictions within the antenna subtraction framework. In doing so we elucidate the highly predictive nature of such a construction, driven by the underlying infrared behaviour. The antenna subtraction formalism has previously been applied successfully to the pure-gluon channel in dijet production at NNLO; we present the extension to processes involving two and four quarks at leading order in colour. We derive explicit expressions for subtracting single and double unresolved contributions to various channels required for dijet production in hadronic collisions. Numerical results are presented to illustrate the validity of the subtraction terms in mimicking the physical cross section in the various unresolved limits.

Declaration

The work in this thesis is based on research carried out at the Institute for Particle Physics Phenomenology, Department of Physics, University of Durham, England. No part of this thesis has been submitted elsewhere for any other degree or qualification. All work is my own in collaboration with my supervisor Professor Nigel Glover, unless referenced to the contrary in the text. Chapters 4 and 5 are based upon research done in collaboration with Professor Nigel Glover and James Currie, and has been published as:

J. Currie, E. W. N. Glover and S. Wells, *Infrared Structure at NNLO Using Antenna Subtraction, JHEP* **1304** (2013) 066, `arXiv:1301.4693`.

Acknowledgements

First and foremost I am immensely grateful to my supervisor Nigel Glover. It has been a privilege to work with him, and I wish to thank him for his support, patient guidance and encouragement over the past four years.

Sincere thanks must also go to my officemates: James Currie, for dealing with so many questions about matrix elements; David Winn for our attempts to Fourier analyse productivity, and also the zoo that is OC118, especially Matthew Yip, Oliver Hall, Dan Busbridge, Jon Davis and Xuan Chen, for our puzzlement over quantum mechanics, the Fine Dining Consortium and far too many stuffed toys. Thank you also to my housemates Simon Gentle and Luke Stanbra, for three years of Coke® -fuelled adventures and for realising that ten sausages for dinner just weren't enough. There are many others too, both within IPPP and otherwise, who have made my time in Durham such an enjoyable experience.

For their love and unfaltering support, I am truly indebted to my parents; I cannot express my gratitude enough for all they have done. I am also very much obliged for the company of my brother Christian as we steadily spend all available funds on classic rock concerts. And finally to Lucy, for making the last year and a half in Durham my happiest. I have lost count of the number of Fortran-induced rages you have quashed. We have been a long way apart: thank you for coming back.

"By the time we've finished with him, he won't know whether he's Number Six or the cube root of infinity" - No.2, *The Schizoid Man*

Contents

List of Tables

List of Figures

Preface

The Large Hadron Collider (LHC) is a masterpiece of engineering and scientific endeavour. With the proliferation of data at unprecedentedly high energies collected since its first successful run in 2010, it has ushered in an exciting new era of physics. Now hitting centre-of-mass energies of 8 TeV, the LHC has successfully rediscovered [1] the Standard Model of particle physics, already establishing challenging results such as diboson and single top production. The crowning success thus far has been the discovery of the scalar particle consistent with the Standard Model Higgs boson, an excitation of the field giving mass to the fundamental matter constituents. Such an event was not confined to the realms of particle physicists; it captured the public interest with only minimal recourse to sensationalist journalism. Yet there still exists a plethora of outstanding and intriguing problems upon which the LHC may begin to shed light: the nature of dark matter, the existence of supersymmetric particles, possible sources of the fermion mass hierarchy to name but a few.

To capture signals of potentially new physics, they must be separated from the huge background present in a collider environment, which requires intimate knowledge of Standard Model phenomenology. In hadron colliders such as the LHC the strong interaction dominates. In order to describe the rich hadronic spectrum, Gell-Mann proposed the quark model, whereby hadrons were constructed in terms of elementary building blocks called quarks. To account for baryonic states existing with quarks of identical spin, the quantum number of colour was introduced. [2]. Colour proved more than merely a workaround for experimental nuances; the exact local symmetry that emerges laid the foundations for **Quantum Chromodynamics** (QCD), the field theoretic framework for the strong interaction.

The work in this thesis focusses on perturbative studies of QCD predictions, pri-

marily the associated infrared behaviour at Next-to-Next-to-Leading Order (NNLO). Infrared divergences plague perturbative calculations at higher orders; **antenna subtraction** offers a general framework by which such divergences can be regulated, and can be applied to processes relevant in hadron colliders. We constrain the infrared structure present within such a formulation, and apply the subtraction method to quark- and gluon- initiated channels required for NNLO dijet production.

This thesis proceeds in the following manner. Chapter 1 reviews a number of basic concepts of QCD that will play an important role in this work, followed by a focussed discussion in Chapter 2 on the infrared divergences present in QCD calculations and the factorisation properties of physical matrix elements in singular limits. Chapter 3 reviews dijet production in hadron colliders, to which later results will apply. Antenna subtraction at NNLO is discussed in Chapter 4, detailing the infrared structures within this framework. With the formalism in place, we construct in Chapters 5 and 6 the subtraction terms for quark-gluon scattering processes relevant for an NNLO treatment of dijet production in hadronic collisions, and test our implementation. Our findings are summarised in Chapter 7.

Chapter 1

Basics in Perturbative QCD

The research presented in this thesis concentrates upon the study of higher order corrections in QCD. To proceed, we lay the foundations of the subject at hand, and introduce the tools required to perform such calculations. This is by no means an in-depth exploration; for comprehensive reviews of QCD and Quantum Field Theory, excellent examples include [3–6].

We first present QCD from a field theory perspective, and then motivate perturbation theory for high energy collider theory. Crucial ideas for field theoretic and perturbative calculations, that of the running of the strong coupling, renormalisation and factorisation, are presented. In Section 1.3 we also introduce colour space as a vital tool for our later analysis of the singular structure of cross section dynamics. Armed with these concepts, and the study of the divergent behaviour of scattering amplitudes that follow in Chapter 2, we are in a favourable position to begin calculations in QCD at higher orders.

1.1 The QCD Lagrangian

The Lagrangian density of QCD can be arranged in terms of four constituent parts;

$$\mathcal{L}_{QCD} = \mathcal{L}_{quark} + \mathcal{L}_{gluon} + \mathcal{L}_{g.f} + \mathcal{L}_{ghost}. \tag{1.1.1}$$

The first two terms $\mathcal{L}_{quark}$ and $\mathcal{L}_{gluon}$ make up what is known as the classical QCD Lagrangian, $\mathcal{L}_{classical}$, and describes the dynamical properties of the quarks and gluons,

$$\mathcal{L}_{classical} = \sum_q \bar{\psi}_q^i (i\slashed{D} - m_q)_{ij} \psi_q^j - \frac{1}{4} G^a_{\mu\nu} G_a^{\mu\nu}, \tag{1.1.2}$$

where the summation is over the q flavours of quarks in the matter sector, the quark fields being represented by ψ_q^j.[1]

The quarks also carry a colour charge $i = 1, 2, 3$ and thus exist in a triplet representation of the group $SU(3)$. The covariant derivative and gluon field strength tensor are given respectively by

$$\slashed{D} = \gamma^\mu (\partial_\mu + ig_s A^a_\mu t^a_{ij}), \tag{1.1.3}$$

$$G^a_{\mu\nu} = \partial_\mu A^a_\nu - \partial_\nu A^a_\mu - g_s f^{abc} A^b_\mu A^c_\nu, \tag{1.1.4}$$

where g_s is the QCD strong coupling and A^a_μ denotes the vector gluon gauge fields. The group elements t^a_{ij} are the fundamental generators of the Lie Algebra of $SU(3)$; there are eight generators, labelled by $a = 1, \ldots 8$. They are used to define the structure constant f^{abc} via the commutation relation

$$[t^a, t^b] = i f^{abc} t^c. \tag{1.1.5}$$

The QCD Lagrangian is invariant under local gauge transformations. That is, it is possible to redefine the quark fields in (1.1.2) independently at any point in spacetime and still keep the physical state of the theory intact. For a rotation of $SU(3)$ by $\Omega(x)$, the quark fields and covariant derivative transform as

$$\psi_q^i \rightarrow \Omega(x) \, \psi_q^i, \tag{1.1.6}$$

$$\bar{\psi}_q^i \rightarrow \bar{\psi}_q^i \, \Omega^{-1}(x), \tag{1.1.7}$$

$$\slashed{D} \psi_q^i \rightarrow \Omega(x) \slashed{D} \, \psi_q^i. \tag{1.1.8}$$

---

[1]The work carried out in this thesis takes massless quark fields for all active flavours.

In order to ascertain the transformation property of the field strength tensor we first use (1.1.8) to derive the transformation of the gluon field A_μ^a as

$$t \cdot A_\mu \to \Omega(x)\Big(t \cdot A_\mu + \frac{i}{g_s}\Omega^{-1}(x)(\partial_\mu\Omega(x))\Big)\Omega^{-1}(x), \qquad (1.1.9)$$

and since the covariant derivative also satisfies the commutation relation

$$[D_\mu, D_\nu] = -ig_s G_{\mu\nu}^a t^a, \qquad (1.1.10)$$

the tranformation of the field strength tensor is found to be

$$t \cdot G_{\mu\nu} \to \Omega(x)\, t \cdot G_{\mu\nu}\Omega^{-1}(x). \qquad (1.1.11)$$

At this juncture we make note of the form of the field strength tensor, where the third term in (1.1.4) describes the gluonic self-interaction and at present prevents gauge invariance. This is unlike the Abelian theory of QED, where the third term is not present. Instead we reconstruct the $\mathcal{L}_{gluon}$ as a trace over the colour indices,

$$-\frac{1}{4}G_{\mu\nu}^a G_a^{\mu\nu} = -\frac{1}{2}\mathrm{Tr}[t \cdot G_{\mu\nu}]^2, \qquad (1.1.12)$$

which is invariant under its transformation in (1.1.11). The combination of these transformations allow the local gauge invariance of $\mathcal{L}_{classical}$ to be transparent. Incidentally, the gluon fields have no associated mass term as the quarks do, since we have no mechanism by which a gluon mass term $m_g^2 A^\mu A_\mu$ can be inserted into the Lagrangian in a gauge-invariant manner.

This is by no means the end of the story. In quantising the (thus far) classical theory, we find a vanishing conjugate gluon momentum which spoils the canonical commutation relations stemming from the gauge freedom enjoyed by the gauge field. Indeed, we have constructed a spin one object with two polarisation states from a four dimensional Lorentz vector. It is thus necessary to impose a constraint on the gluon field such that it is forced to pick a gauge. To accomplish this, a gauge fixing

term is added to the Lagrangian, $\mathcal{L}_{g.f}$, for example

$$\mathcal{L}_{g.f} = -\frac{1}{2\eta}(\partial_\mu A_a^\mu)^2, \tag{1.1.13}$$

which in this case encapsulates the imposition of the Lorentz condition $\partial_\mu A_a^\mu = 0$. The gauge parameter η is arbitrary and parameterises the choice of gauge, for example $\eta = 0$ (Landau gauge), $\eta = 1$ (Feynman gauge) and $\eta = \infty$ (Unitary gauge). Unfortunately, including this term results in the Lagrangian no longer being invariant. Nevertheless, the physical prediction still should be not only gauge invariant, but independent of the choice of gauge.

In the covariant gauges introduced above, the gauge fixing term still leaves the gluon with an unphysical longitudinal degree of freedom that the gauge field's self-interactions require to be eliminated. To proceed, an unphysical complex scalar field ξ^a is introduced, living in the adjoint of $SU(3)$. This **ghost field** satisfies anticommutation properties and thus behaves fermionically. It appears in the Lagrangian as

$$\mathcal{L}_{ghost} = \partial_\mu \xi^{a,\dagger} \partial^\mu \xi^a + g_s f^{abc}(\partial^\mu \xi^{a,\dagger}) A_\mu^b \xi^c, \tag{1.1.14}$$

and the Feynman rules that direct it must be included in any diagrammatic calculations. This inclusion is a result of the non-Abelian nature of QCD; for Abelian theories such as QED, the structure constant f^{abc} vanishes, no interaction terms then exist between it and the physical fields and it can be safely integrated out during the path integral quantisation procedure. It is feasible to avoid the ghost fields entirely by instead working in an axial gauge. However, this often leads to more complicated gluon propagators that may complicate calculations to a greater extent than the additional Feynman diagrams arising from ghost interactions. In either case, the Lagrangian density is established, and the full complement of QCD processes can be accessed via the ensuing Feynman rules.

1.2 Renormalisation of QCD and the running of α_s

The bare parameters and fields, from which the QCD Lagrangian is constructed, are not the fixed quantities we would expect to encounter in an experimental measurement. Rather, they merely parameterise the theory and do not correspond directly to physical observables. Indeed, calculations at higher orders in perturbation theory illustrate the dynamical nature of these parameters, since the quantum corrections are manifest as loops in Feynman diagrams which require integration over internal momenta. For example, a general one-loop tensor integral

$$\mathcal{I}_n^{\mu_1,\cdots\mu_n}(\{p_i\}) = \int \frac{\mathrm{d}^d\ell}{(2\pi)^d} \frac{\ell^{\mu_1}\cdots\ell^{\mu_n}}{\prod_{i=1}^{n}[(\ell^2 - q_i^2) - m_i^2]}, \quad q_i = \sum_{j=0}^{i} p_j, \qquad (1.2.15)$$

where d is the spacetime dimensionality and ℓ denotes the momenta running in the loops, is divergent in four dimensions when the $\ell \to \infty$ limit is taken. Such ultraviolet (UV) singularities are removed by the redefinition of the bare parameters in terms of **renormalised** quantities, rescaling the fields and couplings in the Lagrangian by an overall factor:

$$A_{0,\mu}^a = Z_G^{1/2} A_{ren,\mu}^a \qquad\qquad \psi_{0,q} = Z_q^{1/2}\,\psi_{ren,q} \qquad (1.2.16)$$

$$m_0 = Z_m\,m_{ren} \qquad\qquad g_{s,0}^2 = Z_{g_s^2}\,g_{s,ren}^2 \qquad (1.2.17)$$

where $Z_i = 1 + \delta Z_i$, $\delta Z_i = \mathcal{O}(\alpha_s)$. The terms on the left of the equalities are the parameters found in the bare Lagrangian, whilst the right hand side hold the renormalised quantities. Equation (1.2.16) describes the wave function renormalisations of the gluon and quark fields, whereas (1.2.17) has the mass and coupling constant renormalisation respectively. By absorbing the divergent behaviour into the Z_i parameters, the Green's functions of the renormalised parameters become finite to all orders in perturbation theory [7–9]. In making such a shift, the original Lagrangian is split into two contributions, that of the renormalised Lagrangian (the original written

in terms of renormalised quantities) and a counter term:

$$\mathcal{L}_{0,QCD} = \mathcal{L}_{ren} + \mathcal{L}_{c.t.}, \tag{1.2.18}$$

where $\mathcal{L}_{c.t.}$ holds the multiplicative factors δZ_i.

Whilst the singular terms are fixed in order to cancel the divergences, finite terms can be shifted between the counter term and the renormalised Lagrangian without affecting the full functional integral. Whilst this is safe for an all-orders calculation, in a truncated perturbative expansion, a calculation of an observable may pick up some dependency on the choice of finite terms in the counter term. A **renormalisation scheme** must be chosen, where the structure of the finite terms is made explicit. In the minimal subtraction (MS) scheme, the finite contribution to the counter term is set to zero, whereas in the modified minimal subtraction $(\overline{MS})$ scheme we utilise the fact that, given space-time dimensionality $d = 4 - 2\epsilon$, the finite contribution from the poles are always of the form

$$\frac{\Gamma(1+\epsilon)}{\epsilon}(4\pi)^\epsilon = \frac{1}{\epsilon} + \ln(4\pi) - \gamma + \mathcal{O}(\epsilon) \tag{1.2.19}$$

and thus remove the UV pole

$$\frac{1}{\bar{\epsilon}} = (4\pi)^\epsilon e^{-\epsilon\gamma}\frac{1}{\epsilon} = \bar{C}(\epsilon)\frac{1}{\epsilon}, \tag{1.2.20}$$

which, order by order, moves the finite contribution of the pole into the counter term, out of the renormalised quantities.

The renormalisation of the parameters is defined at an arbitrary scale μ, introduced to maintain a dimensionless action and defining the cutoff for renormalisation conditions. Despite having complete freedom in the choice of μ, it is clear that any physical observable must be invariant under such a choice. The freedom inherited by the addition of μ appears in the renormalised strong coupling as

$$\alpha_{s,0} = Z_\alpha^2(\mu^2)\alpha_{s,ren}. \tag{1.2.21}$$

For the theory to remain consistent, stringent constraints are imposed upon the renormalised quantities as they undergo a shift in the renormalisation scale. We consider a dimensionless observable $\mathcal{R}$ where we are interested in a single scale $\sqrt{s}$ that is larger than all others, $m^2/s \ll 1$. For such an observable, the independence from the renormalisation scale is given by

$$\mu^2 \frac{\mathrm{d}}{\mathrm{d}\mu^2} \mathcal{R}(s/\mu^2, \alpha_s(\mu^2)) = 0, \tag{1.2.22}$$

which, in the strictly massless limit, is expanded via the substitution $t = \log(s/\mu^2)$ to

$$\left[-\frac{\partial}{\partial t} + \beta(\alpha_s(\mu^2)) \frac{\partial}{\partial \alpha_s} \right] \mathcal{R}(e^t, \alpha_s(\mu^2)) = 0, \tag{1.2.23}$$

where $\beta(\alpha_s(\mu^2))$ is the QCD beta-function, defining the running of the coupling with scale, and is given by

$$\beta(\alpha_s(\mu^2)) = \mu^2 \frac{\partial \alpha_s(\mu^2)}{\partial \mu^2}. \tag{1.2.24}$$

We thus see in (1.2.23) that a change in the renormalisation scale can be compensated for by a corresponding change in the coupling. The solution describes the evolution of the coupling as the energy scale shifts from s to μ^2. Given a small coupling, the β-function can be expanded perturbatively in α_s,

$$\frac{1}{2\pi} \beta(\alpha_s(\mu^2)) = -\beta_0 \left(\frac{\alpha_s(\mu^2)}{2\pi} \right)^2 - \beta_1 \left(\frac{\alpha_s(\mu^2)}{2\pi} \right)^3 - \mathcal{O}(\alpha_s(\mu^2)^4), \tag{1.2.25}$$

where the coefficients β_i are extracted by the evaluation of loop corrections to the bare vertices in the theory. Explicitly the coefficients β_0 and β_1 for a theory containing N_F flavours of massless active quarks are given by

$$\beta_0 = \frac{11C_A - 4T_R N_F}{6}, \qquad \beta_1 = \frac{17C_A^2 - 10C_A T_R N_F - 6C_F T_R N_F}{6} \tag{1.2.26}$$

where we introduce the casimirs

$$C_F = \frac{N^2 - 1}{2N}, \qquad C_A = N, \qquad T_R = \frac{1}{2} \tag{1.2.27}$$

for an $SU(N)$ gauge theory with N being the number of colours. Solving an approximate form of (1.2.24) by retaining only the first term in the β-function expansion gives the 1-loop form of the running coupling:

$$\alpha_s(s) = \frac{\alpha_s(\mu^2)}{1 + \alpha_s(\mu^2)(\beta_0/2\pi)\log(s/\mu^2)}. \tag{1.2.28}$$

This provides a link between the couplings at different scales, provided both are small enough to lie in the perturbative regime. The non-Abelian interactions of QCD become immediately apparent, since they produce a positive value for β_0, resulting in the decrease in the coupling strength as the energy scale becomes large[2]. This describes the idea of asymptotic freedom in QCD, and is in stark contrast with QED, in which the coupling is observed to become progressively stronger as the energy is increased.

Returning to the μ-dependence of our observable $\mathcal{R}$ in (1.2.23), it is straightforward to show that $\mathcal{R}(1, \alpha_s(s))$ is a solution. Indeed, any function $f(\alpha_s(s = \mu^2))$ will satisfy the Renormalisation Group Equation, such that the scale dependence of the observable is encapsulated entirely in the scale dependence of the running coupling. Since the analysis of the β-function showed that for large energy scales the coupling α_s will become small, it is feasible to carry out a perturbative expansion of $\mathcal{R}$ in terms of $\alpha_s(s)$,

$$\mathcal{R}(1, \alpha_s(s)) = r_1\alpha_s(s) + r_2\alpha_s(s)^2 + \mathcal{O}(\alpha_s(s)^3). \tag{1.2.29}$$

1.2.1 Scale dependence

The small coupling constant at high energies allows calculations in QCD to be carried out via a perturbative expansion in the coupling. Whilst the observable written as

---

[2]This is provided that $N_F \leqslant 16$, which is happily upheld by the Standard Model.

a full sum over all terms is still independent of renormalisation scale, any practical calculation involves a truncation of the series. Unfortunately this means that the observable, now only in terms of a subset of the expanded terms, no longer enjoys a full cancellation of μ-dependent terms, and is a function of our choice of renormalisation scale. This is clearly of great importance if we wish to compare the theoretical predictions with experiment, which will take no heed of the artificial choice of scale. It is thus necessary to have a firm understanding of the effect on the observable by the renormalisation scale dependence upon truncation of the peturbative series. Expanding our observable in the coupling constant, with the coefficients being a variable in the ratio s/μ^2, reads

$$\mathcal{R}(1, \alpha_s(s)) = \sum_{n=0}^{\infty} r_n \left(\frac{s}{\mu^2} \right) \alpha_s(\mu^2)^n. \qquad (1.2.30)$$

Taking the first N terms and using (1.2.22) to enforce μ-independence of the full expansion, we arrive at

$$\frac{d}{d \log \mu^2} \sum_{n=0}^{N} r_n \left(\frac{s}{\mu^2} \right) \alpha_s(\mu^2)^n = -\frac{d}{d \log \mu^2} \sum_{n=N+1}^{\infty} r_n \left(\frac{s}{\mu^2} \right) \alpha_s(\mu^2)^n = \mathcal{O}(\alpha_s^{N+1}).$$
$$(1.2.31)$$

The truncated series picks up renormalisation scale dependence as expected, which would otherwise vanish with the inclusion of all higher order terms. However, the remainder of the truncated terms go like α_s^{N+1}, indicating that, vitally, the scale dependence decreases as the number of higher order terms is increased - a strong motivation for extending peturbative calculations to higher orders.

1.3   Colour space and matrix elements

The brute-force attack upon scattering problems with the Feynman rules provides an intuitive understanding of the underlying physical calculation. Nevertheless, it becomes rapidly inefficient due to the factorial growth in complexity with increasing multiplicity. A Feynman diagram is in general not gauge invariant, whilst combina-

tions of non-gauge invariant diagrams are often seen to cancel at intermediate levels in the calculation. To overcome the growth of diagrams, a potential step is to separate the gauge and kinematical structures from the outset, thereby avoiding an organisation of factors at odds with the underlying gauge symmetry. We therefore discuss **colour decomposition** as a process by which scattering amplitudes can be written as kinematical objects existing in the space of the different colour structures [10].

A physical matrix element in QCD with n external legs, $\mathcal{M}_n$ can be written as a function of the external momenta p_i, having colour c_i and helicity λ_i. The matrix element is thus realised as a vector projected onto helicity and colour space,

$$\mathcal{M}_n = \mathcal{M}_n^{c_1, c_2, \ldots c_n; \lambda_1, \lambda_2, \ldots \lambda_n}(p_1, p_2, \ldots p_n) = \langle \mathbf{c}, \lambda | \mathcal{M} \rangle, \qquad (1.3.32)$$

where the basis of the helicity and colour space is

$$|\mathbf{c}, \lambda \rangle = |c_1, c_2 \ldots c_n \rangle \otimes |\lambda_1, \lambda_2 \ldots \lambda_n \rangle. \qquad (1.3.33)$$

The possible colour and spin values are naturally defined by the partonic nature of the external states. If parton i is a quark (gluon) it can take a colour value from $c_i = 1, \ldots N$ ($c_i = 1, \ldots N^2 - 1$) and helicity $\lambda_i = 1, 2$ ($\lambda_i = 1, \ldots D - 2$). The squared matrix element can thus be defined, summed over helicity and colour, as

$$
\begin{aligned}
|\mathcal{M}_n|^2 &= \sum_{c_i, \lambda_i} \langle \mathcal{M} | \mathbf{c}, \lambda \rangle \langle \mathbf{c}, \lambda | \mathcal{M} \rangle \\
&= \langle \mathcal{M} | \mathcal{M} \rangle. \qquad (1.3.34)
\end{aligned}
$$

A judicious course of action is to decompose the matrix element according to its colour structures. As aforementioned, the result of such a decomposition is the factorisation of the matrix element into a **partial amplitude** [11] containing only kinematic behaviour, and a function holding all colour information for a given colour structure. For a general scattering process, the decomposition of the matrix element factorises
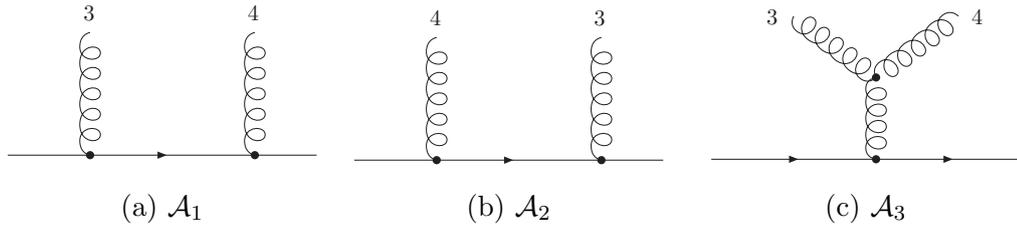
Figure 1.1: Tree-level Feynman diagrams contributing towards two-quark, two-gluon scattering.

as

$$\mathcal{M}_n^{c_1,c_2,\ldots c_n;\lambda_1,\lambda_2,\ldots \lambda_n}(p_1, p_2, \ldots p_n;) = \sum_a \Delta_a^{c_1,c_2,\ldots c_n} \mathbf{M}_n^{\lambda_1,\lambda_2,\ldots \lambda_n;a}(p_1, p_2, \ldots p_n).$$

(1.3.35)

All colour dependence is held within the function Δ_a and M_n is the partial amplitude associated with said colour structure. The partonic nature of the matrix element, including the external states and the loop order, determines fully the subtleties of the decomposition.

The form of the amplitude can then be squared and summed over colours and helicities, resulting in

$$|\mathcal{M}_n|^2 = \sum_{a,b} \sum_{colours} \Delta_a^{\dagger,c_1,c_2,\ldots c_n} \Delta_b^{c_1,c_2,\ldots c_n}$$

$$\times \sum_{hel} \mathbf{M}_n^{\lambda_1,\lambda_2,\ldots \lambda_n;a}(p_1, p_2, \ldots p_n) \mathbf{M}_n^{\lambda_1,\lambda_2,\ldots \lambda_n;b}(p_1, p_2, \ldots p_n), \quad (1.3.36)$$

where we can now carry out independently the squaring of the colour structure Δ and that of the kinematic colour-stripped subamplitude.

At the level of the individual diagram, we see that a Feynman graph consists of a combination of the Feynman propagators and vertices [4]; the colour factor can be stripped outside, and we have just such a factorisation of the colour and kinematic terms. As an example, we consider the tree level contribution to two-quark, two-gluon scattering. This will be required in the dijet production calculations in Chapter 5. There are only three Feynman diagrams that contribute, given in Figure 1.1, where i, j are reserved for quark labels, and a_n denote external gluon indices in the adjoint.

The colour structures associated with each amplitude are

$$\mathcal{A}_1 = (T^{a_1} T^{a_2})_{ij} \mathcal{A}_1, \tag{1.3.37}$$

$$\mathcal{A}_2 = (T^{a_2} T^{a_1})_{ij} \mathcal{A}_2, \tag{1.3.38}$$

$$\mathcal{A}_3 = \text{Tr}(T^{a_1} T^{a_2}) \delta_{ij} \mathcal{A}_3, \tag{1.3.39}$$

where the colour is stripped away, leaving the purely kinematic amplitude $\mathcal{A}_i$. The Fierz identity can be used in conjunction with the structure constant algebra to sum over the internal colour degrees of freedom in (1.3.39), thereby reformulating it in terms of the other two where only external colour degrees of freedom are present:

$$
\begin{aligned}
\mathcal{A}_3 = \text{Tr}(T^{a_1} T^{a_2}) \delta_{ij} \mathcal{A}_3 &= i T^{a_3}_{ij} f^{a_3 a_1 a_2} \delta_{ij} \mathcal{A} \\
&= 2 T^c_{ij} [\text{Tr}(T^{a_3} T^{a_1} T^{a_2}) - \text{Tr}(T^{a_3} T^{a_2} T^{a_1})] \mathcal{A}_3 \\
&= [(\delta_{im}\delta_{kj} - \frac{1}{N}\delta_{ij}\delta_{op}) T^{a_1}_{mn} T^{a_2}_{nk} + (\delta_{ip}\delta_{jo} - \frac{1}{N}\delta_{ij}\delta_{op}) T^{a_2}_{pq} T^{a_1}_{qo}] \mathcal{A}_3 \\
&= [(T^{a_1} T^{a_2})_{ij} - (T^{a_2} T^{a_1})_{ij}] \mathcal{A}_3 \tag{1.3.40}
\end{aligned}
$$

Since the full amplitude is simply the sum of all the diagrams, it can be written in terms of the factorised colour structures,

$$
\begin{aligned}
\mathcal{A}_{full} &= \mathcal{A}_1 + \mathcal{A}_2 + \mathcal{A}_3 \\
&= (T^{a_1} T^{a_2})_{ij} [\mathcal{A}_1 + \mathcal{A}_3] + (T^{a_2} T^{a_1})_{ij} [\mathcal{A}_2 - \mathcal{A}_3] \tag{1.3.41}
\end{aligned}
$$

where we have constructed new, colour ordered partial amplitudes that are a linear combination of individual colour-stripped Feynman diagrams with a particular ordering of the gluons. Importantly, the partial amplitudes are gauge invariant, allowing astute gauge choices to be made independently for each amplitude to simplify calculations. It is these objects that will prove highly useful for later calculations since the Feynman diagrams, now individually hidden inside the partial amplitudes, are

grouped by their colour connectivity into a far smaller set of amplitudes;

$$
\begin{aligned}
\mathcal{A}(q, 3_g, 4_g, \bar{q}) &= \mathcal{A}_1 + \mathcal{A}_3, \\
\mathcal{A}(q, 4_g, 3_g, \bar{q}) &= \mathcal{A}_2 - \mathcal{A}_3.
\end{aligned}
\tag{1.3.42}
$$

The full squared amplitude, summed over colours, is

$$
|\mathcal{A}_{full}|^2 = N(N^2 - 1) \left[\sum_{\{i,j\} \in \{3,4\}} A_4^0(q, i_g, j_g, \bar{q}) - \frac{1}{N^2} \widetilde{A}_4^0(q, 3_g, 4_g, \bar{q}) \right], \tag{1.3.43}
$$

where the square of the colour factors can be carried out utilising the Fierz Identity. In our example here, the leading term is calculated thus

$$
\begin{aligned}
\left[(T^{a_1} T^{a_2})_{ij} \right] \left[(T^{a_1} T^{a_2})_{ij} \right]^\dagger &= \mathrm{Tr}(T^{a_1} T^{a_2} T^{a_2} T^{a_1}) \\
&= N(N^2 - 1)(1 - \frac{1}{N^2}). \tag{1.3.44}
\end{aligned}
$$

The colour calculations can also be carried out in a graphical manner [12], where we can make the replacements in the colour structure of

$$
\delta_i^j : \quad \longrightarrow \quad , \quad \delta^{ab} : \quad \text{ooooo} \quad , \quad (T^a)_{ij} : \quad \underset{}{\overset{\text{oooo}}{\longrightarrow}} \quad . \tag{1.3.45}
$$

In this representation, contracted indices are simply connected by quark or gluon lines, the Fierz identity becomes

$$
\text{[diagram]} \quad = \frac{1}{2} \left[\text{[diagram]} - \frac{1}{N} \text{[diagram]} \right] \tag{1.3.46}
$$

and the properties of the generators can be expressed as

$$\text{Tr}(1) \quad = \quad \bigcirc \quad = N; \quad \text{Tr}(T^a) = \quad \text{(diagram)} \quad = 0; \qquad (1.3.47)$$

$$\text{Tr}(T^a T^b) = \quad \text{(diagram)} \quad = \frac{1}{2} \quad \text{(diagram)} \quad . \qquad (1.3.48)$$

It is now a simple exercise to apply these rules to decompose the squared colour structures, the final result being some function of N. Our above calculation now looks like:

$$\left[(T^{a_1}T^{a_2})_{ij}\right]\left[(T^{a_1}T^{a_2})_{ij}\right]^{\dagger} \quad = \quad \text{(diagram)} \quad = \quad \text{(diagram)}$$

$$= \quad \bigcirc \quad \times \quad \text{(diagram)} \quad - \frac{1}{N} \quad \text{(diagram)}$$

$$= \quad \left(N - \frac{1}{N}\right) \times \left[\quad \bigcirc \quad \times \quad \bigcirc \quad - \frac{1}{N} \quad \bigcirc \quad \right]$$

$$= \quad N(N^2 - 1)(1 - \frac{1}{N^2}). \qquad (1.3.49)$$

It is apparent from (1.3.49) that in squaring the amplitude, the partial amplitude associated with the colour structure $(T^{a_1}T^{a_2})_{ij}$ is going to contribute to both colour-leading and colour-subleading terms. In fact, the subleading contributions in (1.3.43) contain a sum of the partial amplitudes;

$$\widetilde{A}_4^0(q, 3_g, 4_g, \bar{q}) = |\mathcal{A}(q, 3_g, 4_g, \bar{q}) + \mathcal{A}(q, 4_g, 3_g, \bar{q})|^2 = |\mathcal{A}_1 + \mathcal{A}_2|^2 \qquad (1.3.50)$$

where we see that the contribution from the three gluon vertex $\mathcal{A}_3$ has dropped out. Since there are no longer any self-gluon interactions present, it is akin to the gluons in this subamplitude acting under $U(1)$ instead of $SU(3)$ - they are aptly named Abelian gluons. As will be discussed later, this makes significant simplifications to the parton colour-connectivity.

1.4 Factorisation

The cross section for two initial state hadrons with momenta P_1 and P_2 is given by [13]

$$\sigma(P_1, P_2) = \sum_{a,b} \int dz_1\, dz_2\, f_a(z_1, \mu_F^2) f_b(z_2, \mu_F^2)\, \hat{\sigma}_{ab}(p_1, p_2, \alpha_s(\mu_F^2)), \qquad (1.4.51)$$

where the partons carry a momentum fraction z_i of the hadrons, which then participate in the partonic cross section $\hat{\sigma}_{ab}$ with momenta p_1 and p_2. The details of the initial state hadrons and relative partonic momentum distributions are contained within the parton distribution functions (PDFs) for parton a as $f_a(z_a, \mu_F^2)$. The PDFs can be computed independently from the partonic cross section, and are non-perturbative in nature. The factorisation formula of (1.4.51) shows clearly that the total cross section can be constructed via a summation over all possible partonic subprocesses, weighted by the PDF determining the probability of the occurrence of each initial partonic state. For high energies the coupling is small and the partonic cross section can be calculated perturbatively. High momentum transfer is vital; soft effects, characterised by the Λ_{QCD} scale where hadronic effects become dominant, can spoil the factorisation since we can pick up contributions from interactions between long- and short-distance effects. However, for a high centre-of-mass energy the soft effects are subleading, only becoming dominant at lower scales where colour-neutralisation and confinement hadronisation effects begin to occur. It must be noted that the factorisation theorem has only been proven for Deep Inelastic Scattering and Drell-Yan processes [13], and caution must be taken in its direct application to more exclusive processes.

For leading order calculations, the cross section at high energies is simply the product of the partonic cross section with the parton distribution function, as in (1.4.51). However, as we move to higher orders and include radiative corrections to the leading order process, we create an ambiguity in the distinction between what constitutes the hard partonic cross section and the hadronic properties that are dealt with non-perturbatively. Including such corrections in the hard scattering alters the initial state momentum distribution and thus can be at odds with the PDF descrip-

tion. In order to separate which emissions are considered long- and short- distance physics, a factorisation scale μ_F is introduced. Radiated partons with transverse momentum greater than μ_F are considered part of the hard scattering, whilst partons with momentum smaller than μ_F are incorporated into the parton distributions. We have factorised the physics into long and short distance effects, but at the cost of introducing the arbitrary scale μ_F upon which the hard scattering cross section and PDFs are separately dependent upon, although the total hadronic cross section should be independent of μ_F. A greater number of terms included in the perturbative expansion will reduce the μ_F dependence, as with the renormalisation scale dependence discussed in Section 1.2. With this in mind, the calculational path upon which to proceed becomes clear. In a similar fashion to the renormalisation procedure of redefining the bare parameters of the Lagrangian, the parton distributions that enter (1.4.51) are labelled the 'bare' PDFs $\tilde{f}_a(z)$ and are related to the physical PDFs $f_a(z, \mu_F^2)$. In the renormalisation procedure, the bare parameters are merely multiplied by the Z_i factor to produce the renormalised Lagrangian and counter term to deal with the UV divergences, whereas the bare and physical PDFs are related via a convolution,

$$f_a(z, \mu_F^2) = \int \mathrm{d}x \, \mathrm{d}y \tilde{f}_b(x) \Gamma_{ba}(y, \mu_F^2) \delta(z - xy) = [\tilde{f}_b \otimes \Gamma_{ba}](z, \mu_F^2), \qquad (1.4.52)$$

where μ_F^2 is the scale at which the factorisation is defined. The factorisation kernel Γ_{ba} can be perturbatively expanded in the strong coupling as

$$\Gamma_{ba}(y, \mu_F^2) = \delta_{ba}\delta(1 - y) + \left(\frac{\alpha_s}{2\pi}\right) \Gamma_{ba}^1(y, \mu_F^2) + \left(\frac{\alpha_s}{2\pi}\right)^2 \Gamma_{ba}^2(y, \mu_F^2) + \mathcal{O}(\alpha_s^3), \, (1.4.53)$$

given a suitably high μ_F^2. In a practical perturbative calculation, the series is truncated at some order in α_s, and then we acquire dependence on the factorisation scale [14].

By taking the inverse of (1.4.52) we can uncover the bare PDF in terms of the physical one:

$$\tilde{f}_a(z) = \int \mathrm{d}x \, \mathrm{d}y \, f_b(x, \mu_F^2) \, \Gamma_{ba}^{-1}(y, \mu_F^2) \, \delta(z - xy) = [f_b \otimes \Gamma_{ba}^{-1}](z, \mu_F^2), \qquad (1.4.54)$$

where

$$\Gamma_{ba}^{-1}(y, \mu_F^2) = \delta_{ba}\delta(1-y) - \left(\frac{\alpha_s(\mu_F^2)}{2\pi}\right)\Gamma_{ba}^1(y)$$
$$- \left(\frac{\alpha_s(\mu_F^2)}{2\pi}\right)^2\left[\Gamma_{ba}^2(y) - \sum_c[\Gamma_{bc}^1 \otimes \Gamma_{ca}^1](y)\right] + \mathcal{O}(\alpha_s^3).$$

$$(1.4.55)$$

In doing so we have a new expression for the hadronic cross section in terms of the physical PDFs, which now hold dependence on μ_F^2. The partonic cross section, now infrared finite, reads

$$d\hat{\sigma}_{ij}(z_1H_1, z_2H_2) = \int \frac{dx_1}{x_1}\frac{dx_2}{x_2}\Gamma_{ki}^{-1}(x_1\mu_F^2)\Gamma_{lj}^{-1}(x_2\mu_F^2)d\tilde{\sigma}_{kl}(x_1z_1H_1, x_2z_2H_2). \quad (1.4.56)$$

The effect of this factorisation procedure can be seen by pertubatively expanding the partonic cross section - the factorisation kernel according to (1.4.55) and $d\hat{\sigma}$ by (1.4.51) - and equating powers of the coupling. We follow the argument in [15] as it is useful to see this form for later computations. At leading order, only the first term of (1.4.55) will contribute, and immediately produces the expected result

$$d\hat{\sigma}_{ij,LO}(z_1H_1, z_2H_2) = d\tilde{\sigma}_{ij,LO}(z_1H_1, z_2H_2). \quad (1.4.57)$$

For higher orders in α_s the cross section now picks up terms incorporating the factorisation kernels;

$$\begin{aligned}d\hat{\sigma}_{ij,NLO}(z_1H_1, z_2H_2) &= d\tilde{\sigma}_{ij,NLO}(z_1H_1, z_2H_2)\\ &\quad - \int\frac{dx_1}{x_1}\Gamma_{ki}^1(x_1)d\hat{\sigma}_{kj,LO}(x_1z_1H_1, x_2z_2H_2)\\ &\quad - \int\frac{dx_2}{x_2}\Gamma_{lj}^1(x_2)d\hat{\sigma}_{il,LO}(x_1z_1H_1, x_2z_2H_2)\\ &= d\tilde{\sigma}_{ij,NNLO}(z_1H_1, z_2H_2) + d\hat{\sigma}_{ij,NNLO}^{MF}(z_1H_1, z_2H_2),\end{aligned}$$

$$(1.4.58)$$

$$
\begin{aligned}
\mathrm{d}\hat{\sigma}_{ij,NNLO}(z_1 H_1, z_2 H_2) &= \mathrm{d}\tilde{\sigma}_{ij,NNLO}(z_1 H_1, z_2 H_2) \\
&\quad - \int \frac{\mathrm{d}x_1}{x_1} \Gamma^2_{ki}(x_1) \mathrm{d}\hat{\sigma}_{kj,LO}(x_1 z_1 H_1, z_2 H_2) \\
&\quad - \int \frac{\mathrm{d}x_1}{x_1} \Gamma^1_{ki}(x_1) \mathrm{d}\hat{\sigma}_{kj,NLO}(x_1 z_1 H_1, z_2 H_2) \\
&\quad - \int \frac{\mathrm{d}x_2}{x_2} \Gamma^2_{lj}(x_2) \mathrm{d}\hat{\sigma}_{il,LO}(z_1 H_1, x_2 z_2 H_2) \\
&\quad - \int \frac{\mathrm{d}x_2}{x_2} \Gamma^1_{lj}(x_2) \mathrm{d}\hat{\sigma}_{il,NLO}(z_1 H_1, x_2 z_2 H_2) \\
&\quad + \int \frac{\mathrm{d}x_1}{x_1} \int \frac{\mathrm{d}x_2}{x_2} \Gamma^1_{ki}(x_1) \Gamma^1_{lj}(x_2) \mathrm{d}\hat{\sigma}_{kl,LO}(x_1 z_1 H_1, x_2 z_2 H_2) \\
&= \mathrm{d}\tilde{\sigma}_{ij,NNLO}(z_1 H_1, z_2 H_2) + \mathrm{d}\hat{\sigma}^{MF}_{ij,NNLO}(z_1 H_1, z_2 H_2),
\end{aligned}
$$

$$(1.4.59)$$

where we see a further similarity with renormalisation, in that the full cross section at a particular order is given by the cross section containing the physical PDF, plus a **mass factorisation** counter term, built from lower order partonic cross sections.

We are now in a favourable condition. The low energy effects - the physics occurring below the factorisation scale μ_F - is contained within $\mathrm{d}\hat{\sigma}^{MF}_{ij}$, and the combination of this and the hard scattering process gives a finite partonic cross section. The redefined parton distribution function $f_a(x, \mu_F^2)$ containing the long distance physics of the strong interaction can be determined independently from the experimental data at a preferred scale. Given a computation of the PDF at a particular scale, it can be evolved to a new scale by appealing to its all-order independence of the factorisation scale, in a similar vein to renormalisation. The resulting Renormalisation Group Equations are the DGLAP equations [16–18], which can be used to run the parton distributions across resolution scales. The evolution can be written in terms of splitting functions and expanded perturbatively in the strong coupling.

Chapter 2

Infrared Behaviour of QCD Amplitudes

Perturbation theory allows concrete and systematically improvable predictions to be made of scattering processes. By expanding to higher and higher orders we can aim to reduce the large errors introduced by renormalisation scale dependence and gain greater precision in theoretical predictions required for comparison with LHC measurements.

However, in extending to higher orders we immediately encounter singularities that haunt vital aspects of our calculations, those of **ultraviolet** (UV) and **infrared** (IR) divergences, in both the virtual and real radiative corrections to the leading order process. In this chapter we discuss the origin of these singularities, and methods by which they can be brought under control.

2.1 Divergent behaviour

Consider the one loop integral associated with the process in Figure 2.1 such that $p_1^2 = p_2^2 = 0$ (i.e. massless on-shell fermions), namely

$$\mathcal{I} \sim \int \frac{\mathrm{d}^d \ell}{i\pi^{d/2}} \frac{\bar{u}(p_1)[\gamma^\mu(\slashed{\ell} + \slashed{p}_2)\gamma^\nu(\slashed{\ell} + \slashed{p}_1)\gamma^\rho]u(p_2)}{[\ell^2 + i\epsilon][(\ell - p_1)^2 + i\epsilon][(\ell + p_2)^2 + i\epsilon]}, \tag{2.1.1}$$
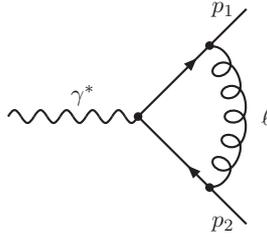
Figure 2.1: NLO virtual correction to $\gamma^* \to q\bar{q}$.

where d is the dimensionality of spacetime. The $i\epsilon$ prescription prevents the enclosure off poles within the contour integral over ℓ. Since we integrate over all possible momenta of the virtual gluon, ultraviolet divergences occur in the high energy massless limit, $|\ell| \to \infty$. In this limit, $\ell > p_1, p_2$ so that

$$\mathcal{I} \sim \int \frac{\mathrm{d}^d \ell}{i\pi^{d/2}} \frac{\bar{u}(p_1)[\gamma^\mu \ell \gamma^\nu \ell \gamma^\rho] u(p_2)}{\ell^6 + (i\epsilon)^3}, \tag{2.1.2}$$

and we observe a logarithmic UV divergence as $d \to 4$. It is removed during the renormalisation procedure detailed in Section 1.2. In a calculation utilising the Feynman diagrammatic approach, the amplitudes are inherently unrenormalised. By considering a perturbative expansion

$$|\mathcal{M}\rangle = \left(\frac{\alpha_s}{2\pi}\right)^n \left[|\mathcal{M}^{(0),un}\rangle + \frac{\alpha_s}{2\pi}|\mathcal{M}^{(1),un}\rangle + \left(\frac{\alpha_s}{2\pi}\right)^2 |\mathcal{M}^{(2),un}\rangle + \mathcal{O}(\alpha_s^3)\right], \tag{2.1.3}$$

and replacing the bare couplings with the renormalised ones, we can determine the renormalised amplitudes as functions of the unrenormalised ones order by order in α_s:

$$\begin{aligned}
|\mathcal{M}^{(0)}\rangle &= |\mathcal{M}^{(0),un}\rangle, \\
|\mathcal{M}^{(1)}\rangle &= \frac{1}{\bar{C}(\epsilon)}|\mathcal{M}^{(1),un}\rangle - \frac{n\beta_0}{\epsilon}|\mathcal{M}^{(0),un}\rangle, \\
|\mathcal{M}^{(2)}\rangle &= \frac{1}{\bar{C}(\epsilon)^2}|\mathcal{M}^{(2),un}\rangle - \frac{(1+n)\beta_0}{\epsilon}\frac{1}{\bar{C}(\epsilon)}|\mathcal{M}^{(1),un}\rangle - \frac{n}{2}\left(\frac{\beta_1}{\epsilon} - \frac{\beta_0^2(1+n)}{\epsilon^2}\right)|\mathcal{M}^{(0),un}\rangle.
\end{aligned} \tag{2.1.4}$$

When considering a theory with massless particles, or in our case the high energy limit at the LHC, we encounter further divergences that arise when particle momenta become negligible with respect to the hard scale involved. In our loop integral above,

this can be seen when one of the propagators vanishes, $|\ell| \to 0, -p_1, -p_2$ [1]. Physically we see this as particles going **soft**, where the energy becoming too small to identify, and **collinear**, where two particles are travelling in the same direction. We now consider these configurations in terms of the real and virtual corrections to a scattering process.

2.1.1 Virtual IR divergences

The infrared singularities stemming from the virtual corrections can be understood by employing the formalism of Catani [19, 20], which provides an algorithmic approach to the formulation of the pole structure of both one and two-loop renormalised amplitudes.

Singular behaviour of one-loop amplitudes

Following on from Section 1.3, we consider the QCD amplitude $|\mathcal{M}\rangle$ in colour space with n external partons. The amplitudes are renormalised in the $\overline{MS}$ scheme and we work in conventional dimensional regularisation (CDR), where all states are treated in d dimensions. The perturbative expansion of the amplitude is

$$|\mathcal{M}\rangle = \left(\frac{\alpha_s}{2\pi}\right)^m \left[|\mathcal{M}^0\rangle + \frac{\alpha_s}{2\pi}|\mathcal{M}^1\rangle + \left(\frac{\alpha_s}{2\pi}\right)^2 |\mathcal{M}^2\rangle + \mathcal{O}(\alpha_s^3)\right], \qquad (2.1.5)$$

with m being process dependent. The singular behaviour of the one-loop amplitude $|\mathcal{M}^1\rangle$, as described in [19], can be separated from the finite part in colour space through the singularity operator $\mathbf{I}^{(1)}(\mu^2, \epsilon)$,

$$|\mathcal{M}^1(\mu^2, \epsilon)\rangle = \mathbf{I}^{(1)}(\mu^2, \epsilon)|\mathcal{M}^0(\mu^2)\rangle + |\mathcal{M}^{1,fin}(\mu^2)\rangle, \qquad (2.1.6)$$

where we make explicit the fact that the amplitudes are dependent on the renormalisation scale μ. $|\mathcal{M}^{1,fin}(\mu^2)\rangle$ is an IR finite function in the limit $\epsilon \to 0$. All divergences associated with $|\mathcal{M}^1(\mu^2, \epsilon)\rangle$ are factorised with respect to the tree level amplitude

---

[1]In a massive theory the mass term in the propagator would act as a regulator. Even so, in QCD we have massless gluons so such a divergence is still present.

$|\mathcal{M}^0(\mu^2)\rangle$, encapsulated inside the IR singularity operator $\mathbf{I}^{(1)}(\mu^2, \epsilon)$ defined as

$$\mathbf{I}^{(1)}(\mu^2, \epsilon) = \frac{e^{\gamma\epsilon}}{2\Gamma(1-\epsilon)} \sum_{i=1}^{n} \frac{1}{\mathbf{T}_i^2} \mathcal{V}_i^{sing}(\epsilon) \sum_{j\neq i} \mathbf{T}_i \cdot \mathbf{T}_j \left(\frac{e^{-i\lambda_{ij}\pi}\mu^2}{s_{ij}}\right)^\epsilon, \qquad (2.1.7)$$

where the summations run over all external legs, and s_{ij} is the usual Mandelstam invariant $s_{ij} = 2p_i \cdot p_j$ for massless partons i and j. Also, there is an additional factor

$$\lambda_{ij} = \begin{cases} 1 & \text{if both particles are incoming or outgoing.} \\ 0 & \text{otherwise.} \end{cases} \qquad (2.1.8)$$

With this construction, it is natural to view the real and virtual emissions as insertions of colour interactions between all the partons in a certain colour state amplitude. To obtain the singular behaviour of the amplitude we use **colour charges** $\mathbf{T}_i$. The matrices T_{cb}^a are defined as: [21]

$$\begin{aligned} T_{cb}^a &= t_{cb}^a && \text{final state quark or initial antiquark emitter,} \\ T_{cb}^a &= -t_{cb}^a && \text{final state antiquark or initial quark emitter,} \\ T_{cb}^a &= if_{cab} && \text{gluon emitter.} \end{aligned}$$

The colour charge algebra is

$$(\mathbf{T}_i)^a(\mathbf{T}_j)^a \equiv \mathbf{T}_i \cdot \mathbf{T}_j = \begin{cases} \mathbf{T}_j \cdot \mathbf{T}_i & \text{if } i \neq j. \\ \mathbf{T}_i^2 = C_i & \text{otherwise.} \end{cases} \qquad (2.1.9)$$

The Casimir operator C_i will be $C_i = C_F(C_i = C_A)$ for the ith parton being a quark (gluon). Since in this notation the vectors $|\mathcal{M}_m(p_1, p_2, \ldots, p_n)\rangle$ are colour singlets, colour conservation allows us to enjoy the property

$$\sum_{i=1}^{n} \mathbf{T}_i |\mathcal{M}_n\rangle = 0, \qquad (2.1.10)$$

providing a stringent self-consistency check on the operators defined in the following section.

The singular contributions are buried in the $\mathcal{V}_i^{sing}(\epsilon)$ function as poles in the

parameter ϵ,

$$\mathcal{V}_i^{sing}(\epsilon) = \frac{1}{\epsilon^2} + \gamma_i \frac{1}{\epsilon} \tag{2.1.11}$$

where γ_i depends on the type of parton involved:

$$\gamma_q = \gamma_{\bar{q}} = \frac{3}{2}, \qquad \gamma_g = \frac{\beta_0}{C_A}. \tag{2.1.12}$$

Here, β_0 is the first term in the perturbative expansion of the beta function, given in (1.2.26). Note that the singularity operator is regularisation scale (RS) independent: the RS dependence is encoded within the tree and one-loop finite pieces.

Example: one loop singularities in $\gamma^* \to q\bar{q}$

As an example we consider again the virtual correction to the quark vertex at NLO, given in Figure 2.1. The colour charge operators are simply $\mathbf{T}_q$ and $\mathbf{T}_{\bar{q}}$, and from (2.1.10),

$$\mathbf{T}_q + \mathbf{T}_{\bar{q}} = 0: \quad \mathbf{T}_{\bar{q}}^2 = \mathbf{T}_q^2 = \mathbf{T}_q \cdot \mathbf{T}_{\bar{q}} = -C_F \mathbf{I}. \tag{2.1.13}$$

We thus construct the singularity operator using (2.1.7), which takes the form

$$\mathbf{I}^{(1)}(\mu^2, \epsilon) = -C_F \frac{e^{\gamma\epsilon}}{2\Gamma(1-\epsilon)} \left[\frac{1}{\epsilon^2} + \frac{3}{2\epsilon} \right] \left(\frac{-\mu^2}{s_{12}} \right)^{\epsilon} \mathbf{I}, \tag{2.1.14}$$

where $\mathbf{I}$ is the identity matrix. The poles of the full squared matrix element can be thus obtained by using (2.1.6),

$$\mathcal{P}oles\left[|\mathcal{M}_2^1(p_1, p_2)|^2 \right] = -C_F \frac{e^{\gamma\epsilon}}{2\Gamma(1-\epsilon)} \left[\frac{1}{\epsilon^2} + \frac{3}{2\epsilon} \right] \left(\frac{-\mu^2}{s_{12}} \right)^{\epsilon} |\mathcal{M}_2^0(p_1, p_2)|^2. \tag{2.1.15}$$

However, by decomposing the amplitude into its colour structures as in the previous section, we can obtain the pole structure for colour ordered squared matrix elements, in which the squared subamplitudes will be multiplied by a scalar function holding the ϵ dependence, its explicit form being the inner product of (2.1.6) with the tree level amplitudes. The processes required in this thesis are calculated explicitly in Appendix A using this formalism. In doing so, we can write the poles of the squared

matrix elements as a sum of colour-ordered, two particle IR singularity operators that run over the colour connected pairs that exist in the colour-ordered squared amplitudes:

$$
\begin{aligned}
\mathcal{P}oles\left[M_n^1(1,\cdots,n)\right] &= 2\sum_{i,j}\mathbf{I}_{ij}^{(1)}(\epsilon,s_{ij})M_n^0(1,\cdots,n) \\
&\equiv 2\,\mathbf{I}_n^{(1)}(\epsilon,1,\cdots,n)M_n^0(1,\cdots,n),
\end{aligned} \tag{2.1.16}
$$

where $M_n^0(1,\cdots,n)$ is a squared colour-ordered partial amplitude. The two particle singularity operators [22] can be constructed in a similar fashion to the example above, changing the partonic content for each of the possible colour structures and parton combinations;

$$
\begin{aligned}
\mathbf{I}_{q\bar{q}}^{(1)}(\epsilon,s_{q\bar{q}}) &= -\frac{e^{\epsilon\gamma}}{2\Gamma(1-\epsilon)}\left[\frac{1}{\epsilon^2}+\frac{3}{2\epsilon}\right]\Re(-s_{q\bar{q}})^{-\epsilon}\,, \\
\mathbf{I}_{qg}^{(1)}(\epsilon,s_{qg}) &= -\frac{e^{\epsilon\gamma}}{2\Gamma(1-\epsilon)}\left[\frac{1}{\epsilon^2}+\frac{5}{3\epsilon}\right]\Re(-s_{qg})^{-\epsilon}\,, \\
\mathbf{I}_{gg}^{(1)}(\epsilon,s_{gg}) &= -\frac{e^{\epsilon\gamma}}{2\Gamma(1-\epsilon)}\left[\frac{1}{\epsilon^2}+\frac{11}{6\epsilon}\right]\Re(-s_{gg})^{-\epsilon}\,, \\
\mathbf{I}_{q\bar{q},F}^{(1)}(\epsilon,s_{q\bar{q}}) &= 0\,, \\
\mathbf{I}_{qg,F}^{(1)}(\epsilon,s_{qg}) &= \frac{e^{\epsilon\gamma}}{2\Gamma(1-\epsilon)}\frac{1}{6\epsilon}\Re(-s_{qg})^{-\epsilon}\,, \\
\mathbf{I}_{gg,F}^{(1)}(\epsilon,s_{gg}) &= \frac{e^{\epsilon\gamma}}{2\Gamma(1-\epsilon)}\frac{1}{3\epsilon}\Re(-s_{gg})^{-\epsilon}\,.
\end{aligned} \tag{2.1.17}
$$

Using this notation the pole structure for our example reads

$$
\mathcal{P}oles\left[M_m^1(1,\cdots,m)\right] = 2\mathbf{I}_{q\bar{q}}^{(1)}(\epsilon,s_{12})M_2^0(p_1,p_2). \tag{2.1.18}
$$

Singular Behaviour of two-loop amplitudes

The double virtual contribution to the $pp\to n$-jet cross section involves the two-loop $(n+2)$-parton matrix elements which have no implicit IR divergence in any regions of the appropriate n-parton phase space. The two loop contribution does contain explicit poles, displaying an inevitable increase in complexity of the singular structure. However, as with the one-loop case, a similar factorisation formula is

observed. Introducing a new insertion operator $\mathbf{I}^{(2)}(\epsilon)$, the pole structure of the two loop amplitude can be expressed as

$$|\mathcal{M}^2(\mu^2,\epsilon)\rangle = \mathbf{I}^{(1)}(\mu^2,\epsilon)|\mathcal{M}^1(\mu^2)\rangle + \mathbf{I}^{(2)}(\mu^2,\epsilon)|\mathcal{M}^0(\mu^2)\rangle + |\mathcal{M}^{2,fin}(\mu^2)\rangle, \quad (2.1.19)$$

where again we have a term $|\mathcal{M}^{2,fin}(\mu^2)\rangle$ that is finite in the limit $\epsilon \to 0$. However, unlike the one-loop case, there are now two terms that contain the singularity structure, and they both must take account of the deeper poles found in two-loop amplitudes, now up to $1/\epsilon^4$.

In a similar fashion to the one loop case, we construct the squared matrix element by taking the interference of the two-loop amplitude with the tree level counterpart, and also the self interference of the one-loop amplitude:

$$M_n^2 = \langle \mathcal{M}_n^0 | \mathcal{M}_n^2 \rangle + \langle \mathcal{M}_n^2 | \mathcal{M}_n^0 \rangle + \langle \mathcal{M}_n^1 | \mathcal{M}_n^1 \rangle. \quad (2.1.20)$$

The application of (2.1.19) thus provides the IR pole structure of the squared, colour-ordered matrix element. This construction reflects the dipole-like singularity structure for two-loop amplitudes made apparent in Catani's two-loop factorisation formula [20],

$$
\begin{aligned}
\mathcal{P}oles\big(M_n^2(1,\cdots,n)\big) &= 2\mathbf{I}_n^{(1)}(\epsilon;1,\cdots,n)\left(M_n^1(1,\cdots,n) - \frac{\beta_0}{\epsilon}M_n^0(1\cdots,n)\right) \\
&- 2\mathbf{I}_n^{(1)}(\epsilon;1,\cdots,n)^2 M_n^0(1,\cdots,n) \\
&+ 2e^{-\epsilon\gamma}\frac{\Gamma(1-2\epsilon)}{\Gamma(1-\epsilon)}\left(\frac{\beta_0}{\epsilon} + K\right)\mathbf{I}_n^{(1)}(2\epsilon;1\cdots,n)M_n^0(1\cdots,n) \\
&+ 2\mathbf{H}^{(2)}(\epsilon)M_n^0(1,\cdots,n), \quad (2.1.21)
\end{aligned}
$$

with $\mathbf{I}_n^{(1)}(\epsilon)$ given by Eq. (2.1.7), and

$$K = N\left(\frac{67}{18} - \frac{\pi^2}{6}\right) - N_F\frac{10}{9}. \quad (2.1.22)$$

The insertion operators also involve the hard radiation functions $\mathbf{H}^{(2)}(\epsilon)$, containing poles of up to $\mathcal{O}(\epsilon^{-1})$, and are not universal; they are both process- and regularisation scheme-dependent. Nevertheless, the poles of the two-loop squared matrix element

are correctly isolated, whilst the finite contributions must be obtained via explicit calculations of the amplitude.

2.1.2 Real IR divergences

The IR divergences stemming from real radiation occur in a different manner to the virtual corrections. The latter, upon integration over the virtual momenta, can be expressed as a Laurent expansion in ϵ via dimensional regularisation (see for example [5]). Real radiative divergences are manifest only after integration over the final state phase space, which will include regions where the invariants, out of which the squared matrix elements are contracted, vanish. This is seen clearly by examining the real radiative correction to our favourite quark vertex diagram:

$$|\mathcal{M}_3^0|^2 \;\; = \;\; \left| \;\; \vcenter{\hbox{}} \;\; + \;\; \vcenter{\hbox{}} \;\; \right|^2 \sim \left(\frac{2s_{12}s_{123}}{s_{13}s_{23}} + \frac{s_{13}}{s_{23}} + \frac{s_{23}}{s_{13}} \right), \quad (2.1.23)$$

which diverges for

$$s_{ij} = 2E_iE_j(1-\cos\theta_{ij}) = \begin{cases} E_g \to 0 & \text{soft} \\ \theta_{ij} \to 0 & \text{collinear} \end{cases} \quad (2.1.24)$$

Since in such limits the final state is indistinguishable from the process with no radiation from the detector viewpoint, we must include this contribution. To gain control of these divergences, we again appeal to the colour-ordering of the matrix elements. These colour subamplitudes will only contain inverse powers of invariants pertaining to colour connected partons, such as that given in Appendix A. In controlling the colour connectivity of the amplitudes, we can also ascertain the divergent limits that exist. The sum of all the colour-ordered amplitudes will thus contain the full extent of divergent behaviour present in the complete process.

Single unresolved limits at tree level

Colour-ordered matrix elements in the single unresolved limit involve a parton becoming either soft or collinear with another parton that is colour-connected to it. In

the unresolved limit, the squared matrix element factorises into a product of a universal function holding the singular behaviour, and a reduced finite squared matrix element,

$$M_n^0(\{p\}) \xrightarrow{\text{singular limit}} U(s_{ij}, z) M_{n-1}^0(\{p\}/\{p_i, p_j\}). \qquad (2.1.25)$$

The explicit form of the universal function $U(s_{ij}, z)$, the momenta present and the structure of the reduced multiplicity squared matrix element are dependent on the singular configuration at hand. Mappings between the sets of momenta must be constructed, and are addressed in Section 4.2.

The singular configurations are built from two possible scenarios:

1. Soft partons: $p \to \xi q$, $\quad \xi \in \mathbb{R} \to 0$,

2. Collinear partons: $p \to \lambda q$, $\quad \lambda \in \mathbb{R}$.

In this thesis we treat all partons as massless, but the quark still cannot become soft since this would break current conservation. In this particular limit the matrix element vanishes; the integration over phase space is unaffected by such a limit.

When a gluon goes soft however, the colour-ordered matrix element is non-vanishing since there is no longer protection from current conservation. Instead we see that the n-parton matrix element factors onto a universal soft eikonal term, multiplied by a reduced $(n-1)$-parton matrix element with the offending gluon removed. For the tree-level squared matrix element we observe explicitly [23],

$$M_n^0(\cdots i, j, k \cdots) \xrightarrow{j_g \to 0} S_{ijk} M_{n-1}^0(\cdots, i, k, \cdots). \qquad (2.1.26)$$

Importantly, the eikonal factor S_{ijk} is independent of the partonic nature of its neighbours: partons i and j in (2.1.26) can be either gluons or quarks and the soft function is unchanged. It is a function only of the momenta,

$$S_{ijk} = \frac{2s_{ik}}{s_{ij}s_{jk}}, \qquad (2.1.27)$$

and holds fully the momenta of the soft gluon; none remains in the reduced matrix

element.

The collinear limit can be treated in a similar fashion, if we consider the limit in which two partons i and j are described by a single parton A, an amalgamation of the two collinear partons. Here the factorisation of the squared matrix element behaves as [16]

$$M_n^0(\cdots i, j \cdots) \xrightarrow{i\|j} \frac{1}{s_{ij}} P_{ij\to A}(z) M_{n-1}^0(\cdots, A, \cdots), \tag{2.1.28}$$

where z is the fraction of the momentum of A contributed by i, that is

$$p_i = zp_A \qquad\qquad p_j = (1-z)p_A \tag{2.1.29}$$

and $P_{ij\to A}$ is a spin-averaged splitting function which, in contrast to the universal soft factor, has a dependency on the species of parton involved in the limit. Considering the allowed vertices in QCD, we have:

$$P_{qq\to G}(z) = \frac{z^2 + (1-z)^2 - \epsilon}{1-\epsilon}; \tag{2.1.30}$$

$$P_{qg\to Q}(z) = \frac{1 + (1-z)^2 - \epsilon z^2}{z}, \tag{2.1.31}$$

$$P_{gg\to G}(z) = 2\Big(\frac{z}{1-z} + \frac{1-z}{z} + z(1-z)\Big). \tag{2.1.32}$$

C-parity provides the other splitting functions: $P_{\bar{q}g\to\bar{Q}} = P_{qg\to q}$.

We extend this formalism to take account for partons crossing into the initial state. For soft partons colour-connected to initial states it is sufficient to modify the Lorentz invariants in the soft eikonal factor: with a final state parton j and an initial state parton $\hat{i}$ we construct the invariant $s_{\hat{i}j} = (p_{\hat{i}} - p_j)^2 = -2p_{\hat{i}} \cdot p_j$. The hatted momenta in this thesis will always denote initial states. For the collinear case the modification is slightly more involved, since the momentum fraction z associated with the split partons is altered: for the case of two final-state partons we invoke (2.1.29), whereas for a final state j and initial state $\hat{i}$ becoming collinear the momentum fractioning behaves as

$$p_j = zp_{\hat{i}}, \qquad\qquad p_j = (1-z)p_{\hat{i}}. \tag{2.1.33}$$

This in turn affects the splitting functions, which will pick up extra factors of $(1 - \epsilon)$ in CDR when there is an alteration in the number of polarizations of the partons as they change type during the hard scattering. The initial-final splitting functions are related to the final-final splitting functions of (2.1.30), (2.1.31) and (2.1.32) by [24]:

$$P_{qq\leftarrow G}(z) = \frac{z^2 + (1-z)^2 - \epsilon}{1-z} = \frac{1-\epsilon}{1-z}P_{qq\to G}(z); \tag{2.1.34}$$

$$P_{qg\leftarrow Q}(z) = \frac{1 + (1-z)^2 - \epsilon z^2}{z(1-z)} = \frac{1}{1-z}P_{qg\to Q}(z), \tag{2.1.35}$$

$$P_{gg\leftarrow G}(z) = \frac{2(1-z+z^2)^2}{z(1-z)^2} = \frac{1}{1-z}P_{gg\to G}(z). \tag{2.1.36}$$

As with the case for the final-final splitting functions, in the singular limit the matrix element factorises into the splitting function multiplied by a reduced matrix element with one fewer parton.

Single unresolved limits at one loop level

The factorisation of one-loop squared matrix elements in single unresolved limits follows a similar pattern to the tree level case [25], except that we must now take into account that the contribution from the loop may sit in either the splitting function or the reduced matrix element. New universal singular functions must be introduced; the single soft limit factorises as

$$M_n^1(\cdots, i, j, k, \cdots) \xrightarrow{j_g \to 0} S_{ijk}M_{n-1}^1(\cdots, i, k, \cdots) + S_{ijk}^1 M_{n-1}^1(\cdots, i, k, \cdots), \tag{2.1.37}$$

where S_{ijk}^1 is the one loop soft function given in [26] and includes singular terms up to $1/\epsilon^2$. In a similar fashion, the factorisation of the one loop squared matrix element in the collinear limit is given by

$$M_n^1(\cdots, i, j, \cdots) \xrightarrow{i||j} \frac{1}{s_{ij}}P_{ij\to A}(z)M_{n-1}^1(\cdots, A, \cdots) + \frac{1}{s_{ij}}P_{ij\to A}^1(z)M_{n-1}^0(\cdots, A, \cdots), \tag{2.1.38}$$

and is given in full at the helicity level in [27]. Implicit singular behaviour of one loop squared matrix elements will naturally appear at NNLO, and thus any subtraction term constructed at this order must contain one loop structures to accommodate the new one-loop splitting functions.

Angular terms

In addition to the momentum fraction z, full splitting functions are dependent on the spin index carried by the parent parton. However, the splitting functions encoding the singular information of the colour ordered matrix elements are spin averaged objects.

For a quark splitting to a quark-gluon pair, there is a trivial helicity dependence and thus the factorisation is simply

$$M_{n+1}^0(\cdots, i, j, \cdots) \xrightarrow{i \| j} \frac{1}{s_{ij}} P_{ij \to A_q}(z) M_n^0(\cdots, A_q, \cdots). \tag{2.1.39}$$

However, when we consider a gluon splitting into either a quark-antiquark pair or two gluons, we must now take into account that the parent gluon is a vector particle, and carries a Lorentz spin index μ. Taking the full splitting function [28] rather than the spin-averaged case we see

$$
\begin{aligned}
P_{q\bar{q} \to G}^{\mu\nu}(z, k_\perp) &= -g^{\mu\nu} + 4z(1-z)\frac{k_\perp^\mu k_\perp^\nu}{k_\perp^2}. \\
P_{gg \to G}^{\mu\nu}(z, k_\perp) &= -2\left[g^{\mu\nu}\left(\frac{1}{1-z} + \frac{1-z}{z}\right) + 2(1-\epsilon)z(1-z)\frac{k_\perp^\mu k_\perp^\nu}{k_\perp^2}\right].
\end{aligned}
\tag{2.1.40}
$$

The full splitting functions have dependency on the component transverse to the collinear splitting axis, $k_\perp$, and the helicity of the parent parton. A parameterisation of the collinear daughter parton momenta in terms of $k_\perp$ is thus introduced in [21]; in order to do so it is also necessary to define an auxiliary light-like vector n, whereby $k_\perp \cdot n = k_\perp \cdot p_A = 0$. Enforcing the daughter and parent momenta to be on-shell, the

collinear partons can be defined as

$$
\begin{aligned}
p_i &= zp_A + k_\perp - \frac{k_\perp^2 n}{2p_A \cdot n}\frac{1}{z}, \\
p_j &= (1-z)p_A - k_\perp - \frac{k_\perp^2 n}{2p_A \cdot n}\frac{1}{1-z}.
\end{aligned}
\tag{2.1.41}
$$

Incorporating all spin-dependencies, the factorisation of the matrix element in the collinear limit of two daughter partons from a parent gluon can be expressed as

$$
\begin{aligned}
M_{n+1}^0(\cdots, i, j, \cdots) \ \xrightarrow{i \| j} \ & \frac{1}{s_{ij}} P_{ij \to A_g}^{\mu\nu}(z, k_\perp) M_{n,\mu\nu}^0(\cdots, A_g, \cdots) \\
= & \ \frac{1}{s_{ij}} P_{ij \to A_g}(z) M_n^0(\cdots, A_g, \cdots) + \text{ang.}
\end{aligned}
\tag{2.1.42}
$$

Since the subtraction method introduced in Chapter 4 utilises spin-averaged functions, the extra angular terms are missed. However, these contributions from the spin correlations will vanish after integration over the azimuthal angle ϕ. A possible approach to account for these correlations is to pair up phase space points that are related by a rotation of the collinear partons by $\Delta\phi = \pi/2$ about the collinear direction. With such a pairing, the correlations from the matrix element in the rotated and unrotated points cancel. The effect of this correction will be considered later in this thesis through analysis of explicit results.

Double unresolved limits at tree level

Calculations at NNLO allow for real radiative corrections to the Born process through the addition of two real unresolved partons. Whilst the unresolved partons can still be either soft or collinear as in the single unresolved case, there are now naturally a wider range of configurations stemming from two partons going simultaneously unresolved [29]. In the limit we observe a similar factorisation into a reduced matrix element multiplied by a singular factor, where the structure of the factorised object is determined by the unresolved behaviour and the colour-connectivity of the partons involved. With double unresolved limits we can identify three configurations of colour connections between partons:

1. **Colour connected double unresolved**: A common pair of hard radiators

separate two partons going unresolved - the unresolved partons are colour adjacent, as in Figure 2.2a.

2. **Almost colour-connected double unresolved**: The two unresolved partons are colour-adjacent to hard radiators, one of which is shared between them, given in Figure 2.2b.

3. **Colour-unconnected double unresolved**: Each unresolved parton is sandwiched between two hard radiators, but separated by at least one other hard radiator (Figure 2.2c).

$$\qquad\qquad\text{(a)}\qquad\qquad\qquad\qquad\text{(b)}\qquad\qquad\qquad\qquad\text{(c)}$$
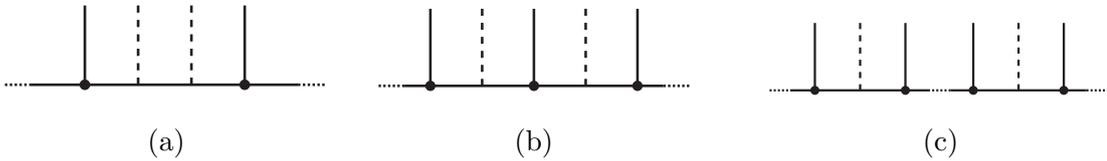
Figure 2.2: Colour connectivity configurations for doubly unresolved partons (dashed vertical lines) between hard radiators (solid vertical lines). The unresolved partons can be (a) colour connected, (b) almost colour connected or (c) colour unconnected.

Since there is an additional parton becoming unresolved it is possible to have additional classes of singular limits to those at NLO:

1. **Double soft unresolved partons**

   The double soft configurations consist of both partons going soft simultaneously between a single pair of hard radiators, and will fall into one of the three colour configurations detailed above. When the two partons are colour connected, the factorisation is simple [30]:

   $$M_n^0(\cdots, a, i, j, b, \cdots) \xrightarrow{i,j \to 0} S_{aijb} M_{n-2}^0(\cdots, a, b, \cdots), \qquad (2.1.43)$$

   where we reserve labels $a, \ldots, d$ for hard radiators. When the two soft partons are gluons, the form of the double soft gluon function S_{aijb} is universal as for the single unresolved case. However, it is now possible for a quark-antiquark pair to go soft simultaneously, the source being a soft gluon splitting to such a pair. In this case the soft function must be differentiated from the pure gluon case

as it takes a different form [22], but is universal for this scenario nonetheless. For the almost-colour connected and colour unconnected configurations, we find again straightforward factorisation behaviour, since the limit can be taken by considering an iteration of the single unresolved procedure. The factorisation for colour-unconnected unresolved partons reads

$$M_n^0(\cdots, a, i, b \cdots, c, j, d, \cdots) \xrightarrow{i,j \to 0} S_{aib} \, S_{cjd} M_{n-2}^0(\cdots a, b, \cdots, c, d, \cdots).$$

(2.1.44)

and is simply extended to allow for the almost colour-connected configuration by letting $b = c$.

2. **Collinear unresolved partons**

For limits involving partons going collinear only, we encounter two setups. Firstly that of a pair of NLO-type collinear limits in which pairs of partons separately go collinear, the double collinear limit, which will occur in the almost colour-connected and colour-unconnected configurations. However, it is now possible for three partons to become simultaneously collinear with each other, called the triple collinear limit.

In the colour connected configuration where three partons merge to form a single parent parton, the triple collinear limit factorises the squared subamplitude as

$$M_n^0(\cdots, i, j, k, \cdots) \xrightarrow{i||j||k} P_{ijk \to A}(z_1, z_2, z_3) M_{n-2}^0(\cdots, A, \cdots), \quad (2.1.45)$$

where again A is the composite parton. The form of the splitting functions are, similarly to the single splittings, dependent on the nature of the unresolved partons and are collected in [22], the momentum fractions of each parton here given by z_1, z_2 and z_3. The triple collinear limit when two of the three partons are colour connected also produces a singular outcome,

$$M_n^0(\cdots, i, \cdots, j, k, \cdots) \xrightarrow{i||j||k} \frac{1}{s_{jk}}.$$

(2.1.46)

However, the integration of phase space in the region of this limit also contains the same invariants, which vanish more rapidly than the divergent squared matrix element such that no IR singularity is formed. Furthermore, when all three partons are colour-unconnected, the matrix element is finite in the triple collinear regions.

When there are two colour connected pairs of collinear partons, we again observe an iterated NLO-type factorisation:

$$M_n^0(\cdots, i, j, \cdots, k, l, \cdots) \xrightarrow{i||j,k||l} \frac{1}{s_{ij}} P_{ij \to A}(z_1) \frac{1}{s_{kl}} P_{kl \to B}(z_2) M_{n-2}^0(\cdots, A, \cdots B, \cdots).$$

$$(2.1.47)$$

As before, if the collinear limit stems from a gluon pair or quark-antiquark pair collapsing onto a parent gluon, then azimuthal corrections described previously must be taken into account.

In a similar vein to the colour-unconnected triple collinear limit, if all four partons are separated in the colour string, then the matrix element provides no contribution of the order $1/s_{ij} s_{kl}$; in the integration over this phase space region we receive a negligible contribution.

3. **Soft- collinear unresolved partons**

   A combination of both soft and collinear unresolved limits is possible at NNLO, where a single pair of partons goes collinear, and another goes soft, simultaneously. For colour-connected scenarios in the limit, the squared matrix element factorises into a product of a soft factor and a splitting function:

$$M_n^0(\cdots, i, j, k, b \cdots) \xrightarrow{i||j,k \to 0} \frac{1}{s_{ij}} P_{ij \to A}(z_1) S_{b,kji} M_{n-2}^0(\cdots, A, b, \cdots).$$

$$(2.1.48)$$

where b is a hard radiator [31]. For the case where j is the soft parton and i and k go collinear, the matrix element factorises into a less singular object, resulting in a vanishing contribution. For the case where the soft and collinear pair are colour unconnected, we see once more an iteration of the single unresolved

limits, namely

$$M_n^0(\cdots, a, i, b, \cdots, j, k, \cdots) \xrightarrow{j||k, i \to 0} \frac{1}{s_j k} P_{jk \to A}(z_1) S_{aib} M_{n-2}^0(\cdots, a, b, \cdots, A, \cdots).$$

(2.1.49)

2.1.3 Singularity cancellation

As we have already seen, the explicit pole structure of one-loop amplitudes, and thus the squared matrix elements, can be written as a Laurent expansion in the dimension parameter ϵ via dimensional regularisation. Analysis by Bloch and Nordseick [32], and Kinoshita [33], Lee and Nauenberg [34] (KLN) proved that all IR singularities present in the virtual corrections combined with the real emission will cancel when summed over all degenerate states, leaving a finite cross section.

The inclusion of the real emission makes heuristic sense; their divergences occur in the limits where additional radiated parton would be unobserved by a physical detector. Thus, the process would be indistinguishable from the one with lower multiplicity, and should therefore be considered as a contribution to the underlying process' final state.

To observe explicitly such a cancellation in perturbative calculations, we are required to perform the phase space integration analytically over the unresolved regions, such that the real and virtual phase spaces are of the same size. Thus at NLO we sum over all the real emission diagrams which contain singly unresolved limits. These are at the same order in α_s as the virtual corrections. The full cross section for n partons in the final state is then

$$d\hat{\sigma}_{ij}^{NLO} = \int_{d\Phi_{n+1}} d\hat{\sigma}_{ij}^R + \int_{d\Phi_n} d\hat{\sigma}_{ij}^V,$$

(2.1.50)

where we must integrate over the unresolved phase space. The extension to NNLO of course increases the complexity, since now double unresolved emission can occur at tree level, and single emission from the one loop corrections;

$$d\hat{\sigma}_{ij}^{NNLO} = \int_{d\Phi_{n+2}} d\hat{\sigma}_{ij}^{RR} + \int_{d\Phi_{n+1}} d\hat{\sigma}_{ij}^{RV} + \int_{d\Phi_n} d\hat{\sigma}_{ij}^{VV}.$$

(2.1.51)

2.2 Colour ordered strings

Before introducing in the following chapters the mechanism by which the singularities are cancelled, we review the possible structures available for colour ordered matrix elements, with reference to the colour decomposition reviewed in Section 1.3. There are two basic objects from which all colour structures can be assembled: gluon strings and quark strings. A gluon string is characterised by a trace over $SU(N)$ generators, where a_k denotes the generator associated with external gluon k, e.g., an n-gluon colour ordered matrix element is associated with the colour structure,

$$\mathrm{Tr}(T^{a_1} T^{a_2} \cdots T^{a_{n-1}} T^{a_n}) \equiv (a_1 a_2 \cdots a_{n-1} a_n). \tag{2.2.52}$$

The colour ordered partial amplitude associated with this colour structure contains IR divergences between colour connected partons, i.e., those external legs whose associated generators are adjacent in the colour structure. Due to the trace nature of the colour factors, the partial amplitudes display cyclic symmetry, which means that the colour connection not only exists between adjacent partons in the notation defined above, but also between the endpoints a_1 and a_n.

The quark string is given by a string of gluon generators sandwiched between fundamental quark indices, e.g., a quark string containing a quark-antiquark pair and n gluons has the colour structure,

$$(T^{a_1} T^{a_2} \cdots T^{a_{n-1}} T^{a_n})_{ij} \equiv (a_1 a_2 \cdots a_{n-1} a_n)_{ij}, \tag{2.2.53}$$

where i, j denote the fundamental (antifundamental) colour indices carried by the quark (antiquark). The IR divergences of the partial amplitude associated with this colour structure also exist for unresolved configurations involving colour connected partons. The gluons at each end of the quark string are not colour connected to each other but are colour connected to the quark endpoints instead. What happens when partons become collinear across colour structures?

If the quark-antiquark pair become collinear to form a composite gluon, the colour structure pinches down to a trace structure and the surviving reduced matrix element

(multiplied by the universal splitting function) tends to a gluonic partial amplitude,

$$(a_1 a_2 \cdots a_{n-1} a_n)_{ij} \xrightarrow{q_i \| \bar{q}_j} (a_1 a_2 \cdots a_{n-1} a_n a_{(ij)}). \qquad (2.2.54)$$

Sub-leading colour structures also arise at the amplitude level according to the distribution of fundamental indices among the endpoints. For example, the four-quark two-gluon partial amplitudes have twelve colour structures. Six of the structures are given according to the permutations of gluons within the structures,

$$(a_1 a_2)_{il}(\oslash)_{kj} \qquad (a_1)_{il}(a_2)_{kj} \qquad (\oslash)_{il}(a_1 a_2)_{kj}, \qquad (2.2.55)$$

where i, k and j, l denote the fundamental and anti-fundamental indices of the quarks and antiquarks respectively and $(\oslash)_{il} = \delta_{il}$ is an empty quark string whose colour factor is simply a Kronecker delta in fundamental indices. The six sub-leading colour structures are obtained by the substitution $j \leftrightarrow l$.

As discussed above, in the case of a quark string, a $q \| \bar{q}$ limit causes the quark string to collapse onto a gluon string. With multiple quark strings, a quark-antiquark collinear limit can cause quark strings to merge, with the composite gluon contributing to the gluon string by connecting the fundamental indices of the quark endpoints, e.g.,

$$(a_{i_1} \cdots a_{i_n})_{ij}(a_{j_1} \cdots a_{j_m})_{kl} \xrightarrow{q_k \| \bar{q}_j} (a_{i_1} \cdots a_{i_n} a_{(kj)} a_{j_1} \cdots a_{j_m})_{il}. \qquad (2.2.56)$$

The same behaviour is exhibited in the reduced partial amplitude in the limits. When multiple strings are present in a single colour ordered partial amplitude, the partons involved in each quark string are separated from those involved in other strings by a semi-colon, e.g.,

$$M_n^0(\cdots ; q_1, g_1, g_2, \bar{q}_1; q_3, g_1, \bar{q}_2; \cdots). \qquad (2.2.57)$$

Sub-leading colour

The sub-leading colour contribution cannot, in general, be written in the form of an incoherent sum of squared partial amplitudes. However for low multiplicity final-states the sub-leading colour contribution can often be rewritten as the square of a coherent sum of QCD partial amplitudes where one or more gluons behave in an Abelian fashion.

Matrix elements containing "Abelian gluons" obey the usual QCD factorisation formulae in all the unresolved limits of the non-Abelian gluons. The Abelian gluons do not couple to the non-Abelian gluons and only couple to quarks; therefore they can only be considered colour-connected to the quarks. A sub-leading colour matrix element can thus be considered to contain two colour structures: a pure QCD colour structure formed from all quarks and non-Abelian gluons, the factorisation properties of which are identical to those of leading colour squared matrix element, and a QED-like colour structure containing quark pairs and colour disconnected Abelian gluons [35]. As an example, consider a squared partial amplitude with two quarks, n non-Abelian gluons and one Abelian gluon, $\tilde{i}$, is denoted $M_{n+3}^0(q, g_1, \cdots, \tilde{g}_i, \cdots, g_n, \bar{q})$. The colour structure is of the form

$$(q, 1, \cdots, \tilde{i}, \cdots, n, \bar{q})_{ij} \quad \sim \quad (q, 1, \cdots, n, \bar{q})_{ij} \otimes (q, \tilde{i}, \bar{q})_{ij}. \qquad (2.2.58)$$

The Abelian gluon can have collinear limits with the quarks and also become soft,

$$M_{n+3}^0(q, g_1, \cdots, \tilde{g}_i, \cdots, g_n, \bar{q}) \quad \xrightarrow{i||q} \quad \frac{1}{s_{qi}} P_{qg\to Q}(z) \, M_{n+2}^0(Q, g_1, \cdots, g_n, \bar{q}), \quad (2.2.59)$$

$$M_{n+3}^0(q, g_1, \cdots, \tilde{g}_i, \cdots, g_n, \bar{q}) \quad \xrightarrow{i\to 0} \quad S_{qi\bar{q}} \, M_{n+2}^0(q, g_1, \cdots, g_n, \bar{q}), \qquad (2.2.60)$$

where $P_{qg\to Q}(z)$ and $S_{qi\bar{q}}$ are the time-like quark-gluon splitting function and soft function respectively. The collinear limit with the antiquark is given by exchanging $q \leftrightarrow \bar{q}$. When the sub-leading colour matrix elements can be re-written in terms of squared matrix elements involving Abelian gluons then the IR divergent limits can be subtracted using antenna functions just as at leading colour. For six or more coloured particles, the sub-leading colour contribution cannot be written purely in

terms of squared matrix elements with Abelian gluons. Nevertheless, the sub-leading colour contributions will in general contain fewer and less intricate divergent limits than their leading colour counterparts. Any finite contribution to the cross section can be immediately integrated numerically.

<div align="center">*</div>

The discussion of this chapter has illustrated the universal behaviour of the real emission in the single and double unresolved limit. What will follow for the remainder of this thesis is the application of these properties in creating counter terms that can be constructed in such a way that can render the real emission finite, whilst simultaneously employing the KLN theorem to deal with the explicit poles from the virtual contributions. We will focus on the leading colour contribution for clarity but it is clear that a similar treatment can be reproduced for sub-leading colour contributions in future studies.

Chapter 3

Dijet Production at the LHC

By far the most dominant hard process in collider experiments is the QCD production of jets, which provide an excellent testing ground for probing the Standard Model and possibly detecting hints of new physics. In this chapter we discuss jet cross sections in collider experiments, and examine leading order dijet production and motivations for extending our calculations to higher orders. Dijet production will be our primary calculational focus in subsequent chapters.

3.1 Jet cross sections

The final state quarks and gluons emitted in a hard scattering process are not the particles we observe in the detector. Indeed, since the first experiments at SLAC to probe the proton substructure, bare quarks have yet to be detected. Quark confinement is a solution to this potential discrepancy with theory, whereby the net colour of the partons are always confined inside hadrons, with only colour singlets being observable. We see in the discussion of the running coupling that at large separations, the coupling becomes large also. At distances on the scale of the hadron diameter, the strong interaction is sufficiently strong such that pair production can occur. Successively stronger gluons can be radiated also, often close to being collinear to the parent parton, and join non-perturbatively to form colour-neutral mesons and baryons. The result is a collimated **jet** of hadrons, which are the objects measured in the detector. The energy and mass of the jet is somewhat indicative of that of the parton in the

hard scattering. Figure 3.1 shows a dijet event taken at the ATLAS detector with the LHC running at a centre of mass energy of 2.8 TeV. Two back to back collimated clusters of energy deposits are clear, each with a high transverse momentum. The event was collected on 8th August 2010.

Creating qualitative analyses of jet structure is vital, and a crucial postulate to link theory and experimental data is local parton hadron duality (LPHD) [36]. Most of the energy and momentum is found to be contained within a single hadron on the jet; LPHD asserts that in addition, the momentum flow and quantum numbers of the hadrons are mimicked at the parton level by those partons initiating the jets. With hadronisation effects taken to be minimal, the association of the fixed state partons at the hard scattering with a jet should be a reasonable assertion. In extending the hard scattering computations to higher orders in α_s we allow for a richer partonic final state to potentially cluster to form jets. Nevertheless, completely reproducing the full final state emissions within the matrix element calculation is highly impractical, and matching to a parton shower, which simulates the soft and collinear radiation from the hard scattering scale to hadronisation, is required.
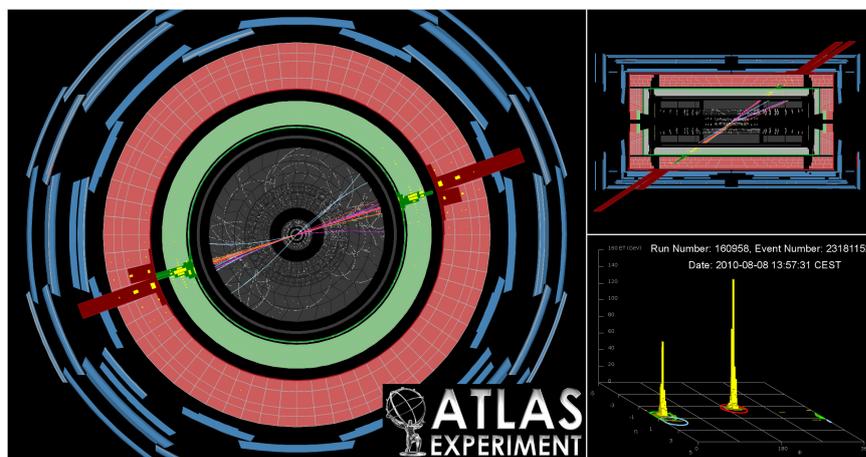
Figure 3.1: Dijet event recorded at ATLAS with jets from pp collision of invariant mass 2.8 TeV. A track p_T cut of 2.5 GeV is applied.

The incoming hadrons contain a spectrum of longitudinal momenta, modelled by PDFs. With respect to these hadrons, the centre-of-mass of the partonic interaction is often boosted since the partons hold only a fraction of the hadronic momenta. It is judicious therefore to define variables that transform as simply as possible under

such a longitudinal boost. We define the hyperbolic angle rapidity, y, as

$$y = \frac{1}{2}\ln\left(\frac{E + p_z}{E - p_z}\right), \tag{3.1.1}$$

where the difference in rapidity between particles Δy_{ij} is boost invariant. For the massless of high energy regime suitable at the LHC, pseudo rapidity is preferred, defined as

$$\eta = -\ln\left(\tan\left(\frac{\theta}{2}\right)\right), \tag{3.1.2}$$

which is experimentally favourable since θ, the angle from the beam direction, is measured directly in a detector. Hadron calorimeters also measure the transverse energy E_T, rather than the transverse momenta:

$$E_T = E\sin(\theta). \tag{3.1.3}$$

It is now possible to rewrite the four-momentum of a particle as

$$p = (m_T\cosh y, p_T\sin y, p_T\cos y, p_T\sinh y), \tag{3.1.4}$$

where the transverse mass $m_T = \sqrt{p_T^2 + m^2}$ is also boost invariant. Given suitable kinematic variables for describing jets, the jet itself must be defined. Rather than studiously (and unrealistically) examining by eye each individual event collected on tape, it is prudent to define a set of rules, a **jet definition**, that will control the way in which a list of jets will be returned, when provided with a set of particle momenta in a given event. In the construction of jet algorithms it is imperative that they are not affected to their detriment by IR contributions: explicitly, the jet distributions produced by the jet algorithm must be insensitive to soft and collinear radiation. That is, they display **infrared safety**. For example, a quark-antiquark pair accompanied by any number of soft and collinear gluons and quark-antiquark pairs should all contribute to the same observable. In the context of a theoretical calculation, we encounter cross sections given in terms of functions describing kinematics and

dynamics of the physical process, accompanied by a jet function,

$$\frac{\mathrm{d}\hat{\sigma}}{dX} \sim \int \mathrm{d}\Phi_n \sum |\mathcal{M}_n\{p_i\}|^2 J_n^{(m)}(\{p_i\}) \tag{3.1.5}$$

where we sum over all n-parton final state contributions and define the measurement by the jet function $J_n^{(m)}(\{p_i\})$. For IR safety, we require that

$$\left.\begin{array}{l} J_{n+1}^{(m)}(p_1, \cdots, \xi p_n, (1-\xi)p_n) \\ J_{n+1}^{(m)}(p_1, \cdots, \xi p_n, 0) \end{array}\right\} = J_n^{(m)}(p_1, \cdots, p_n), \tag{3.1.6}$$

that is, the jet function for n and $n+1$ partons must become equal in the the one-parton unresolved limit. As discussed previously, in a fully inclusive cross section calculation the soft and collinear singularities should cancel between real and virtual corrections. A singularity-free transition rate in the massless limit is guaranteed if all degenerate states are incorporated; we sum over all radiative corrections in the soft/collinear limits that contribute to the same final state. However, if the jet function is sensitive to the IR radiation, cancellation can no longer occur since the real and virtual configurations contribute to different jet multiplicities - the KLN theorem will no longer hold.

Two major classes of jet algorithm present themselves for hadron colliders, that of **sequential recombination** and **cone** algorithms. They are briefly discussed here, although extensive reviews can be found in [37, 38].

3.1.1 Sequential recombination algorithms

Sequential recombination algorithms take a bottom up approach, in that they behave in a manner akin to inverting the sequence of splitting in a parton shower. Starting with the set of final states, the jets are defined by repeatedly combining particles into composite objects that fall within some distance measure x_{ij}. Once all the particles have passed the selection criteria for recombination, the remaining composite particles can be identified as jets. These algorithms are therefore infrared and collinear safe, since soft or collinear particles are immediately recombined in the initial clustering. The algorithm for hadronic colliders proceeds as follows:

i - For every pair of partons in the final state, calculate a distance measure x_{ij}, and x_{iB}, the distance between the parton i and the beam axis.

ii - Extract the minimum distance measure x_{ij}^{min}.

iii - If the minimum x_{ij}^{min} is below some jet resolution threshold x_{cut}, recombine the particles i and j into a single composite particle and return to (i).

iv - If the minimum is instead one of the x_{iB}, allow i to be a jet and remove from the list of particles.

v - All remaining particles can be assigned as jets, and iteration is terminated.

In such an algorithm, the number of jets is controlled exclusively by the jet resolution threshold x_{cut}. The two extrema set the precedent: as $x_{cut} \to 0$, the jet width is becoming extremely narrow and eventually all final state hadrons become individual jets, whereas x_{cut} becoming large broadens the jets and encapsulates far more final state hadrons, resulting in far fewer occurrences of multi-jet events.

Various sequential jet algorithms exist, notably the k_t [39], anti-k_t [40] and Cambridge/Aachen [41]. They are differentiated through the definition of the distance measure for recombination. Most generally, it is given as

$$
\begin{aligned}
x_{ij} &= \min(k_{t_i}^{2p}, k_{t_j}^{2p}) \frac{\Delta R_{ij}^2}{R^2}, \\
d_{i,B} &= p_{t_i}^{2p},
\end{aligned}
\tag{3.1.7}
$$

where R defines the radial extent of the jet in the $y - \phi$ plane when pictured as a cone, and

$$
\Delta R^2 = (\Delta y_{ij})^2 + (\Delta \phi_{ij})^2,
\tag{3.1.8}
$$

where y_i and ϕ_i are the rapidity and azimuth of particle i respectively. Here, R is taking on the role of x_{cut}. The minimum function returns the smaller of the two arguments. Choosing the value for $p \in \{-1, 0, 1\}$ determines the specific algorithm: k_t, anti-k_t and Cambridge/Aachen use $p = 1, -1$ and 0 respectively.

The k_t algorithm was used extensively at LEP, and since it is closely related to the divergences that appear in QCD emissions, can represent an approximate inversion of the branching process. The k_t algorithm clusters the softest particles first and can often lead to experimentally unaesthetic jets with jagged edges [37]. This is remedied by the anti-k_t algorithm, such that now it is the hardest particles that cluster first. In doing so, the jets emanate from the hardest particle and produce cone-shaped jets. The Cambridge/Aachen algorithm has the distance measure based only on a geometric scale, that is the particles are clustered by their spatial separation. It privileges the collinear divergences of QCD, favouring them over the soft divergences, and is useful for jet substructure analysis.

In addition to the choice of algorithm, defining the radial extent of the jet has a marked effect; large jet radii will capture most of the radiative emissions of a particle in a single jet, whereas for small jet radii one can see a splitting of the particle producing two separate jets. The details of the collider processes can give an indication of a preferred choice. For example, high transverse momenta events can produce a large amount of QCD radiation, and thus a large jet radius is desirable if we wish to minimise loss of radiation from a jet. Conversely, a large radius includes more particles from the underlying event.

Typically at ATLAS at the LHC, an anti-k_t algorithm is used with R = 0.6. To interface jet algorithms with Monte Carlo simulations, FastJet [42] is used. As its name suggests, FastJet can implement sequential recombination algorithms over a time of $\mathcal{O}(N\ln N)$, significantly faster than up to $\mathcal{O}(N^3)$ seen in original implementations of the k_t algorithm in hadron-hadron collisions [43].

3.1.2 Cone algorithms

Cone algorithms were chronologically the first used and follow an approach whereby some initial direction is specified by a seed particle, around which a cone of radius R, azimuth ϕ and rapidity y are constructed. Particles falling within the cone are summed. The direction of the resultant momenta defines the new seed direction, and the process is iterated until the cone direction is stable. To construct the algorithm, a seed must first be chosen, the cone identified and a split merging procedure carried

out to convert the cones into jets. Initiating the seeds with jets however, can result in IR unsafety. For example, picking the highest transverse momenta as the seed can result in different numbers of final states if it splits into a collinear pair, altering the order of hardness of the final state partons. This problem is remedied in the SISCone algorithm [44]. Rather than picking a seed, from all subsets of particles within the cone a momentum is calculated: if it lies within the cone it is stable. A split merging can then be used to remove overlap of stable cones. For some threshold fraction f of the softer of a pair of cones being shared with its harder partner, the cones are either merged if f is exceeded (typically $f = 0.5$ or 0.75), otherwise the overlapping particles are assigned to whichever cone is closer in angle. Since there is no hard seed, and requiring the definition of the cones to have no effect on the split merging, SIScone provides an example of an IR safe cone algorithm. Cone algorithms are now less favoured than sequential recombination algorithms.

3.2 Dijet production

3.2.1 Leading order cross section

Inclusive dijet production at the LHC,

$$p + p \rightarrow j + j + X, \tag{3.2.9}$$

consists of the scattering of partonic elements off hadrons, namely quarks and gluons, at large angles relative to the beam direction, following a proton-proton collision. Here j is a jet defined with a suitable algorithm and X represents the other particles in the final state, including the proton debris.

The study of dijet production is a prime candidate for both the construction of high precision tests of QCD, as well as providing a possible window into new physics.

The use of jet algorithms to determine single inclusive and dijet observables allows for fundamental QCD processes to be measured in hadronic collider environments, including the determination of the parton distributions inside protons [46,47], and as a direct probe of a measurement of α_s [48,49]. The angular distribution of dijets can

also be an indication of new physics; large modifications in the LHC dijet angular distribution from the Standard Model prediction can be a hint at quark contact interactions [45].

Following from (1.4.51), we can consider the leading order partonic cross section

$$d\hat{\sigma}_{ab}^{LO} = d\Phi_2(p_i, p_j; p_a, p_b)\frac{1}{S_2}\overline{\sum}|\mathcal{M}_{ab\to ij}|^2 J_2^{(2)}(p_i, p_j), \qquad (3.2.10)$$

where S_2 is a symmetry factor associated with identical final states. The graphs contributing to the leading order matrix element $|\mathcal{M}_{ab\to ij}|^2$ are given in Figure 3.2, and all processes (including crossings thereof)

$$
\begin{aligned}
q + Q &\to q + Q & q + q &\to q + q \\
q + \bar{q} &\to g + g & g + g &\to g + g
\end{aligned}
\qquad (3.2.11)
$$

must be considered. The squared matrix elements for $2 \to 2$ scattering are well known up to two-loop level [50] which we require for NNLO calculations. The squared matrix
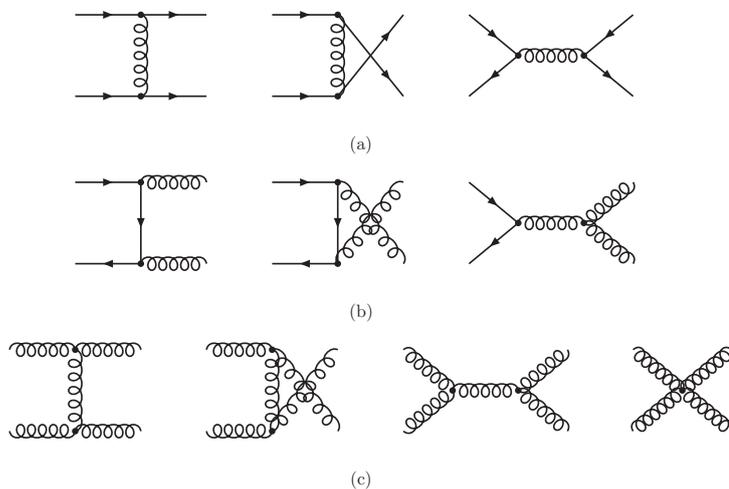
Figure 3.2: Diagrams for dijet production: (a) quark scattering, (b) quark-gluon scattering and (c) gluon scattering.

elements are summed and averaged over the appropriate spins and colours for the particular incoming and outgoing particles. Initial quarks obtain a colour average of $1/N$, whilst initial gluons gain a factor of $1/(N^2 - 1)$. Unpolarised particles will

also pick up an additional spin average factor of $1/2$. The n- parton final state phase space is given by

$$\mathrm{d}\Phi_n(p_1,\ldots,p_n;p_a,p_b) = \prod_{i=1}^{n} \frac{\mathrm{d}^{d-1}p_i}{2E_i(2\pi)^{d-1}}(2\pi)^d\delta^d(p_a + p_b - \sum_{i=1}^{n} p_i), \qquad (3.2.12)$$

whilst the jet function $J_n^{(m)}(p_1,\ldots,p_m)$ defines an n-jet final state via cuts on an m-parton final state.

3.2.2 Motivation for higher order calculations

Truncating the pertubative series at leading order, whilst a fine starting point, is plagued with limitations. As previously discussed in the context of LPHD, we only have a single parton to identify with the jet, and no further emission to provide any richness of jet shape: the cross section is independent of our jet radius R, contrary to detector measurements. The results are also strongly scale dependent thanks to the running of the coupling. A lack of initial state radiation provides no opportunity to theoretically model a non-trivial initial state transverse momentum distribution. We therefore appeal to higher order corrections for a solution.

As discussed in the general case, incorporating higher order corrections increases the accuracy of the prediction, where already excellent agreement between data and NLO QCD is observed over several orders of magnitude. So why go beyond NLO, when even a preliminary study presented thus far indicates excessive calculational complexity?

A major motivation, mentioned in Section 1.2, is that the scale dependence of an observable decreases as more orders in perturbation theory are included. Leading order results can see a 30% change, whereas in some regions a NNLO calculation can decrease the sensitivity of μ_R to less than 1%. This is clear both in Figure 3.3 and Figure 3.4, where in the latter we see a significant range over which μ_R can be varies with minimal change in the value of the cross section. The improvement in scheme independence shown here in Figure 3.4 for 100 GeV at CDF, is given for LO, NLO and NNLO predictions over the often used range of varying μ_R by a factor of two around the hard scale. A parallel can also be drawn with the factorisation scale

dependence that is introduced for hadronic initial states.
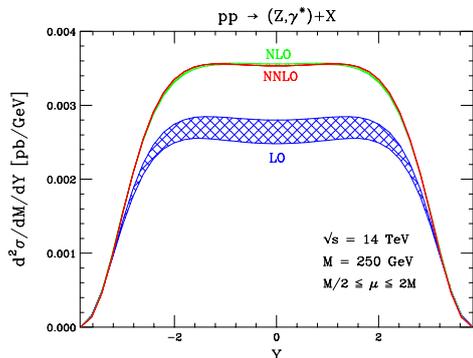
Figure 3.3: Differential cross section for inclusive Z^0 production from pp collisions [51], across a rapidity gap $-4 < Y < 2$. The centre-of-mass energy is $\sqrt{s} = 14$ TeV.
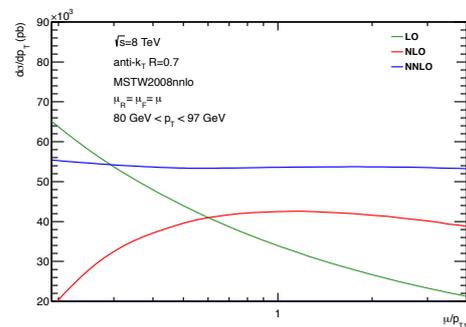
Figure 3.4: Renormalisation scale dependence for single jet production in pp collision at $\sqrt{s} = 8$ TeV, for various orders in the perturbative series. The jet has $80 < p_T < 97$ GeV [52].

From Section 1.4, the NNLO hard scattering must be convolved with the PDFs accurate to the same order. For parton distributions at NNLO it is necessary to acquire a global fit to the data on various observables computed at this order, in addition to the PDF running obtained through the evaluation of three-loop splitting functions [46]. The LHC is an excellent laboratory for probing the gluon distributions, since the initial state hadrons have a large gluon momentum fraction. Previously, quark distributions have been probed by DIS data [53], whilst inclusive jet data from the Tevatron [102] attacked the gluon distribution at NLO.

Higher order corrections are not only changing the global normalisation of the leading order prediction; the opening of phase space allows for more complex final states and thus an alteration of the distribution shape itself [52]. Furthermore, the addition of virtual corrections add new kinematical contributions, manifest in higher weight polylogarithms of scale ratios. As is evident in Figure 3.3, a mere scaling of the leading order calculation is often not a good model of higher order effects.

As aforementioned, the jet algorithms take inputs from final state momenta of a hard process to generate a number of jets constructed via a series of criteria required via the chosen jet definition. The description of the jet can be improved by considering higher order corrections at the level of the hard scattering. Opening up the final state phase space for additional partonic structure immediately implies an improvement on

(a) LO   (b) NLO   (c) NNLO
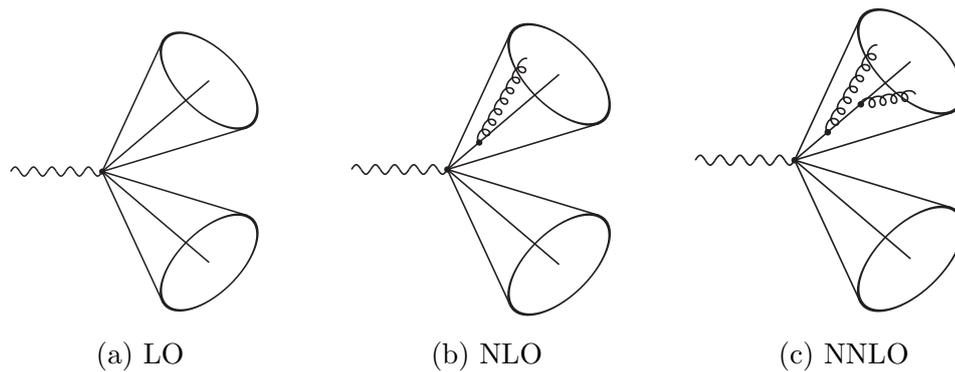
Figure 3.5: Jets modelled by extra final state partons at NNLO.

the matching between theoretical and experimental jet reconstruction. Considering a generic final state pair production in Figure 3.5 we see that at LO the single hard final state parton will directly correspond to the jet. However, once we extend this to NNLO there is now room for up to three final state partons contributing to the jet, offering a richer momentum and parton distribution from which to construct the jet shape. The additional final states in the perturbative calculation can be thought of as the initial emission of radiation otherwise carried out by the parton shower. We can consider similar improvements to the initial state. At leading order the incoming partons have no transverse momentum relative to the beam direction. By allowing for radiation from the initial state partons, there is a non-trivial transverse component, resulting in a more complex momentum distribution in the final state.

Chapter 4

Antenna Subtraction

The primary goal of this thesis is to gain control of the infra-red structures present in a NNLO QCD calculation. This chapter begins by examining the procedures by which such singularities can first be isolated and extracted, focussing on the particular method of **antenna subtraction**. We discuss this formalism at both NLO and NNLO, elucidating the link between the various structures present in the calculation, via their infrared structure. This will stand us in good stead for the application of antenna subtraction to hadro-produced dijet production at NNLO in the chapters that follow.

4.1 Singularity isolation

Let us first consider the structure of an m-jet cross section up to NNLO. The partonic cross sections for a $2 \to m$ process, with m partons in the final state have the form

$$
\mathrm{d}\hat{\sigma}_{LO} = \int_{d\Phi_m} \mathrm{d}\hat{\sigma}^B, \tag{4.1.1}
$$

$$
\mathrm{d}\hat{\sigma}_{NLO} = \int_{d\Phi_{m+1}} \mathrm{d}\hat{\sigma}^R + \int_{d\Phi_m} [\mathrm{d}\hat{\sigma}^V + \mathrm{d}\hat{\sigma}^{MF}], \tag{4.1.2}
$$

$$
\mathrm{d}\hat{\sigma}_{NNLO} = \int_{d\Phi_{m+2}} \mathrm{d}\hat{\sigma}^{RR} + \int_{d\Phi_{m+1}} [\mathrm{d}\hat{\sigma}^{RV} + \mathrm{d}\hat{\sigma}^{MF,RV}] + \int_{d\Phi_m} [\mathrm{d}\hat{\sigma}^{VV} + \mathrm{d}\hat{\sigma}^{MF,VV}]. \tag{4.1.3}
$$

The leading order cross section is straightforward, including only the Born level cross section constructed from the tree level m-parton matrix element and integrated over phase space:

$$\mathrm{d}\hat{\sigma}^B \sim \mathrm{d}\Phi_m(\{p_i\})\langle\mathcal{M}^0_{m+2}|\mathcal{M}^0_{m+2}\rangle. \tag{4.1.4}$$

At NLO the additional power of α_s means that we are not only opening up the phase space for a further final state parton, but also incorporating virtual corrections to the Born process. We now encounter an $(m+3)$-parton real radiation correction $\mathrm{d}\hat{\sigma}^R$, the $(m+2)$-parton virtual correction $\mathrm{d}\hat{\sigma}^V$ that holds loop corrections to the Born term, and the mass factorisation term $\mathrm{d}\hat{\sigma}^{MF}$ to account for the initial state collinear radiation in the parton densities. The real and virtual corrections at NLO are of the form

$$
\begin{aligned}
\mathrm{d}\hat{\sigma}^R &\sim \mathrm{d}\Phi_{m+1}(\{p_i\})\langle\mathcal{M}^0_{m+3}|\mathcal{M}^0_{m+3}\rangle, \\
\mathrm{d}\hat{\sigma}^V &\sim \mathrm{d}\Phi_m(\{p_i\})[\langle\mathcal{M}^1_{m+2}|\mathcal{M}^0_{m+2}\rangle + \langle\mathcal{M}^0_{m+2}|\mathcal{M}^1_{m+2}\rangle].
\end{aligned} \tag{4.1.5}
$$

Finally, at NNLO we are again opening up the phase space for an additional parton, such that double real radiation from the Born process is now possible. There is now a double real radiation contribution (RR) over the $(m+4)$-parton phase space $\mathrm{d}\hat{\sigma}^{RR}$, a real virtual (RV) correction $\mathrm{d}\hat{\sigma}^{RV}$ over $(m+3)$-parton phase space which incorporates a one loop matrix element, and a double virtual (VV) contribution $\mathrm{d}\hat{\sigma}^{VV}$ that holds two loop matrix elements, proportional to $(m+2)$-parton phase space:

$$
\begin{aligned}
\mathrm{d}\hat{\sigma}^{RR} &\sim \mathrm{d}\Phi_{m+2}(\{p_i\})\langle\mathcal{M}^0_{m+4}|\mathcal{M}^0_{m+4}\rangle. \\
\mathrm{d}\hat{\sigma}^{RV} &\sim \mathrm{d}\Phi_{m+1}(\{p_i\})[\langle\mathcal{M}^1_{m+3}|\mathcal{M}^0_{m+3}\rangle + \langle\mathcal{M}^0_{m+3}|\mathcal{M}^1_{m+3}\rangle]. \\
\mathrm{d}\hat{\sigma}^{VV} &\sim \mathrm{d}\Phi_m(\{p_i\})[\langle\mathcal{M}^1_{m+2}|\mathcal{M}^1_{m+2}\rangle + \langle\mathcal{M}^0_{m+2}|\mathcal{M}^2_{m+2}\rangle + \langle\mathcal{M}^2_{m+2}|\mathcal{M}^0_{m+2}\rangle].
\end{aligned}
$$

$$\tag{4.1.6}$$

Taking first the NLO cross section we find that each term on the right hand side of (4.1.2) is independently divergent, containing both UV and IR (soft and collinear) singularities. After removal of the UV divergences via renormalisation, the sum of

the terms renders the full cross section finite.

As discussed in Chapter 2, whilst the IR singularities from $d\hat{\sigma}^V$ are immediately obtained after the loop integration, the soft and collinear divergences in the real radiation contribution are only made explicit after the integration over phase space, a calculation that is often not analytically feasible. In order to construct a Monte Carlo program that can be be adapted to incorporate various jet observables, the IR singularities of the real radiative corrections must first be isolated such that they can be cancelled, thus leaving a finite remainder that can be safely integrated numerically.

Such a bottleneck has opened up broad research into the isolation of singularities. Phase space slicing [55] has been utilised successfully in NLO calculations of electron-positron collisions [56]. It has allowed for a high degree of automation through colour decomposition of the amplitude and factorisation of the phase space in the unresolved region. It does however introduce a theoretical parameter into the calculation, defining the resolution around the singular limit which, although in principle allowed to be arbitrarily close to the limit, must be chosen carefully to avoid large numerical errors. Sector decomposition [57] involves the iterated splitting of the matrix element and final state phase space into sectors, with numerical integration of the ensuing integrals. It has been carried out for specific observables [58–60], notably vector boson [61] and Higgs [62] production at NNLO. However, sector decomposition must be carried out explicitly for each individual process, and with increasing complexity of said process comes an inevitable proliferation of integrals to compute.

The preferred method at NLO is **subtraction** [63,64]. Unlike procedures such as phase space slicing, subtraction introduces counterterms $d\hat{\sigma}^S$ into the cross section, which are not only exact, but also analytic, allowing for a transparent cancellation of singularities. The counterterms mimic the real radiation cross section $d\hat{\sigma}^R$ in all singular limits such that the difference between $d\hat{\sigma}^R$ and $d\hat{\sigma}^S$ in a particular limit is finite. They must also be simple enough to be integrated analytically over the unresolved region of the particle phase space in d dimensions, such that the explicit poles can be cancelled against those emanating from the virtual corrections. This thesis focusses on the extension to NNLO predictions, where a similar procedure can be followed. The subtraction method can in principle be extended to higher

orders in perturbation theory, where the goal then becomes constructing counterterms with increasing multiplicity that maintain the both the analytic integrability and the correct mimicry of the singular regions of the physical cross sections.

A number of schemes exist utilising the subtraction method, since the construction of the counter terms is by no means unique.

At NLO, the FKS [63] subtraction by Frixione, Kunszt and Signer and the Catani-Syemour dipole formalism [64] have been implemented in an automated fashion [65, 66]. At NNLO, the q_T subtraction [67] utilises the fact that real emissions have universal IR structure; such emissions can be obtained via transverse-momentum resummation techniques. However, it only deals with colourless final states; as such it has been applied at NNLO to processes such as Higgs [68] and photon pair [69] production. Sector-improved residue subtraction [70] employs a novel isolation of phase space in the singular regions whilst utilising FKS subtraction methods, and has been applied to top quark pair production [71, 72] and Higgs plus single jet production [73]. This thesis focusses on a particular subtraction scheme, that of **antenna subtraction** [22]. It has been successfully applied to the structure of three-jet events in electron-positron annihilation at NNLO [35, 74, 75], and subsequent numerical calculation of the NNLO corrections to event shapes, jet rates and event-shape moments [76–78]. For hadron colliders, the antenna method has been applied at NNLO to the all gluon contribution to dijet production [15, 79, 80] and the production of heavy particles [81, 82].

This chapter will proceed as follows. First, the building blocks and tools required for antenna subtraction will be explored, along with a description of the functional form of the subtraction terms at both NLO and NNLO. We will then investigate in detail the infrared structures that present themselves during the calculation and how obtaining a stranglehold on the singularity structure provides a vital insight into the cancellations that must occur at each level of the subtraction calculation.

Before the subtraction term can be constructed, the ingredients vital to the success of the antenna formalism must be introduced, that of the **factorisation of phase space**, and the **antenna functions** and their integrated form. We describe each in turn.

4.2 Phase space factorisation

A vital component in the construction of the subtraction terms, along with the factorisation of the squared matrix element in unresolved limits, is the mapping of phase space. These involve sending original momenta involved in the limit - the hard radiators and the unresolved particles - into a redefined set of on-shell momenta. The new set will be a linear combination of the original momenta, but by construction free from dynamical poles involving those original momenta. With such a mapping we see factorisation for a single unresolved particle of the form

$$
\mathrm{d}\Phi_{m+1}(p_1, \cdots, p_i, p_j, p_k, \cdots, p_{m+1})
$$
$$
= \mathrm{d}\Phi_m(p_1, \cdots, p_I, p_K, \cdots, p_{m+1}) \mathrm{d}\Phi_{X_{ijk}}(p_i, p_j, p_k),
$$

$$(4.2.7)$$

where the reduced multiplicity phase space is independent of the momenta p_i, p_j and p_k, but instead depends on the composite momenta p_I, p_K; all dependence on p_i, p_j, p_k is contained within the antenna phase space $\mathrm{d}\Phi_{X_{ijk}}$.

For double unresolved configurations we require a mapping to allow for a similar factorisation of the phase space as

$$
\mathrm{d}\Phi_{m+2}(p_1, \cdots, p_i, p_j, p_k, p_l, \cdots, p_{m+2})
$$
$$
= \mathrm{d}\Phi_m(p_1, \cdots, p_I, p_L, \cdots, p_{m+1}) \mathrm{d}\Phi_{X_{ijkl}}(p_i, p_j, p_k, p_l).
$$

$$(4.2.8)$$

In doing so we allow the subtraction term to be completely factorised. The mappings required at NNLO are that of a four-to-two momenta mapping,

$$
\mathcal{F}(4 \rightarrow 2) : \{p_i, p_j, p_k, p_l\} \rightarrow \{p_{\widetilde{(ijk)}}, p_{\widetilde{(jkl)}}\}, \tag{4.2.9}
$$

where we make explicit in the mapped momenta labels which original momenta are involved, as well as NLO-type three-to-two mappings, which can be iteratively re-

peated, of the form

$$\mathcal{F}(3 \to 2) : \{p_i, p_j, p_k\} \to \{p_{\widetilde{(ij)}}, p_{\widetilde{(jk)}}\}. \tag{4.2.10}$$

The mappings must conserve momenta between mapped and unmapped sets, with the former remaining on-shell, and be able to collapse onto a subset of the unmapped momenta in a particular implicit divergent limit. We must also recognise different mappings according to the presence of initial states in the unresolved limits; final-final, initial-final and initial-initial exist for the hard radiators. They are derived in [24, 83], and we discuss each in turn here.

Final-final mapping

For a single parton j becoming unresolved between hard radiators i and k where, keeping only the momentum indices for notational ease, we see the mapping $\{i, j, k\} \to \{\widetilde{(ij)}, \widetilde{(jk)}\}$ [84],

$$
\begin{aligned}
p_{\widetilde{(ij)}} &= z_1 p_i + z_2 p_j + z_3 p_k \\
p_{\widetilde{(jk)}} &= (1 - z_1)p_i + (1 - z_2)p_j + (1 - z_3)p_k
\end{aligned} \tag{4.2.11}
$$

where

$$
\begin{aligned}
z_1 &= \frac{1}{2(s_{ij} + s_{ik})}\Big[(1 + \rho)\, s_{ijk} - 2\, z_2\, s_{jk}\Big], \\
z_2 &= \frac{s_{jk}}{(s_{ij} + s_{jk})}, \\
z_3 &= \frac{1}{2(s_{jk} + s_{ik})}\Big[(1 - \rho)\, s_{ijk} - 2\, z_2\, s_{ij}\Big], \\
\rho^2 &= 1 + \frac{4\, z_2(1 - z_2)\, s_{ij} s_{jk}}{s_{ijk} s_{ik}}.
\end{aligned} \tag{4.2.12}
$$

The mappings display momentum conservation and satisfy the following properties:

$$
\begin{aligned}
p^2_{\widetilde{(ij)}} &= 0, & p^2_{\widetilde{(jk)}} &= 0, \\
p_{\widetilde{(ij)}} &\to p_i, & p_{\widetilde{(jk)}} &\to p_k & \text{for } j \to 0 \text{ (soft)},
\end{aligned}
$$

$$p_{\widetilde{(ij)}} \to p_i + p_j, \qquad\qquad p_{\widetilde{(jk)}} \to p_k \qquad\qquad \text{for } i||j \text{ (collinear)},$$

$$p_{\widetilde{(ij)}} \to p_i, \qquad\qquad p_{\widetilde{(jk)}} \to p_j + p_k \qquad \text{for } j||k \;.$$

For the double unresolved limits two, partons become unresolved and as such we require a single map to reduce four partons to two. Using the notation $\{i, j, k, l\} \to \{\widetilde{(ijk)}, \widetilde{(jkl)}\}$ the maps are constructed as

$$p_{\widetilde{(ijk)}} = z_1 p_i + z_2 p_j + z_3 p_k + z_4 p_l$$

$$p_{\widetilde{(jkl)}} = (1 - z_1)p_i + (1 - z_2)p_j + (1 - z_3)p_k + (1 - z_4)p_l, \qquad (4.2.13)$$

with the parameterisation variables defined as [83]

$$\begin{aligned}
z_1 &= \frac{1}{2(s_{ij} + s_{ik} + s_{il})}\Big[(1 + \rho)\, s_{ijkl} \\
&\quad - z_2 \left(s_{jk} + 2\, s_{jl}\right) - z_3 \left(s_{jk} + 2\, s_{kl}\right) \\
&\quad + (z_2 - z_3)\frac{s_{ij}s_{kl} - s_{ik}s_{jl}}{s_{il}}\Big] \\
z_2 &= \frac{s_{jk} + s_{jl}}{s_{ij} + s_{jk} + s_{jl}} \\
z_3 &= \frac{s_{kl}}{s_{ik} + s_{jk} + s_{kl}} \\
z_4 &= \frac{1}{2(s_{il} + s_{jl} + s_{kl})}\Big[(1 - \rho)\, s_{ijkl} \\
&\quad - z_2 \left(s_{jk} + 2\, s_{ij}\right) - z_3 \left(s_{jk} + 2\, s_{ik}\right) \\
&\quad - (z_2 - z_3)\frac{s_{ij}s_{kl} - s_{ik}s_{jl}}{s_{il}}\Big] \\
\rho &= \Big[1 + \frac{(z_2 - z_3)^2}{s_{il}^2\, s_{ijkl}^2}\lambda(s_{ij}\, s_{kl}, s_{il}\, s_{jk}, s_{ik}\, s_{jl}) \\
&\quad + \frac{1}{s_{il}\, s_{ijkl}}\Big\{2\left(z_2\left(1 - z_3\right) + z_3(1 - z_2)\right)\left(s_{ij}s_{kl} + s_{ik}s_{jl} - s_{jk}s_{il}\right) \\
&\qquad\qquad + 4\, z_2\left(1 - z_2\right) s_{ij}s_{jl} + 4\, z_3\left(1 - z_3\right) s_{il}s_{kl}\Big\}\Big]^{\frac{1}{2}}, \\
\lambda(u, v, w) &= u^2 + v^2 + w^2 - 2(uv + uw + vw)\;. \qquad\qquad (4.2.14)
\end{aligned}$$

Again, in the various unresolved singular limits, the behaviour of the mapped momenta can be seen to obey correctly the necessary requirements. We also note that in single unresolved limits, the map $\mathcal{F}(4 \to 2)$ reproduces the same mapped momenta

as for the map $\mathcal{F}(3 \to 2)$. As an example we take the soft j limit, $p_j \to 0$, which results in negligible contributions from the p_j-dependent pieces in (4.2.13), whilst the behaviour of the $z_{1,2,3,4}$ and ρ becomes

$$
\begin{aligned}
z_1 &\to \frac{1}{2(s_{ik} + s_{il})}\Big[(1 + \rho)\, s_{ikl} - 2\, z_3\, s_{kl}\Big], \\
z_2 &\to \frac{s_{kl}}{(s_{ik} + s_{kl})}, \\
z_3 &\to \frac{1}{2(s_{il} + s_{kl})}\Big[(1 - \rho)\, s_{ikl} - 2\, z_3\, s_{ik}\Big],
\end{aligned}
$$

$$
\rho \to \left[1 + \frac{4\, z_3(1 - z_3)\, s_{il}s_{kl}}{s_{ikl}s_{il}}\right]^{\frac{1}{2}}.
\tag{4.2.15}
$$

Relabelling the momenta as $\{i, k, l\} \to \{i, j, k\}$ reproduces the parameters in (4.2.12), thus leaving us with the $\mathcal{F}(3 \to 2)$ map.

Initial-final mapping

For the case where one of the hard radiators is in the initial state, we require a new mapping. Rather than a full remapping, the initial momentum is rescaled such that it remains on beamline. The final state particles remaining are mapped into a single composite momentum [24]. Using the notation $\{\hat{1}, i, j\} \to \{\hat{1}, \widetilde{(ij)}\}$ the maps $\mathcal{F}(3 \to 2)$ are constructed as

$$
\begin{aligned}
\bar{p}_1 &= x p_1 \\
\bar{p}_{\widetilde{(ij)}} &= p_i + p_j - (1 - x)p_1,
\end{aligned}
\tag{4.2.16}
$$

where

$$
x = \frac{s_{1i} + s_{1j} + s_{ij}}{s_{1i} + s_{1j}}
\tag{4.2.17}
$$

for massless composite momenta. Again, momentum conservation and on-shellness is maintained. In doing so, we can write the phase space in terms of a two parton

phase space and the standard reduced particle multiplicity phase space:

$$
\begin{aligned}
&\mathrm{d}\Phi_{m+1}(p_1, p_2; \cdots, p_i, p_j, \cdots) \\
&= \mathrm{d}\Phi_m(\bar{p}_1, p_2; \cdots, p_{\widetilde{(ij)}}, \cdots)\mathrm{d}\Phi_2(p_1, q; p_i, p_j)\frac{Q^2}{2\pi}\frac{\mathrm{d}x}{x}\delta(x - \hat{x}).
\end{aligned}
\quad (4.2.18)
$$

The scale is $Q^2 = -q^2 = -(p_i + p_j - p_1)^2$, and $\hat{x}$ is given in (4.2.17). For the case of double unresolved configurations we can employ a similar rescaling, $\{\hat{1}, i, j, k\} \to \{\hat{1}, \widetilde{(ijk)}\}$ [24], with the mapping parameters given by

$$
\begin{aligned}
\bar{p}_1 &= xp_1 \\
\bar{p}_{\widetilde{(ij)}} &= p_i + p_j + p_k - (1 - x)p_1,
\end{aligned}
\quad (4.2.19)
$$

with

$$
x = \frac{s_{1i} + s_{1j} + s_{1k} + s_{ij} + s_{jk} + s_{ik}}{s_{1i} + s_{1j} + s_{1k}}.
\quad (4.2.20)
$$

The factorisation of the phase space behaves as

$$
\begin{aligned}
&\mathrm{d}\Phi_{m+2}(p_1, p_2; \cdots, p_i, p_j, p_k, \cdots) \\
&= \mathrm{d}\Phi_m(\bar{p}_1, p_2; \cdots, p_{\widetilde{(ijk)}}, \cdots)\mathrm{d}\Phi_3(p_1, q; p_i, p_j, p_k)\frac{Q^2}{2\pi}\frac{\mathrm{d}x}{x}\delta(x - \hat{x}).
\end{aligned}
\quad (4.2.21)
$$

Initial-initial mapping

In the case where the antenna function contains two initial state partons, a phase space map is required that will rescale the two initial states. In any antennae, these will always be acting as hard radiators. However, unlike the initial-final case, there is no final state parton in the mapped set of momenta to hold the overall momentum rescaling, and we naïvely observe failure of momentum conservation between mapped and unmapped momenta. To remedy this, all final state mapped momenta are remapped [64], even if they are not explicitly involved in the unresolved limit. We rescale the initial particles by

$$
\bar{p}_1 = z_1 p_1
$$

$$\bar{p}_2 = z_2 p_2 \tag{4.2.22}$$

However, the final state momenta $q = p_1 + p_2 - p_i$ with p_i being involved in the limit, does not in general lie along the beam axis and thus a transformation of the final state must take place. The rescaling of the initial states is determined by performing a (Lorentz-invariant) boost of q onto the beam axis, fixing the rescaling parameters as

$$z_1 = \sqrt{\frac{(s_{12} - s_{2i})(s_{12} - s_{1i} - s_{2i})}{s_{12}(s_{12} - s_{1i})}},$$

$$z_1 = \sqrt{\frac{(s_{12} - s_{1i})(s_{12} - s_{1i} - s_{2i})}{s_{12}(s_{12} - s_{2i})}}. \tag{4.2.23}$$

To subsequently maintain momentum conservation, all the final state momenta - including those not involved in the unresolved limit - must be boosted as

$$p_i \to \tilde{p}_i = p_i - \frac{2p_i \cdot (q + \tilde{q})}{(q + \tilde{q})^2}(q + \tilde{q}) + \frac{2p_i \cdot q}{q^2}\tilde{q}, \tag{4.2.24}$$

where $\tilde{q} = \bar{p}_1 + \bar{p}_2$ is the combination of the rescaled initial state momenta, lying on beam axis. This allows the phase space to be factorised as

$$\begin{aligned}
&\mathrm{d}\Phi_{m+1}(p_1, p_2; p_3, \cdots, p_i, \cdots, p_{m+1}) \\
&= \mathrm{d}\Phi_m(\bar{p}_1, \bar{p}_2; \tilde{p}_3, \cdots, \tilde{p}_{m+1})\mathrm{d}^d p_i \frac{\delta^+(p_i^2)}{(2\pi)^{d-1}} \frac{\mathrm{d}x_1}{x_1} \frac{\mathrm{d}x_2}{x_2} \delta(x_1 - \hat{x}_1)\delta(x_2 - \hat{x}_2)x_1 x_2.
\end{aligned} \tag{4.2.25}$$

Although this mapping is not unique, it is highly constrained; to treat the initial state rescaling parameters symmetrically, a rotation (rather than a boost) is forbidden since a rotation towards the beam axis would have to be chosen, thus favouring x_1 or x_2.

We can play a similar game for the double unresolved mapping. The mapping goes as $\{\hat{1}, i, j, \hat{2}\} \to \{\hat{\hat{1}}, \hat{\hat{2}}\}$, with $q = p_1 + p_2 - p_i - p_j$ and

$$z_1 = \sqrt{\frac{(s_{12} - s_{2i} - s_{2j})(s_{12} - s_{1i} - s_{1j} - s_{2i} - s_{2j} + s_{ij})}{s_{12}(s_{12} - s_{1i} - s_{1j})}}$$

$$z_2 = \sqrt{\frac{(s_{12} - s_{1i} - s_{2j})(s_{12} - s_{1i} - s_{1j} - s_{2i} - s_{2j} + s_{ij})}{s_{12}(s_{12} - s_{2i} - s_{2j})}} \qquad (4.2.26)$$

which results in a double convolution in the factorised phase space

$$d\Phi_{m+2}(p_1, p_2; p_3, \cdots, p_i, p_j, \cdots, p_{m+1}) = d\Phi_m(\bar{p}_1, \bar{p}_2; \tilde{p}_3, \cdots, \tilde{p}_{m+1})$$
$$\times d^d p_i \frac{\delta^+(p_i^2)}{(2\pi)^{d-1}} d^d p_j \frac{\delta^+(p_j^2)}{(2\pi)^{d-1}} \frac{dx_1}{x_1} \frac{dx_2}{x_2} \delta(x_1 - \hat{x}_1)\delta(x_2 - \hat{x}_2)x_1 x_2. \qquad (4.2.27)$$

4.3   Antenna functions

Antenna functions are the building blocks of the antenna subtraction terms. They are constructed from colour-ordered physical matrix elements and can contain multiple singular limits, which will be utilised in matching with the QCD matrix element under consideration. For NNLO calculations, we require antenna functions consisting of three and four partons, where the underlying structure holds a pair of hard *radiators*, and up to two partons that can go unresolved. We will also require antenna functions at both tree and one-loop level. Since they are built from colour-ordered matrix elements, the antenna functions will follow the same factorisation properties laid out in Chapter 2.

We can categorise the antenna functions depending on the hard radiator partons onto which the full antenna collapses in the unresolved limits. In general, we have three possibilities: quark-antiquark, quark-gluon and gluon-gluon radiators. From these two-parton processes, gluons and quark-antiquark pairs can be radiated to construct the antenna functions. The quark-antiquark antennae are derived from virtual photon decay $\gamma^* \to q\bar{q} + \text{partons}$ [85], the quark-gluon antennae form neutralino decay into gluinos, $\tilde{\chi} \to \tilde{g} + \text{partons}$ [86], and the gluon-gluon antennae from Higgs decay [87], $H \to gg + \text{partons}$. As a teaser to the later results, note that the quark-gluon antenna are constructed from processes involving supersymmetric particles. Whilst QCD is supersymmetric at tree level, at one loop the additional colour flows from the gluino (acting as a quark) require care to be taken in constructing the subtraction term involving such antennae. The explicit three- and four-parton antennae required for each colour ordered strings will be given in Section 4.4.

The tree-level antennae are constructed from colour-ordered, three and four parton squared tree level matrix elements, normalised to the underlying two parton process of the hard radiators:

$$X_3^0(i,j,k) = S_{ijk:IK} \frac{M_3^0(i,j,k)}{M_2^0(I,K)}, \tag{4.3.28}$$

$$X_4^0(i,j,k,l) = S_{ijkl:IL} \frac{M_4^0(i,j,k,l)}{M_2^0(I,L)}. \tag{4.3.29}$$

The symmetry factor S accounts for the degenerate antenna setup in the two parton process, and also for identical final state symmetry. The three parton, one-loop antenna functions are constructed similarly, and have factorisation behaviour of the form (tree $\times$ loop) + (loop $\times$ tree), following that of Section 2.1.2. They are constructed from colour-ordered, three parton matrix elements at one-loop level [22]:

$$X_3^1(i,j,k) = S_{ijk:IK} \frac{M_3^1(i,j,k)}{M_2^0(I,K)} - X_3^0(i,j,k) \frac{M_2^1(I,K)}{M_2^0(I,K)}. \tag{4.3.30}$$

These completely define all the antenna functions required for the subtraction term at NNLO; all one and two parton unresolved limits of the physical matrix element can be recreated using the antennae given here. Not only that, but all antenna functions have been analytically integrated [88–91] over the unresolved phase space. Provided this can be carried out with higher multiplicity and loops, the extension of the antenna formalism to higher order calculations is feasible.

We can also categorise the antenna functions by whether any of the partons involved are in the initial state, since their behaviour in the singular limits changes in such configurations, such as in the form of the collinear splitting functions. In the analytic form of the unintegrated antenna functions, this is achieved simply via crossing. Allowing for initial states can alter the number of limits that the antenna deals with: initial partons cannot go soft, and if there are two initial states there will be no collinear limit between them.

Although we wish to encapsulate as many limits as possible within a single antenna function, oversubtraction of divergences must be prevented, that is the antenna should ideally not contain singular limits not present in the matrix element it is trying

to mimic. Quark-gluon and gluon-gluon antenna functions have ambiguity in what constitutes the hard radiator due to the cyclic nature of the colour flow. An example is that of the $D_3^0(q, i_g, j_g)$, where there are more than one antenna configuration present. It is thus judicious to split the antenna function into sub antennae that share the full set of limits between them (symmetrically if possible). This can be achieved via partial fractioning of the terms in the antenna to isolate particular divergences. The full tree-level $D_3^0(q, i_g, j_g)$ is of the form [22]

$$
D_3^0(q, i_g, j_g) = \frac{1}{s_{134}^2} \left(\frac{2s_{134}^2 s_{14}}{s_{13}s_{34}} + \frac{2s_{134}^2 s_{13}}{s_{14}s_{34}} + \frac{s_{14}s_{34} + s_{34}^2}{s_{13}} \right.
$$
$$
\left. + \frac{s_{13}s_{34} + s_{34}^2}{s_{14}} + \frac{2s_{13}s_{14}}{s_{34}} + 5s_{134} + s_{34} \right) + \mathcal{O}(\epsilon). \quad (4.3.31)
$$

In matching with a physical matrix element, the $q||j_g$ is often unwanted, since in a colour string of the physical matrix element they are colour unconnected; here the antenna cyclic colour-connection betrays us. The antenna is thus split into two,

$$
D_3^0(q, i_g, j_g) = d_3^0(q, i_g, j_g) + d_3^0(q, j_g, i_g), \quad (4.3.32)
$$

such that

$$
d_3^0(q, i_g, j_g) = \frac{1}{s_{134}^2} \left(\frac{2s_{134}^2 s_{14}}{s_{13}s_{34}} + \frac{s_{14}s_{34} + s_{34}^2}{s_{13}} + \frac{s_{13}s_{14}}{s_{34}} + \frac{5}{2}s_{134} + \frac{1}{2}s_{34} \right) + \mathcal{O}(\epsilon).
$$
$$
\quad (4.3.33)
$$

Now the sub antenna only contains collinear limits $q||i_g$ and $i_g||j_g$, and only gluon i_g goes soft: gluon j_g and the quark are unambiguously the hard radiators. This game can also be played with the $F_3^0(i_g, j_g, k_g)$ antenna where it is split into three symmetric sub antennae $f_3^0(i_g, j_g, k_g)$ [22], containing the full soft j_g limit and partial limits for the $i_g||j_g$ and $j_g||k_g$ collinear limits. In a single sub antenna of this type, there is no $i_g||k_g$ collinear limit. Again, the hard radiators are no longer ambiguous.

In order to utilise this at NNLO, the partial fractioning must also be implemented at the one-loop level. In general, the one-loop antenna function can be written as a

sum of the poles contribution and a finite remainder,

$$X_3^1(i,j,k) = \mathcal{P}oles(X_3^1(i,j,k)) + \mathcal{F}inite(X_3^1(i,j,k)) \tag{4.3.34}$$

where, following the formalism of Chapter 2, the pole contribution is of the form

$$\mathcal{P}oles(X_3^1(i,j,k)) = \mathbf{I}_n^{(1)}(i,j,k)X_3^0(i,j,k). \tag{4.3.35}$$

Immediately, we see that the pole contribution to the one loop antenna can be easily split, since it is just the tree-level antenna multiplied by a singular factor dependent only on the momenta involved (which are unchanged). The finite contributions are equally malleable and can be partial fractioned separately. We examine the $D_3^1(q, i_g, j_g)$:

$$D_3^1(q,i_g,j_g) = \mathbf{I}_n^{(1)}(i,j,k)D_3^0(q,i_g,j_g) + \mathbb{F}(s_{ij}, s_{qi}, s_{qj})D_3^0(q,i_g,j_g) + \frac{1}{3s_{ij}} \tag{4.3.36}$$

where $\mathbb{F}$ is a finite function involving logarithms of ratios of invariants. The pole contributions and $\mathbb{F}$ term are both proportional to $D_3^0(q, i_g, j_g)$, which is partial fractioned as above. The final term can be simply separated symmetrically, so that

$$d_3^1(q,i_g,j_g) = \mathbf{I}_n^{(1)}(i,j,k)d_3^0(q,i_g,j_g) + \mathbb{F}(s_{ij}, s_{qi}, s_{qj})d_3^0(q,i_g,j_g) + \frac{1}{6s_{ij}} \tag{4.3.37}$$

and we find the correct behaviour and limit that are required. Note that for all partons in the final state (and indeed, crossing the quark to the initial state), the splitting of the $D_3^0(q, i_g, j_g)$ is symmetric amongst the subantennae. As we see in the following chapters, gluon initiated processes can result in flavour changing initial states and a symmetric splitting is undesirable.

Defining the hard radiators without ambiguity in four-parton antennae is also problematic, with the initial state gluon again being a primary source of distress. The final-final D_4^0 and F_4^0 are discussed in [35]. For initial states in F_4^0 we can consult [79], but the full role of the D_4^0 with initial gluons is still under development.

4.3.1   Integrated antenna functions

The antenna functions will contain all the required implicit singular divergences in the matrix element and, with the factorisation of phase space, allow all divergent structures to be factorised into their own separate region of phase space. What remains to be done is to integrate analytically the antenna functions over this region of phase space.

We split the notation and definitions of the integrated antenna into three regimes according to the number of hard radiators in the initial state. When all three partons are in the final state, called the final-final configuration, the integration over the antenna phase space $\mathrm{d}\Phi_{X_{ijk}}$ takes the form

$$\mathcal{X}_3^\ell(s_{ijk}) = \frac{1}{C(\epsilon)} \int \mathrm{d}\Phi_{X_{ijk}} X_3^\ell(i, j, k), \qquad (4.3.38)$$

where the factor $C(\epsilon) = \bar{C}(\epsilon)/(8\pi^2)$ emanates from the coupling constant renormalisation, and $\ell = 0, 1$ is the number of loops. The integration is performed in d dimensions to make the IR singularities explicit. For the four-parton final-final antenna we have a similar expression [22]:

$$\mathcal{X}_4^0(s_{ijkl}) = \frac{1}{|C(\epsilon)|^2} \int \mathrm{d}\Phi_{X_{ijkl}} X_4^0(i, j, k, l). \qquad (4.3.39)$$

For the initial-final case where one of the two hard radiators is in the initial state, the phase space is slightly modified, since we are incorporating the rescaling of the initial parton $x_i p_i$. The integrated three-parton antenna has the form [24]

$$\mathcal{X}_3^\ell(s_{1ij}; x_1) = \frac{1}{C(\epsilon)} \int \mathrm{d}\Phi_2 X_{3,a}^\ell(\hat{1}, j, k) \frac{Q^2}{2\pi} \delta(x_1 - \hat{x}_1), \qquad (4.3.40)$$

whereas the four parton antenna [88] is defined

$$\mathcal{X}_4^0(s_{1ijk}; x_1) = \frac{1}{|C(\epsilon)|^2} \int \mathrm{d}\Phi_2 X_{4,a}^0(\hat{1}, i, j, k) \frac{Q^2}{2\pi} \delta(x_1 - \hat{x}_1). \qquad (4.3.41)$$

The last configuration sees both the hard radiators in the initial state. The initial-initial phase space is somewhat simpler due to the double delta function [24], and

integrating over the factorised phase space from Section 4.2 gives

$$\mathcal{X}_3^\ell(s_{1i2}; x_1, x_2) = \frac{1}{C(\epsilon)} \int \mathrm{d}^d k \frac{\delta^+(k^2)}{(2\pi)^{d-1}} X_{3,ab}^\ell(\hat{1}, i, \hat{2}) x_1 x_2 \delta(x_1 - \hat{x}_1)\delta(x_2 - \hat{x}_2)$$

(4.3.42)

for the three parton antennae, and [90]

$$
\begin{aligned}
\mathcal{X}_4^0(s_{1ij2}; x_1, x_2) &= \frac{1}{|C(\epsilon)|^2} \int \mathrm{d}^d k_i \frac{\delta^+(k_i^2)}{(2\pi)^{d-1}} \mathrm{d}^d k_j \frac{\delta^+(k_j^2)}{(2\pi)^{d-1}} \\
&\times \ X_{4,ab}^0(\hat{1}, i, j, \hat{2})\, x_1 x_2\, \delta(x_1 - \hat{x}_1)\delta(x_2 - \hat{x}_2)
\end{aligned}
$$

(4.3.43)

for the four parton antennae, where the initial state partons are explicitly labelled in the integrated antenna by the subscripts a and b. This will prove vital later when identifying integrated forms of flavour changing antenna. The integrals are carried out using a variety of multi-loop techniques, including Integration-By-Parts (IBP) [92,93] to reduce tensor integrals to a set of master integrals,[1] and mutiparticle phase space integration [94].

4.3.2 Singular structure

As we shall see, the antenna approach successfully isolates the infrared singularities, which themselves have a very particular structure. Therefore, one can ask the questions:

1. How does the infrared structure guide the construction of the real radiation subtraction terms?

2. How do the integrated subtraction terms relate to the known infrared structure of the loop amplitudes?

The main aim of this section is to develop the systematics of the antenna subtraction scheme at NLO and particularly at NNLO by focussing on the structure of the subtraction terms for the double real, real-virtual and double virtual channels.

---

[1]One loop tensor graphs can always be reduced down to a set of scalar integrals [95], but this this not necessarily the case for higher loop graphs.

It is well known that the explicit poles of the virtual contributions are described by Catani's one- and two-loop factorisation formulae [19, 20]. It is well established (and in fact the keystone of all subtraction methods) that real radiation amplitudes factorise in IR divergent limits following an antenna factorisation pattern whereby a pair of hard partons radiate unresolved partons. The unintegrated antenna functions are used to mimic the implicit divergence of the real contributions while the poles associated with the integrated antenna functions directly cancel the explicit poles of the virtual contributions.

From the predictive structure apparent in the subtraction terms due to the colour ordering of the matrix elements, a number of structures, which we call **integrated dipoles**, emerge after integration and combination with the relevant mass factorisation contributions. At one-loop, $\boldsymbol{J}_2^{(1)}$ is related to an integrated three-particle tree-level antenna and describes the unresolved radiation between two colour connected particles. Similarly, at two-loops, $\boldsymbol{J}_2^{(2)}$ fulfills the same role for double unresolved radiation and involves integrated four-particle tree-level antennae, three-particle one-loop antennae and products of three-parton tree-level antennae.

The IR structure of any two-loop contribution is given by one- and two-loop **integrated antenna strings** [97] which are simply formed from $\boldsymbol{J}_2^{(1)}$ and $\boldsymbol{J}_2^{(2)}$. For a given colour ordering of a particular n-particle process, $\boldsymbol{J}_n^{(1)}$ and $\boldsymbol{J}_n^{(2)}$ can be written down as a sum over integrated dipoles that involve colour connected particles,

$$\boldsymbol{J}_n^{(\ell)}(1, \cdots, n) \;\; = \;\; \sum_{(i,j)} \boldsymbol{J}_2^{(\ell)}(i, j), \qquad\qquad (4.3.44)$$

where $\ell = 1, 2$ denotes the single and double unresolved integrated antenna strings respectively and the sum is over colour connected pairs of partons. Equivalently, the pole structure is identified as a sum of dipole-like terms proportional to $(|s_{ij}|)^{-\ell\epsilon}$ that link the colour connected particles i and j.

Of course, the form of $\boldsymbol{J}_n^{(1)}$ and $\boldsymbol{J}_n^{(2)}$ in terms of integrated antennae imposes a particular structure on the unintegrated antennae that make up the real radiation subtraction terms. Understanding the explicit pole structure of virtual amplitudes in terms of integrated antenna strings gives a direct connection between the block

structure of the unintegrated subtraction terms and the explicit pole structure of virtual contributions, thereby simplifying the construction of the double real, real-virtual and double virtual subtraction terms.

4.4 Antenna subtraction at NLO

We first concentrate on the structure of NLO calculations within the antenna subtraction formalism. Whilst relatively simple, it elucidates notable features relevant to NNLO calculations which are fully explained in this section.

We are interested in the higher-order corrections to the underlying leading-order (LO) cross section. The hadro-production of n jets is given by

$$\mathrm{d}\hat{\sigma}_{ij,LO}(\xi_1 H_1, \xi_2 H_2) \;\; = \;\; \int_n \mathrm{d}\hat{\sigma}^B_{ij,LO}(\xi_1 H_1, \xi_2 H_2), \qquad (4.4.45)$$

where the Born-level cross section is obtained by evaluating the tree-level contributions for $(n+2)$-parton scattering with partons i, j in the initial-state carrying a fraction $\xi_{1,2}$ of the parent hadron's momentum $H_{1,2}$. We then integrate over the final-state phase space, where to keep track of the number n of final state particles we use the shorthand notation,

$$\int_n. \qquad (4.4.46)$$

Explicitly, the Born-level cross section is given by,

$$\begin{aligned}
\mathrm{d}\hat{\sigma}^B_{ij,LO} \;\; &= \;\; \mathcal{N}_{LO} \sum_\sigma \mathrm{d}\Phi_n(p_3, \cdots, p_{n+2}; p_1, p_2) \, \frac{1}{S_n} \\
&\times \; \left[M^0_{n+2}(\sigma(1, \cdots, n+2)) \, J_n^{(n)}(\{p\}_n) + \mathcal{O}\!\left(\frac{1}{N^2}\right) \right], \qquad (4.4.47)
\end{aligned}$$

where S_n is a final-state symmetry factor, and $\{p\}_n$ denotes the set of n final-state momenta. M^0_{n+2} is an $(n+2)$-parton squared partial amplitude with a given colour ordering denoted by σ and i labels the parton with momentum p_i. The factor $\mathcal{N}_{LO}$ contains all non-QCD factors and some overall QCD factors such as the overall power

of the coupling. As in Section 3.2, we define the $2 \to n$ particle phase space as

$$
\begin{aligned}
\mathrm{d}\Phi_n(p_3, \cdots, p_{n+2}; p_1, p_2) = & \\
\frac{\mathrm{d}^{d-1}p_3}{2E_3(2\pi)^{d-1}} \cdots \frac{\mathrm{d}^{d-1}p_{n+2}}{2E_{n+2}(2\pi)^{d-1}} & (2\pi)^d \delta^d(p_1 + p_2 - p_3 - \cdots - p_{n+2}). \quad (4.4.48)
\end{aligned}
$$

where the jet algorithm $J_n^{(m)}$ constructs n jets from m final-state partons with momenta labelled by the set $\{p\}_m$. For the leading-order cross section in Eq. (4.4.47) $m = n$ and there is an exact parton-jet correspondence.

The NLO correction to the n-jet cross section contains three contributions and is given by,

$$
\mathrm{d}\hat{\sigma}_{ij,NLO} \;\; = \;\; \int_{n+1} \mathrm{d}\hat{\sigma}_{ij,NLO}^R \;\; + \;\; \int_n \left(\mathrm{d}\hat{\sigma}_{ij,NLO}^V + \mathrm{d}\hat{\sigma}_{ij,NLO}^{MF} \right), \qquad (4.4.49)
$$

where $\mathrm{d}\hat{\sigma}_{ij}^R$ and $\mathrm{d}\hat{\sigma}_{ij,NLO}^V$ are the real and virtual NLO corrections and $\mathrm{d}\hat{\sigma}_{ij,NLO}^{MF}$ is the NLO mass factorisation contribution,

$$
\begin{aligned}
\mathrm{d}\hat{\sigma}_{ij,NLO}^{MF}(\xi_1 H_1, \xi_2 H_2) \;\; = \;\; & -\int \frac{\mathrm{d}z_1}{z_1} \frac{\mathrm{d}z_2}{z_2} \left(\frac{\alpha_s N}{2\pi} \right) \bar{C}(\epsilon)\, \Gamma_{ij;kl}^{(1)}(z_1, z_2) \\
& \times \mathrm{d}\hat{\sigma}_{kl,LO}(z_1 \xi_1 H_1, z_2 \xi_2 H_2),
\end{aligned}
$$

$$(4.4.50)$$

where $\bar{C}(\epsilon) = (4\pi)^\epsilon e^{-\epsilon\gamma}$. The mass factorisation contribution serves to remove all initial-state collinear singularities from the cross section by absorbing them into the redefined physical PDF and can be written in terms of the one-loop Altarelli-Parisi kernels as discussed in Section 1.4;

$$
\Gamma_{ij;kl}^{(1)}(z_1, z_2) \;\; = \;\; \delta(1 - z_2)\delta_{lj}\Gamma_{ki}^{(1)}(z_1) + \delta(1 - z_1)\delta_{ki}\Gamma_{lj}^{(1)}(z_2). \qquad (4.4.51)
$$

The real cross section contains soft and collinear IR divergences and so we must construct a subtraction term, $\mathrm{d}\hat{\sigma}_{ij,NLO}^S$, from antenna functions and reduced multiplicity matrix elements. It must remove all implicit singularities from the real emission cross section without introducing further spurious singularities of its own and be local in the sense that the subtraction is successful point-by-point in phase space. As

aforementioned, the subtraction term must be analytically integrable in order to convert the implicit divergence of the subtraction term into the explicit singularities of the integrated subtraction term.[2] When combined with the mass factorisation contribution, these terms combine to cancel the explicit poles of the virtual contribution and produce a finite NLO cross section. Since all three- and four-parton antenna functions have been successfully integrated for FF, IF and II configurations [88–91], analytic integrability is a solved issue.

Subsequently, the NLO cross section can be reorganised in such a way that each square bracket is free from both implicit divergence and explicit poles,

$$
\mathrm{d}\hat{\sigma}_{ij,NLO} \;=\; \int_{n+1} \left[\mathrm{d}\hat{\sigma}^R_{ij,NLO} - \mathrm{d}\hat{\sigma}^S_{ij,NLO}\right] + \int_n \left[\mathrm{d}\hat{\sigma}^V_{ij,NLO} - \mathrm{d}\hat{\sigma}^T_{ij,NLO}\right], \quad (4.4.52)
$$

where the virtual subtraction term is given by the real subtraction term integrated over the single unresolved phase space and the NLO mass factorisation contribution,

$$
\mathrm{d}\hat{\sigma}^T_{ij,NLO} \;=\; -\int_1 \mathrm{d}\hat{\sigma}^S_{ij,NLO} - \mathrm{d}\hat{\sigma}^{MF}_{ij,NLO}. \quad (4.4.53)
$$

4.4.1 NLO real emission subtraction term

The single real emission cross section takes the form,

$$
\begin{aligned}
\mathrm{d}\hat{\sigma}^R_{ij,NLO} \;=\;& \mathcal{N}^R_{NLO} \sum_\sigma \mathrm{d}\Phi_{n+1}(p_3, \cdots, p_{n+3}; p_1, p_2) \, \frac{1}{S_{n+1}} \\
&\times \left[M^0_{n+3}(\sigma(1, \cdots, n+3)) \, J^{(n+1)}_n(\{p\}_{n+1}) + \mathcal{O}\!\left(\frac{1}{N^2}\right) \right], \quad (4.4.54)
\end{aligned}
$$

where, as in Eq. (4.4.47), S_{n+1} is a final-state symmetry factor, $\{p\}_{n+1}$ denotes the set of $(n+1)$ final-state momenta, M^0_{n+3} denotes an $(n+3)$-parton squared partial amplitude for a given colour ordering denoted by σ and i labels the parton with momentum p_i. The overall coupling is given by

$$
\mathcal{N}^R_{NLO} \;=\; \mathcal{N}_{LO} \left(\frac{\alpha_s N}{2\pi}\right) \frac{\bar{C}(\epsilon)}{C(\epsilon)} \quad (4.4.55)
$$

---

[2]One could equally well numerically integrate the subtraction term as in Ref. [70] or [98, 99].

where again $C(\epsilon) = \bar{C}(\epsilon)/8\pi^2$.

Subtraction terms

At NLO we must take account of the single unresolved limits in the matrix element at hand. The full subtraction term is a sum of contributions of the type,

$$
\begin{aligned}
\mathrm{d}\hat{\sigma}_{NLO}^S &= \mathcal{N}_{NLO}^R \sum_{\text{perms}} \sum_{j} \mathrm{d}\Phi_{n+1}(p_3, \cdots, p_{n+3}; p_1, p_2) \frac{1}{S_{n+1}} \\
&\times X_3^0(\cdot, j, \cdot) \, M_{n+2}^0(\cdots, j, \cdots) \, J_n^{(n)}(\{p\}_n).
\end{aligned} \tag{4.4.56}
$$

where X_3^0 is the NLO antenna function, M_{n+2}^0 the reduced matrix element with a particular colour ordering and the sum runs over all the possible unresolved particles j. As previously intimated, there are three separate cases that correspond to the hard radiators being in the final state (FF), both in the initial state (II) or one in the initial-state and one in the final-state (IF). For DIS processes $\mathrm{d}\hat{\sigma}_{NLO}^{S,II} = 0$ while for e^+e^- annihilation $\mathrm{d}\hat{\sigma}_{NLO}^{S,IF} = \mathrm{d}\hat{\sigma}_{NLO}^{S,II} = 0$. At NLO it is possible to write the subtraction terms explicitly for all configurations at leading colour and for an arbitrary number of partons.

When the unresolved parton j is colour connected to the final-state hard radiators i and k, the subtraction term for the partial amplitude $M_{n+3}^0(\cdots, i, j, k, \cdots)$ takes the form,

$$
M_{n+3}^0(\cdots, i, j, k, \cdots) \longrightarrow X_3^0(i, j, k) \, M_{n+2}^0(\cdots, I, K, \cdots). \tag{4.4.57}
$$

The identity of colour ordered partons in the limit fix the species of the antenna function, shown in Table 4.1. There are five possibilities reflecting the different particle assignments and possible colour structures. The sum over j takes into account all the possible unresolved partons in the colour-ordered matrix element fitting the final-final configuration. The final-final phase space map [84], $(i, j, k) \rightarrow (\widetilde{(ij)}, \widetilde{(jk)})$, ensures that the momenta involved in the antenna function are mapped onto two hard composite momenta. The IR divergence associated with the configuration where j becomes unresolved is described by the appropriate antenna function and, in the

singular limit, the subtraction term tends to the value of the real emission cross section. The various antennae and reduced matrix elements appropriate for a particular colour ordered matrix element in the real emission are listed in Table. 4.1.

Final-Final Unintegrated Antennae		
Matrix element, M_{n+3}^0	Antenna, X_3^0	Reduced matrix element, M_{n+2}^0
$(\cdots; i_q, j_g, k_{\bar{q}}; \cdots)$	$A_3^0(i, j, k)$	$(\cdots; I_q, K_{\bar{q}}; \cdots)$
$(\cdots; i_q, j_g, k_g, \cdots)$	$d_3^0(i, j, k)$	$(\cdots; I_q, K_g, \cdots)$
$(\cdots; i_{q'}, j_{\bar{q}}; k_q, \cdots)$	$E_3^0(i, j, k)$	$(\cdots; I_{q'}, K_g, \cdots)$
$(\cdots, i_g, j_g, k_g, \cdots)$	$f_3^0(i, j, k)$	$(\cdots, I_g, K_g, \cdots)$
$(\cdots, i_g, j_{\bar{q}}; k_q, \cdots)$	$G_3^0(i, j, k)$	$(\cdots, I_g, K_g, \cdots)$

Table 4.1: The NLO antennae, X_3^0, and reduced matrix elements, M_{n+2}^0, appropriate for the various particle assignments and colour structures in the real radiation partial amplitudes, M_{n+3}^0 for the final-final configuration.

In configurations with initial-state partons, an initial-final antenna is necessary and the initial-final phase space map [24] $(\hat{1}, i, j) \rightarrow (\hat{\bar{1}}, \widetilde{(ij)})$ is employed to generate the composite momenta for the reduced matrix element so that

$$M_{n+3}^0(\cdots, \hat{1}_a, i, j, \cdots) \longrightarrow X_{3,a\rightarrow b}^0(\hat{1}, i, j) \, M_{n+2}^0(\cdots, \hat{\bar{1}}_b, \widetilde{(ij)}, \cdots) \qquad (4.4.58)$$

where the initial-state parton labelled $\hat{1}_a$ where a is the species of the initial-state parton, either q or g for a quark or gluon respectively. The various antennae and reduced matrix elements for a particular colour ordered matrix element in the real emission are listed in Table. 4.2. In hadron-hadron collisions, an analogous subtraction term exists for the second initial-state parton, i.e., $\hat{1}_a \rightarrow \hat{2}_b$ where b is the species of the second initial-state parton. For processes where $a = b$, we drop the subscript $a \rightarrow b$ for simplicity and only retain the label in the species changing cases.

Finally we must consider the initial-initial configuration where an unresolved parton is emitted between two initial-state partons of species a and b. The subtraction term uses an initial-initial antenna function and the appropriate initial-initial phase space map [24] $(\hat{1}, i, \hat{2}) \rightarrow (\hat{\bar{1}}, \hat{\bar{2}})$,

$$M_{n+3}^0(\cdots, \hat{1}_a, i, \hat{2}_b, \cdots) \longrightarrow X_{3,a\rightarrow c,b\rightarrow d}^0(\hat{1}, i, \hat{2}) \, M_{n+2}^0(\cdots, \hat{\bar{1}}_c, \hat{\bar{2}}_d, \cdots). \qquad (4.4.59)$$

Initial-Final Unintegrated Antennae		
Matrix element, M^0_{n+3}	Antenna, X^0_3	Reduced matrix element, M^0_{n+2}
$(\cdots ; \hat{1}_q, i_g, j_{\bar{q}}; \cdots)$	$A^0_3(\hat{1}, i, j)$	$(\cdots ; \hat{\bar{1}}_q, J_{\bar{q}}; \cdots)$
$(\cdots ; \hat{1}_q, i_g, j_g, \cdots)$	$d^0_3(\hat{1}, i, j)$	$(\cdots ; \hat{\bar{1}}_q, J_g, \cdots)$
$(\cdots ; i_q, j_g, \hat{1}_g, \cdots)$	$d^0_3(i, j, \hat{1})$	$(\cdots ; J_q, \hat{\bar{1}}_g, \cdots)$
$(\cdots ; \hat{1}_{q'}, i_{\bar{q}}; j_q, \cdots)$	$E^0_3(\hat{1}, i, j)$	$(\cdots ; \hat{\bar{1}}_{q'}, J_g, \cdots)$
$(\cdots , \hat{1}_g, i_g, j_g, \cdots)$	$f^0_3(\hat{1}, i, j)$	$(\cdots , \hat{\bar{1}}_g, J_g, \cdots)$
$(\cdots , \hat{1}_g, i_{\bar{q}}; j_q, \cdots)$	$G^0_3(\hat{1}, i, j)$	$(\cdots , \hat{\bar{1}}_g, J_g, \cdots)$
$(\cdots ; i_q, \hat{1}_g, j_{\bar{q}}, \cdots)$	$-a^0_{3,g \to q}(i, \hat{1}; j)$	$(\cdots ; \hat{\bar{1}}_q, J_g, \cdots)$
$(\cdots ; i_q, \hat{1}_g, j_g, \cdots)$	$-d^0_{3,g \to q}(i, \hat{1}; j)$	$(\cdots ; \hat{\bar{1}}_q, J_g, \cdots)$
$(\cdots ; i_{q'}, \hat{1}_q; j_q, \cdots)$	$-E^0_{3,q \to g}(i, \hat{1}, j)$	$(\cdots ; J_{q'}, \hat{\bar{1}}_g, \cdots)$
$(\cdots , i_g, \hat{1}_q; j_q, \cdots)$	$-G^0_{3,q \to g}(i, \hat{1}, j)$	$(\cdots , J_g, \hat{\bar{1}}_g, \cdots)$

Table 4.2: The NLO antennae, X^0_3, and reduced matrix elements, M^0_{n+2}, appropriate for the various particle assignments and colour structures in the real radiation partial amplitudes, M^0_{n+3} for the initial-final configuration. The identity changing antennae are collected at the bottom of this table.

The various antennae and reduced matrix elements appropriate for a particular colour ordered matrix element in the real emission are listed in Table 4.3. As in the initial-final case, the subscripts are only retained in the species changing cases, $a \neq c$ or $b \neq d$.

Initial-Initial Unintegrated Antennae		
Matrix element, M^0_{n+3}	Antenna, X^0_3	Reduced matrix element, M^0_{n+2}
$(\cdots ; \hat{1}_q, i_g, \hat{2}_{\bar{q}}, \cdots)$	$A^0_3(\hat{1}, i, \hat{2})$	$(\cdots ; \hat{\bar{1}}_q, \hat{\bar{2}}_{\bar{q}}; \cdots)$
$(\cdots ; \hat{1}_q, i_g, \hat{2}_g, \cdots)$	$D^0_3(\hat{1}, i, \hat{2})$	$(\cdots ; \hat{\bar{1}}_q, \hat{\bar{2}}_g, \cdots)$
$(\cdots , \hat{1}_g, i_g, \hat{2}_g, \cdots)$	$F^0_3(\hat{1}, i, \hat{2})$	$(\cdots , \hat{\bar{1}}_g, \hat{\bar{2}}_g, \cdots)$
$(\cdots ; \hat{1}_q, \hat{2}_g, i_{\bar{q}}; \cdots)$	$-A^0_{3,g \to q}(\hat{1}, \hat{2}, i)$	$(\cdots ; \hat{\bar{1}}_q, \hat{\bar{2}}_{\bar{q}}; \cdots)$
$(\cdots ; i_q, \hat{1}_g, \hat{2}_g, \cdots)$	$-d^0_{3,g \to q}(i, \hat{1}; \hat{2})$	$(\cdots ; \hat{\bar{1}}_q, \hat{\bar{2}}_g, \cdots)$
$(\cdots ; \hat{1}_{q'}, \hat{2}_{\bar{q}}; i_q, \cdots)$	$-E^0_{3,q \to g}(\hat{1}, \hat{2}, i)$	$(\cdots ; \hat{\bar{1}}_{q'}, \hat{\bar{2}}_g, \cdots)$
$(\cdots , \hat{1}_g, \hat{2}_{\bar{q}}; i_q, \cdots)$	$-G^0_{3,q \to g}(\hat{1}, \hat{2}, i)$	$(\cdots , \hat{\bar{1}}_g, \hat{\bar{2}}_g, \cdots)$

Table 4.3: The NLO antennae, X^0_3, and reduced matrix elements, M^0_{n+2}, appropriate for the various particle assignments and colour structures in the real radiation partial amplitudes, M^0_{n+3} for the initial-initial configuration.

4.4.2 NLO mass factorisation term

The notation for the NLO mass factorisation contribution was presented at the beginning of this section in Eq. (4.4.50) and in Section 1.4. Writing the Born cross section out in terms of the matrix elements being integrated over the final-state phase space, the mass factorisation contribution at NLO is given by

$$
\begin{aligned}
\mathrm{d}\hat{\sigma}_{ij,NLO}^{MF} &= -\mathcal{N}_{NLO}^{V} \sum_{\text{perms}} \mathrm{d}\Phi_n(p_3, \cdots, p_{n+1}; x_1 p_1, x_2 p_2) \int \frac{\mathrm{d}z_1}{z_1} \frac{\mathrm{d}z_2}{z_2} \frac{1}{S_n} \\
&\times \ \Gamma_{ij;kl}^{(1)}(z_1, z_2) \ M_n^0(\cdots, \hat{k}, \cdots, \hat{l}, \cdots) \ J_n^{(n)}(p_3, \cdots, p_{n+1}).
\end{aligned}
\tag{4.4.60}
$$

In this formula there is an implicit sum over k and l, denoting the particle types of the initial-state partons. The explicit forms for the various mass factorisation kernels and their associated colour decompositions are given in [97]. The overall factor is given by

$$
\mathcal{N}_{NLO}^{V} = \mathcal{N}_{LO} \left(\frac{\alpha_s N}{2\pi} \right) \bar{C}(\epsilon) = \mathcal{N}_{NLO}^{R} \ C(\epsilon).
\tag{4.4.61}
$$

4.4.3 NLO virtual subtraction term

The virtual subtraction term is constructed from the integrated real subtraction term and the mass factorisation contribution. For a single colour connected pair in the colour ordering of the virtual matrix element, a virtual subtraction term will have the form

$$
\begin{aligned}
\mathrm{d}\hat{\sigma}_{NLO}^{T} &= -\mathcal{N}_{NLO}^{V} \int \frac{\mathrm{d}x_1}{x_1} \frac{\mathrm{d}x_2}{x_2} \frac{1}{S_n} \sum_{\text{perms}} \mathrm{d}\Phi_n(p_3, \cdots, p_n; x_1 p_1, x_2 p_2) \\
&\times \sum_{I,K} \boldsymbol{J}_2^{(1)}(I, K) \ M_{n+2}^0(\cdots, I, K, \cdots) \ J_n^{(n)}(\{p\}_n).
\end{aligned}
\tag{4.4.62}
$$

where in Figure 4.1, the singular integrated dipole factor, $\boldsymbol{J}_2^{(1)}$ is directly related to the integration of the X_3^0 antenna function over the single unresolved phase space, and is defined to all orders in ϵ. The precise form of $\boldsymbol{J}_2^{(1)}$ depends on the species of the resolved hard radiator partons in the real radiation matrix elements that produced this integrated dipole contribution and the kinematic configuration. Connecting to-
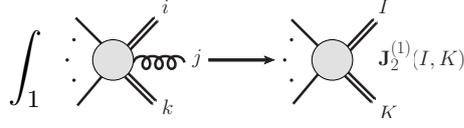
Figure 4.1: NLO virtual structure. Integration of the tree-level real emission over the single unresolved phase space for particle j generates an integrated dipole $\boldsymbol{J}_2^{(1)}(I, K)$ for each dipole pair I, K, containing the explicit IR poles of the virtual contribution.

gether the various integrated dipoles to form a single integrated antenna string for each reduced matrix element forms the full virtual subtraction term.

In the final-final configuration, the generic virtual subtraction term for a pair of colour connected partons I, K is produced by integrating the subtraction term associated with the real radiation matrix element $M_{n+3}^0(\cdots, i, j, k, \cdots)$ with the mapping $(i, j, k) \to (I, K)$ and has the form,

$$M_{n+3}^0(\cdots, i, j, k, \cdots) \longrightarrow \boldsymbol{J}_2^{(1)}(\widetilde{(ij)}, \widetilde{(jk)}) \; M_{n+2}^0(\cdots, \widetilde{(ij)}, \widetilde{(jk)}, \cdots). \quad (4.4.63)$$

This equation is the analogue of Eq. (4.4.57). The details of the integrated dipoles depends on the species of parton under consideration and all possibilities are listed in Table 4.4.

Final-Final Integrated Antennae		
Matrix element, M_{n+3}^0	Integrated dipole, $\boldsymbol{J}_2^{(1)}$	Reduced matrix element, M_{n+2}^0
$(\cdots; i_q, j_g, k_{\bar{q}}; \cdots)$	$\boldsymbol{J}_2^{(1)}(I_q, K_{\bar{q}}) = \mathcal{A}_3^0(s_{IK})$	$(\cdots; I_q, K_{\bar{q}}; \cdots)$
$(\cdots; i_q, j_g, k_g, \cdots)$	$\boldsymbol{J}_2^{(1)}(I_q, K_g) = \frac{1}{2}\mathcal{D}_3^0(s_{IK})$	$(\cdots; I_q, K_g, \cdots)$
$(\cdots; i_{q'}, j_{\bar{q}}; k_q, \cdots)$	$\boldsymbol{J}_{2,N_F}^{(1)}(I_q, K_g) = \frac{1}{2}\mathcal{E}_3^0(s_{IK})$	$(\cdots; I_q, K_g, \cdots)$
$(\cdots, i_g, j_g, k_g, \cdots)$	$\boldsymbol{J}_2^{(1)}(I_g, K_g) = \frac{1}{3}\mathcal{F}_3^0(s_{IK})$	$(\cdots, I_g, K_g, \cdots)$
$(\cdots, i_g, j_{\bar{q}}; k_q, \cdots)$	$\boldsymbol{J}_{2,N_F}^{(1)}(I_g, K_g) = \mathcal{G}_3^0(s_{IK})$	$(\cdots, I_g, K_g, \cdots)$

Table 4.4: The correspondence between the real radiation matrix elements, M_{n+3}^0 and the integrated NLO dipoles $\boldsymbol{J}_2^{(1)}$ and reduced matrix elements, M_{n+2}^0 for various particle assignments and colour structures for the final-final configuration.

When one of the partons making up the hard dipole is in the initial-state then the analogous formula to Eq. (4.4.63) now contains the appropriate mass factorisation

kernels from Eq. (4.4.60),

$$M_{n+3}^0(\cdots , \hat{1}, i, j, \cdots) \longrightarrow \boldsymbol{J}_2^{(1)}(\hat{\bar{1}}, \widetilde{(ij)})\; M_{n+2}^0(\cdots , \hat{\bar{1}}, \widetilde{(ij)}, \cdots), \qquad (4.4.64)$$

where the only modification is the form of the integrated dipoles, listed in Table 4.5. The substitution $\hat{1} \to \hat{2}$ allows the subtraction term including initial parton $\hat{2}$ to be constructed.

Initial-Final Integrated Antennae		
Matrix element, M_{n+3}^0	Integrated dipole, $\boldsymbol{J}_2^{(1)}$	Reduced matrix element, M_{n+2}^0
$(\cdots ; \hat{1}_q, i_g, j_{\bar{q}}; \cdots)$	$\boldsymbol{J}_2^{(1)}(\hat{\bar{1}}_q, J_{\bar{q}}) = \mathcal{A}_{3,q}^0(s_{\bar{1}J}) - \Gamma_{qq}^{(1)}(x_1)\delta_2$	$(\cdots ; \hat{\bar{1}}_q, J_{\bar{q}}; \cdots)$
$(\cdots ; \hat{1}_q, i_g, j_g; \cdots)$	$\boldsymbol{J}_2^{(1)}(\hat{\bar{1}}_q, J_g) = \frac{1}{2}\mathcal{D}_{3,q}^0(s_{\bar{1}J}) - \Gamma_{qq}^{(1)}(x_1)\delta_2$	$(\cdots ; \hat{\bar{1}}_q, J_g; \cdots)$
$(\cdots ; i_q, j_g, \hat{1}_g; \cdots)$	$\boldsymbol{J}_2^{(1)}(J_q, \hat{\bar{1}}_g) = \mathcal{D}_{3,g,qg}^0(s_{\bar{1}J}) - \frac{1}{2}\Gamma_{gg}^{(1)}(x_1)\delta_2$	$(\cdots ; J_q, \hat{\bar{1}}_g; \cdots)$
$(\cdots ; \hat{1}_{q'}, i_{\bar{q}}; j_q, \cdots)$	$\boldsymbol{J}_{2,N_F}^{(1)}(\hat{\bar{1}}_q, J_g) = \frac{1}{2}\mathcal{E}_{3,q',q\bar{q}}^0(s_{\bar{1}J})$	$(\cdots ; \hat{\bar{1}}_q, J_g; \cdots)$
$(\cdots , \hat{1}_g, i_g, j_g; \cdots)$	$\boldsymbol{J}_2^{(1)}(\hat{\bar{1}}_g, J_g) = \frac{1}{2}\mathcal{F}_{3,g}^0(s_{\bar{1}J}) - \frac{1}{2}\Gamma_{gg}^{(1)}(x_1)\delta_2$	$(\cdots , \hat{\bar{1}}_g, J_g; \cdots)$
$(\cdots , \hat{1}_g, i_{\bar{q}}; j_q, \cdots)$	$\boldsymbol{J}_{2,N_F}^{(1)}(\hat{\bar{1}}_g, J_g) = \mathcal{G}_{3,g}^0(s_{\bar{1}J})$	$(\cdots , \hat{\bar{1}}_g, J_g; \cdots)$
$(\cdots ; i_q, \hat{1}_g, j_{\bar{q}}; \cdots)$	$\boldsymbol{J}_{2,g\to q}^{(1)}(\hat{\bar{1}}_q, J_{\bar{q}}) = -\frac{1}{2}\mathcal{A}_{3,g,q\bar{q}}^0(s_{\bar{1}J}) - \Gamma_{qg}^{(1)}(x_1)\delta_2$	$(\cdots ; \hat{\bar{1}}_q, J_{\bar{q}}; \cdots)$
$(\cdots ; i_q, \hat{1}_g, j_g; \cdots)$	$\boldsymbol{J}_{2,g\to q}^{(1)}(\hat{\bar{1}}_q, J_g) = -\mathcal{D}_{3,g,qg}^0(s_{\bar{1}J}) - \Gamma_{qg}^{(1)}(x_1)\delta_2$	$(\cdots ; \hat{\bar{1}}_q, J_g; \cdots)$
$(\cdots ; i_{q'}, \hat{1}_q; j_q, \cdots)$	$\boldsymbol{J}_{2,q\to g}^{(1)}(J_q, \hat{\bar{1}}_g) = -\mathcal{E}_{3,q,qq'}^0(s_{\bar{1}J}) - \Gamma_{gq}^{(1)}(x_1)\delta_2$	$(\cdots ; J_q, \hat{\bar{1}}_g; \cdots)$
$(\cdots , i_g; \hat{1}_q, j_q, \cdots)$	$\boldsymbol{J}_{2,q\to g}^{(1)}(J_g, \hat{\bar{1}}_g) = -\mathcal{G}_{3,q}^0(s_{\bar{1}J}) - \Gamma_{gq}^{(1)}(x_1)\delta_2$	$(\cdots , J_g, \hat{\bar{1}}_g; \cdots)$

Table 4.5: The correspondence between the real radiation matrix elements, M_{n+3}^0 and the integrated NLO dipoles $\boldsymbol{J}_2^{(1)}$ and reduced matrix elements, M_{n+2}^0 for various particle assignments and colour structures for the initial-final configuration. For brevity $\delta(1 - x_i) = \delta_i$ for $i = 1, 2$.

The final kinematic configuration is when both hard radiators in the dipole are in the initial-state. In this case, the relevant subtraction term is

$$M_{n+3}^0(\cdots , \hat{1}, i, \hat{2}, \cdots) \longrightarrow \boldsymbol{J}_2^{(1)}(\hat{\bar{1}}, \hat{\bar{2}})\; M_{n+2}^0(\cdots , \hat{\bar{1}}, \hat{\bar{2}}, \cdots), \qquad (4.4.65)$$

where once again, only the form of the integrated dipole is different from Eqs. (4.4.63) and (4.4.64) and the initial-initial integrated dipoles are listed in Table 4.6.

The relationship between the real radiation subtraction term $\mathrm{d}\hat{\sigma}^S$ and the virtual subtraction term $\mathrm{d}\hat{\sigma}^T$ is shown in Figure 4.2. The full virtual subtraction term is generated by summing over the colour connected pairs in the virtual matrix element's colour ordering. For example, consider an $(n + 3)$-parton squared partial amplitude,

Initial-Initial Integrated Antennae		
Matrix element, M_{n+3}^0	Integrated dipole, $\boldsymbol{J}_2^{(1)}$	Reduced matrix element, M_{n+2}^0
$(\cdots, \hat{1}_q, i_g, \hat{2}_{\bar{q}}, \cdots)$	$\boldsymbol{J}_2^{(1)}(\hat{\bar{1}}_q, \hat{\bar{2}}_{\bar{q}}) = \mathcal{A}_{3,q\bar{q}}^0(s_{\bar{1}\bar{2}}) - \Gamma_{qq}^{(1)}(x_1)\delta_2 - \Gamma_{qq}^{(1)}(x_2)\delta_1$	$(\cdots; \hat{\bar{1}}_q, \hat{\bar{2}}_{\bar{q}}; \cdots)$
$(\cdots; \hat{1}_q, i_g, \hat{2}_g, \cdots)$	$\boldsymbol{J}_2^{(1)}(\hat{\bar{1}}_q, \hat{\bar{2}}_g) = \mathcal{D}_{3,qg}^0(s_{\bar{1}\bar{2}}) - \Gamma_{qq}^{(1)}(x_1)\delta_2 - \frac{1}{2}\Gamma_{gg}^{(1)}(x_2)\delta_1$	$(\cdots; \hat{\bar{1}}_q, \hat{\bar{2}}_g, \cdots)$
$(\cdots, \hat{1}_g, i_g, \hat{2}_g, \cdots)$	$\boldsymbol{J}_2^{(1)}(\hat{\bar{1}}_g, \hat{\bar{2}}_g) = \mathcal{F}_{3,gg}^0(s_{\bar{1}\bar{2}}) - \frac{1}{2}\Gamma_{gg}^{(1)}(x_1)\delta_2 - \frac{1}{2}\Gamma_{gg}^{(1)}(x_2)\delta_1$	$(\cdots, \hat{\bar{1}}_g, \hat{\bar{2}}_g, \cdots)$
$(\cdots; \hat{1}_q, \hat{2}_g, i_{\bar{q}}; \cdots)$	$\boldsymbol{J}_{2,g\to q}^{(1)}(\hat{\bar{1}}_q, \hat{\bar{2}}_{\bar{q}}) = -\mathcal{A}_{3,qg}^0(s_{\bar{1}\bar{2}}) - \Gamma_{qg}^{(1)}(x_2)\delta_1$	$(\cdots; \hat{\bar{1}}_q, \hat{\bar{2}}_{\bar{q}}; \cdots)$
$(\cdots; i_q, \hat{1}_g, \hat{2}_g, \cdots)$	$\boldsymbol{J}_{2,g\to q}^{(1)}(\hat{\bar{1}}_q, \hat{\bar{2}}_g) = -\mathcal{D}_{3,qg}^0(s_{\bar{1}\bar{2}}) - \Gamma_{qg}^{(1)}(x_1)\delta_2$	$(\cdots; \hat{\bar{1}}_q, \hat{\bar{2}}_g, \cdots)$
$(\cdots; \hat{1}_{q'}, \hat{2}_{\bar{q}}; i_q, \cdots)$	$\boldsymbol{J}_{2,q\to g}^{(1)}(\hat{\bar{1}}_q, \hat{\bar{2}}_g) = -\mathcal{E}_{3,q'q,q}^0(s_{\bar{1}\bar{2}}) - \Gamma_{gq}^{(1)}(x_2)\delta_1$	$(\cdots; \hat{\bar{1}}_{q'}, \hat{\bar{2}}_g, \cdots)$
$(\cdots, \hat{1}_g, \hat{2}_{\bar{q}}; i_q, \cdots)$	$\boldsymbol{J}_{2,q\to g}^{(1)}(\hat{\bar{1}}_g, \hat{\bar{2}}_g) = -\mathcal{G}_{3,gq}^0(s_{\bar{1}\bar{2}}) - \Gamma_{gq}^{(1)}(x_2)\delta_1$	$(\cdots, \hat{\bar{1}}_g, \hat{\bar{2}}_g, \cdots)$

Table 4.6: The correspondence between the real radiation matrix elements, M_{n+3}^0 and the integrated NLO dipoles $\boldsymbol{J}_2^{(1)}$ and reduced matrix elements, M_{n+2}^0 for various particle assignments and colour structures for the initial-initial configuration. For brevity $\delta(1-x_1) = \delta_1$, $\delta(1-x_2) = \delta_2$.

containing a quark-antiquark pair and $(n+1)$ gluons, that maps onto the $(n+2)$-parton squared partial amplitude $M_{n+2}^0(\hat{\bar{1}}_q, i_g, \cdots, j_g, \hat{\bar{2}}_{\bar{q}})$. Once the leading colour single unresolved subtraction term for this matrix element has been integrated and combined with the mass factorisation terms, the resulting virtual subtraction term is simply given by,

$$
\begin{aligned}
\mathrm{d}\hat{\sigma}_{NLO}^T &= -\mathcal{N}_{NLO}^V \int \frac{\mathrm{d}x_1}{x_1} \frac{\mathrm{d}x_2}{x_2} \frac{1}{S_n} \sum_{\text{perms}} \mathrm{d}\Phi_n(p_3, \cdots, p_n; x_1 p_1, x_2 p_2) \\
&\times \boldsymbol{J}_{n+2}^{(1)}(\hat{\bar{1}}_q, i_g, \cdots, j_g, \hat{\bar{2}}_{\bar{q}}) M_{n+2}^0(\hat{\bar{1}}_q, i_g, \cdots, j_g, \hat{\bar{2}}_{\bar{q}}) J_n^{(n)}(p_3, \cdots, p_n), \quad (4.4.66)
\end{aligned}
$$

where the full integrated antenna string is formed from the sum of integrated dipoles,

$$
\begin{aligned}
\boldsymbol{J}_{n+2}^{(1)}(\hat{\bar{1}}_q, i_g, j_g, \cdots, k_g, l_g, \hat{\bar{2}}_{\bar{q}}) &= \boldsymbol{J}_2^{(1)}(\hat{\bar{1}}_q, i_g) + \boldsymbol{J}_2^{(1)}(i_g, j_g) + \cdots \\
&+ \boldsymbol{J}_2^{(1)}(k_g, l_g) + \boldsymbol{J}_2^{(1)}(\hat{\bar{2}}_q, l_g). \quad (4.4.67)
\end{aligned}
$$

Each term in $\boldsymbol{J}_{n+2}^{(1)}$ is proportional to a particular kinematic factor, $(|s_{ij}|)^{-\epsilon}$. We therefore see that the singularities present in each term correspond to a particular singular contribution $\boldsymbol{I}_{ij}^{(1)}$. The full singularity structure is simply obtained by summing the integrated dipoles to form $\boldsymbol{J}_{n+2}^{(1)}$, or equivalently by summing $\boldsymbol{I}_{ij}^{(1)}$. Using Catani's one-loop factorisation formula, discussed in Chapter 2 and [20],

$$
\mathcal{P}oles\big(M_{n+2}^1(1, \cdots, n+2)\big) = 2\boldsymbol{I}_{n+2}^{(1)}(\epsilon; 1, \cdots, n+2)M_{n+2}^0(1, \cdots, n+2),
$$

$$\mathrm{d}\hat\sigma^T : \qquad \boxed{\mathrm{d}\hat\sigma^T \sim \boldsymbol{J}_n^{(1)} M_n^0}$$

$$\mathrm{d}\hat\sigma^S : \qquad \boxed{\mathrm{d}\hat\sigma^S \sim X_3^0 M_n^0}$$
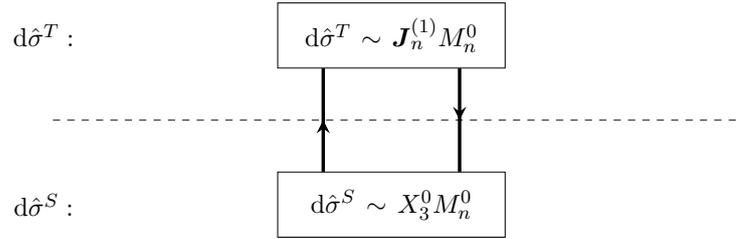
Figure 4.2: The NLO correction to n-parton scattering requires the construction of the subtraction term $\mathrm{d}\hat\sigma_{NLO}^S$ to remove all IR divergent behaviour of the $(n + 1)$-parton real emission. Integrating this subtraction term and combining with the NLO mass factorisation terms generates the virtual subtraction term, $\mathrm{d}\hat\sigma_{NLO}^T$. Antenna subtraction allows $\mathrm{d}\hat\sigma_{NLO}^T$ to be generated by first constructing $\mathrm{d}\hat\sigma_{NLO}^S$ or vice versa.

$$\tag{4.4.68}$$

where $\boldsymbol{I}_{n+2}^{(1)}(\epsilon; 1, \cdots, n + 2)$ is the n-parton IR singularity operator, which can be written as a sum of dipole contributions,

$$\boldsymbol{I}_{n+2}^{(1)}(\epsilon; 1, \cdots, n) \;\; = \;\; \sum_{(i,j)} \boldsymbol{I}_{ij}^{(1)}(\epsilon; s_{ij}), \tag{4.4.69}$$

and the sum runs over colour connected pairs of partons.

The integrated antenna strings that form the virtual subtraction term exactly mimic the virtual cross section poles, such that the NLO calculation is now infrared finite.

The correspondence between the poles of $\boldsymbol{J}_{n+2}^{(1)}$ and the one-loop matrix elements removes the need for the $\boldsymbol{I}_{n+2}^{(1)}$. This correspondence is particularly clear because of the way the integrated antenna string has been constructed as a sum of dipole-like antenna contributions. Recognising that the mass factorisation contributions fit naturally into the structure of the integrated antenna strings, means that only the genuine final-state IR poles remain in the virtual subtraction term. This puts the virtual subtraction term in a particularly convenient form for carrying out the explicit pole cancellation against the virtual contribution.We now extend the antenna subtraction formalism to NNLO calculations.

4.5 Antenna subtraction at NNLO

At NNLO we must now consider cross sections involving two additional particles in the scattering process, appearing as either real or virtual particles. These additional particles lead to three distinct contributions: double real $d\hat{\sigma}^{RR}_{ij,NNLO}$, real-virtual $d\hat{\sigma}^{RV}_{ij,NNLO}$ or double virtual $d\hat{\sigma}^{VV}_{ij,NNLO}$, containing $(n+4)$-, $(n+3)$-, $(n+2)$-partons and zero-, one-, two-loops respectively, where n is the number of jets in the final-state,

$$
\begin{aligned}
d\hat{\sigma}_{ij,NNLO} &= \int_{n+2} d\hat{\sigma}^{RR}_{ij,NNLO} + \int_{n+1} \left(d\hat{\sigma}^{RV}_{ij,NNLO} + d\hat{\sigma}^{MF,1}_{ij,NNLO} \right) \\
&+ \int_n \left(d\hat{\sigma}^{VV}_{ij,NNLO} + d\hat{\sigma}^{MF,2}_{ij,NNLO} \right).
\end{aligned}
\tag{4.5.70}
$$

The integration measure $\int_{d\Phi_n}$ is defined in (4.4.46). Following the discussion in Chapter 1.4, the NNLO mass factorisation terms are naturally partitioned into terms containing $(n+1)$- or n-parton final-states, which are given by,

$$
\begin{aligned}
d\hat{\sigma}^{MF,1}_{ij,NNLO}(\xi_1 H_1, \xi_2 H_2) &= -\int \frac{dz_1}{z_1} \frac{dz_2}{z_2} \\
\times \quad &\left(\frac{\alpha_s N}{2\pi} \right) \bar{C}(\epsilon) \, \Gamma^{(1)}_{ij;kl}(z_1, z_2) \left(d\hat{\sigma}^R_{kl,NLO} - d\hat{\sigma}^S_{kl,NLO} \right)(z_1 \xi_1 H_1, z_2 \xi_2 H_2),
\end{aligned}
\tag{4.5.71}
$$

$$
\begin{aligned}
d\hat{\sigma}^{MF,2}_{ij,NNLO}(\xi_1 H_1, \xi_2 H_2) &= -\int \frac{dz_1}{z_1} \frac{dz_2}{z_2} \Bigg\{ \\
&\left(\frac{\alpha_s N}{2\pi} \right)^2 \bar{C}(\epsilon)^2 \, \Gamma^{(2)}_{ij;kl}(z_1, z_2) d\hat{\sigma}_{kl,LO}(z_1 \xi_1 H_1, z_2 \xi_2 H_2) \\
+ \quad &\left(\frac{\alpha_s N}{2\pi} \right) \bar{C}(\epsilon) \, \Gamma^{(1)}_{ij;kl}(z_1, z_2) \left(d\hat{\sigma}^V_{kl,NLO} - d\hat{\sigma}^T_{kl,NLO} \right)(z_1 \xi_1 H_1, z_2 \xi_2 H_2) \Bigg\},
\end{aligned}
\tag{4.5.72}
$$

where the new ingredient at NNLO, $\Gamma^{(2)}_{ij;kl}$, can be written in terms of one- and two-loop Altarelli-Parisi kernels,

$$
\Gamma^{(2)}_{ij;kl}(z_1, z_2) = \delta(1 - z_2)\delta_{lj}\Gamma^{(2)}_{ki}(z_1) + \delta(1 - z_1)\delta_{ki}\Gamma^{(2)}_{lj}(z_2) + \Gamma^{(1)}_{ki}(z_1)\Gamma^{(1)}_{lj}(z_2).
\tag{4.5.73}
$$

At NNLO, the subtraction terms are now constructed from both three and four parton antennae to account for the double unresolved radiation. The one-loop three parton antennae now also appear to mimic the single unresolved limits of the one-loop physical matrix element. They will remove all implicit divergence of the double real and real-virtual contributions. Introducing a double real subtraction term $d\hat{\sigma}^{S}_{ij,NNLO}$, a real-virtual subtraction term $d\hat{\sigma}^{VS}_{ij,NNLO}$, their corresponding integrated forms and the NNLO mass factorisation contributions, the NNLO cross section can be reorganised such that each term in square brackets is rendered free from implicit divergence and explicit poles and thus suitable for a numerical implementation;

$$
\begin{aligned}
d\hat{\sigma}_{ij,NNLO} &= \int_{n+2} \left[d\hat{\sigma}^{RR}_{ij,NNLO} - d\hat{\sigma}^{S}_{ij,NNLO} \right] \\
&+ \int_{n+1} \left[d\hat{\sigma}^{RV}_{ij,NNLO} - d\hat{\sigma}^{T}_{ij,NNLO} \right] \\
&+ \int_{n} \left[d\hat{\sigma}^{VV}_{ij,NNLO} - d\hat{\sigma}^{U}_{ij,NNLO} \right],
\end{aligned}
\tag{4.5.74}
$$

where the real-virtual and double virtual subtraction terms are given by,

$$
d\hat{\sigma}^{T}_{ij,NNLO} = d\hat{\sigma}^{VS}_{ij,NNLO} - \int_{1} d\hat{\sigma}^{S,1}_{ij,NNLO} - d\hat{\sigma}^{MF,1}_{ij,NNLO},
\tag{4.5.75}
$$

$$
d\hat{\sigma}^{U}_{ij,NNLO} = - \int_{1} d\hat{\sigma}^{VS}_{ij,NNLO} - \int_{2} d\hat{\sigma}^{S,2}_{ij,NNLO} - d\hat{\sigma}^{MF,2}_{ij,NNLO}.
\tag{4.5.76}
$$

The integrated double real subtraction terms are decomposed explicitly into a piece that is integrated over the single unresolved particle phase space and a piece that is integrated over the phase space of two unresolved particles, since integration of the subtraction term $d\hat{\sigma}^{S}_{NNLO}$ gives contributions to both the $(n+1)$- and n-parton final states

$$
\int_{n+2} d\hat{\sigma}^{S}_{ij,NNLO} = \int_{n+1} \int_{1} d\hat{\sigma}^{S,1}_{ij,NNLO} + \int_{n} \int_{2} d\hat{\sigma}^{S,2}_{ij,NNLO}.
\tag{4.5.77}
$$

The construction of subtraction terms at the double real, real-virtual and double virtual levels requires an intimate understanding of the explicit IR singularity structure and implicit IR divergent behaviour of both the physical matrix elements and the subtraction terms for different final-state multiplicities. The colour connectivity completely informs the construction of the double real subtraction term as there are no

explicit IR poles to consider. The double virtual subtraction term, which is free from implicit IR divergences, deals solely with explicit IR cancellation. The real-virtual subtraction term contains both explicit poles and implicit divergent behaviour and so its structure must take into account both parton colour connection and explicit pole cancellation.

In the proceeding sections below, we will see how the $\mathrm{d}\hat{\sigma}^S_{NNLO}$, $\mathrm{d}\hat{\sigma}^T_{NNLO}$ and $\mathrm{d}\hat{\sigma}^U_{NNLO}$ subtraction terms each contain components, fulfilling a particular rôle in the construction of the correct infrared structure. It is the nature of any subtraction scheme, that whatever is subtracted from a final state with a particular multiplicity, must be added back in either integrated or unintegrated form to a final state with a different multiplicity. The "roadmap" in Figure 4.3 illustrates how the subtraction terms $\mathrm{d}\hat{\sigma}^S_{NNLO}$, $\mathrm{d}\hat{\sigma}^T_{NNLO}$ and $\mathrm{d}\hat{\sigma}^U_{NNLO}$ are related.

The five terms introduced in the double real subtraction term are directly linked with specific terms in the real-virtual and double virtual subtraction terms. Similarly, terms in the real-virtual subtraction term are composed partly of integrated terms from the double real subtraction term $\int_1 \mathrm{d}\hat{\sigma}^S_{ij,NNLO}$ and new virtual subtraction terms, $\mathrm{d}\hat{\sigma}^{VS}_{ij,NNLO}$. The remaining terms, $\int_2 \mathrm{d}\hat{\sigma}^S_{ij,NNLO}$ and $\int_1 \mathrm{d}\hat{\sigma}^{VS}_{ij,NNLO}$, combine to produce the structures present in $\mathrm{d}\hat{\sigma}^U_{ij,NNLO}$. As the discussion unfolds, we anticipate that it will help to refer back to Figure 4.3.

4.5.1 Construction of the double real subtraction term

At NNLO the double real radiative $(n + 4)$-parton correction to the $pp \rightarrow n$ jets process, must be included integrated over the full $(n + 2)$-parton phase space, given the constraint that n jets are observed. In order for this to be achieved, the IR divergent behaviour of the partonic cross section must be isolated. By construction, the double real subtraction term mimics the IR divergence and factorisation of the real radiation matrix elements in all relevant single and double unresolved limits, referring back to the limits in Chapter 2. At NNLO there are four colour configurations to consider when constructing the subtraction term for n-jet production [22, 35, 75, 79]:

1. $\mathrm{d}\hat{\sigma}^{S,a}$

   A single unresolved final-state parton but the remaining $(n + 1)$ final-state

$d\hat{\sigma}^U$:

$$d\hat{\sigma}^{U,A} \sim \left(-\frac{\mathcal{B}_0}{\epsilon}\boldsymbol{J}_n^{(1)}M_n^1 + \boldsymbol{J}_n^{(1)}M_n^1\right)$$

$$d\hat{\sigma}^{U,B} \sim \frac{1}{2}\boldsymbol{J}_n^{(1)} \otimes \boldsymbol{J}_n^{(1)}M_n^0$$

$$d\hat{\sigma}^{U,C} \sim \boldsymbol{J}_n^{(2)}M_n^0$$

$d\hat{\sigma}^T$:

$$d\hat{\sigma}^{T,a} \sim \boldsymbol{J}_{n+1}^{(1)}M_{n+1}^0$$

$$d\hat{\sigma}^{T,b_3} \sim \left(-\frac{\mathcal{B}_0}{\epsilon}X_3^0 M_n^0 + \frac{\mathcal{B}_0}{\epsilon}X_3^0\left(\frac{|s|}{\mu^2}\right)^{-\epsilon}M_n^0\right)$$

$$d\hat{\sigma}^{T,b_1} \sim \left(X_3^0 M_n^1 + X_3^0 \boldsymbol{J}_n^{(1)}M_n^0\right)$$

$$d\hat{\sigma}^{T,c} \sim \left(-\int_1 d\hat{\sigma}^{S,c} + d\hat{\sigma}^{T,c_1} + d\hat{\sigma}^{T,c_2}\right)$$

$$d\hat{\sigma}^{T,b_2} \sim \left(X_3^1 M_n^0 + \boldsymbol{J}_X^{(1)}X_3^0 M_n^0 - \boldsymbol{J}_X X_3^0 \boldsymbol{J}_2^{(1)}M_n^0\right)$$

$d\hat{\sigma}^S$:

$$d\hat{\sigma}^{S,a}$$
$$d\hat{\sigma}^{S,d}$$
$$d\hat{\sigma}^{S,c}$$
$$d\hat{\sigma}^{S,b_2}$$
$$d\hat{\sigma}^{S,b_1}$$
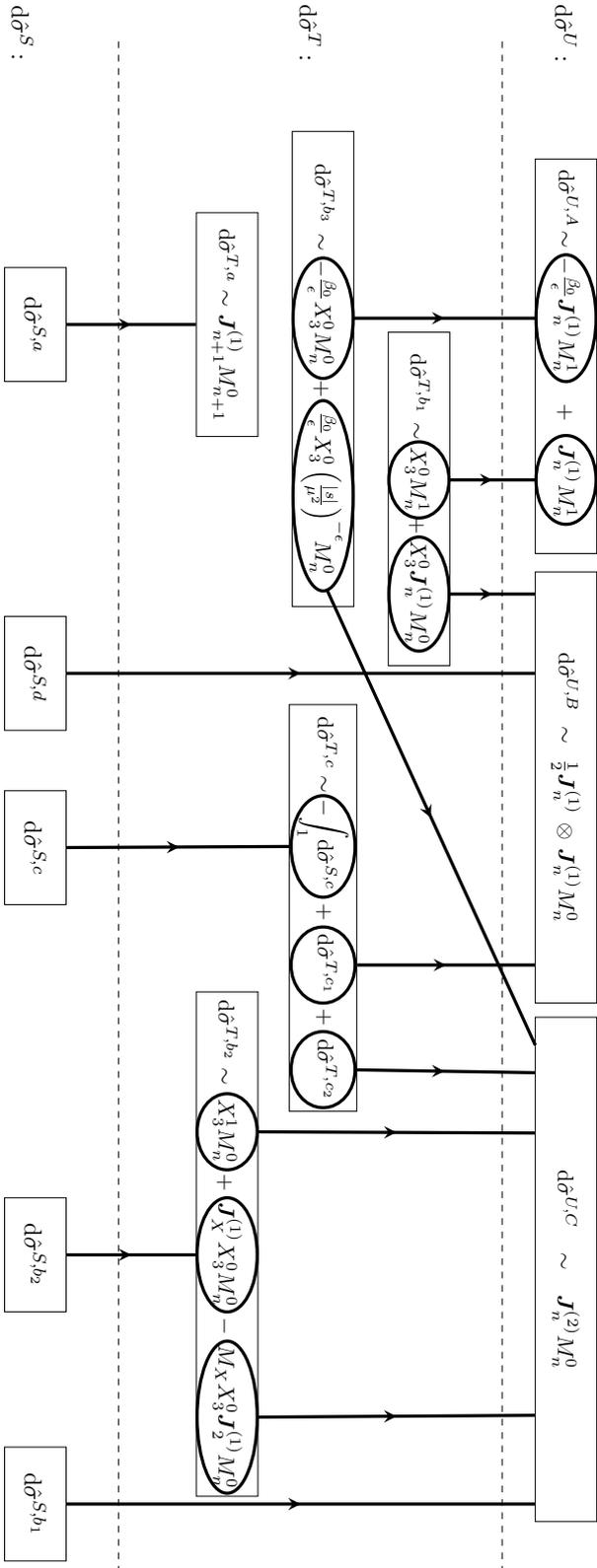
Figure 4.3: The NNLO correction to n-parton scattering contains three contributions: double real, real-virtual and double virtual, with the associated subtraction terms denoted $d\hat{\sigma}^S_{NNLO}$, $d\hat{\sigma}^T_{NNLO}$ and $d\hat{\sigma}^U_{NNLO}$ discussed in Secs. 4.5.1, 4.5.2 and 4.5.3 respectively. Each distinct contribution to the subtraction terms is shown in a rectangular box. Individual terms within a box flow between boxes after integration, indicated by the arrows.

partons will still form n jets.

2. $\mathrm{d}\hat{\sigma}^{S,b}$

   Two colour-connected unresolved partons, i.e., two unresolved partons radiated between a single pair of hard radiators.

3. $\mathrm{d}\hat{\sigma}^{S,c}$

   Two almost colour-connected unresolved partons, i.e., two colour disconnected unresolved partons sharing a common radiator, and including large angle soft radiation.

4. $\mathrm{d}\hat{\sigma}^{S,d}$

   Two colour disconnected unresolved partons, i.e., two colour disconnected unresolved partons with no radiators in common.

The four possible colour configurations for the single and double unresolved limits of the $(n + 4)$-parton matrix elements provide a natural way to divide the subtraction term into pieces, as has been emphasised in previous works [22,35]. It should be noted that although the factorisation of the matrix elements is strictly classified according to the colour connection of unresolved partons, the associated subtraction terms readily communicate with one another in most unresolved limits due to the existence and cross cancellation of spurious singularities. These systematic cross cancellations suggest that structures exist in the subtraction term other than those dictated by the colour connection of unresolved partons.

In the following sections we make a further reorganisation of the double real subtraction term into five contributions,

$$\mathrm{d}\hat{\sigma}^{S}_{NNLO} = \mathrm{d}\hat{\sigma}^{S,a}_{NNLO} + \mathrm{d}\hat{\sigma}^{S,b_1}_{NNLO} + \mathrm{d}\hat{\sigma}^{S,b_2}_{NNLO} + \mathrm{d}\hat{\sigma}^{S,c}_{NNLO} + \mathrm{d}\hat{\sigma}^{S,d}_{NNLO}. \quad (4.5.78)$$

Such an organisation of the double real subtraction term allows a transparent understanding of how various terms from the double real level cascade down the calculation upon integration. Understanding this structure also permits a systematic construction of the double real subtraction term built from predictable blocks of terms.

Single unresolved subtraction term, $\mathrm{d}\hat{\sigma}^{S,a}_{NNLO}$

The removal of single unresolved limits from the $(n+4)$-parton contribution to the n-jet cross section at NNLO is not dissimilar from the subtraction term constructed to isolate single unresolved limits from the $(n+4)$-parton contribution to the $(n+1)$-jet cross section at NLO. The two subtraction terms differ only in the number of jets allowed by the jet function,

$$\mathrm{d}\hat{\sigma}^{S,a}_{NNLO}(\{p\}_{n+4}) = \mathrm{d}\hat{\sigma}^{S}_{NLO}(\{p\}_{n+4})\Big|_{J^{(n+1)}_{n+1} \to J^{(n+1)}_{n}}. \tag{4.5.79}$$

The discussion about constructing the NLO subtraction terms given in Section 4.4 is then sufficient to construct the single unresolved NNLO subtraction term $\mathrm{d}\hat{\sigma}^{S,a}_{NNLO}$. Although this part of the subtraction term removes single unresolved divergences of the physical matrix elements for n-jet selecting observables, it also generates additional spurious singularities in the almost colour connected and colour disconnected limits, over-subtracting the divergence in each case. This is because the $(n+3)$-parton reduced matrix elements allow an additional parton to become unresolved and yet still form n-jets. This contribution is reintroduced at the real-virtual level and cancel the explicit poles in the real-virtual contribution upon analytic integration.

Four-parton antenna subtraction term, $\mathrm{d}\hat{\sigma}^{S,b_1}_{NNLO}$

At NNLO there are essential new ingredients in the form of four-parton tree level antenna functions that are required to faithfully reproduce the colour connected double unresolved divergences of the physical matrix elements. The momentum map associated with a four-parton antenna function is the $(n+4) \to (n+2)$ map that maps the four antenna momenta i, j, k, l down to two composite momenta $\widetilde{(ijk)}, \widetilde{(jkl)}$, which is different for the final-final [84], initial-final and initial-initial [24] configurations. This group of terms has the form,

$$\begin{aligned}
\mathrm{d}\hat{\sigma}^{S,b_1}_{NNLO} &= \mathcal{N}^{RR}_{NNLO} \sum_{n+2} \mathrm{d}\Phi_{n+2}(p_3, \ldots, p_{n+4}; p_1, p_2) \frac{1}{S_{n+2}} \\
&\times \sum_{j,k} X^0_4(i, j, k, l) \, M^0_{n+2}(\cdots, \widetilde{(ijk)}, \widetilde{(jkl)}, \cdots) \, J^{(n)}_n(\{p\}_n), \tag{4.5.80}
\end{aligned}$$

where $\mathcal{N}_{NNLO}^{RR}$ contains the overall QCD coupling, colour and non-QCD factors appropriate for the double real radiation contribution,

$$\mathcal{N}_{NNLO}^{RR} = \mathcal{N}_{LO} \left(\frac{\alpha_s N}{2\pi} \right)^2 \frac{\bar{C}(\epsilon)^2}{C(\epsilon)^2}. \tag{4.5.81}$$

This term is generic to all three kinematic configurations, (FF, IF and II), with the specific antenna functions and momentum maps depending on which configuration the term belongs to. The four-parton antenna functions displays further divergent behaviour including single unresolved and almost colour connected singularities that may not match up with the physical matrix element, all of which must be properly removed elsewhere in the subtraction term. The analytic integration of the four-parton antenna functions is carried out over the double unresolved antenna phase space and so the terms in $\mathrm{d}\hat{\sigma}_{NNLO}^{S,b_1}$ are reintroduced as part of the double virtual subtraction term.

Four-parton single unresolved subtraction term, $\mathrm{d}\hat{\sigma}_{NNLO}^{S,b_2}$

As mentioned in the previous section, four-parton antenna functions contain single unresolved spurious singularities which must be removed to ensure a proper subtraction of the IR divergence in the physical matrix elements. For each four-parton antenna, the single unresolved limits are removed by constructing a subtraction term along the lines of $\mathrm{d}\hat{\sigma}_{NNLO}^{S,a}$ but now applying this method to the four-parton antenna function rather than the physical matrix elements. This highlights one of the beauties of antenna subtraction; since the subtraction terms are constructed from physical processes themselves, any spurious singularities can be treated identically to the physical matrix element. As such, the terms are built from three-parton antennae (used to remove the single unresolved limits) multiplied by another three-parton antenna (the remnant of the four-parton antenna after the single unresolved limit is taken) and a reduced matrix element which in the single unresolved limit maps on to the matrix element associated with the four-parton antenna. For a four-parton antenna

Configuration	X_4^0	$\tilde{X}_4^0$
Final-final	$A_4^0, B_4^0, C_4^0, D_{4,a}^0, E_{4,a}^0, \tilde{E}_4^0, F_{4,a}^0, G_4^0, \tilde{G}_4^0, H_4^0$	$\tilde{A}_4^0, D_{4,c}^0, E_{4,b}^0, F_{4,b}^0,$
Initial-final	$A_4^0, B_4^0, C_4^0, G_4^0, \tilde{G}_4^0, H_4^0$	$\tilde{A}_4^0, D_4^0, E_4^0, F_4^0$
Initial-initial	$A_4^0, B_4^0, C_4^0, D_{4,\text{adj}}^0 F_{4,\text{adj}}^0, G_4^0, \tilde{G}_4^0, H_4^0$	$\tilde{A}_4^0, D_{4,\text{n.adj}}^0, E_4^0, F_{4,\text{n.adj}}^0$

Table 4.7: The classification of the four-parton antenna functions based upon whether they contain almost colour-connected limits. The final state D_4^0, E_4^0 and F_4^0 antennae are decomposed into sub-antennae [35, 79] for numerical implementation.

function, this block has the generic form

$$
\begin{aligned}
\mathrm{d}\hat{\sigma}_{NNLO}^{S,b_2} &= -\mathcal{N}_{NNLO}^{RR} \sum_{n+2} \mathrm{d}\Phi_{n+2}(p_3, \ldots, p_{n+4}; p_1, p_2) \, \frac{1}{S_{n+2}} \\
&\times \sum_j X_3^0(i,j,k) \, X_3^0(I,K,l) \, M_{n+2}^0(\cdots, I', L, \cdots) \, J_n^{(n)}(\{p\}_n),
\end{aligned}
$$

(4.5.82)

where the sum is over all partons in the four-parton antenna which allow a single unresolved singularity. This block may also contain spurious almost colour connected singularities of its own, which can arise when the secondary antenna in (4.5.82) also contains single unresolved limits. The block of terms associated with each four-parton antenna encapsulates all of the single unresolved singularities of the four-parton antenna. As discussed in Section 4.5.2, a collection of terms which correctly mimic the single unresolved limits of the four-parton antenna functions performs a specific role when reintroduced as part of the real-virtual subtraction term.

Almost colour connected subtraction term, $\mathrm{d}\hat{\sigma}_{NNLO}^{S,c}$

This scenario occurs only when there are at least five partons in the scattering process. It is intimately linked to the four-parton antenna functions that contain almost colour connected unresolved partons, denoted by $\tilde{X}_4^0$; X_4^0 antennae do not give a contribution to $\mathrm{d}\hat{\sigma}_{NNLO}^{S,c}$. The classification of the four-parton antenna functions into X_4^0 and $\tilde{X}_4^0$ types is displayed in Table 4.7.

In almost colour connected limits, the terms in $\mathrm{d}\hat{\sigma}_{NNLO}^{S,b_2}$ can over-subtract the divergences of the associated $\tilde{X}_4^0$. In the same limits $\mathrm{d}\hat{\sigma}_{NNLO}^{S,a}$ contributes twice the subtraction required by the matrix elements. Both of these over-subtractions have

to be accounted for by $d\hat{\sigma}_{NNLO}^{S,c}$, which also includes the wide angle soft subtraction term [35, 108].

As a general algorithm for the construction of $d\hat{\sigma}_{NNLO}^{S,c}$, consider the four parton antenna $\tilde{X}_4^0(j, i, k, l)$. Partons j and l are hard radiators, bookending unresolved partons i and k. It is a final-final double unresolved configuration for clarity but the strategy also applies to initial-final and initial-initial configurations. Each $\tilde{X}_4^0$, in $d\hat{\sigma}_{NNLO}^{S,b_1}$ generates a block of terms in $d\hat{\sigma}_{NNLO}^{S,c}$, in addition to that in $d\hat{\sigma}_{NNLO}^{S,b_1}$ which is of the form

$$\tilde{X}_4^0(j, i, k, l) M_{n+2}^0(\cdots, a, \widetilde{(jik)}, \widetilde{(lki)}, b, \cdots), \tag{4.5.83}$$

where a and b are further hard partons in the colour ordering, as in Figure 4.4. The underlying colour ordering without the unresolved partons is thus $(\cdots a, j, l, b \cdots)$. The construction follows as

1. Radiate i from region I in Figure 4.4, then radiate k from region I of the remapped colour ordering, given that i is unresolved:

$$X_3^0(j, i, l) \; X_3^0(\widetilde{(ji)}, k, \widetilde{(il)}) \; M_n^0(\ldots, a, \widetilde{((ji)k)}, \widetilde{(k(il))}, b, \ldots). \tag{4.5.84}$$

   The reduced matrix element has a multiplicity of two fewer since two single unresolved mappings have taken place. This is the first term of the block.

2. Two further terms are produced by radiating i from region II or III first, followed by the radiation of k from region I of the remapped colour ordering. These terms come with a relative minus sign.

3. Repeat for the reverse ordering of the unresolved partons by making the substitution $i \leftrightarrow k$.

Written in terms of antennae, this contribution thus has the form,

$$+ \quad \frac{1}{2} X_3^0(j, i, l) \; X_3^0(\widetilde{(ji)}, k, \widetilde{(il)}) \; M_n^0(\ldots, a, \widetilde{((ji)k)}, \widetilde{(k(il))}, b, \ldots)$$
$$- \quad \frac{1}{2} X_3^0(a, i, j) \; X_3^0(\widetilde{(ji)}, k, l) \; M_n^0(\ldots, \widetilde{(ai)}, \widetilde{((ji)k)}, \widetilde{(kl)}, b, \ldots)$$
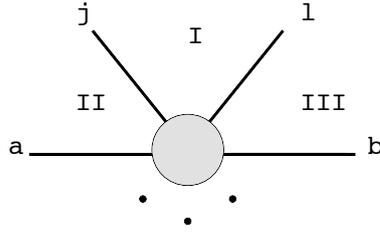
Figure 4.4: The three regions associated with the radiation of the primary unresolved parton. Region I: between the hard radiators of the four-parton antenna, j, l. Region II: one place to the left in the colour ordering between partons a, j. Region III: one place to the right in the colour ordering between partons l, b.

$$- \frac{1}{2} X_3^0(l, i, b) \, X_3^0(j, k, \widetilde{(li)}) \, M_n^0(\ldots, a, \widetilde{(jk)}, \widetilde{(k(li))}, \widetilde{(ib)}, \ldots) + (i \leftrightarrow k).$$

$$(4.5.85)$$

The large angle soft terms can also be included in this structure. Two almost colour-connected unresolved partons are removed from the underlying colour ordering and we impose the same radiation pattern of these partons from the underlying colour ordering as in (4.5.85). The mapping applied to the primary antenna does not matter because this term only contributes in the soft limit where all mappings become identical. For six or more parton processes, the large angle soft terms can be generated by allowing the first radiation to be between a pair of final-state partons [15]. In the special case of hadron-hadron initiated six parton scattering there will only ever be two hard final-state partons so the choice of final-state partons, between which the first unresolved parton is radiated, is unambiguous. However for five-parton processes there simply are not enough final-state partons and the first mapping should be of initial-final type. Four parton processes would require an initial-initial mapping, however in such a simple case there is no almost colour connected contribution. With the first mapping fixed to be of a particular type, the secondary antenna (which describes the radiation of the second unresolved parton) has common arguments across all terms, unlike in (4.5.85) where the arguments depend on the specific mapping inherited from the primary antenna. As a consequence, the secondary antenna can be factored out with the reduced matrix element so that, for example, in the final-final

mapping case, the large angle soft can have the form,

$$Y \cdot X_3^0(\widetilde{(ij)}, k, \widetilde{(il)}) \, M_n^0(\ldots, a, \widetilde{((ij)k)}, \widetilde{(k(il))}, b, \ldots), \tag{4.5.86}$$

where Y is a sum of large angle soft antennae. A similar structure emerges in the initial-final mapping case. The structure of this term can be understood with reference to Figure 4.4. For each region into which an unresolved parton can be radiated there is a term in Y given by,

$$-\frac{1}{2} \left[S_{\alpha i \beta} - S_{AIB} \right], \tag{4.5.87}$$

where I denotes the momentum of the unresolved parton i after the first mapping and for the example configuration considered in (4.5.85),

$$\begin{aligned}
(\alpha, \beta) &= \left\{ \left(a, \widetilde{(ij)} \right), \left(\widetilde{(ij)}, \widetilde{(il)} \right), \left(\widetilde{(il)}, b \right) \right\}, \\
(A, B) &= \left\{ \left(a, \widetilde{((ij)k)} \right), \left(\widetilde{((ij)k)}, \widetilde{(k(il))} \right), \left(\widetilde{(k(il))}, b \right) \right\},
\end{aligned} \tag{4.5.88}$$

The pair of soft functions for each region comes with an overall sign depending on which region the primary antenna belongs to, i.e., a relative minus sign for the regions II and III. Collecting the terms in (4.5.85) and the large angle soft terms produces a block of terms for a given $\tilde{X}_4^0$; the sum of such blocks constitutes $\mathrm{d}\hat{\sigma}_{NNLO}^{S,c}$,

$$\begin{aligned}
\mathrm{d}\hat{\sigma}_{NNLO}^{S,c} &= \mathcal{N}_{NNLO}^{RR} \sum_{n+2} \mathrm{d}\Phi_{n+2}(p_3, \ldots, p_{n+4}; p_1, p_2) \frac{1}{S_{n+2}} \sum_{i,k} \Bigg\{ \\
&+ \frac{1}{2} X_3^0(j, i, l) \, X_3^0(\widetilde{(ji)}, k, \widetilde{(il)}) \, M_n^0(\ldots, a, \widetilde{((ji)k)}, \widetilde{(k(il))}, b, \ldots) \\
&- \frac{1}{2} X_3^0(a, i, j) \, X_3^0(\widetilde{(ji)}, k, l) \, M_n^0(\ldots, \widetilde{(ai)}, \widetilde{((ji)k)}, \widetilde{(kl)}, b, \ldots) \\
&- \frac{1}{2} X_3^0(l, i, b) \, X_3^0(j, k, \widetilde{(li)}) \, M_n^0(\ldots, a, \widetilde{(jk)}, \widetilde{(k(li))}, \widetilde{(ib)}, \ldots) \\
&- \frac{1}{2} \Bigg[\left(S_{\widetilde{(ij)}, i, \widetilde{(il)}} - S_{\widetilde{((ij)k)} i \widetilde{(k(il))}} \right) \\
&\qquad - \left(S_{ai\widetilde{(ij)}} - S_{ai\widetilde{((ij)k)}} \right) - \left(S_{bi\widetilde{(il)}} - S_{bi\widetilde{((il)k)}} \right) \Bigg] \\
&\qquad X_3^0(\widetilde{(ij)}, k, \widetilde{(il)}) \, M_n^0(\ldots, a, \widetilde{((ij)k)}, \widetilde{(k(il))}, b, \ldots) \Bigg\} J_n^{(n)}(\{p\}_n),
\end{aligned}$$

$$(4.5.89)$$

where the sum over i, k denotes the set of almost colour-connected pairs contained within the $\tilde{X}_4^0$ antennae in $\mathrm{d}\hat{\sigma}_{NNLO}^{S,b_1}$. The blocks in $\mathrm{d}\hat{\sigma}_{NNLO}^{S,c}$ have a common secondary antenna and so when integrated over the single unresolved phase space of the primary antenna, will stay together as a group of integrated antenna functions factoring onto a common unintegrated antenna.

Colour disconnected subtraction term, $\mathrm{d}\hat{\sigma}_{NNLO}^{S,d}$

It is feasible for unresolved partons to be separated by greater than one hard radiator in a colour ordering when there are at least six coloured particles present. The subtraction terms in $\mathrm{d}\hat{\sigma}_{NNLO}^{S,a}$ take into account all possible single unresolved partons and so for each colour disconnected pair of unresolved partons, j and m, where parton j lies in the antenna function and m in the reduced matrix element, there is the corresponding subtraction term where m lies in the antenna and j in the reduced matrix element. In this double unresolved limit both of these subtraction terms tend to the same value and $\mathrm{d}\hat{\sigma}_{NNLO}^{S,a}$ exactly double-counts the divergence of the matrix elements.

To correct for this over-subtraction, a block of terms is introduced with the form,

$$
\begin{aligned}
\mathrm{d}\hat{\sigma}_{NNLO}^{S,d} \;=\; & -\mathcal{N}_{NNLO}^{RR} \sum_{n+2} \mathrm{d}\Phi_{n+2}(p_3, \ldots, p_{n+4}; p_1, p_2) \, \frac{1}{S_{n+2}} \\
& \times \; \sum_{j,m} X_3^0(i,j,k) \, X_3^0(l,m,n) \, M_{n+2}^0(\cdots, I, K, \cdots, L, N, \cdots) \, J_n^{(n)}(\{p\}_n).
\end{aligned}
$$

$$(4.5.90)$$

where the sum runs over pairs of partons separated by more than one hard parton in the ordering.

Both the unresolved partons can be integrated out immediately, since the regions of phase space over which they contribute are disconnected. With this in mind, we will add the integrated form of $\mathrm{d}\hat{\sigma}_{NNLO}^{S,d}$ back into the double virtual subtraction term.

4.5.2 Construction of the real-virtual subtraction term

The one-loop $(n+3)$-parton matrix elements contain both explicit poles and implicit IR divergences, both of which must be dealt with by the real-virtual subtraction term. In addition to imitating the physical one-loop matrix elements, the real-virtual subtraction term inherits terms from the double real subtraction term after analytic integration over a single unresolved parton. We see $\mathrm{d}\hat{\sigma}^T_{NNLO}$ containing three types of contribution:

1. $\mathrm{d}\hat{\sigma}^{T,a}$

    Terms of the type $\mathcal{X}^0_3$ that cancel the explicit poles in the virtual one-loop $(m+3)$-parton matrix elements.

2. $\mathrm{d}\hat{\sigma}^{T,b}$

    Terms that describe the single unresolved limits of the virtual one-loop $(m+3)$-parton matrix elements.

3. $\mathrm{d}\hat{\sigma}^{T,c}$

    Almost colour-connected contributions of the type $\mathcal{X}^0_3 X^0_3$.

The subtraction term for the real-virtual contribution can be further sub-divided into five contributions,

$$\mathrm{d}\hat{\sigma}^T_{NNLO} = \mathrm{d}\hat{\sigma}^{T,a}_{NNLO} + \mathrm{d}\hat{\sigma}^{T,b_1}_{NNLO} + \mathrm{d}\hat{\sigma}^{T,b_2}_{NNLO} + \mathrm{d}\hat{\sigma}^{T,b_3}_{NNLO} + \mathrm{d}\hat{\sigma}^{T,c}_{NNLO}. \quad (4.5.91)$$

We proceed by describing each in turn, including whether the terms originate and terminate in the double real, real-virtual and double virtual contribution. First however we introduce the mass factorisation term at real-virtual level.

Real-virtual mass factorisation term, $\mathrm{d}\hat{\sigma}^{MF,1}_{ij,NNLO}$

The NNLO real-virtual mass factorisation contribution of Eq. (4.5.71) can be further divided,

$$\mathrm{d}\hat{\sigma}^{MF,1}_{ij,NNLO} = \mathrm{d}\hat{\sigma}^{MF,1,a}_{ij,NNLO} + \mathrm{d}\hat{\sigma}^{MF,1,b}_{ij,NNLO}, \quad (4.5.92)$$

such that $\mathrm{d}\hat{\sigma}_{ij,NNLO}^{MF,1,a}$ is proportional to the $(n+3)$-parton matrix elements,

$$
\begin{aligned}
\mathrm{d}\hat{\sigma}_{ij,NNLO}^{MF,1,a}(\xi_1 H_1, \xi_2 H_2) &= -\int \frac{\mathrm{d}x_1}{x_1}\frac{\mathrm{d}x_2}{x_2} \\
&\times \left(\frac{\alpha_s N}{2\pi}\right) \bar{C}(\epsilon)\, \Gamma_{ij;kl}^{(1)}(x_1, x_2)\, \mathrm{d}\hat{\sigma}_{kl,NLO}^{R}(x_1\xi_1 H_1, x_2\xi_2 H_2),
\end{aligned}
$$

$$(4.5.93)$$

which will contribute to $\mathrm{d}\hat{\sigma}_{NNLO}^{T,a}$ and $\mathrm{d}\hat{\sigma}_{ij,NNLO}^{MF,1,b}$, which contributes to $\mathrm{d}\hat{\sigma}_{NNLO}^{T,b}$.

$$
\mathrm{d}\hat{\sigma}_{ij,NNLO}^{MF,1,b} = \mathrm{d}\hat{\sigma}_{ij,NNLO}^{MF,1,b_2}, \tag{4.5.94}
$$

where,

$$
\begin{aligned}
\mathrm{d}\hat{\sigma}_{ij,NNLO}^{MF,1,b_2}(\xi_1 H_1, \xi_2 H_2) &= \int \frac{\mathrm{d}x_1}{x_1}\frac{\mathrm{d}x_2}{x_2} \\
&\times \left(\frac{\alpha_s N}{2\pi}\right) \bar{C}(\epsilon)\, \Gamma_{ij;kl}^{(1)}(x_1, x_2)\, \mathrm{d}\hat{\sigma}_{kl,NLO}^{S}(x_1\xi_1 H_1, x_2\xi_2 H_2).
\end{aligned}
$$

$$(4.5.95)$$

However, to simplify the book-keeping in the construction of the real-virtual subtraction terms it proves useful to trivially rewrite $\mathrm{d}\hat{\sigma}_{ij,NNLO}^{MF,1,b}$ in the following way,

$$
\mathrm{d}\hat{\sigma}_{ij,NNLO}^{MF,1,b} = \mathrm{d}\hat{\sigma}_{ij,NNLO}^{MF,1,b_1} + \mathrm{d}\hat{\sigma}_{ij,NNLO}^{MF,1,b_2} + \mathrm{d}\hat{\sigma}_{ij,NNLO}^{MF,1,b_3}, \tag{4.5.96}
$$

where we have added and subtracted,

$$
\begin{aligned}
\mathrm{d}\hat{\sigma}_{ij,NNLO}^{MF,1,b_1}(\xi_1 H_1, \xi_2 H_2) &= \int \frac{\mathrm{d}x_1}{x_1}\frac{\mathrm{d}x_2}{x_2} \\
&\times \left(\frac{\alpha_s N}{2\pi}\right) \bar{C}(\epsilon)\, \Gamma_{ab;ab}^{(1)}(x_1, x_2)\, \mathrm{d}\hat{\sigma}_{ij,NLO}^{S}(x_1\xi_1 H_1, x_2\xi_2 H_2),
\end{aligned}
$$

$$(4.5.97)$$

$$
\mathrm{d}\hat{\sigma}_{ij,NNLO}^{MF,1,b_3}(\xi_1 H_1, \xi_2 H_2) = -\mathrm{d}\hat{\sigma}_{ij,NNLO}^{MF,1,b_1}(\xi_1 H_1, \xi_2 H_2). \tag{4.5.98}
$$

The parton distributions that multiply these contributions to the partonic cross section are always fixed by the identity of partons i and j, which, in the initial-final (and initial-initial) configurations, are always of the same type as one (or both) partons

involved in the antenna. However, in certain collinear limits, the type of parton can change, e.g. a gluon may transform into a quark or vice versa. Eqs. (4.5.97) and (4.5.98) describe these situations. In such a situation, there is a change in the parton flavour in the reduced matrix element, even though the antenna correctly describes the singularity of the physical matrix element. In Eq. (4.5.97) a and b represent the species of the initial-state partons in the reduced matrix element in $d\hat{\sigma}^S_{ij,NLO}$ rather than the initial-state partons i and j that are involved in the antenna. Thus for unresolved limits that do not change the identities of initial-state partons then $a = i$ and $b = j$. However, in an identity changing initial-state collinear limit there will be a discrepancy between the parton species in the antenna, i, j and those in the reduced matrix element, a, b. For example, consider a subtraction term $d\hat{\sigma}^S_{qg,NLO}$ that contains a term,

$$d\hat{\sigma}^S_{qg,NLO} \quad \sim \quad \cdots + A^0_3(\hat{1}_q, \hat{2}_g, 3_{\bar{q}}) \, M^0_n(\cdots ; \hat{\bar{1}}_q, \hat{\bar{2}}_{\bar{q}}; \cdots) \, J^{(n)}_n(\{p\}_n), \quad (4.5.99)$$

where in the $\hat{2}_g || 3_{\bar{q}}$ limit, the initial state gluon transforms into an antiquark. In this case the initial-state partons involved in the antenna $A^0_3(\hat{1}_q, \hat{2}_g, 3_{\bar{q}})$ are $(i, j) \equiv (q, g)$ while the initial-state parton species in the reduced matrix element $M^0_n(\cdots ; \hat{\bar{1}}_q, \hat{\bar{2}}_{\bar{q}}; \cdots)$ are $(a, b) \equiv (q, \bar{q})$. In other words, $i = a = q$, while the labels associated with parton $\hat{2}$ differ, $j = g$ and $b = \bar{q}$. In this example the mass factorisation kernel used in Eq. (4.5.97) is given by $\Gamma^{(1)}_{q\bar{q};q\bar{q}}(x_1, x_2)$.

One-loop explicit pole subtraction term, $d\hat{\sigma}^{T,a}_{NNLO}$

It was emphasised in Section 4.5.1 that the construction of $d\hat{\sigma}^{S,a}_{NNLO}$ follows the same lines as constructing $d\hat{\sigma}^S_{NLO}$ with a modified jet function and an additional parton. This matches the interpretation of the mass factorisation contribution $d\hat{\sigma}^{MF,1,a}_{NNLO}$ and so integrating the antennae in $d\hat{\sigma}^{S,a}_{NNLO}$ and combining with the mass factorisation kernels in $d\hat{\sigma}^{MF,1,a}_{NNLO}$ will generate precisely the same type of integrated antenna strings seen at NLO but with one additional parton,

$$d\hat{\sigma}^{T,a}_{NNLO} \quad = \quad -\int_1 d\hat{\sigma}^{S,a}_{NNLO} - d\hat{\sigma}^{MF,1,a}_{NNLO}$$

$$
\begin{aligned}
= \ & -\mathcal{N}_{NNLO}^{RV} \sum_{n+1} \int \frac{\mathrm{d}x_1}{x_1} \frac{\mathrm{d}x_2}{x_2} \, \mathrm{d}\Phi_{n+1}(p_3, \ldots, p_{n+3}; x_1 p_1, x_2 p_2) \, \frac{1}{S_{n+1}} \\
& \times \ \boldsymbol{J}_{n+3}^{(1)}(1, \ldots, n+3) \, M_{n+3}^0(1, \ldots, n+3) \, J_n^{(n+1)}(\{p\}_{n+1}),
\end{aligned}
\qquad (4.5.100)
$$

where $\mathcal{N}_{NNLO}^{RV} = C(\epsilon)\mathcal{N}_{NNLO}^{RR}$. We showed in Section 4.4 that the poles of $\boldsymbol{J}_{n+2}^{(1)}$ are simply related to the poles of the $(n+2)$-parton one-loop matrix elements. Using this fact, it is clear that the term $\mathrm{d}\hat{\sigma}_{NNLO}^{T,a}$ correctly subtracts the explicit poles of the real-virtual matrix elements. This holds for all points in phase space; we must now address the dynamic poles of the one-loop matrix element arising in single unresolved scenarios.

Tree $\times$ loop subtraction term, $\mathrm{d}\hat{\sigma}_{NNLO}^{T,b_1}$

One-loop matrix elements factorise in implicit IR singular limits into two terms [27] which can be schematically understood as,

$$
\text{1-loop} \ \longrightarrow \ (\text{tree} \times \text{loop}) \ + \ (\text{loop} \times \text{tree}).
$$

The first term is the product of a tree-level singular function factoring onto a one-loop reduced matrix element and is subtracted using a tree level antenna function and a one-loop reduced matrix element. This term by itself removes part of the implicit IR divergence of the one-loop matrix elements but introduces explicit poles associated with the one-loop $(n+2)$-parton reduced matrix element. The explicit poles of this matrix element can be removed by introducing the appropriate integrated antenna string so that, after including the mass factorisation contribution $\mathrm{d}\hat{\sigma}_{NNLO}^{MF,1,b_1}$, defined in Eq. (4.5.97),

$$
\begin{aligned}
\mathrm{d}\hat{\sigma}_{NNLO}^{T,b_1} = \ & \mathcal{N}_{NNLO}^{RV} \sum_{n+1} \int \frac{\mathrm{d}x_1}{x_1} \frac{\mathrm{d}x_2}{x_2} \, \mathrm{d}\Phi_{n+1}(p_3, \ldots, p_{n+3}; x_1 p_1, x_2 p_2) \, \frac{1}{S_{n+1}} \\
& \times \sum_j X_3^0(i,j,k) \Bigg\{ \delta(1-x_1)\delta(1-x_2) \, M_{n+2}^1(1, \ldots, n+2) \\
& \qquad\qquad + c_J \boldsymbol{J}_{n+2}^{(1)}(1, \ldots, n+2) \, M_{n+2}^0(1, \ldots, n+2) \Bigg\} J_n^{(n)}(\{p\}_n),
\end{aligned}
$$
$$
(4.5.101)
$$

is free from explicit IR poles and where the sum is over the final-state unresolved partons. c_J is a constant equal to unity unless $n = 0$ and all particles are gluons in which case $c_J = 2$ to account for both colour orderings of the gluons. This formula can be applied to final-final, initial-final and initial-initial configurations.

Loop × tree subtraction term, $\mathrm{d}\hat{\sigma}_{NNLO}^{T,b_2}$

To account for the contribution from the one-loop singular function factoring onto the tree-level matrix element, a subtraction term is constructed from a one-loop antenna function and a tree-level reduced matrix element. The one-loop antenna function contains explicit IR poles which must be removed to ensure a finite total contribution. This goal is achieved by a difference of integrated antenna strings which contains the IR explicit poles of the one-loop antenna, and reflects the construction of X_3^1 in (4.3.30). The mass factorisation terms $\mathrm{d}\hat{\sigma}_{NNLO}^{MF,1,b_2}$ and $\mathrm{d}\hat{\sigma}_{NNLO}^{MF,1,b_3}$, defined in Eqs. (4.5.95) and (4.5.98) respectively, are combined with the integrated antennae to cancel fully the explicit IR poles of the one-loop antenna functions:

$$
\begin{aligned}
\mathrm{d}\hat{\sigma}_{NNLO}^{T,b_2} \;=\; & \mathcal{N}_{NNLO}^{RV} \sum_{n+1} \int \frac{\mathrm{d}x_1}{x_1} \frac{\mathrm{d}x_2}{x_2} \, \mathrm{d}\Phi_{n+1}(p_3,\ldots,p_{n+3};x_1 p_1, x_2 p_2) \, \frac{1}{S_{n+1}} \\
\times \; & \sum_j \Big[X_3^1(i,j,k)\delta(1-x_1)\delta(1-x_2) + \boldsymbol{J}_X^{(1)}(i,j,k) X_3^0(i,j,k) \\
- \; & M_X X_3^0(i,j,k) \boldsymbol{J}_2^{(1)}(I,K) \Big] M_{n+2}^0(\cdots,I,K,\cdots) \, J_n^{(n)}(\{p\}_n),
\end{aligned}
$$

$$(4.5.102)$$

where M_X is a constant which depends on the species of one-loop antenna, X_3^1. The string $\boldsymbol{J}_X^{(1)}$ is constructed as a sum of N_X two-particle integrated antenna strings,

$$
\boldsymbol{J}_X^{(1)} \;=\; \sum_{(i,j)=1}^{N_X} \boldsymbol{J}_2^{(1)}(i,j),
\tag{4.5.103}
$$

where N_X counts the number of colour-connected pairs of partons in the one-loop antenna. The values of M_X and N_X are displayed in Table 4.8. This subtraction term applies to all kinematic configurations and particle combinations. The mass

X_3^1	A_3^1	$\tilde{A}_3^1$	$\hat{A}_3^1$	D_3^1	$\hat{D}_3^1$	E_3^1	$\tilde{E}_3^1$	$\hat{E}_3^1$	F_3^1	$\hat{F}_3^1$	G_3^1	$\tilde{G}_3^1$	$\hat{G}_3^1$
N_X	2	1	2	3	3	2	1	0	3	3	2	1	0
M_X	1	1	0	2	2	2	0	2	2	2	2	0	2

Table 4.8: Number of colour-connected pairs N_X for the one-loop antenna X_3^1, and the associated constant M_X.

factorisation kernels used to form the $\boldsymbol{J}_X^{(1)}$ come from $\mathrm{d}\hat{\sigma}_{NNLO}^{MF,1,b_2}$ and those used to generate $\boldsymbol{J}_2^{(1)}$ come from $\mathrm{d}\hat{\sigma}_{NNLO}^{MF,1,b_3}$. The term proportional to $\boldsymbol{J}_X^{(1)}$ is derived from the integral of the double real subtraction term. Following the discussion in Section 4.4, the poles of a four-parton matrix element integrated over the single unresolved phase space may be encapsulated by an integrated antenna string. Schematically,

$$\mathcal{P}oles\left[\int_1 M_4^0\right] = \mathcal{P}oles\left[\boldsymbol{J}_3^{(1)} M_3^0\right] = -\mathcal{P}oles\left[M_3^1\right], \qquad (4.5.104)$$

and therefore the single unresolved poles of a four-parton antenna are also described by,

$$\mathcal{P}oles\left[\int_1 X_4^0\right] = \mathcal{P}oles\left[\boldsymbol{J}_X^{(1)} X_3^0\right] = -\mathcal{P}oles\left[X_3^1\right]. \qquad (4.5.105)$$

In Section 4.5.1, $\mathrm{d}\hat{\sigma}_{NNLO}^{S,b}$ was constructed to have no single unresolved limits such that,

$$\mathcal{P}oles\left[\int_1 \mathrm{d}\hat{\sigma}_{NNLO}^{S,b}\right] = 0. \qquad (4.5.106)$$

Equivalently,

$$\mathcal{P}oles\left[\int_1 \mathrm{d}\hat{\sigma}_{NNLO}^{S,b_1}\right] = -\mathcal{P}oles\left[\int_1 \mathrm{d}\hat{\sigma}_{NNLO}^{S,b_2}\right]. \qquad (4.5.107)$$

For each X_4^0 or $\tilde{X}_4^0$ contributing to $\mathrm{d}\hat{\sigma}_{NNLO}^{S,b_1}$, the associated block of iterated antennae in $\mathrm{d}\hat{\sigma}_{NNLO}^{S,b_2}$ integrated over the single unresolved phase space therefore systematically generates a singular contribution of the form, $\boldsymbol{J}_X^{(1)}(i,j,k)X_3^0(i,j,k)$, as required by Eq. (4.5.102).

The one-loop antenna term, X_3^1, and the two-parton integrated antenna string,

$J_2^{(1)}$, in Eq. (4.5.102) do not come from the double real subtraction term and so must be compensated for in the double virtual subtraction term.

One-loop renormalisation subtraction term, $d\hat{\sigma}_{NNLO}^{T,b_3}$

In the real-virtual subtraction term, two one-loop quantities are introduced: the one-loop reduced matrix elements in (4.5.101) and the one-loop antenna functions in (4.5.102). The one-loop matrix elements are renormalised at the renormalisation scale μ^2 whereas the one-loop antenna is renormalised at the mass scale of the antenna s_{ijk}. To ensure both quantities are renormalised at the same scale, the replacement is made,

$$X_3^1(i,j,k) \quad \rightarrow \quad X_3^1(i,j,k) + \frac{\beta_0}{\epsilon} X_3^0(i,j,k) \left(\left(\frac{|s_{ijk}|}{\mu^2} \right)^{-\epsilon} - 1 \right). \quad (4.5.108)$$

In doing so, we pick up a further term proportional to β_0, via an expansion in the ratio of scales;

$$
\begin{aligned}
d\hat{\sigma}_{NNLO}^{T,b_3} &= \mathcal{N}_{NNLO}^{RV} \sum_{n+1} \int \frac{dx_1}{x_1} \frac{dx_2}{x_2} \, d\Phi_{n+1}(p_3, \ldots, p_{n+3}; x_1 p_1, x_2 p_2) \, \frac{1}{S_{n+1}} \\
&\times \quad \sum_j \beta_0 \log\left(\frac{\mu^2}{|s_{ijk}|} \right) X_3^0(i,j,k) \delta(1-x_1)\delta(1-x_2) \\
&\times \quad M_{n+2}^0(\cdots, I, K, \cdots) \, J_n^{(n)}(\{p\}_n),
\end{aligned}
\quad (4.5.109)
$$

where the sum is the same as in (4.5.102). There is also a colour decomposition of β_0 into terms proportional to N and N_F,

$$\beta_0 = b_0 N + b_{0,F} N_F, \quad (4.5.110)$$

where $b_0 = 11/6$ and $b_{0,F} = -1/3$. The terms in $d\hat{\sigma}_{NNLO}^{T,b_3}$ originate in the real-virtual subtraction term and so, by integrating the three-parton antenna over the single-unresolved phase space, are reintroduced as part of the double virtual subtraction term.

Integrated almost colour connected subtraction term, $\mathrm{d}\hat{\sigma}_{NNLO}^{T,c}$

To complete the real-virtual subtraction term, we must include the analytic integration of $\mathrm{d}\hat{\sigma}_{NNLO}^{S,c}$ over the single unresolved antenna phase space with additional predictable terms to ensure an IR finite contribution. Integrating Eq. (4.5.89) over the single unresolved phase space and introducing three additional terms to ensure all explicit IR poles are cancelled yields,

$$
\begin{aligned}
\mathrm{d}\hat{\sigma}_{NNLO}^{T,c} =\ & -\mathcal{N}_{NNLO}^{RV} \sum_{n+1} \int \frac{\mathrm{d}x_1}{x_1}\frac{\mathrm{d}x_2}{x_2}\, \mathrm{d}\Phi_{n+1}(p_3,\ldots,p_{n+3};x_1 p_1, x_2 p_2)\, \frac{1}{S_{n+1}} \Bigg\{ \\
& \frac{1}{2} \sum_j \Bigg[\Bigg(\left(\mathcal{X}_3^0(s_{ik}) - \mathcal{X}_3^0(s_{(ij)(jk)})\right) \\
& - \left(\mathcal{X}_3^0(s_{ai}) - \mathcal{X}_3^0(s_{a(ij)})\right) - \left(\mathcal{X}_3^0(s_{kb}) - \mathcal{X}_3^0(s_{(kj)b})\right) \Bigg) \\
& - \Bigg(\left(\mathcal{S}(s_{ik}, s_{ik}, 1) - \mathcal{S}(s_{(ij)(jk)}, s_{ik}, x_{(ij)(jk),ik})\right) \\
& - \left(\mathcal{S}(s_{ai}, s_{ik}, x_{ai,ik}) - \mathcal{S}(s_{a(ij)}, s_{ik}, x_{a(ij),ik})\right) \\
& - \left(\mathcal{S}(s_{kb}, s_{ik}, x_{kb,ik}) - \mathcal{S}(s_{(kj)b}, s_{ik}, x_{(kj)b,ik})\right) \Bigg) \delta(1-x_1)\delta(1-x_2) \Bigg] \Bigg\} \\
& \times\ X_3^0(i,j,k)\, M_{n+2}^0(\cdots, I, K, \cdots)\, J_n^{(n)}(\{p\}_n). \tag{4.5.111}
\end{aligned}
$$

In this equation, the terms introduced to ensure IR finiteness are those involving the integrated antennae with mapped momenta, $\mathcal{X}_3^0(s_{(ij)(jk)})$, $\mathcal{X}_3^0(s_{a(ij)})$ and $\mathcal{X}_3^0(s_{(kj)b})$. These terms must therefore appear in the double virtual subtraction term. For future reference we label these as,

$$
\begin{aligned}
\mathrm{d}\hat{\sigma}_{NNLO}^{T,c_1} =\ & -\mathcal{N}_{NNLO}^{RV} \sum_{n+1} \int \frac{\mathrm{d}x_1}{x_1}\frac{\mathrm{d}x_2}{x_2}\, \mathrm{d}\Phi_{n+1}(p_3,\ldots,p_{n+3};x_1 p_1, x_2 p_2)\, \frac{1}{S_{n+1}} \\
& \times\ \frac{1}{2} \sum_j \left[\mathcal{X}_3^0(s_{(ij)(jk)}) + \mathcal{X}_3^0(s_{a(ij)}) + \mathcal{X}_3^0(s_{(kj)b}) \right] \\
& \times\ X_3^0(i,j,k)\, M_{n+2}^0(\cdots, I, K, \cdots)\, J_n^{(n)}(\{p\}_n), \tag{4.5.112} \\
\mathrm{d}\hat{\sigma}_{NNLO}^{T,c_2} =\ & +\mathcal{N}_{NNLO}^{RV} \sum_{n+1} \int \frac{\mathrm{d}x_1}{x_1}\frac{\mathrm{d}x_2}{x_2}\, \mathrm{d}\Phi_{n+1}(p_3,\ldots,p_{n+3};x_1 p_1, x_2 p_2)\, \frac{1}{S_{n+1}} \\
& \times\ \sum_j \mathcal{X}_3^0(s_{(ij)(jk)})\, X_3^0(i,j,k)\, M_{n+2}^0(\cdots, I, K, \cdots)\, J_n^{(n)}(\{p\}_n).
\end{aligned}
$$

$$\tag{4.5.113}$$

The integrated soft function for the final-final mapping is denoted by $\mathcal{S}(s_{ac}, s_{ik}, x_{ac,ik})$. An explicit expression can be found in Ref. [15]. As discussed in Section 4.5.1, for five-parton processes it is necessary to use a soft function with an initial-final map. In this case one finds an analogous equation to Eq. (4.5.111) involving the integrated initial-final soft function, $\mathcal{S}^{IF}(s_{ac}, s_{IK}, y_{ac,iK})$, which is given explicitly in [97].

4.5.3   Double virtual subtraction term structure

The double virtual contribution to the $pp \to n$-jet cross section involves the two-loop $(n + 2)$-parton matrix elements, which have no implicit IR divergence in any regions of the appropriate n-parton phase space. The explicit IR poles of the two-loop contribution are cancelled by the remaining integrated form of the subtraction terms, combined with the double-virtual mass factorisation terms. The main result here is that the double virtual subtraction term is constructed from three terms,

$$\mathrm{d}\hat{\sigma}^{U}_{ij,NNLO} = \mathrm{d}\hat{\sigma}^{U,A}_{ij,NNLO} + \mathrm{d}\hat{\sigma}^{U,B}_{ij,NNLO} + \mathrm{d}\hat{\sigma}^{U,C}_{ij,NNLO}. \tag{4.5.114}$$

We shall now demonstrate the origin of each of these terms. This construction reflects the dipole-like singularity structure for two-loop amplitudes made apparent in Catani's two-loop factorisation formula introduced in (2.1.19) and [20].

$$
\begin{aligned}
\mathcal{P}oles\big(M_n^2(1,\cdots,n)\big) = \; & 2\boldsymbol{I}_n^{(1)}(\epsilon; 1, \cdots, n)\left(M_n^1(1,\cdots,n) - \frac{\beta_0}{\epsilon} M_n^0(1 \cdots, n) \right) \\
& - \; 2\boldsymbol{I}_n^{(1)}(\epsilon; 1, \cdots, n)^2 M_n^0(1, \cdots, n) \\
& + \; 2e^{-\epsilon\gamma} \frac{\Gamma(1-2\epsilon)}{\Gamma(1-\epsilon)}\left(\frac{\beta_0}{\epsilon} + K \right) \boldsymbol{I}_n^{(1)}(2\epsilon; 1 \cdots, n) M_n^0(1 \cdots, n) \\
& + \; 2\boldsymbol{H}^{(2)}(\epsilon) M_n^0(1, \cdots, n), \tag{4.5.115}
\end{aligned}
$$

with $\boldsymbol{I}_n^{(1)}(\epsilon)$ given by Eq. (4.4.69) and where the form of the hard function, $\boldsymbol{H}^{(2)}(\epsilon)$ and the constant K depends on the particle content and order in N under consideration.

Double virtual mass factorisation terms, $d\hat{\sigma}_{NNLO}^{MF,2}$

The general form of the double virtual mass factorisation contribution was given in Eq. (4.5.72). To elucidate the construction of the double virtual subtraction term, $\Gamma_{ij;kl}^{(2)}(z_1, z_2)$ may be decomposed in the following way,

$$\Gamma_{ij;kl}^{(2)}(z_1, z_2) = \overline{\Gamma}_{ij;kl}^{(2)}(z_1, z_2) - \frac{\beta_0}{\epsilon}\Gamma_{ij;kl}^{(1)}(z_1, z_2) + \frac{1}{2}\big[\Gamma_{ij;ab}^{(1)} \otimes \Gamma_{ab;kl}^{(1)}\big](z_1, z_2),$$
(4.5.116)

such that,

$$\overline{\Gamma}_{ij;kl}^{(2)}(z_1, z_2) = \overline{\Gamma}_{ik}^{(2)}(z_1)\delta_{jl}\delta(1 - z_2) + \overline{\Gamma}_{jl}^{(2)}(z_2)\delta_{ik}\delta(1 - z_1),$$
$$\overline{\Gamma}_{ij}^{(2)}(z) = -\frac{1}{2\epsilon}\left(p_{ij}^1(z) + \frac{\beta_0}{\epsilon}p_{ij}^0(z)\right).$$
(4.5.117)

The double virtual mass factorisation contribution can be recast into three terms,

$$d\hat{\sigma}_{ij,NNLO}^{MF,2} = d\hat{\sigma}_{ij,NNLO}^{MF,2,A} + d\hat{\sigma}_{ij,NNLO}^{MF,2,B} + d\hat{\sigma}_{ij,NNLO}^{MF,C},$$
(4.5.118)

where the individual contributions are given by:

$$d\hat{\sigma}_{ij,NNLO}^{MF,2,A} = -\int \frac{dz_1}{z_1}\frac{dz_2}{z_2}\left(\frac{\alpha_s N}{2\pi}\right)\bar{C}(\epsilon)\,\Gamma_{ij;kl}^{(1)}\left(d\hat{\sigma}_{kl,NLO}^V - \frac{\beta_0}{\epsilon}d\hat{\sigma}_{kl,LO}\right),$$
(4.5.119)

$$d\hat{\sigma}_{ij,NNLO}^{MF,2,B} = +\int \frac{dz_1}{z_1}\frac{dz_2}{z_2}\left(\frac{\alpha_s N}{2\pi}\right)\bar{C}(\epsilon)\,\Gamma_{ij;kl}^{(1)}d\hat{\sigma}_{kl,NLO}^T$$
$$-\int \frac{dz_1}{z_1}\frac{dz_2}{z_2}\left(\frac{\alpha_s N}{2\pi}\right)^2\bar{C}(\epsilon)^2\frac{1}{2}\big[\Gamma_{ij;ab}^{(1)} \otimes \Gamma_{ab;kl}^{(1)}\big]d\hat{\sigma}_{kl,LO},$$
(4.5.120)

$$d\hat{\sigma}_{ij,NNLO}^{MF,2,C} = -\int \frac{dz_1}{z_1}\frac{dz_2}{z_2}\left(\frac{\alpha_s N}{2\pi}\right)^2\bar{C}(\epsilon)^2\overline{\Gamma}_{ij;kl}^{(2)}\,d\hat{\sigma}_{kl,LO}.$$
(4.5.121)

The convolution of two functions $f(x_1, x_2)$ and $g(y_1, y_2)$ is defined as

$$\big[f \otimes g\big](z_1, z_2) \equiv \int dx_1 dx_2 dy_1 dy_2 f(x_1, x_2)g(y_1, y_2)\delta(z_1 - x_1 y_1)\delta(z_2 - x_2 y_2).$$
(4.5.122)

Each of these terms naturally fits into the corresponding piece of the double virtual subtraction term $\mathrm{d}\hat{\sigma}_{ij,NNLO}^{U,A}$, $\mathrm{d}\hat{\sigma}_{ij,NNLO}^{U,B}$, and $\mathrm{d}\hat{\sigma}_{ij,NNLO}^{U,C}$, to render each contribution free from initial-state collinear poles.

$\mathrm{d}\hat{\sigma}_{NNLO}^{U,A}$ subtraction term

The first double virtual subtraction term is constructed from the integrated real-virtual subtraction terms, and the appropriate mass factorisation contributions. This includes the integrated $\mathrm{d}\hat{\sigma}_{NNLO}^{T,b_1}$ given in Eq. (4.5.101), the tree level antennae multiplying the one loop matrix element. The second term comes from the integrated form of $\mathrm{d}\hat{\sigma}_{NNLO}^{T,b_3}$,

$$
\begin{aligned}
\int_1 \mathrm{d}\hat{\sigma}_{ij,NNLO}^{T,b_3} &= -\mathcal{N}_{NNLO}^{VV} \sum_n \int \frac{\mathrm{d}z_1}{z_1}\frac{\mathrm{d}z_2}{z_2}\, \mathrm{d}\Phi_n(p_3,\ldots,p_{n+2};z_1p_1,z_2p_2)\, \frac{1}{S_n} \\
&\times \sum_{\{i,j\}} \frac{\beta_0}{\epsilon}\left(\left(\frac{|s_{ij}|}{\mu^2}\right)^{-\epsilon} - 1\right) \mathcal{X}_3^0(s_{ij}) M_{n+2}^0(1,\cdots,n+2) J_n^{(n)}(\{p\}_n),
\end{aligned}
$$

$$(4.5.123)$$

where $\mathcal{N}_{NNLO}^{VV} = C(\epsilon)\mathcal{N}_{NNLO}^{RV} = C(\epsilon)^2 \mathcal{N}_{NNLO}^{RR}$. We extract two separate terms from (4.5.123), sending the first term (proportional to $(|s_{ij}|^{-\epsilon})$) into $\mathrm{d}\hat{\sigma}_{NNLO}^{U,C}$, whilst the second, proportional to -1, is combined with the one-loop matrix element term from the integral of $\mathrm{d}\hat{\sigma}_{NNLO}^{T,b_1}$ and the mass factorisation term $\mathrm{d}\hat{\sigma}_{NNLO}^{MF,2,A}$. The result is the first double virtual subtraction term,

$$
\begin{aligned}
\mathrm{d}\hat{\sigma}_{ij,NNLO}^{U,A} = -\mathcal{N}_{NNLO}^{VV} \sum_n \int \frac{\mathrm{d}z_1}{z_1}\frac{\mathrm{d}z_2}{z_2}\, \mathrm{d}\Phi_n(p_3,\ldots,p_{n+2};z_1p_1,z_2p_2)\, \frac{1}{S_n} \\
\times\ \boldsymbol{J}_{n+2}^{(1)}(1,\cdots,n+2)\left(M_{n+2}^1(1,\cdots,n+2) - \frac{\beta_0}{\epsilon}\, M_{n+2}^0(1,\cdots,n+2)\right) J_n^{(n)}(\{p\}_n).
\end{aligned}
$$

$$(4.5.124)$$

The poles of the integrated antenna string are directly related to the poles of Catani's one-loop insertion operator; this contribution to the double virtual cross section contains the $1/\epsilon^4$ and $1/\epsilon^3$ singular contributions given in the first line of Eq. (4.5.115).

Crucially, $\mathrm{d}\hat{\sigma}_{NNLO}^{U,A}$ does not contain precisely the same singularities at $1/\epsilon^2$ and

above as the first line of Eq. (4.5.115) because the finite difference between $\boldsymbol{J}_n^{(1)}$ and $\boldsymbol{I}_n^{(1)}$ is formally of order ϵ^0. These differences ultimately cancel against similar terms in $\mathrm{d}\hat{\sigma}_{NNLO}^{U,B}$ and $\mathrm{d}\hat{\sigma}_{NNLO}^{U,C}$.

$\mathrm{d}\hat{\sigma}_{NNLO}^{U,B}$ subtraction term

The second double virtual subtraction term is formed from the integral of the remaining term from $\mathrm{d}\hat{\sigma}_{ij,NNLO}^{T,b_1}$ (4.5.101) proportional to M_n^0, the integral of $\mathrm{d}\hat{\sigma}_{NNLO}^{T,c_1}$ (4.5.113) and $\mathrm{d}\hat{\sigma}_{NNLO}^{S,d}$ (4.5.90), and the mass factorisation contribution $\mathrm{d}\hat{\sigma}_{NNLO}^{MF,2,B}$. The resultant subtraction term is given by,

$$
\begin{aligned}
\mathrm{d}\hat{\sigma}_{ij,NNLO}^{U,B} \;=\; & -\mathcal{N}_{NNLO}^{VV} \sum_n \int \frac{\mathrm{d}z_1}{z_1}\frac{\mathrm{d}z_2}{z_2}\, \mathrm{d}\Phi_n(p_3,\dots,p_{n+2};z_1p_1,z_2p_2)\,\frac{1}{S_n} \\
& \times\; \frac{1}{2}\big[\boldsymbol{J}_{n+2}^{(1)}(1,\cdots,n+2)\otimes\boldsymbol{J}_{n+2}^{(1)}(1,\cdots,n+2)\big](z_1,z_2) \\
& \times\; M_{n+2}^0(1,\cdots,n+2)\,J_n^{(n)}(\{p\}_n).
\end{aligned}
\tag{4.5.125}
$$

It can be seen that this expression matches up with the pole structure of the second line of Eq. (4.5.115) with additional singular contributions arising from the finite differences between $\boldsymbol{J}_n^{(1)}$ and $\boldsymbol{I}_n^{(1)}$ at $\mathcal{O}(\epsilon^0)$ and higher orders.

Note that the combination of Eqs. (4.5.124) and (4.5.125) reproduce the pole structure of the first two lines of Eq. (4.5.115) up to $\mathcal{O}(1/\epsilon)$.

$\mathrm{d}\hat{\sigma}_{NNLO}^{U,C}$ subtraction term

The last term is constructed by integrating appropriate terms in the remaining double real and real-virtual subtraction terms, $\mathrm{d}\hat{\sigma}_{NNLO}^{S,b_1}$ (4.5.80), $\mathrm{d}\hat{\sigma}_{NNLO}^{T,b_2}$ (4.5.102), $\mathrm{d}\hat{\sigma}_{NNLO}^{T,c_2}$ (4.5.113), the term proportional to $|s_{ij}|^{-\epsilon}$ generated by expanding the bracket in Section 4.5.3 and the mass factorisation contribution $\mathrm{d}\hat{\sigma}_{NNLO}^{MF,2,C}$ (4.5.121). We write this term as

$$
\begin{aligned}
\mathrm{d}\hat{\sigma}_{NNLO}^{U,C} \;=\; & -\mathcal{N}_{NNLO}^{VV} \sum_n \int \frac{\mathrm{d}z_1}{z_1}\frac{\mathrm{d}z_2}{z_2}\, \mathrm{d}\Phi_n(p_3,\dots,p_{n+2};z_1p_1,z_2p_2)\,\frac{1}{S_n} \\
& \boldsymbol{J}_{n+2}^{(2)}(1,\cdots,n+2)\,M_{n+2}^0(1,\cdots,n+2)\,J_n^{(n)}(\{p\}_n),
\end{aligned}
\tag{4.5.126}
$$

where we have introduced the double unresolved integrated antenna string, $\boldsymbol{J}^{(2)}_{n+2}$ as a sum over double unresolved integrated dipoles, $\boldsymbol{J}^{(2)}_2$,

$$\boldsymbol{J}^{(2)}_{n+2}(1, \cdots, n+2) = \sum_{(i,j)} \boldsymbol{J}^{(2)}_2(i,j), \tag{4.5.127}$$

and the sum runs over colour connected pairs of partons in the $(n+2)$-parton ordering. The matrix element is at tree level. This new set of integrated dipoles depend on the type of particle in the scattering process, the order in the colour decomposition under consideration and the kinematic configuration (FF, IF or II) of the dipole. Schematically, we construct the double virtual dipole from the integrated three- and four-parton tree level and one loop antennae. The final-final case takes the form

$$\begin{aligned}
\boldsymbol{J}^{(2)}_2(I,J) &= c_1^{FF}\mathcal{X}_4^0(s_{IJ}) + c_2^{FF}\tilde{\mathcal{X}}_4^0(s_{IJ}) + c_3^{FF}\mathcal{X}_3^1(s_{IJ}) \\
&+ c_4^{FF}\frac{\beta_0}{\epsilon}\left(\frac{|s_{IJ}|}{\mu^2}\right)^{-\epsilon}\mathcal{X}_3^0(s_{IJ}) + c_5^{FF}\mathcal{X}_3^0(s_{IJ}) \otimes \mathcal{X}_3^0(s_{IJ}),
\end{aligned} \tag{4.5.128}$$

where c_n^{FF}, are constants associated with each integrated dipole. For an initial-final integrated dipole, the form of the integrated dipole is modified by the use of initial-final integrated antennae and the inclusion of the necessary mass factorisation contribution to remove all initial-state collinear poles,

$$\begin{aligned}
\boldsymbol{J}^{(2)}_2(\hat{\bar{1}},I) &= c_1^{IF}\mathcal{X}_4^0(s_{\bar{1}I}) + c_2^{IF}\tilde{\mathcal{X}}_4^0(s_{\bar{1}I}) + c_3^{IF}\mathcal{X}_3^1(s_{\bar{1}I}) + c_4^{IF}\frac{\beta_0}{\epsilon}\left(\frac{|s_{\bar{1}I}|}{\mu^2}\right)^{-\epsilon}\mathcal{X}_3^0(s_{\bar{1}I}) \\
&+ c_5^{IF}\mathcal{X}_3^0(s_{\bar{1}I}) \otimes \mathcal{X}_3^0(s_{\bar{1}I}) - \overline{\Gamma}^{(2)}_{ik}(z_1)\delta(1-z_2),
\end{aligned} \tag{4.5.129}$$

where i labels the species of parton in the initial-state and k is the parton involved in the matrix element in Eq. (4.5.126). The initial-initial integrated dipole is formed from initial-initial antennae and includes a mass factorisation contribution with non-trivial z_1 and z_2 dependence,

$$\begin{aligned}
\boldsymbol{J}^{(2)}_2(\hat{\bar{1}},\hat{\bar{2}}) &= c_1^{II}\mathcal{X}_4^0(s_{\bar{1}\bar{2}}) + c_2^{II}\tilde{\mathcal{X}}_4^0(s_{\bar{1}\bar{2}}) + c_3^{II}\mathcal{X}_3^1(s_{\bar{1}\bar{2}}) + \frac{\beta_0}{\epsilon}\left(\frac{|s_{\bar{1}\bar{2}}|}{\mu^2}\right)^{-\epsilon}c_4^{II}\mathcal{X}_3^0(s_{\bar{1}\bar{2}}) \\
&+ c_5^{II}\mathcal{X}_3^0(s_{\bar{1}\bar{2}}) \otimes \mathcal{X}_3^0(s_{\bar{1}\bar{2}}) - \overline{\Gamma}^{(2)}_{ij;kl}(z_1)\delta(1-z_2),
\end{aligned} \tag{4.5.130}$$

where the i, j labels carried by $\overline{\Gamma}^{(2)}_{ij;kl}$ are the species of initial-state parton carried by the cross section and k, l denote those carried by the matrix element in Eq. (4.5.126).

The full double virtual subtraction term, $\mathrm{d}\hat{\sigma}^U_{NNLO}$

The full double virtual subtraction term is given by the sum of $\mathrm{d}\hat{\sigma}^{U,A}_{NNLO}$ (4.5.124), $\mathrm{d}\hat{\sigma}^{U,B}_{NNLO}$ (4.5.125) and $\mathrm{d}\hat{\sigma}^{U,C}_{NNLO}$ (4.5.126) so that,

$$
\begin{aligned}
\mathrm{d}\hat{\sigma}^U_{NNLO} = -\mathcal{N}^{VV}_{NNLO} \sum_n \int \frac{\mathrm{d}z_1}{z_1} \frac{\mathrm{d}z_2}{z_2} \, \mathrm{d}\Phi_n(p_3, \ldots, p_{n+2}; z_1 p_1, z_2 p_2) \, \frac{1}{S_n} \Bigg\{ \\
\boldsymbol{J}^{(1)}_{n+2}(1, \cdots, n+2) \left(M^1_{n+2}(1, \cdots, n+2) - \frac{\beta_0}{\epsilon} \, M^0_{n+2}(1, \cdots, n+2) \right) \\
+ \frac{1}{2} \left[\boldsymbol{J}^{(1)}_{n+2}(1, \cdots, n+2) \otimes \boldsymbol{J}^{(1)}_{n+2}(1, \cdots, n+2) \right](z_1, z_2) \, M^0_{n+2}(1, \cdots, n+2) \\
+ \boldsymbol{J}^{(2)}_{n+2}(1, \cdots, n+2) \, M^0_{n+2}(1, \cdots, n+2) \Bigg\} J^{(n)}_n(\{p\}_n).
\end{aligned}
\tag{4.5.131}
$$

This master equation encapsulates the IR poles generated by the integration of the tree-level double real emission over the double unresolved phase space, plus the integration of the one-loop real-virtual contribution over the single unresolved phase space.

As previously discussed, the first term in Eq. (4.5.131) reflects the pole structure of the first line in Eq. (4.5.115). The second term similarly reflects the structure of the second line in Eq. (4.5.115). The third term introduces the double unresolved integrated antenna string, $\boldsymbol{J}^{(2)}_{n+2}$, which is summed over colour-connected dipoles. This term corresponds to the terms proportional to $\boldsymbol{I}^{(1)}_{n+2}(2\epsilon)$ and $\boldsymbol{H}^{(2)}(\epsilon)$ in the last two lines of Eq. (4.5.115). When adding together all contributions in the double-virtual channel, we observe that contributions of order ϵ or higher to the one-loop amplitude cancel, even though they are multiplied with divergent factors in individual terms (one-loop self-interference and integrated real-virtual subtraction terms). This cancellation can be understood in detail from the NNLO infrared singularity structure [20, 100].

Chapter 5

Dijet Production from Two-Quark Processes

The treatment of Chapter 4 provides the tools necessary to calculate jet production cross sections for massless jets at NNLO, using antenna subtraction to control the infra-red behaviour. The first step towards a complete treatment of $pp \to jj$ was completed earlier this year [101] with the construction of the full leading colour subtraction term for the pure gluon contribution. Figure 5.1 displays the doubly differential jet cross sections, presented for pp collisions at $\sqrt{s} = 8$ TeV over a range of rapidities for the anti-k_t algorithm with $R = 0.7$. The calculation was carried out using the MSTW08NNLO gluon distribution function [102]. The renormalisation scale was set at $\mu_F = \mu_R \equiv \mu$ with μ being the transverse momenta of the leading jet.

This can be compared indicatively with experimental results taken from CMS with data from LHC proton-proton collisions at $\sqrt{s} = 8$ TeV, corresponding to an integrated luminosity of 10.71fb^{-1}, given here in Figure 5.2. The theoretical k-factors for the cross section are also determined in [101] and given here in Figure 5.3, where the corrections consistently increase the cross section for high p_T with respect to the NLO results, a tantalising indication of the necessity for extending calculations to higher orders in perturbation theory. This is only for the gluon-only channel however. We must also consider jet production from different partonic processes, namely those involving quarks. Quarks can appear in both the initial and final state for a full prediction of dijet production in perturbation theory.
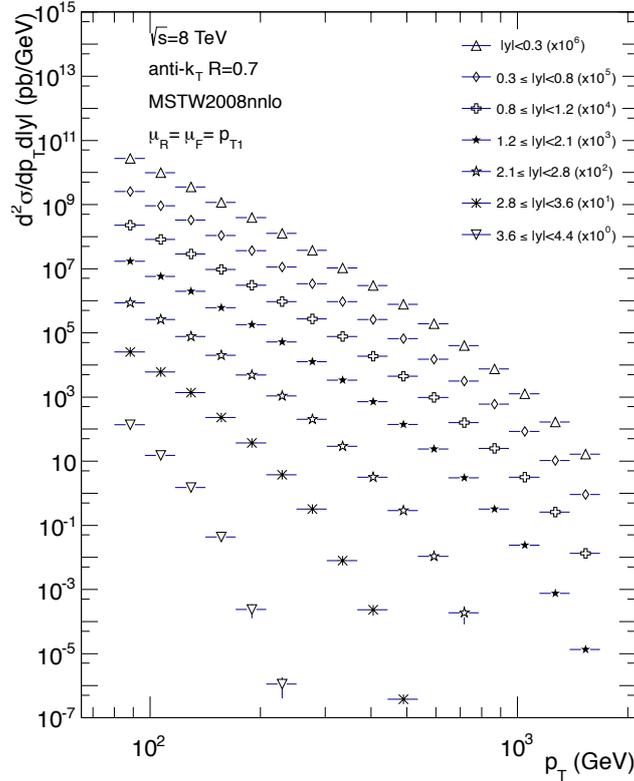
Figure 5.1: All-gluon contribution to the double-differential inclusive jet transverse energy distribution at $\sqrt{s} = 8$ TeV for anti-k_t algorithm with $R = 0.7$ and $E_T > 80$ GeV, taken at various rapidity slices [101].

This chapter focusses on dijet production at NNLO involving one quark pair, extending the antenna subtraction formalism for the pure gluonic channel both at double real and real-virtual level. As in the gluon-only channel, the calculation of NNLO dijet production requires the following ingredients:

- tree level, six parton matrix elements for the double real radiation, where two partons can go unresolved.

- interference of tree and one-loop, five parton amplitudes (real-virtual) where a single parton can go unresolved.

- interference of tree and two-loop amplitudes, and self-interference of one-loop amplitudes, both involving four partons. There are no implicit poles at the double virtual level.
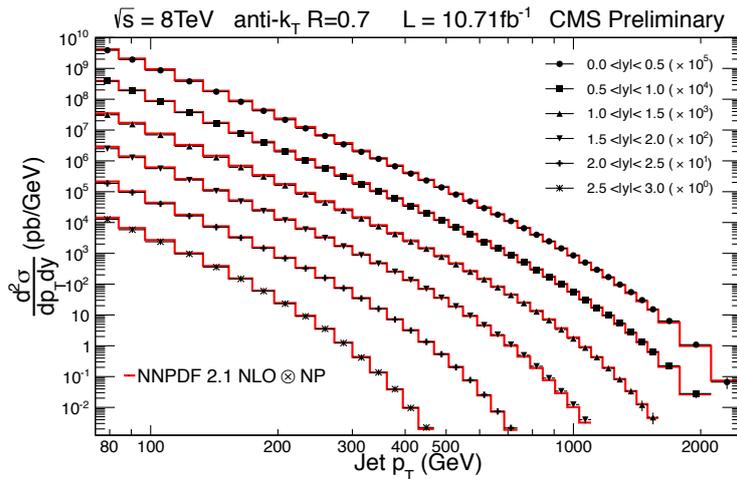
Figure 5.2: A measurement of the inclusive jet cross section, double-differential in jet transverse momentum p_T and absolute jet rapidity. The data is from the LHC proton-proton collisions at $\sqrt{s} = 8$ TeV collected with the CMS detector. Jets are reconstructed with the anti-k_t algorithm for R=0.7 in a phase space region ranging up to jet transverse momenta of $p_T = 2.5$TeV and an absolute rapidity of $|y| = 3.0$. The measured jet cross section is corrected for detector effects and compared to predictions of perturbative QCD at next-to-leading order using various sets of parton distribution functions [103].
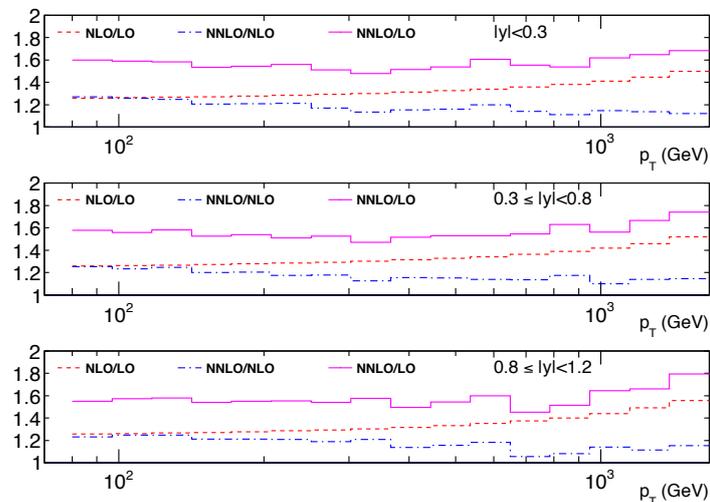
Figure 5.3: Double differential k-factors for rapidity slices of $|y| < 0.3, 0.3 < |y| < 0.8, 0.8 < |y| < 1.2$, with $p_T > 80$ GeV [101].

The pole structure of the matrix elements involving loop corrections will be constructed using the formalism in Section 2.1.1, and recast in terms of the integrated antenna strings. Before launching into the leading colour NNLO $q\bar{q} \to gg$ channel, it

is judicious to consider first the NLO correction to the same channel, in which only the tree-level five parton matrix elements and one-loop four parton matrix elements are required. This will be carried out to all orders in colour, whilst setting $N_F = 0$, using antenna subtraction. This chapter will proceed as follows. We first introduce the notation for both squared and unsquared amplitudes, and then construct the partonic matrix elements required for NLO and NNLO quark-antiquark scattering at leading colour. The real and virtual quark initiated subtraction terms are then discussed at NLO, where the cancellation of poles is transparent. The NNLO double real (RR), real-virtual (RV) and double virtual (VV) subtraction terms are given, along with numerical checks on the implicit pole cancellation. The quark-gluon and gluon-gluon initiated processes are then addressed, and expressions for the leading colour NNLO real-virtual and double virtual subtraction terms constructed.

5.1 Notation and amplitudes

Here we first review our notation for amplitudes involving quarks. In previous chapters the symbol M_n^l was used to denote a generic l-loop, n-parton, squared partial amplitude. In previous works [15,80] the symbol A_n^l was used to denote the l-loop, n-parton all-gluon squared partial amplitudes. Following this example, squared partial amplitudes involving one quark-antiquark pair and $(n-2)$ gluons will be represented by the symbol B_n^l and we will reserve C_n^l (D_n^l) for processes involving two non-identical (identical) quark-antiquark pairs and $(n-4)$ gluons respectively.

In our notation, the leading colour l-loop amplitude for $(m+2)$-parton scattering with one quark-antiquark pair in the initial-state is given by,

$$
\begin{aligned}
\boldsymbol{\mathcal{B}}_{m+2}^l(\{p_i, \lambda_i, a_i, i, j\}) &= 2^{m/2} g^m \left(\frac{g^2 N C(\epsilon)}{2} \right)^l \sum_{\sigma \in S_m} \\
&\times \left(T^{a_{\sigma(1)}} \cdots T^{a_{\sigma(m)}} \right)_{ij} \mathcal{B}_{m+2}^l(\hat{1}_q, \sigma(3)_g, \cdots, \sigma(m+2)_g, \hat{2}_{\bar{q}}),
\end{aligned}
\tag{5.1.1}
$$

where the permutation sum S_m is the group of permutations of m symbols. The $SU(N)$ algebra is normalised according to the convention, $\text{Tr}(T^a T^b) = \delta^{ab}/2$. For notational consistency we take the quarks to be in the initial state, although this

extends naturally to gluonic initial states via crossing. It will be made explicit if the initial states change functional form of the analytic expressions given. The initial states are labelled $\hat{1}$ and $\hat{2}$.

Squaring and summing over helicities and colours gives the leading colour l-loop $q\bar{q} \to m$ gluon contribution to the n-jet cross section,

$$
\begin{aligned}
\mathrm{d}\hat{\sigma}_{ij} &= \mathcal{N}^l_{ij,m+2}\mathrm{d}\Phi_m(p_3,\ldots,p_{m+2};p_1,p_2)\frac{1}{m!} \\
&\times \sum_{\sigma \in S_m} B^l_{m+2}(\hat{1}_q,\sigma(3)_g,\ldots,\sigma(m+2)_g,\hat{2}_{\bar{q}})J_n^{(m)}(\{p\}_m),
\end{aligned}
\tag{5.1.2}
$$

where B^l_{m+2} denotes the l-loop, $(m+2)$-parton, colour-ordered helicity summed, squared partial amplitude. The tree-level, one-loop and two-loop squared partial amplitudes are defined according to:

$$
\begin{aligned}
B^0_{m+2}(\sigma) &= |\mathcal{B}^0_{m+2}(\sigma)|^2, \\
B^1_{m+2}(\sigma) &= 2\mathrm{Re}\big[\mathcal{B}^{0,\dagger}_{m+2}(\sigma)\mathcal{B}^1_{m+2}(\sigma)\big], \\
B^2_{m+2}(\sigma) &= 2\mathrm{Re}\big[\mathcal{B}^{0,\dagger}_{m+2}(\sigma)\mathcal{B}^2_{m+2}(\sigma)\big] + |\mathcal{B}^1_{m+2}(\sigma)|^2,
\end{aligned}
\tag{5.1.3}
$$

where σ denotes a given colour ordering. The normalisation factor $\mathcal{N}^l_{ij,m+2}$ includes the average over initial spins and colours and is given by

$$
\mathcal{N}^l_{ij,m+2} = \mathcal{N}_{ij,LO} \times \left(\frac{\alpha_s N}{2\pi}\right)^{m+l-2}\frac{\bar{C}(\epsilon)^{m+l-2}}{C(\epsilon)^{m-2}}.
\tag{5.1.4}
$$

The i,j subscripts indicate the initial state partons; we thus have

$$
\mathcal{N}_{q\bar{q},LO} = \frac{1}{2s} \times \frac{1}{4N^2} \times \left(g^2N\right)^2\frac{(N^2-1)}{N},
\tag{5.1.5}
$$

$$
\mathcal{N}_{qg,LO} = \frac{1}{2s} \times \frac{1}{4N(N^2-1)} \times \left(g^2N\right)^2\frac{(N^2-1)}{N},
\tag{5.1.6}
$$

$$
\mathcal{N}_{gg,LO} = \frac{1}{2s} \times \frac{1}{4(N^2-1)^2} \times \left(g^2N\right)^2\frac{(N^2-1)}{N}.
\tag{5.1.7}
$$

The coupling g^2 has been converted into α_s using the factors $C(\epsilon)$ and $\bar{C}(\epsilon)$,

$$
g^2NC(\epsilon) = \left(\frac{\alpha_s N}{2\pi}\right)\bar{C}(\epsilon).
\tag{5.1.8}
$$

For low multiplicity matrix elements ($m \leqslant 3$), the sub-leading colour contributions can be written as an incoherent sum of squared partial amplitudes. The treatment of the NLO $q\bar{q} \to gg$ process will elucidate this idea.

5.2 Matrix elements for up to six partons

5.2.1 Four-parton matrix elements

The four parton contribution contains a quark-antiquark pair and two gluons, and consists of a tree level Born cross section, along with its one-loop real-virtual and two-loop double virtual corrections. The tree level, Born cross section can be colour decomposed as following:

$$
\mathrm{d}\hat{\sigma}_{q\bar{q},LO} = \mathcal{N}_{q\bar{q},LO} \int \mathrm{d}\Phi_2(p_3, p_4; p_1, p_2) \frac{1}{2!} \sum_{P(i,j)} \Bigg\{
$$
$$
\left(B_4^0(\hat{1}_q, i_g, j_g, \hat{2}_{\bar{q}}) - \frac{1}{2N^2} \widetilde{B}_4^0(\hat{1}_q, i_g, j_g, \hat{2}_{\bar{q}}) \right) J_2^{(2)}(p_3, p_4) \Bigg\}, \quad (5.2.9)
$$

where $P(i,j)$ denotes the two permutations of the gluons 3 and 4 in the colour ordering. The sub-leading colour contribution is formed from the square of a coherent sum of colour-ordered matrix elements,

$$
\widetilde{B}_4^0(\hat{1}_q, i_g, j_g, \hat{2}_{\bar{q}}) = |\mathcal{B}_4^0(\hat{1}_q, i_g, j_g, \hat{2}_{\bar{q}}) + \mathcal{B}_4^0(\hat{1}_q, j_g, i_g, \hat{2}_{\bar{q}})|^2. \quad (5.2.10)
$$

In such a structure subleading in colour, there are no three-gluon couplings between i and j, and this contribution is sometimes referred to as QED-like, or as involving Abelian gluons. This altered colour connectivity must be taken into account when constructing the subtraction terms.

The full colour decomposition of the one-loop cross section can be similarly constructed, but now including subleading terms deeper in powers of N and additional terms emanating from quark loops resulting in matrix elements accompanied by fac-

tors of N_F. The decomposition reads

$$
\begin{aligned}
\mathrm{d}\hat{\sigma}^V_{q\bar{q},NLO} = \ & \mathcal{N}^1_{q\bar{q},4} \int \mathrm{d}\Phi_2(p_3,p_4;p_1,p_2)\frac{\mathrm{d}x_1}{x_1}\frac{\mathrm{d}x_2}{x_2}\delta(1-x_1)\delta(1-x_2)\frac{1}{2}\sum_{P(i,j)}\Bigg\{ \\
& B^1_4(\hat{\bar{1}}_q,i_g,j_g,\hat{\bar{2}}_{\bar{q}}) - \frac{1}{N^2}\left[\widetilde{B^1_{4,a}}(\hat{\bar{1}}_q,i_g,j_g,\hat{\bar{2}}_{\bar{q}}) + \frac{1}{2}\widetilde{B^1_{4,b}}(\hat{\bar{1}}_q,i_g,j_g,\hat{\bar{2}}_{\bar{q}})\right] \\
& + \ \frac{1}{2N^4}\widetilde{\widetilde{B^1_4}}(\hat{\bar{1}}_q,i_g,j_g,\hat{\bar{2}}_{\bar{q}}) + NN_F\widehat{B^1_4}(\hat{\bar{1}}_q,i_g,j_g,\hat{\bar{2}}_{\bar{q}}) + \frac{N_F}{N}\widehat{\widetilde{B^1_4}}(\hat{\bar{1}}_q,i_g,j_g,\hat{\bar{2}}_{\bar{q}})\Bigg\} \\
& \times J^{(2)}_2(p_i,p_j)
\end{aligned}
\tag{5.2.11}
$$

where the overall factor is,

$$
\mathcal{N}^1_{q\bar{q},4} = \mathcal{N}_{q\bar{q},LO}\left(\frac{\alpha_s N}{2\pi}\right)\bar{C}(\epsilon).
\tag{5.2.12}
$$

The various contributions are formed from the projection of one-loop partial amplitudes onto tree-level amplitudes. The first sub-leading colour contribution is split into two terms, $\widetilde{B^1_{4,a}}$ and $\widetilde{B^1_{4,b}}$ to reflect the fact that the explicit poles of these contributions factor onto different tree-level matrix elements.

The pole structure, which is derived in Appendix A, can be written as sums of the singularity operators multiplied by squared tree-level, colour ordered matrix elements and, using the formalism in Chapter 4, expressed in terms of integrated antenna strings,

$$
\begin{aligned}
\mathcal{P}oles\left[B^1_4(\hat{\bar{1}}_q,i_g,j_g,\hat{\bar{2}}_{\bar{q}})\right] &= -\boldsymbol{J}^{(1)}_4(\hat{\bar{1}}_q,i_g,j_g,\hat{\bar{2}}_{\bar{q}})\,B^0_4(\hat{\bar{1}}_q,i_g,j_g,\hat{\bar{2}}_{\bar{q}}), \\
\mathcal{P}oles\left[\widetilde{B^1_{4,a}}(\hat{\bar{1}}_q,i_g,j_g,\hat{\bar{2}}_{\bar{q}})\right] &= -\boldsymbol{J}^{(1)}_2(\hat{\bar{1}}_q,\hat{\bar{2}}_{\bar{q}})\,B^0_4(\hat{\bar{1}}_q,i_g,j_g,\hat{\bar{2}}_{\bar{q}}), \\
\mathcal{P}oles\left[\widetilde{B^1_{4,b}}(\hat{\bar{1}}_q,i_g,j_g,\hat{\bar{2}}_{\bar{q}})\right] &= -\left(\boldsymbol{J}^{(1)}_3(\hat{\bar{1}}_q,i_g,\hat{\bar{2}}_{\bar{q}}) + \boldsymbol{J}^{(1)}_3(\hat{\bar{1}}_q,j_g,\hat{\bar{2}}_{\bar{q}})\right)\widetilde{B^0_4}(\hat{\bar{1}}_q,i_g,j_g,\hat{\bar{2}}_{\bar{q}}) \\
&\quad +\boldsymbol{J}^{(1)}_2(\hat{\bar{1}}_q,\hat{\bar{2}}_{\bar{q}})\,\widetilde{B^0_4}(\hat{\bar{1}}_q,i_g,j_g,\hat{\bar{2}}_{\bar{q}}), \\
\mathcal{P}oles\left[\widetilde{\widetilde{B^1_4}}(\hat{\bar{1}}_q,i_g,j_g,\hat{\bar{2}}_{\bar{q}})\right] &= -\boldsymbol{J}^{(1)}_2(\hat{\bar{1}}_q,\hat{\bar{2}}_{\bar{q}})\,\widetilde{B^0_4}(\hat{\bar{1}}_q,i_g,j_g,\hat{\bar{2}}_{\bar{q}}).
\end{aligned}
\tag{5.2.13}
$$

Following the discussion of Sec. 4.4, the integrated antenna strings are formed from

sums of integrated dipoles,

$$
\begin{aligned}
\boldsymbol{J}_4^{(1)}(\hat{\bar{1}}_q, i_g, j_g, \hat{\bar{2}}_{\bar{q}}) &= \boldsymbol{J}_2^{(1)}(\hat{\bar{1}}_q, i_g) + \boldsymbol{J}_2^{(1)}(i_g, j_g) + \boldsymbol{J}_2^{(1)}(j_g, \hat{\bar{2}}_{\bar{q}}), \\
\boldsymbol{J}_3^{(1)}(\hat{\bar{1}}_q, i_g, \hat{\bar{2}}_{\bar{q}}) &= \boldsymbol{J}_2^{(1)}(\hat{\bar{1}}_q, i_g) + \boldsymbol{J}_2^{(1)}(j_g, \hat{\bar{2}}_{\bar{q}}), \\
\boldsymbol{J}_2^{(1)}(j_g, \hat{\bar{2}}_{\bar{q}}) &= \boldsymbol{J}_2^{(1)}(\hat{\bar{2}}_q, j_g),
\end{aligned}
\tag{5.2.14}
$$

where the relevant integrated dipoles are given in Tabs. 4.4 and 4.5.

Using these relations, the poles of the N_F independent virtual cross section from the channel $q\bar{q} \to gg$ can be rewritten in the form,

$$
\begin{aligned}
\mathcal{P}oles\left(\mathrm{d}\hat{\sigma}_{q\bar{q},NLO}^V\right) &= -\mathcal{N}_{q\bar{q},4}^1 \int \mathrm{d}\Phi_2(p_3, p_4; p_1, p_2) \frac{\mathrm{d}x_1}{x_1} \frac{\mathrm{d}x_2}{x_2} \frac{1}{2} \sum_{P(i,j)} \Bigg\{ \\
&\quad \left[\boldsymbol{J}_4^{(1)}(\hat{\bar{1}}_q, i_g, j_g, \hat{\bar{2}}_{\bar{q}}) \, B_4^0(\hat{\bar{1}}_q, i_g, j_g, \hat{\bar{2}}_{\bar{q}}) \right] \\
&\quad -\frac{1}{N^2} \left[\boldsymbol{J}_2^{(1)}(\hat{\bar{1}}_q, \hat{\bar{2}}_{\bar{q}}) \, B_4^0(\hat{\bar{1}}_q, i_g, j_g, \hat{\bar{2}}_{\bar{q}}) + \boldsymbol{J}_3^{(1)}(\hat{\bar{1}}_q, i_g, \hat{\bar{2}}_{\bar{q}}) \, \widetilde{B}_4^0(\hat{\bar{1}}_q, i_g, j_g, \hat{\bar{2}}_{\bar{q}}) \right] \\
&\quad +\left(\frac{N^2+1}{2N^4}\right) \left[\boldsymbol{J}_2^{(1)}(\hat{\bar{1}}_q, \hat{\bar{2}}_{\bar{q}}) \, \widetilde{B}_4^0(\hat{\bar{1}}_q, 3_g, 4_g, \hat{\bar{2}}_{\bar{q}}) \right] \Bigg\} J_2^{(2)}(p_i, p_j).
\end{aligned}
\tag{5.2.15}
$$

The leading colour contribution to the two-loop $q\bar{q} \to gg$ cross section is given by,

$$
\begin{aligned}
\mathrm{d}\hat{\sigma}_{q\bar{q},NNLO}^{VV} &= \mathcal{N}_{q\bar{q},4}^2 \int \mathrm{d}\Phi_2(p_3, p_4; p_1, p_2) \frac{1}{2!} \frac{\mathrm{d}z_1}{z_1} \frac{\mathrm{d}z_2}{z_2} \sum_{P(i,j)} \\
&\quad \times \ B_4^2(\hat{\bar{1}}_q, i_g, j_g, \hat{\bar{2}}_{\bar{q}}) \delta(1-x_1) \delta(1-x_2) \, J_2^{(2)}(p_i, p_j),
\end{aligned}
\tag{5.2.16}
$$

where the overall factor is,

$$
\mathcal{N}_{q\bar{q},4}^2 = \mathcal{N}_{q\bar{q},LO} \left(\frac{\alpha_s N}{2\pi}\right)^2 \bar{C}(\epsilon)^2.
\tag{5.2.17}
$$

As in [15, 80] and Eq. (5.1.3), the two-loop matrix element contains the projection of the two-loop amplitude onto the tree-level amplitude and the self-interference of the one-loop amplitude.

5.2.2   Five-parton matrix elements

The five parton contribution includes an additional gluon in the process compared to that of the four-parton case. For the purpose of dijet production, the five parton contributions will be required for a) the tree level single real emission contribution for the NLO cross section, and b) the one-loop real-virtual contribution to the NNLO cross section.

At tree level, the real emission contribution to the N_F independent $q\bar{q} \to gg$ NLO cross section is

$$
\begin{aligned}
\mathrm{d}\hat{\sigma}^R_{q\bar{q},NLO} \;=\;& \mathcal{N}^0_{q\bar{q},5}\, \mathrm{d}\Phi_3(p_3,p_4,p_5;p_1,p_2)\, \frac{1}{3!} \sum_{P(i,j,k)} \Bigg\{ \Bigg[B^0_5(\hat{1}_q, i_g, j_g, k_g, \hat{2}_{\bar{q}}) \\
& -\frac{1}{N^2}\, \widetilde{B}^0_5(\hat{1}_q, i_g, j_g, k_g, \hat{2}_{\bar{q}}) + \frac{1}{3!}\left(\frac{N^2+1}{N^4}\right) \widetilde{\widetilde{B}}^0_5(\hat{1}_q, i_g, j_g, k_g, \hat{2}_{\bar{q}}) \Bigg] \\
& \times J^{(3)}_2(p_i, p_j, p_k) \Bigg\},
\end{aligned}
\tag{5.2.18}
$$

where $P(i,j,k)$ is the set of six permutations of the gluons in the colour ordering and the overall factor is given by,

$$
\mathcal{N}^0_{q\bar{q},5} \;=\; \mathcal{N}_{q\bar{q},LO}\left(\frac{\alpha_s N}{2\pi}\right)\frac{\bar{C}(\epsilon)}{C(\epsilon)}.
\tag{5.2.19}
$$

The subleading colour matrix element $\widetilde{B}^0_5(\hat{1}_q, i_g, j_g, k_g, \hat{2}_{\bar{q}})$ is given by,

$$
\begin{aligned}
&\widetilde{B}^0_5(\hat{1}_q, i_g, j_g, k_g, \hat{2}_{\bar{q}}) = \\
&|\mathcal{B}^0_5(\hat{1}_q, i_g, j_g, k_g, \hat{2}_{\bar{q}}) + \mathcal{B}^0_5(\hat{1}_q, j_g, i_g, k_g, \hat{2}_{\bar{q}}) + \mathcal{B}^0_5(\hat{1}_q, j_g, k_g, i_g, \hat{2}_{\bar{q}})|^2,
\end{aligned}
\tag{5.2.20}
$$

such that gluon i behaves in an Abelian fashion. The most subleading contribution is given by the QED-like matrix element, formed by averaging over all colour-ordered matrix elements,

$$
\widetilde{\widetilde{B}}^0_5(\hat{1}_q, i_g, j_g, k_g, \hat{2}_{\bar{q}}) \;=\; \left| \sum_{P(i,j,k)} \mathcal{B}^0_5(\hat{1}_q, i_g, j_g, k_g, \hat{2}_{\bar{q}}) \right|^2.
\tag{5.2.21}
$$

All gluons in this contribution are Abelian in nature.

The one-loop contribution has a more complex structure than the four-parton case, since the additional gluon allows for new emergent colour structures. Following the notation in Sec 5.1, the one loop amplitude is

$$
\begin{aligned}
\mathcal{B}_5^1(\{p_i, \lambda_i, a_i, i, j\}) \;=\; & 2^{3/2}g^3\left(\frac{g^2 N C(\epsilon)}{2}\right) \times \Bigg\{ \\
& N_c \sum_{P(i,j,k)} (T^{a_i}T^{a_j}T^{a_k})_{q\bar{q}} \mathcal{B}_5^{1,l}(1_q, i, j, k, 2_{\bar{q}}) \\
+ \; & N_F \sum_{P(i,j,k)} (T^{a_i}T^{a_j}T^{a_k})_{q\bar{q}} \mathcal{B}_5^{1,f}(1_q, i, j, k, 2_{\bar{q}}) \\
+ \; & \frac{1}{N_c} \sum_{P(i,j,k)} (T^{a_i}T^{a_j}T^{a_k})_{q\bar{q}} \mathcal{B}_5^{1,s}(1_q, i, j, k, 2_{\bar{q}}) \\
+ \; & \sum_{(i,j,k)} (T^{a_i})_{q\bar{q}}\mathrm{Tr}(T^{a_j}T^{a_k}) \mathcal{B}_5^{1,d}(1_q, i, 2_{\bar{q}}; j, k) \\
+ \; & \mathrm{Tr}(T^{a_3}T^{a_4}T^{a_5})\delta_{q\bar{q}} \mathcal{B}_5^{1,q}(1_q, 2_{\bar{q}}; 3, 4, 5) \\
+ \; & \mathrm{Tr}(T^{a_5}T^{a_4}T^{a_3})\delta_{q\bar{q}} \mathcal{B}_5^{1,q}(1_q, 2_{\bar{q}}; 3, 4, 5) \\
+ \; & \frac{N_F}{N_c}(\mathrm{Tr}(T^{a_3}T^{a_4}T^{a_5}) + \mathrm{Tr}(T^{a_5}T^{a_4}T^{a_3}))\delta_{q\bar{q}} \mathcal{B}_5^{1,q,f}(1_q, 2_{\bar{q}}; 3, 4, 5) \Bigg\}.
\end{aligned}
$$

$$(5.2.22)$$

In addition to the tree-type colour structures, one now encounters loop-type structures coming from quark colour loops with two and three gluonic legs. Taking the interference of (5.2.22) with its tree-level counterpart can be simplified by observing a number of properties of the amplitude itself. Whereas the leading tree-type subamplitude $\mathcal{B}_5^{1,l}$ has associated subleading and flavour contributions, it should be noted that there is no N_F-dependent term for the amplitude $\mathcal{B}_5^{1,d}$ proportional to $T_{q\bar{q}}^{a_i} \mathrm{Tr}(T^{a_j}T^{a_k})$. Although there are diagrams that contribute towards this subamplitude, they contain fermion loops, and cancel by Furry's theorem.

The loop-type colour structures indicate symmetries present in the subamplitudes, as with the tree-type structures. The trace over the gluons imposes a cyclic symmetry in the gluon permutations within the amplitude; indeed, the partial amplitude $\mathcal{B}_5^{1,q,f}$ is accompanied by two traces of opposite cyclicity, resulting in it being maximally symmetric under gluon exchange. In principle, it is possible to rewrite the subleading contributions in terms of the leading colour subamplitudes [104]. However, this has the effect of contorting the colour connectivity of the amplitudes which, for the

purposes of utilising antenna subtraction, one wishes to avoid. The squared matrix element, summed over colours and helicities, is given by

$$
\begin{aligned}
\mathrm{d}\hat{\sigma}_{q\bar{q},NNLO}^{RV} = \ & \mathcal{N}_{q\bar{q},5}^{1}\mathrm{d}\Phi_3(p_3,p_4,p_5;p_1,p_2)\frac{\mathrm{d}x_1}{x_1}\frac{\mathrm{d}x_2}{x_2}\delta(1-x_1)\delta(1-x_2)\frac{1}{3!} \times \Bigg\{ \\
& \sum_{P(i,j,k)} \left(B_5^{1,l}(\hat{1}_q,i_g,j_g,k_g,\hat{2}_{\bar{q}}) + \frac{1}{N^2}B_5^{1,s}(\hat{1}_q,i_g,j_g,k_g,\hat{2}_{\bar{q}}) \right) \\
& - \frac{1}{N^2}\sum_{P(i,j,k)} \widetilde{B}_5^{1,l}(\hat{1}_q,\tilde{i},j,k,\hat{2}_{\bar{q}}) - \frac{1}{N^4}\sum_{P(i,j,k)} \widetilde{B}_5^{1,s}(\hat{1}_q,\tilde{i},j,k,\hat{2}_{\bar{q}}) \\
& + \left(\frac{N^2+1}{N^4}\right)\left[\widetilde{B}_5^{1,l}(\hat{1}_q,\tilde{3}_g,\tilde{4}_g,\tilde{5}_g,\hat{2}_{\bar{q}}) + \frac{1}{N^2}\widetilde{B}_5^{1,s}(\hat{1}_q,\tilde{3}_g,\tilde{4}_g,\tilde{5}_g,\hat{2}_{\bar{q}}) \right] \\
& + \left(\frac{1}{2N^2}\right)\left[\sum_i B_5^{1,d}(\hat{1}_q,i,\hat{2}_{\bar{q}};\tilde{j}_g,\tilde{k}_g) - \frac{1}{N^2}\widetilde{B}_5^{1,d}(\hat{1}_q,\tilde{3}_g,\hat{2}_{\bar{q}};\tilde{4}_g,\tilde{5}_g) \right] \\
& + \frac{1}{N^2}\left[\sum_{P(i,j,k)} B_5^{1,q}(\hat{1}_q,\hat{2}_{\bar{q}};i_g,j_g,k_g) - \frac{2}{3N^2}\widetilde{B}_5^{1,q}(\hat{1}_q,\hat{2}_{\bar{q}};\tilde{3}_g,\tilde{4}_g,\tilde{5}_g) \right] \Bigg\},
\end{aligned}
$$

$$(5.2.23)$$

where again the sum is over the leading colour gluon permuations and the flavour-dependent terms are omitted. The overall factor can be derived from (5.1.4),

$$
\mathcal{N}_{q\bar{q},5}^{1} = \mathcal{N}_{q\bar{q},LO}\left(\frac{\alpha_s N}{2\pi}\right)^2 \frac{\bar{C}(\epsilon)^2}{C(\epsilon)},
$$

$$(5.2.24)$$

and

$$
\mathcal{N}_{NNLO}^{RV} = \mathcal{N}_{q\bar{q},LO}\left(\frac{\alpha_s N}{2\pi}\right)^2 \frac{\bar{C}(\epsilon)^2}{C(\epsilon)} = \mathcal{N}_{NNLO}^{RV} C(\epsilon).
$$

$$(5.2.25)$$

The Abelian structures also behave in a similar fashion as their tree level counterparts. However, we now encounter new objects B_5^d and B_5^q due to the loop-level colour structures that do not have analogues at tree level. The squared matrix element B_5^d originates from amplitudes in which there is a colour string between the quarks and a single gluon, whilst the remaining external gluons make up a second colour structure involving a fermion loop, and thus are colour disconnected from the quarks. This is indicated by the B_5^d arguments: the sum being over each gluon, with the last two arguments being the remaining gluons. Similarly for B_5^q, where now there is direct colour connection between the quarks, and all three gluons forming a separate colour

structure. This can be seen at the amplitude level by noting the form of the $SU(3)$ generators multiplying each amplitude in (5.2.22).

The pole structure for the full squared matrix element is derived in Appendix A. For the purposes of this thesis we are only considering the leading colour matrix elements: the pole structure in terms of integrated antenna strings reads

$$
\mathcal{P}oles\big(\mathrm{d}\hat{\sigma}_{NNLO}^{RV}\big) \;=\; -\mathcal{N}_{q\bar{q},4}^{1} \int \mathrm{d}\Phi_3(p_3,p_4,p_5;p_1,p_2)\frac{\mathrm{d}x_1}{x_1}\frac{\mathrm{d}x_2}{x_2}\frac{1}{2}\sum_{P(i,j,k)}\Bigg\{
$$
$$
\boldsymbol{J}_5^{(1)}(\hat{\bar{1}}_q, i_g, j_g, k_g, \hat{\bar{2}}_{\bar{q}})\; B_5^0(\hat{\bar{1}}_q, i_g, j_g, k_g, \hat{\bar{2}}_{\bar{q}})\Bigg\}. \qquad (5.2.26)
$$

Numerical Checks

The calculations of both the four and five parton one-loop matrix elements were performed contemporaneously by Badger *et al.* in `Njet` [105]. The matrix elements constructed by this author are derived from the amplitudes given in [106] and [107], rewritten in the form given in (5.2.23) and (5.2.15) respectively, and implemented in the Fortran code `NNLOJET`. The `Njet` code evaluates the full squared matrix element, including all subleading effects, whereas the colour decomposition employed here ideally requires checks on the individual colour-ordered squared subamplitudes, in addition to the full squared matrix element. Nevertheless, both methods allow for a manual variation of the renormalisation scale, number of colours and quark flavours so particular orders in colour can be isolated. Both approaches can be evaluated in conventional dimensional regularisation, and also shifted to the 't Hooft-Veltman scheme, allowing for further corroboration of the finite terms.

The results used here (averaged over initial spins and colours) can be directly compared with the `Njet` result for the total squared matrix element at specific points in phase space. We calculate the ratio

$$
\frac{1}{g^2}\frac{|M_5^1(\{p_i\})|^2}{|M_5^0(\{p_i\})|^2}, \qquad (5.2.27)
$$

for two four-parton phase space points and two five-parton phase space points. The channel given is that of gluon production from quark-antiquark collision, and the results between `NNLOJET` and `Njet` are given in Tables 5.1 and 5.2 respectively.

		$\bar{q}q \to gg$		
		$1/\epsilon^2$	$1/\epsilon$	$1/\epsilon^0$
PS #1	NNLOJET	-16.6666666666	13.3561829169717	21.9879375396124
	Njet	-1.6666666666722	13.3561820813345	21.9879372288741
PS #2	NNLOJET	-16.666666666666	8.79545993894548	-78.4933926511771
	Njet	-16.6666666666722	8.79546007470786	-78.4933892819566

Table 5.1: Comparison of NNLOJET and Njet [105] for value of R in (5.2.27), for $\bar{q}q \to gg$ at leading colour.

		$\bar{q}q \to ggg$		
		$1/\epsilon^2$	$1/\epsilon$	$1/\epsilon^0$
PS #1	NNLOJET	-23.333333333	-11.3640062833269	-91.3387887430282
	Njet	-23.333333333	-11.3640059348231	-9.13387867405098
PS #2	NNLOJET	-23.333333333	6.56701820268222	-1.49785922157793
	Njet	-23.333333333	6.567017843280173	-1.49785955162316

Table 5.2: Comparison of NNLOJET and Njet [105] for value of R in (5.2.27), for $\bar{q}q \to ggg$.

We see good agreement for both multiplicity channels. For the leading colour comparisons in Table 5.1, a small discrepancy is expected, since in order to compare the single colour-ordered amplitudes constructed here with the full matrix element in Njet, the large N limit ($N = 3000$) is taken so as to isolate the colour-leading contribution. Naturally in this region the subleading effects are small but still contributing.

5.2.3   Six-parton matrix elements

Only at NNLO do we require a six-parton matrix element for dijet production, namely for the tree level contribution which allows for double real radiation. The process again adds a further gluon, and at leading colour is given by

$$
\begin{aligned}
\mathrm{d}\hat{\sigma}^{RR}_{q\bar{q},NNLO} &= \mathcal{N}^0_{q\bar{q},6} \, \mathrm{d}\Phi_4(p_3,\ldots,p_6; p_1, p_2) \, \frac{1}{4!} \sum_{P(i,j,k,l)} \\
&\times B^0_6(\hat{1}_q, i_g, j_g, k_g, l_g, \hat{2}_{\bar{q}}) \, J^{(4)}_2(p_i, p_j, p_k, p_l),
\end{aligned}
\tag{5.2.28}
$$

where $P(i, j, k, l)$ denotes the 24 possible permutations of gluons in the colour ordering and the overall factor is given by,

$$\mathcal{N}_{q\bar{q},6}^0 \;=\; \mathcal{N}_{q\bar{q},LO}\left(\frac{\alpha_s N}{2\pi}\right)^2 \frac{\bar{C}(\epsilon)^2}{C(\epsilon)^2}. \tag{5.2.29}$$

It is convenient to rearrange the 24 squared amplitudes present in Eq. (5.2.28) into three terms,

$$\sum_{P(i,j,k,l)} M_6^0(\hat{1}_q, i_g, j_g, k_g, l_g, \hat{2}_{\bar{q}}) \;=\; X_6^0(\hat{1}_q, 3_g, 4_g, 5_g, 6_g, \hat{2}_{\bar{q}})$$
$$+\;\; X_6^0(\hat{1}_q, 3_g, 5_g, 4_g, 6_g, \hat{2}_{\bar{q}})$$
$$+\;\; X_6^0(\hat{1}_q, 3_g, 4_g, 6_g, 5_g, \hat{2}_{\bar{q}}), \tag{5.2.30}$$

where each X_6^0 contains eight colour ordered squared amplitudes obtained by the four cyclic permutations of the final state gluons and their line reversals:

$$X_6^0(\hat{1}_q, 3_g, 4_g, 5_g, 6_g, \hat{2}_{\bar{q}}) \;=\; B_6^0(\hat{1}_q, 3_g, 4_g, 5_g, 6_g, \hat{2}_{\bar{q}}) + B_6^0(\hat{1}_q, 6_g, 5_g, 4_g, 3_g, \hat{2}_{\bar{q}})$$
$$+\;\; B_6^0(\hat{1}_q, 4_g, 5_g, 6_g, 3_g, \hat{2}_{\bar{q}}) + B_6^0(\hat{1}_q, 3_g, 6_g, 5_g, 4_g, \hat{2}_{\bar{q}})$$
$$+\;\; B_6^0(\hat{1}_q, 5_g, 6_g, 3_g, 4_g, \hat{2}_{\bar{q}}) + B_6^0(\hat{1}_q, 4_g, 3_g, 6_g, 5_g, \hat{2}_{\bar{q}})$$
$$+\;\; B_6^0(\hat{1}_q, 6_g, 3_g, 4_g, 5_g, \hat{2}_{\bar{q}}) + B_6^0(\hat{1}_q, 5_g, 4_g, 3_g, 6_g, \hat{2}_{\bar{q}}).$$
$$\tag{5.2.31}$$

As will be seen, it is sufficient to apply the subtraction technique to one block of orderings, since the other two are related by symmetry and contribute numerically the same result after integration over the phase space.

5.3 Quark-antiquark initiated dijet production at NLO

5.3.1 Real radiation subtraction term, $\mathrm{d}\hat{\sigma}^S_{NLO}$

The subtraction term for the real cross section presented in Eq. (5.2.18) is given by,

$$
\begin{aligned}
\mathrm{d}\hat{\sigma}^S_{q\bar{q},NLO} \;=\; & \mathcal{N}^0_{q\bar{q},5}\;\mathrm{d}\Phi_3(p_3,p_4,p_5;p_1,p_2)\,\frac{1}{3!}\sum_{P(i,j,k)}\Bigg\{ \\
& \Bigg[\; d^0_3(\hat{1},i,j)\;B^0_4(\hat{\tilde{1}}_q,\widetilde{(ij)}_g,k_g,\hat{2}_{\bar{q}})\;J^{(2)}_2(p_{(ij)},p_k) \\
& +\; f^0_3(i,j,k)\;B^0_4(\hat{1}_q,\widetilde{(ij)}_g,\widetilde{(jk)}_g,\hat{2}_{\bar{q}})\;J^{(2)}_2(p_{(ij)},p_{(jk)}) \\
& +\; d^0_3(\hat{2},k,j)\;B^0_4(\hat{1}_q,i_g,\widetilde{(jk)}_g,\hat{\tilde{2}}_{\bar{q}})\;J^{(2)}_2(p_i,p_{(jk)})\Bigg] \\
& -\frac{1}{N^2}\;\Bigg[\; A^0_3(\hat{1},i,\hat{2})\;B^0_4(\hat{\tilde{1}}_q,\tilde{j}_g,\tilde{k}_g,\hat{\tilde{2}}_{\bar{q}})\;J^{(2)}_2(p_j,p_k) \\
& +\; d^0_3(\hat{1},j,k)\;\widetilde{B}^0_4(\hat{\tilde{1}}_q,i_g,\widetilde{(jk)}_g,\hat{2}_{\bar{q}})\;J^{(2)}_2(p_i,p_{(jk)}) \\
& +\; d^0_3(\hat{2},k,j)\;\widetilde{B}^0_4(\hat{1}_q,i_g,\widetilde{(jk)}_g,\hat{\tilde{2}}_{\bar{q}})\;J^{(2)}_2(p_i,p_{(jk)})\Bigg] \\
& +\frac{1}{3!}\left(\frac{N^2+1}{N^4}\right)\;\Bigg[\; A^0_3(\hat{1},i,\hat{2})\;\widetilde{B}^0_4(\hat{\tilde{1}}_q,\tilde{j}_g,\tilde{k}_g,\hat{\tilde{2}}_{\bar{q}})\;J^{(2)}_2(p_j,p_k) \\
& +\; A^0_3(\hat{1},j,\hat{2})\;\widetilde{B}^0_4(\hat{\tilde{1}}_q,\tilde{i}_g,\tilde{k}_g,\hat{\tilde{2}}_{\bar{q}})\;J^{(2)}_2(p_i,p_k) \\
& +\; A^0_3(\hat{1},k,\hat{2})\;\widetilde{B}^0_4(\hat{\tilde{1}}_q,\tilde{i}_g,\tilde{j}_g,\hat{\tilde{2}}_{\bar{q}})\;J^{(2)}_2(p_i,p_j)\Bigg]\Bigg\}. \qquad (5.3.32)
\end{aligned}
$$

5.3.2 Virtual subtraction term, $\mathrm{d}\hat{\sigma}^T_{NLO}$

Integrating the real subtraction term over the single unresolved phase space and combining with the appropriate NLO mass factorisation kernels allows the virtual subtraction term to be constructed from integrated antenna strings,

$$
\begin{aligned}
\mathrm{d}\hat{\sigma}^T_{q\bar{q},NLO} \;=\; & -\mathcal{N}^1_{q\bar{q},4}\;\mathrm{d}\Phi_2(p_3,p_4;p_1,p_2)\,\frac{1}{2}\sum_{P(i,j)}\int\frac{\mathrm{d}x_1}{x_1}\frac{\mathrm{d}x_2}{x_2}\Bigg\{ \\
& \boldsymbol{J}^{(1)}_4(\hat{\tilde{1}}_q,i_g,j_g,\hat{\tilde{2}}_{\bar{q}})\;B^0_4(\hat{\tilde{1}}_q,i_g,j_g,\hat{\tilde{2}}_{\bar{q}}) \\
& -\frac{1}{N^2}\;\Bigg[\; \boldsymbol{J}^{(1)}_2(\hat{\tilde{1}}_q,\hat{\tilde{2}}_{\bar{q}})\;B^0_4(\hat{\tilde{1}}_q,i_g,j_g,\hat{\tilde{2}}_{\bar{q}}) + \boldsymbol{J}^{(1)}_3(\hat{\tilde{1}}_q,i_g,\hat{\tilde{2}}_{\bar{q}})\;\widetilde{B}^0_4(\hat{\tilde{1}}_q,i_g,j_g,\hat{\tilde{2}}_{\bar{q}})\Bigg] \\
& +\left(\frac{N^2+1}{2N^4}\right)\;\Bigg[\; \boldsymbol{J}^{(1)}_2(\hat{\tilde{1}}_q,\hat{\tilde{2}}_{\bar{q}})\;\widetilde{B}^0_4(\hat{\tilde{1}}_q,i_g,j_g,\hat{\tilde{2}}_{\bar{q}})\Bigg]\Bigg\}\,J^{(2)}_2(p_i,p_j). \qquad (5.3.33)
\end{aligned}
$$

From the definition of these strings, the connection to the unintegrated subtraction term in Eq. (5.3.32) is clear. This expression exactly matches that of Eq. (5.2.15), i.e.,

$$\mathcal{P}oles\left(\mathrm{d}\hat{\sigma}^V_{q\bar{q},NLO}\right) - \mathcal{P}oles\left(\mathrm{d}\hat{\sigma}^T_{q\bar{q},NLO}\right) \;=\; 0. \tag{5.3.34}$$

5.4 Quark-antiquark initiated dijet production at NNLO

As aforementioned, the leading colour NNLO contribution to dijet production has previously been studied using the antenna subtraction formalism for purely gluonic channels at the double real [108], real-virtual [15] and double virtual [80] levels.

This section will focus on the leading colour NNLO corrections to dijet production from quark-antiquark scattering. These corrections include the double real tree-level contribution $q\bar{q} \to gggg$, the real-virtual one-loop contribution $q\bar{q} \to ggg$ and the double virtual two-loop contribution $q\bar{q} \to gg$, all of which were examined using the methods of Section 4.5.

5.4.1 Double real subtraction term, $\mathrm{d}\hat{\sigma}^S_{NNLO}$

The leading colour contribution to the squared matrix element is an incoherent sum of squared colour-ordered partial amplitudes. The sum over colour orderings can be partitioned into three blocks of orderings as described in Sec. 5.2.3, such that a subtraction term may be constructed for a block of orderings, rather than the entire squared matrix element. Following the general discussion of Sec. 4.5, the NNLO subtraction term for the block of orderings in Eq. (5.2.31) is given by,

$$\mathrm{d}\hat{\sigma}^{S,X_6}_{q\bar{q},NNLO} = \mathcal{N}^0_{q\bar{q},6}\, \mathrm{d}\Phi_4(p_3,\ldots,p_6;p_1,p_2)\, \frac{1}{4!} \sum_{P_C(ijkl)} \left\{ \vphantom{\sum} \right.$$

$$+ f^0_3(i,j,k)\, B^0_5(\hat{1}_q, \widetilde{(i,j)}_g, \widetilde{(jk)}_g, l_g, \hat{2}_{\bar{q}})\, J^{(3)}_2(p_{(ij)}, p_{(jk)}, p_l)$$

$$+ f^0_3(j,k,l)\, B^0_5(\hat{1}_q, i_g, \widetilde{(jk)}_g, \widetilde{(kl)}_g, \hat{2}_{\bar{q}})\, J^{(3)}_2(p_{(i)}, p_{(jk)}, p_{(kl)})$$

$$+ d^0_3(\hat{1},i,j)\, B^0_5(\hat{\bar{1}}_q, \widetilde{(ij)}_g, k_g, l_g, \hat{2}_{\bar{q}})\, J^{(3)}_2(p_{(ij)}, p_k, p_l)$$

$$+d_3^0(\hat{2},l,k)\,B_5^0(\hat{1}_q,i_g,j_g,\widetilde{(kl)}_g,\hat{\bar{2}}_{\bar{q}})\,J_2^{(3)}(p_i,p_j,p_{(kl)})$$

$$+f_3^0(l,k,j)\,B_5^0(\hat{1}_q,\widetilde{(lk)}_g,\widetilde{(kj)}_g,i_g,\hat{2}_{\bar{q}})\,J_2^{(3)}(p_{(lk)},p_{(kj)},p_i)$$

$$+f_3^0(k,j,i)\,B_5^0(\hat{1}_q,l_g,\widetilde{(kj)}_g,\widetilde{(ji)}_g,\hat{2}_{\bar{q}})\,J_2^{(3)}(p_l,p_{(kj)},p_{(ji)})$$

$$+d_3^0(\hat{1},l,k)\,B_5^0(\hat{\bar{1}}_q,\widetilde{(lk)}_g,j_g,i_g,\hat{2}_{\bar{q}})\,J_2^{(3)}(p_{(lk)},p_j,p_i)$$

$$+d_3^0(\hat{2},i,j)\,B_5^0(\hat{1}_q,l_g,k_g,\widetilde{(ji)}_g,\hat{\bar{2}}_{\bar{q}})\,J_2^{(3)}(p_l,p_k,p_{(ji)})$$

$$+F_{4,a}^0(i,j,k,l)\,B_4^0(\hat{1}_q,\widetilde{(ijk)}_g,\widetilde{(jkl)}_g,\hat{2}_{\bar{q}})\,J_2^{(2)}(p_{(ijk)},p_{(jkl)})$$

$$+F_{4,b}^0(i,j,l,k)\,B_4^0(\hat{1}_q,\widetilde{(ijl)}_g,\widetilde{(jlk)}_g,\hat{2}_{\bar{q}})\,J_2^{(2)}(p_{(ijk)},p_{(jlk)})$$

$$+F_{4,a}^0(l,k,j,i)\,B_4^0(\hat{1}_q,\widetilde{(lkj)}_g,\widetilde{(kji)}_g,\hat{2}_{\bar{q}})\,J_2^{(2)}(p_{(lkj)},p_{(kji)})$$

$$+F_{4,b}^0(l,k,i,j)\,B_4^0(\hat{1}_q,\widetilde{(lki)}_g,\widetilde{(kij)}_g,\hat{2}_{\bar{q}})\,J_2^{(2)}(p_{(lki)},p_{(kij)})$$

$$+D_4^0(\hat{1},i,j,k)\,B_4^0(\hat{\bar{1}}_q,\widetilde{(ijk)}_g,l_g,\hat{2}_{\bar{q}})\,J_2^{(2)}(p_{(ijk)},p_l)$$

$$+D_4^0(\hat{2},l,k,j)\,B_4^0(\hat{1}_q,i_g,\widetilde{(lkj)}_g,\hat{\bar{2}}_{\bar{q}})\,J_2^{(2)}(p_i,p_{(lkj)})$$

$$-\tilde{A}_4^0(\hat{1},i,k,\hat{2})\,B_4^0(\hat{\bar{1}}_q,\tilde{j}_g,\tilde{l}_g,\hat{\bar{2}}_{\bar{q}})\,J_2^{(2)}(p_{\tilde{j}},p_{\tilde{l}})$$

$$-f_3^0(i,j,k)\,f_3^0(\widetilde{(ij)},\widetilde{(jk)},l)\,B_4^0(\hat{1}_q,\widetilde{((ij)(jk))}_g,\widetilde{((jk)l)}_g,\hat{2}_{\bar{q}})\,J_2^{(2)}(p_{((ij)(jk))},p_{((jk)l)})$$

$$-f_3^0(j,k,l)\,f_3^0(i,\widetilde{(jk)},\widetilde{(kl)})\,B_4^0(\hat{1}_q,\widetilde{(i(jk))}_g,\widetilde{((jk)(kl))}_g,\hat{2}_{\bar{q}})\,J_2^{(2)}(p_{((ij)(jk))},p_{((jk)l)})$$

$$-f_3^0(i,j,k)\,f_3^0(\widetilde{(ij)},l,\widetilde{(jk)})\,B_4^0(\hat{1}_q,\widetilde{((ij)l)}_g,\widetilde{((jk)l)}_g,\hat{2}_{\bar{q}})\,J_2^{(2)}(p_{((ij)l)},p_{((jk)l)})$$

$$-f_3^0(l,k,j)\,f_3^0(\widetilde{(lk)},\widetilde{(kj)},i)\,B_4^0(\hat{1}_q,\widetilde{((lk)(kj))}_g,\widetilde{((kj)i)}_g,\hat{2}_{\bar{q}})\,J_2^{(2)}(p_{((lk)(kj))},p_{((kj)i)})$$

$$-f_3^0(k,j,i)\,f_3^0(l,\widetilde{(kj)},\widetilde{(ji)})\,B_4^0(\hat{1}_q,\widetilde{(l(kj))}_g,\widetilde{((kj)(ji))}_g,\hat{2}_{\bar{q}})\,J_2^{(2)}(p_{(kj)},p_{((kj)(ji))})$$

$$-f_3^0(l,k,j)\,f_3^0(\widetilde{(lk)},i,\widetilde{(kj)})\,B_4^0(\hat{1}_q,\widetilde{((lk)i)}_g,\widetilde{((kj)i)}_g,\hat{2}_{\bar{q}})\,J_2^{(2)}(p_{((lk)i)},p_{((kj)i)})$$

$$-d_3^0(\hat{1},i,j)\,D_3^0(\hat{\bar{1}},\widetilde{(ij)},k)\,B_4^0(\hat{\bar{\bar{1}}}_q,\widetilde{((ij)k)}_g,l_g,\hat{2}_{\bar{q}})\,J_2^{(2)}(p_{((ij),k)},p_l)$$

$$-f_3^0(i,j,k)\,D_3^0(\hat{1},\widetilde{(i,j)},\widetilde{(jk)})\,B_4^0(\hat{\bar{1}}_q,\widetilde{((ij)(jk))}_g,l_g,\hat{2}_{\bar{q}})\,J_2^{(2)}(p_{((ij)(jk))},p_l)$$

$$-d_3^0(\hat{1},k,j)\,D_3^0(\hat{\bar{1}},\widetilde{(kj)},i)\,B_4^0(\hat{\bar{\bar{1}}}_q,\widetilde{((kj)i)}_g,l_g,\hat{2}_{\bar{q}})\,J_2^{(2)}(p_{((kj)i)},p_l)$$

$$-d_3^0(\hat{2},l,k)\, D_3^0(\hat{\tilde{2}},\widetilde{(lk)},j)\, B_4^0(\hat{1}_q,i_g,\widetilde{((lk)j)}_g,\hat{\tilde{\tilde{2}}}_{\bar{q}})\, J_2^{(2)}(p_{((lk)j)},p_i)$$

$$-f_3^0(l,k,j)\, D_3^0(\hat{2},\widetilde{(lk)},\widetilde{(kj)})\, B_4^0(\hat{1}_q,i_g,\widetilde{((lk)(kj))}_g,\hat{\tilde{2}}_{\bar{q}})\, J_2^{(2)}(p_i,p_{((lk)(kj))})$$

$$-d_3^0(\hat{2},j,k)\, D_3^0(\hat{\tilde{2}},\widetilde{(jk)},l)\, B_4^0(\hat{1}_q,i_g,\widetilde{((jk)l)}_g,\hat{\tilde{\tilde{2}}}_{\bar{q}})\, J_2^{(2)}(p_i,p_{((jk)l)})$$

$$+A_3^0(\hat{1},i,\hat{2})\, A_3^0(\hat{\tilde{1}},\tilde{k},\hat{\tilde{2}})\, B_4^0(\hat{\tilde{\tilde{1}}}_q,\tilde{\tilde{j}}_g,\tilde{\tilde{l}}_g,\hat{\tilde{\tilde{2}}}_{\bar{q}})\, J_2^{(2)}(p_{\tilde{j}},p_{\tilde{l}})$$

$$+A_3^0(\hat{1},k,\hat{2})\, A_3^0(\hat{\tilde{1}},\tilde{i},\hat{\tilde{2}})\, B_4^0(\hat{\tilde{\tilde{1}}}_q,\tilde{\tilde{j}}_g,\tilde{\tilde{l}}_g,\hat{\tilde{\tilde{2}}}_{\bar{q}})\, J_2^{(2)}(p_{\tilde{j}},p_{\tilde{l}})$$

$$+\frac{1}{2} f_3^0(i,l,k)\, f_3^0(\widetilde{(il)},j,\widetilde{(lk)})\, B_4^0(\hat{1}_q,\widetilde{((il)j)}_g,\widetilde{((lk)j)}_g,\hat{2}_{\bar{q}})\, J_2^{(2)}(p_{((il)j)},p_{((lk)j)})$$

$$-\frac{1}{2} d_3^0(\hat{1},l,i)\, f_3^0(\widetilde{(li)},j,k)\, B_4^0(\hat{\tilde{1}}_q,\widetilde{((il)j)}_g,\widetilde{(jk)}_g,\hat{2}_{\bar{q}})\, J_2^{(2)}(p_{((il)j)},p_{(jk)})$$

$$-\frac{1}{2} d_3^0(\hat{2},l,k)\, f_3^0(i,j,\widetilde{(kl)})\, B_4^0(\hat{1}_q,\widetilde{(ij)}_g,\widetilde{(j(kl))}_g,\hat{\tilde{2}}_{\bar{q}})\, J_2^{(2)}(p_{(ij)},p_{(j(kl))})$$

$$-\frac{1}{2}\Bigg[\Big(S_{(il)l(lk)} - S_{((il)j)l(j(lk))}\Big) - \Big(S_{1l(il)} - S_{1l((il)j)}\Big) - \Big(S_{2l(lk)} - S_{2l(j(lk))}\Big) \Bigg]$$

$$\times f_3^0(\widetilde{(il)},j,\widetilde{(lk)})\, B_4^0(\hat{1}_q,\widetilde{((il)j)}_g,\widetilde{(j(lk))}_g,\hat{2}_{\bar{q}})\, J_2^{(2)}(p_{((il)j)},p_{(j(lk))})$$

$$+\frac{1}{2} f_3^0(l,i,j)\, f_3^0(\widetilde{(li)},k,\widetilde{(ij)})\, B_4^0(\hat{1}_q,\widetilde{((li)k)}_g,\widetilde{((ij)k)}_g,\hat{2}_{\bar{q}})\, J_2^{(2)}(p_{((li)k)},p_{((ij)k)})$$

$$-\frac{1}{2} d_3^0(\hat{1},i,l)\, f_3^0(\widetilde{(il)},k,j)\, B_4^0(\hat{\tilde{1}}_q,\widetilde{((il)k)}_g,\widetilde{(kj)}_g,\hat{2}_{\bar{q}})\, J_2^{(2)}(p_{((il)k)},p_{(kj)})$$

$$-\frac{1}{2} d_3^0(\hat{2},i,j)\, f_3^0(l,k,\widetilde{(ij)})\, B_4^0(\hat{1}_q,\widetilde{(lk)}_g,\widetilde{(k(ij))}_g,\hat{\tilde{2}}_{\bar{q}})\, J_2^{(2)}(p_{(lk)},p_{(k(ij))})$$

$$-\frac{1}{2}\Bigg[\Big(S_{(li)i(ij)} - S_{((li)k)i(k(ij))}\Big) - \Big(S_{1i(li)} - S_{1i((li)k)}\Big) - \Big(S_{2i(ij)} - S_{2i(k(ij))}\Big) \Bigg]$$

$$\times f_3^0(\widetilde{(li)},k,\widetilde{(ij)})\, B_4^0(\hat{1}_q,\widetilde{((li)k)}_g,\widetilde{(k(ij))}_g,\hat{2}_{\bar{q}})\, J_2^{(2)}(p_{((li)k)},p_{(k(ij))})$$

$$+\frac{1}{2} d_3^0(\hat{1},k,j)\, d_3^0(\hat{\tilde{1}},i,\widetilde{(kj)})\, B_4^0(\hat{\tilde{\tilde{1}}}_q,\widetilde{((kj)i)}_g,l_g,\hat{2}_{\bar{q}})\, J_2^{(2)}(p_{((kj)i)},p_l)$$

$$-\frac{1}{2} f_3^0(j,k,l)\, d_3^0(\hat{1},i,\widetilde{(jk)})\, B_4^0(\hat{\tilde{1}}_q,\widetilde{(i(jk))}_g,\widetilde{(kl)}_g,\hat{2}_{\bar{q}})\, J_2^{(2)}(p_{(i(jk))},p_{(kl)})$$

$$-\frac{1}{2} A_3^0(\hat{1},k,\hat{2})\, d_3^0(\hat{\tilde{1}},\tilde{i},\tilde{j})\, B_4^0(\hat{\tilde{\tilde{1}}}_q,\widetilde{(ij)}_g,\tilde{l}_g,\hat{\tilde{2}}_{\bar{q}})\, J_2^{(2)}(p_{(i,j)},p_{\tilde{l}})$$

$$-\frac{1}{2}\Bigg[\Big(S_{1k(jk)} - S_{\bar{1}k(i(jk))}\Big) - \Big(S_{(jk)k(kl)} - S_{(i(jk))k(kl)}\Big) - \underbrace{\Big(S_{1k2} - S_{\bar{1}k2}\Big)}_{0} \Bigg]$$

$$\times d_3^0(\hat{1},i,\widetilde{(jk)})\, B_4^0(\hat{\tilde{1}}_q,\widetilde{(i(jk))}_g,\widetilde{(kl)}_g,\hat{2}_{\bar{q}})\, J_2^{(2)}(p_{(i(jk))},p_{(kl)})$$

$$+\frac{1}{2}\,d_3^0(\hat{1},i,j)\,d_3^0(\hat{\tilde{1}},k,\widetilde{(ij)})\,B_4^0(\hat{\tilde{\tilde{1}}}_q,\widetilde{((ij)k)}_g,l_g,\hat{2}_{\bar{q}})\,J_2^{(2)}(p_{((ij)k)},p_l)$$

$$-\frac{1}{2}\,f_3^0(j,i,l)\,d_3^0(\hat{1},k,\widetilde{(ji)})\,B_4^0(\hat{\tilde{1}}_q,\widetilde{(k(ji))}_g,\widetilde{(il)}_g,\hat{2}_{\bar{q}})\,J_2^{(2)}(p_{(k,(j,i))},p_{(i,l)})$$

$$-\frac{1}{2}\,A_3^0(\hat{1},i,\hat{2})\,d_3^0(\hat{\tilde{1}},\tilde{k},\tilde{j})\,B_4^0(\hat{\tilde{\tilde{1}}}_q,\widetilde{(kj)}_g,\tilde{l}_g,\hat{\tilde{2}}_{\bar{q}})\,J_2^{(2)}(p_{(kj)},p_{\tilde{l}})$$

$$-\frac{1}{2}\bigg[\Big(S_{1i(ji)}-S_{\bar{1}i(k(ji))}\Big)-\Big(S_{(k(ji))i(il)}-S_{(ji)i(il)}\Big)-\underbrace{\Big(S_{1i2}-S_{\bar{1}i2}\Big)}_{0}\bigg]$$

$$\times d_3^0(\hat{1},k,\widetilde{(ji)})\,B_4^0(\hat{\tilde{1}}_q,\widetilde{(k(ji))}_g,\widetilde{(il)}_g,\hat{2}_{\bar{q}})\,J_2^{(2)}(p_{(k(ji))},p_{(il)})$$

$$+\frac{1}{2}\,d_3^0(\hat{2},j,k)\,d_3^0(\hat{\tilde{2}},l,\widetilde{(jk)})\,B_4^0(\hat{1}_q,i_g,\widetilde{((jk)l)}_g,\hat{\tilde{\tilde{2}}}_{\bar{q}})\,J_2^{(2)}(p_i,p_{((jk)l)})$$

$$-\frac{1}{2}\,f_3^0(i,j,k)\,d_3^0(\hat{2},l,\widetilde{(jk)})\,B_4^0(\hat{1}_q,\widetilde{(ij)}_g,\widetilde{(l(jk))}_g,\hat{\tilde{2}}_{\bar{q}})\,J_2^{(2)}(p_{(i,j)},p_{(l,(j,k))})$$

$$-\frac{1}{2}\,A_3^0(\hat{1},j,\hat{2})\,d_3^0(\hat{\tilde{2}},\tilde{l},\tilde{k})\,B_4^0(\hat{\tilde{1}}_q,\tilde{i}_g,\widetilde{(lk)}_g,\hat{\tilde{\tilde{2}}}_{\bar{q}})\,J_2^{(2)}(p_{\tilde{i}},p_{(lk)})$$

$$-\frac{1}{2}\bigg[\Big(S_{2j(jk)}-S_{\bar{2}j(l(jk))}\Big)-\Big(S_{(ij)j(jk)}-S_{(ij)j((jk)l)}\Big)-\underbrace{\Big(S_{1j2}-S_{1j\bar{2}}\Big)}_{0}\bigg]$$

$$\times d_3^0(\hat{2},l,\widetilde{(jk)})\,B_4^0(\hat{1}_q,\widetilde{(ij)}_g,\widetilde{((jk)l)}_g,\hat{\tilde{2}}_{\bar{q}})\,J_2^{(2)}(p_{(ij)},p_{((jk)l)})$$

$$+\frac{1}{2}\,d_3^0(\hat{2},l,k)\,d_3^0(\hat{\tilde{2}},j,\widetilde{(lk)})\,B_4^0(\hat{1}_q,i_g,\widetilde{((lk)j)}_g,\hat{\tilde{\tilde{2}}}_{\bar{q}})\,J_2^{(2)}(p_{((lk)j)},p_i)$$

$$-\frac{1}{2}\,f_3^0(i,l,k)\,d_3^0(\hat{2},j,\widetilde{(lk)})\,B_4^0(\hat{1}_q,\widetilde{(il)}_g,\widetilde{(j(lk))}_g,\hat{\tilde{2}}_{\bar{q}})\,J_2^{(2)}(p_{(il)},p_{(j(lk))})$$

$$-\frac{1}{2}\,A_3^0(\hat{1},l,\hat{2})\,d_3^0(\hat{\tilde{2}},\tilde{j},\tilde{k})\,B_4^0(\hat{\tilde{1}}_q,\tilde{i}_g,\widetilde{(jk)}_g,\hat{\tilde{\tilde{2}}}_{\bar{q}})\,J_2^{(2)}(p_{\tilde{i}},p_{(jk)})$$

$$-\frac{1}{2}\bigg[\Big(S_{2l(lk)}-S_{\bar{2}l(j(lk))}\Big)-\Big(S_{(il)l((lk)j)}-S_{(il)l(lk)}\Big)-\underbrace{\Big(S_{1l2}-S_{1l\bar{2}}\Big)}_{0}\bigg]$$

$$\times d_3^0(\hat{2},j,\widetilde{(lk)})\,B_4^0(\hat{1}_q,\widetilde{(il)}_g,\widetilde{((lk)j)}_g,\hat{\tilde{2}}_{\bar{q}})\,J_2^{(2)}(p_{(il)},p_{((lk)j)})$$

$$-\frac{1}{2}\,A_3^0(\hat{1},i,\hat{2})\,A_3^0(\hat{\tilde{1}},\tilde{k},\hat{\tilde{2}})\,B_4^0(\hat{\tilde{\tilde{1}}}_q,\tilde{\tilde{j}}_g,\tilde{\tilde{l}}_g,\hat{\tilde{\tilde{2}}}_{\bar{q}})\,J_2^{(2)}(p_{\tilde{\tilde{j}}},p_{\tilde{\tilde{l}}})$$

$$+\frac{1}{2}\,d_3^0(\hat{1},i,j)\,A_3^0(\hat{\tilde{1}},k,\hat{2})\,B_4^0(\hat{\tilde{\tilde{1}}}_q,\widetilde{(ij)}_g,\tilde{l}_g,\hat{\tilde{2}}_{\bar{q}})\,J_2^{(2)}(p_{(\widetilde{ij})},p_{\tilde{l}})$$

$$+\frac{1}{2}\,d_3^0(\hat{2},i,l)\,A_3^0(\hat{1},k,\hat{\tilde{2}})\,B_4^0(\hat{\tilde{1}}_q,\tilde{j}_g,\widetilde{(il)}_g,\hat{\tilde{\tilde{2}}}_{\bar{q}})\,J_2^{(2)}(p_{\tilde{j}},p_{(\widetilde{il})})$$

$$+\frac{1}{2}\bigg[\Big(S_{1i2}-S_{\bar{1}i\bar{2}}\Big)-\Big(S_{1i(ji)}-S_{\bar{1}i(\widetilde{ji})}\Big)-\Big(S_{2i(il)}-S_{\bar{2}i(\widetilde{il})}\Big)\bigg]$$

$$\times A_3^0(\hat{1},k,\hat{2})\,B_4^0(\hat{\tilde{1}}_q,\widetilde{(ji)}_g,\widetilde{(il)}_g,\hat{\tilde{2}}_{\bar{q}})\,J_2^{(2)}(p_{(\widetilde{ji})},p_{(\widetilde{il})})$$

$$-\frac{1}{2} A_3^0(\hat{1}, k, \hat{2}) \, A_3^0(\hat{\bar{1}}, \tilde{i}, \hat{\bar{2}}) \, B_4^0(\hat{\bar{\bar{1}}}_q, \tilde{\tilde{j}}_g, \tilde{\tilde{l}}_g, \hat{\bar{\bar{2}}}_{\bar{q}}) \, J_2^{(2)}(p_{\tilde{j}}, p_{\tilde{l}})$$

$$+\frac{1}{2} d_3^0(\hat{1}, k, j) \, A_3^0(\hat{\bar{1}}, i, \hat{2}) \, B_4^0(\hat{\bar{\bar{1}}}_q, \widetilde{(kj)}_g, \tilde{l}_g, \hat{\bar{2}}_{\bar{q}}) \, J_2^{(2)}(p_{\widetilde{(kj)}}, p_{\tilde{l}})$$

$$+\frac{1}{2} d_3^0(\hat{2}, k, l) \, A_3^0(\hat{1}, i, \hat{\bar{2}}) \, B_4^0(\hat{\bar{1}}_q, \tilde{j}_g, \widetilde{(kl)}_g, \hat{\bar{\bar{2}}}_{\bar{q}}) \, J_2^{(2)}(p_{\tilde{j}}, p_{\widetilde{(kl)}})$$

$$+\frac{1}{2}\left[\left(S_{1k2} - S_{\bar{1}\tilde{k}\bar{2}}\right) - \left(S_{1k(jk)} - S_{\bar{1}\tilde{k}(\widetilde{jk})}\right) - \left(S_{2k(kl)} - S_{\bar{2}\tilde{k}(\widetilde{kl})}\right) \right]$$

$$\times A_3^0(\hat{1}, i, \hat{2}) \, B_4^0(\hat{\bar{1}}_q, \widetilde{(jk)}_g, \widetilde{(kl)}_g, \hat{\bar{2}}_{\bar{q}}) \, J_2^{(2)}(p_{\widetilde{(jk)}}, p_{\widetilde{(kl)}})$$

$$-d_3^0(\hat{1}, i, j) \, d_3^0(\hat{2}, l, k) \, B_4^0(\hat{\bar{1}}_q, \widetilde{(ij)}_g, \widetilde{(kl)}_g, \hat{\bar{2}}_{\bar{q}}) \, J_2^{(2)}(p_{(ij)}, p_{(kl)})$$

$$-d_3^0(\hat{1}, l, k) \, d_3^0(\hat{2}, i, j) \, B_4^0(\hat{\bar{1}}_q, \widetilde{(lk)}_g, \widetilde{(ij)}_g, \hat{\bar{2}}_{\bar{q}}) \, J_2^{(2)}(p_{(lk)}, p_{(ij)}) \bigg\}, \tag{5.4.35}$$

where $P_C(i, j, k, l)$ denotes the set of cyclic permutations of the gluons.

It is interesting to note the appearance of the sub-leading colour quark-antiquark antenna $\tilde{A}_4^0$ and the accompanying A_3^0 antennae. The $\tilde{A}_4^0$ antenna is introduced to remove spurious divergent behaviour of the D_4^0 antenna in the triple collinear limit. Specifically, the D_4^0 antenna contains the IR divergent limit involving colour-disconnected gluons,

$$D_4^0(i, j, k, l) \xrightarrow{j||i||l} \tilde{P}_{ijl \to Q}(x, y, z), \tag{5.4.36}$$

where the antenna tends to the QED-like triple collinear splitting function. This divergent limit has no analogue in the leading colour physical matrix elements and must be removed. In QCD, the quark resides in the fundamental representation and so always terminates a string of gluons which lie to the right (left) of the quark (antiquark) in the colour ordering, e.g.,

$$M_n^0(\cdots; \hat{1}_q, i_g, j_g, k_g, \cdots, l_g, m_g, n_g, \hat{2}_{\bar{q}}; \cdots). \tag{5.4.37}$$

The D_4^0 antenna is derived from the decay of a neutralino to a gluino and gluons, $\tilde{\chi} \to \tilde{g}ggg$, where the gluino plays the role of the quark. In contrast to the quarks, the gluino resides in the adjoint representation and so can sit anywhere in the colour ordering, including configurations with gluons either side of the gluino. For example,

the D_4^0 is derived from the squared partial amplitude $M_4^0(i_{\tilde{g}}, j_g, k_g, l_g)$ which is symmetric under cyclic permutations of its partons. The cyclic symmetry of this matrix element gives rise to the spurious divergent limit described in Eq. (5.4.36).

In any QCD calculation involving a quark-antiquark pair, the subtraction term will contain two D_4^0 antennae, one for the quark and the other for the antiquark, each containing a spurious limit of the kind in Eq. (5.4.36). For example, for the matrix element in Eq. (5.4.37), the subtraction term contains the antennae[1], $D_4^0(\hat{1}, i, j, k)$ and $D_4^0(\hat{2}, n, m, l)$. The subtraction term is constructed for a block of colour orderings related by cyclic permutations of gluons. Using this fact, the subtraction term will always contain the antennae $D_4^0(\hat{1}, i, j, k)$ and $D_4^0(\hat{2}, k, j, i)$, where the arguments of the second antenna are obtained by cyclically permuting the gluons in Eq. (5.4.37). Both of these antennae contain spurious limits of the kind in Eq. (5.4.36), involving gluons i and k and the antenna's fermion. The spurious limits of both D_4^0 antennae can therefore be removed using an $\tilde{A}_4^0(\hat{1}, i, k, \hat{2})$ antenna, as is done in Eq. (5.4.35).

Using D_4^0 antennae to isolate divergences associated with the quark and antiquark endpoints of a quark string, forces us to construct the subtraction term for a block of colour orderings related by cyclic permutations of gluons. Exploiting the cyclic permutations, the spurious limits of the D_4^0 antennae can be systematically removed using an $\tilde{A}_4^0$ antenna. It is noted that this argument holds no matter how many gluons are present in the quark string[2] and the technique is not a special case of the six parton scattering process considered here.

With the modifications due to the spurious limits of the quark-gluon antennae, the double real subtraction term fits the general structure derived in Section 4.5. Due to the non-trivial factorisation of the four-parton final-final antennae and the large sum of permutations, it is not straightforward to show analytically that this subtraction term correctly mimics the IR divergent behaviour of the physical cross section. However, to demonstrate its validity, the subtraction term has been tested numerically.

---

[1]Here the quark-antiquark pair is in the initial state (IF D_4^0 antennae) for consistency with the process considered in this section but the argument is generic to FF, IF and II antennae.

[2]The number of gluons should be more than two. In the case of two gluons an A_4^0 antenna is used instead of the D_4^0 and the issue does not arise.
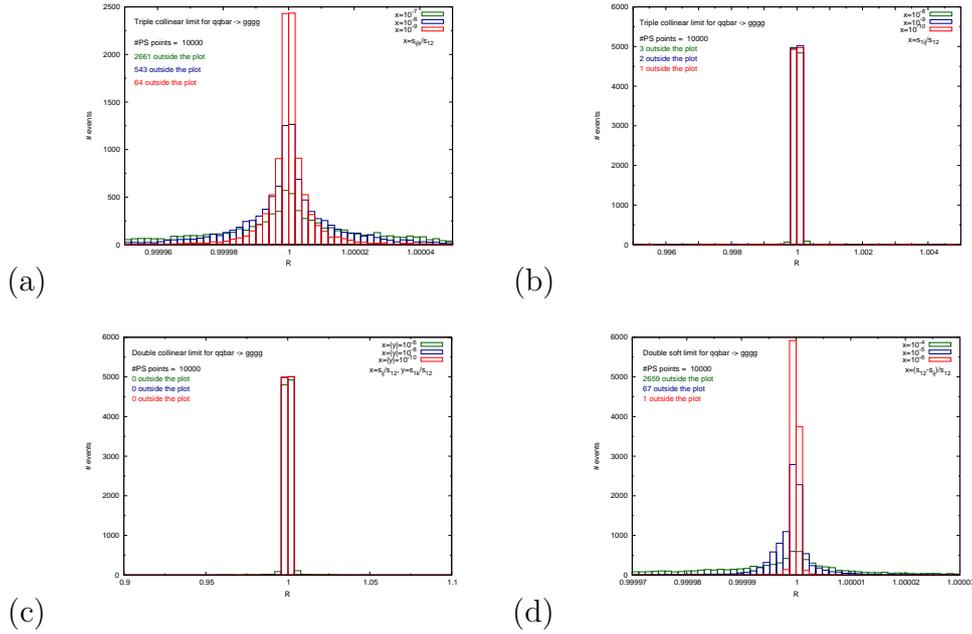
Figure 5.4: Plots displaying the convergence of the double real subtraction term to the physical matrix element in various unresolved limits. The green data is furthest from the singular configuration with the blue data closer to the singular region and the red data the closest. (a) Final-state triple collinear limit between partons i, j, k such that $x = s_{ijk}/s_{12}$. (b) Triple collinear limit between final-state partons i, j and initial-state parton 1, such that $x = s_{1ij}/s_{12}$. (c) Double collinear limit between final-state partons i, j and the initial-final pair $1, k$ such that $x = s_{ij}/s_{12}$, $y = s_{1k}/s_{12}$. (d) Double soft limit for soft partons i, j such that $x = (s_{12} - s_{ij})/s_{12}$.

For each IR divergent configuration, a set of momenta were generated using RAMBO [109] such that the momenta fulfil a set of constraints defining the unresolved configuration. In this configuration, we compute the ratio of the physical matrix element to the subtraction term:

$$R \;=\; \frac{\mathrm{d}\hat{\sigma}^{RR}_{NNLO}}{\mathrm{d}\hat{\sigma}^{S}_{NNLO}}. \qquad (5.4.38)$$

This procedure is then repeated for 10,000 different phase space points in the unresolved configuration defined by the constraints. The constraints are then tightened to force the phase space points closer to the unresolved singular point and the ratio calculated for another 10,000 points. The procedure is repeated once more for a set of points even closer to the singular point and the histogram of ratios for the three sets of constraints plotted.
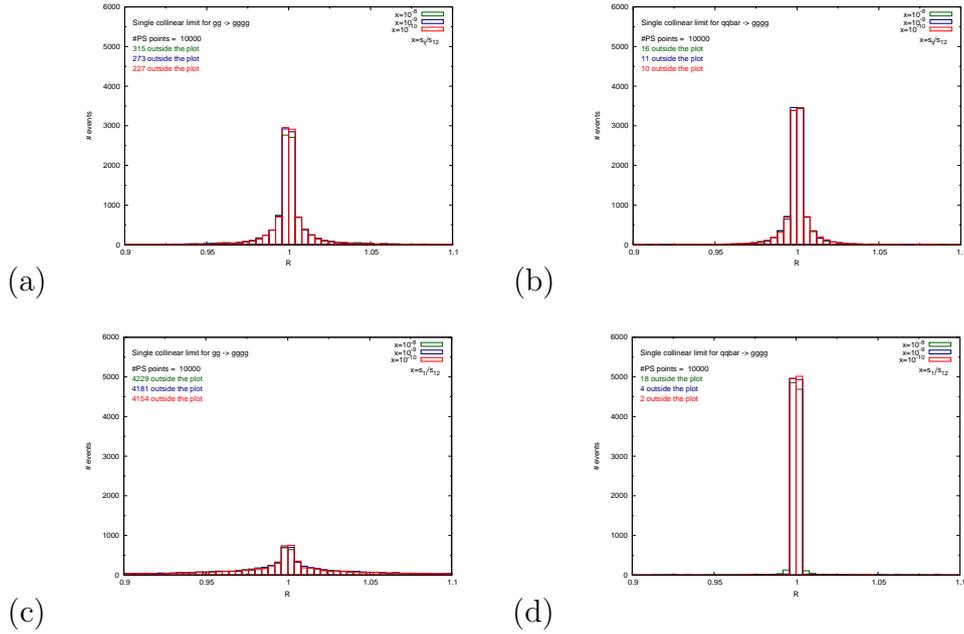
Figure 5.5: Distributions of R without azimuthal angular rotations for single collinear limits: final-final collinear limit for (a) $gg \rightarrow gggg$ and (b) $q\bar{q} \rightarrow gggg$ and initial-final gluon-gluon collinear limit for (c) $gg \rightarrow gggg$ and (d) $q\bar{q} \rightarrow gggg$. The parameter x controls how closely the singular limit is approached, close (dark green), closer (blue) and closest (red).

A selection of plots from four different unresolved configurations is shown in Figure 5.4. In each plot we see that the distribution of R becomes more sharply peaked around one as the unresolved singular limit is approached, i.e., as the parameter x gets smaller. This provides statistical evidence for the convergence of the subtraction term to the physical cross section in the IR divergent limits.

Testing the subtraction term in this way also gives a clear demonstration of the presence of azimuthal correlations in the single collinear limits. The origin and solution to this problem have been discussed in [22, 35, 108]. It was shown that the azimuthal correlations, which spoil the subtraction in the single collinear limit, arise from splitting functions where a parent gluon splits into two daughter gluons or a quark-antiquark pair (and the various crossings of this configuration to include initial-state partons). The $q\bar{q} \rightarrow gggg$ process contains the same final state as the $gg \rightarrow gggg$ process, studied in [79]. Therefore, by turning off the angular rotations when computing the ratio R, both subtraction terms should display similar behaviour when testing the single collinear limit between two final-state partons. This is seen

in Figure 5.5(a) and (b), where the subtraction terms for both processes display a broad peak, characteristic of the presence of uncompensated angular terms. An interesting comparison between the two processes is seen in the initial-final collinear limit. The collinear limit between an initial-state gluon and a final-state gluon does display azimuthal correlations while the collinear limit between an initial-state quark and a final-state gluon does not. We see that the limit involving the initial-state quark shown in Figure 5.5(d) is sharply peaked while the corresponding limit in the purely gluonic process seen in Figure 5.5(c) displays a broad peak because of the uncompensated azimuthal correlations.

5.4.2 Real-virtual subtraction term, $\mathrm{d}\hat{\sigma}^{T}_{NNLO}$

Following the discussion in Sec. 4.5, the real-virtual subtraction term is given by,

$$
\begin{aligned}
\mathrm{d}\hat{\sigma}^{T}_{q\bar{q},NNLO} = \ & \mathcal{N}^{1}_{q\bar{q},5} \int \mathrm{d}\Phi_3(p_3,\ldots,p_5;x_1 p_1, x_2 p_2)\frac{1}{3!}\frac{\mathrm{d}x_1}{x_1}\frac{\mathrm{d}x_2}{x_2} \sum_{P(i,j,k)} \Bigg\{ \\
- \ & \boldsymbol{J}^{(1)}_5(\hat{\bar{1}}_q, i_g, j_g, k_g, \hat{\bar{2}}_{\bar{q}})\ B^0_5(\hat{\bar{1}}_q, i_g, j_g, k_g, \hat{\bar{2}}_{\bar{q}})\ J^{(3)}_2(p_i, p_j, p_k) \\
+ \ & d^0_3(\hat{\bar{1}}, i, j)\Bigg[B^1_4(\hat{\bar{1}}_q, \widetilde{(ij)}_g, k_g, \hat{\bar{2}}_{\bar{q}})\delta(1-x_1)\delta(1-x_2) \\
& + \boldsymbol{J}^{(1)}_4(\hat{\bar{1}}_q, \widetilde{(ij)}_g, k_g, \hat{\bar{2}}_{\bar{q}})\ B^0_4(\hat{\bar{1}}_q, \widetilde{(ij)}_g, k_g, \hat{\bar{2}}_{\bar{q}})\Bigg]\ J^{(2)}_2(p_{\widetilde{ij}}, p_k) \\
+ \ & f^0_3(i, j, k)\Bigg[B^1_4(\hat{\bar{1}}_q, \widetilde{(ij)}_g, \widetilde{(jk)}_g, \hat{\bar{2}}_{\bar{q}})\delta(1-x_1)\delta(1-x_2) \\
& + \boldsymbol{J}^{(1)}_4(\hat{\bar{1}}_q, \widetilde{(ij)}_g, \widetilde{(jk)}_g, \hat{\bar{2}}_{\bar{q}})\ B^0_4(\hat{\bar{1}}_q, \widetilde{(ij)}_g, \widetilde{(jk)}_g, \hat{\bar{2}}_{\bar{q}})\Bigg]\ J^{(2)}_2(p_{\widetilde{ij}}, p_{\widetilde{jk}}) \\
+ \ & d^0_3(\hat{\bar{2}}, k, j)\Bigg[B^1_4(\hat{\bar{1}}_q, i_g, \widetilde{(kj)}_g, \hat{\bar{2}}_{\bar{q}})\delta(1-x_1)\delta(1-x_2) \\
& + \boldsymbol{J}^{(1)}_4(\hat{\bar{1}}_q, i_g, \widetilde{(kj)}_g, \hat{\bar{2}}_{\bar{q}})\ B^0_4(\hat{\bar{1}}_q, i_g, \widetilde{(kj)}_g, \hat{\bar{2}}_{\bar{q}})\Bigg]\ J^{(2)}_2(p_i, p_{\widetilde{jk}}) \\
+ \ & \Bigg[d^1_3(\hat{\bar{1}}, i, j)\delta(1-x_1)\delta(1-x_2) + \boldsymbol{J}^{(1)}_D(\hat{\bar{1}}_g, i_g, j_g)\ d^0_3(\hat{\bar{1}}, i, j) \\
& -2\, d^0_3(\hat{\bar{1}}, i, j)\ \boldsymbol{J}^{(1)}_2(\hat{\bar{1}}_q, \widetilde{(ij)})\Bigg]\ B^0_4(\hat{\bar{1}}_q, \widetilde{(ij)}_g, k_g, \hat{\bar{2}}_{\bar{q}})\ J^{(2)}_2(p_{\widetilde{ij}}, p_k) \\
+ \ & \Bigg[f^1_3(i, j, k)\delta(1-x_1)\delta(1-x_2) + \boldsymbol{J}^{(1)}_F(i_g, j_g, k_g)\ f^0_3(i, j, k) \\
& -2\, f^0_3(i, j, k)\ \boldsymbol{J}^{(1)}_2(\widetilde{(ij)}_g, \widetilde{(jk)}_g)\Bigg]\ B^0_4(\hat{\bar{1}}_q, \widetilde{(ij)}_g, \widetilde{(jk)}_g, \hat{\bar{2}}_{\bar{q}})\ J^{(2)}_2(p_{\widetilde{ij}}, p_{\widetilde{jk}})
\end{aligned}
$$

$$
\begin{aligned}
+ \; & \Big[d_3^1(\hat{\bar{2}}, k, j)\delta(1-x_1)\delta(1-x_2) + \boldsymbol{J}_D^{(1)}(\hat{\bar{2}}_q, k_g, j_g) \; d_3^0(\hat{\bar{2}}, k, j) \\
& -2 \; d_3^0(\hat{\bar{2}}, k, j) \; \boldsymbol{J}_2^{(1)}(\hat{\bar{\bar{2}}}_q, \widetilde{(kj)}_g) \Big] B_4^0(\hat{\bar{1}}_q, i_g, \widetilde{(kj)}_g, \hat{\bar{\bar{2}}}_{\bar{q}}) \; J_2^{(2)}(p_i, p_{\widetilde{jk}}) \\
- \; & \Big[\tilde{A}_3^1(\hat{\bar{1}}, i, \hat{\bar{2}})\delta(1-x_1)\delta(1-x_2) + \boldsymbol{J}_{\tilde{A}}^{(1)}(\hat{\bar{1}}_q, i_g, \hat{\bar{2}}_{\bar{q}}) \; A_3^0(\hat{\bar{1}}, i, \hat{\bar{2}}) \\
& -A_3^0(\hat{\bar{1}}, i, \hat{\bar{2}}) \; \boldsymbol{J}_2^{(1)}(\hat{\bar{\bar{1}}}_q, \hat{\bar{\bar{2}}}_{\bar{q}}) \Big] B_4^0(\hat{\bar{\bar{1}}}_q, \tilde{j}_g, \tilde{k}_g, \hat{\bar{\bar{2}}}_{\bar{q}}) \; J_2^{(2)}(p_{\tilde{j}}, p_{\tilde{k}}) \\
+ \; & b_0 \log\left(\frac{\mu^2}{|s_{1ij}|}\right) d_3^0(\hat{\bar{1}}, i, j)\delta(1-x_1)\delta(1-x_2) \; B_4^0(\hat{\bar{\bar{1}}}_q, \widetilde{(ij)}_g, k_g, \hat{\bar{2}}_{\bar{q}}) J_2^{(2)}(p_{\widetilde{ij}}, p_k) \\
+ \; & b_0 \log\left(\frac{\mu^2}{s_{ijk}}\right) f_3^0(i, j, k)\delta(1-x_1)\delta(1-x_2) \; B_4^0(\hat{\bar{1}}_q, \widetilde{(ij)}_g, \widetilde{(jk)}_g, \hat{\bar{2}}_{\bar{q}}) J_2^{(2)}(p_{\widetilde{ij}}, p_{\widetilde{jk}}) \\
+ \; & b_0 \log\left(\frac{\mu^2}{|s_{2kj}|}\right) d_3^0(\hat{\bar{2}}, k, j)\delta(1-x_1)\delta(1-x_2) \; B_4^0(\hat{\bar{1}}_q, i_g, \widetilde{(jk)}_g, \hat{\bar{\bar{2}}}_{\bar{q}}) J_2^{(2)}(p_i, p_{\widetilde{jk}}) \\
+ \; & \frac{1}{2}\Big[\frac{1}{2}\mathcal{D}_{3,q}^0(s_{\hat{\bar{1}}\widetilde{(ij)}}) - \frac{1}{2}\mathcal{D}_{3,q}^0(s_{\hat{\bar{1}}j}) - \frac{1}{3}\mathcal{F}_3^0(s_{\widetilde{(ij)}k}) + \frac{1}{3}\mathcal{F}_3^0(s_{jk}) + \mathcal{A}_{3,q\bar{q}}^0(s_{\hat{\bar{1}}\hat{\bar{2}}}) - \mathcal{A}_{3,q\bar{q}}^0(s_{\hat{\bar{1}}\hat{\bar{2}}}) \\
& +\delta(1-x_1)\delta(1-x_2)\Big(\mathcal{S}(s_{\widetilde{(ij)}k}, s_{jk}, x_{\widetilde{(ij)}k,jk}) - \mathcal{S}(s_{jk}, s_{jk}, 1) - \mathcal{S}(s_{\hat{\bar{1}}\widetilde{(ij)}}, s_{jk}, x_{\hat{\bar{1}}\widetilde{(ij)},jk}) \\
& +\mathcal{S}(s_{\hat{\bar{1}}j}, s_{jk}, x_{\hat{\bar{1}}j,jk})\Big)\Big] d_3^0(\hat{\bar{1}}, i, j) \; B_4^0(\hat{\bar{\bar{1}}}_q, \widetilde{(ij)}_g, k_g, \hat{\bar{2}}_{\bar{q}}) \; J_2^{(2)}(p_{\widetilde{ij}}, p_k) \\
+ \; & \frac{1}{2}\Big[-\frac{1}{2}\mathcal{D}_{3,q}^0(s_{\hat{\bar{1}}\widetilde{(ij)}}) + \frac{1}{2}\mathcal{D}_{3,q}^0(s_{\hat{\bar{1}}i}) - \frac{1}{2}\mathcal{D}_{3,q}^0(s_{\hat{\bar{2}}\widetilde{(jk)}}) + \frac{1}{2}\mathcal{D}_{3,q}^0(s_{\hat{\bar{2}}k}) + \frac{1}{3}\mathcal{F}_3^0(s_{\widetilde{(ij)}\widetilde{(jk)}}) \\
& -\frac{1}{3}\mathcal{F}_3^0(s_{ik}) + \delta(1-x_1)\delta(1-x_2)\Big(-\mathcal{S}(s_{\widetilde{(ij)}\widetilde{(jk)}}, s_{ik}, x_{\widetilde{(ij)}\widetilde{(jk)},ik}) + \mathcal{S}(s_{ik}, s_{ik}, 1) \\
& +\mathcal{S}(s_{\hat{\bar{1}}\widetilde{(ij)}}, s_{ik}, x_{\hat{\bar{1}}\widetilde{(ij)},ik}) - \mathcal{S}(s_{\hat{\bar{1}}i}, s_{ik}, x_{\hat{\bar{1}}i,ik}) + \mathcal{S}(s_{\hat{\bar{2}}\widetilde{(jk)}}, s_{ik}, x_{\hat{\bar{2}}\widetilde{(jk)},ik}) \\
& -\mathcal{S}(s_{\hat{\bar{2}}k}, s_{ik}, x_{\hat{\bar{2}}k,ik})\Big)\Big] f_3^0(i, j, k) \; B_4^0(\hat{\bar{1}}_q, \widetilde{(ij)}_g, \widetilde{(jk)}_g, \hat{\bar{2}}_{\bar{q}}) \; J_2^{(2)}(p_{\widetilde{ij}}, p_{\widetilde{jk}}) \\
+ \; & \frac{1}{2}\Big[\frac{1}{2}\mathcal{D}_{3,q}^0(s_{\hat{\bar{2}}\widetilde{(jk)}}) - \frac{1}{2}\mathcal{D}_{3,q}^0(s_{\hat{\bar{2}}j}) - \frac{1}{3}\mathcal{F}_3^0(s_{i\widetilde{(jk)}}) + \frac{1}{3}\mathcal{F}_3^0(s_{ij}) + \mathcal{A}_{3,q\bar{q}}^0(s_{\hat{\bar{1}}\hat{\bar{2}}}) - \mathcal{A}_{3,q\bar{q}}^0(s_{\hat{\bar{1}}\hat{\bar{2}}}) \\
& +\delta(1-x_1)\delta(1-x_2)\Big(\mathcal{S}(s_{i\widetilde{(jk)}}, s_{ij}, x_{i\widetilde{(jk)},ij}) - \mathcal{S}(s_{ij}, s_{ij}, 1) \\
& -\mathcal{S}(s_{\hat{\bar{2}}\widetilde{(kj)}}, s_{ij}, x_{\hat{\bar{2}}\widetilde{(kj)},ij}) + \mathcal{S}(s_{\hat{\bar{2}}j}, s_{ij}, x_{\hat{\bar{2}}j,ij})\Big)\Big] \\
& \times d_3^0(\hat{\bar{2}}, k, j) \; B_4^0(\hat{\bar{1}}_q, i_g, \widetilde{(kj)}_g, \hat{\bar{\bar{2}}}_{\bar{q}}) \; J_2^{(2)}(p_i, p_{\widetilde{jk}}) \\
+ \; & \frac{1}{2}\Big[-\mathcal{A}_{3,q\bar{q}}^0(s_{\hat{\bar{1}}\hat{\bar{2}}}) + \mathcal{A}_{3,q\bar{q}}^0(s_{\hat{\bar{1}}\hat{\bar{2}}}) + \frac{1}{2}\mathcal{D}_{3,q}^0(s_{\hat{\bar{1}}\tilde{j}}) - \frac{1}{2}\mathcal{D}_{3,q}^0(s_{\hat{\bar{1}}j}) + \frac{1}{2}\mathcal{D}_{3,q}^0(s_{\hat{\bar{2}}\tilde{k}}) \\
& -\frac{1}{2}\mathcal{D}_{3,q}^0(s_{\hat{\bar{2}}k}) + \delta(1-x_1)\delta(1-x_2)\Big(\mathcal{S}(s_{\hat{\bar{1}}\hat{\bar{2}}}, s_{\tilde{j}k}, x_{\hat{\bar{1}}\hat{\bar{2}},\tilde{j}k}) - \mathcal{S}(s_{\hat{\bar{1}}\hat{\bar{2}}}, s_{jk}, x_{\hat{\bar{1}}\hat{\bar{2}},jk}) \\
& -\mathcal{S}(s_{\hat{\bar{1}}\tilde{j}}, s_{\tilde{j}k}, x_{\hat{\bar{1}}\tilde{j},\tilde{j}k}) + \mathcal{S}(s_{\hat{\bar{1}}j}, s_{jk}, x_{\hat{\bar{1}}j,jk}) - \mathcal{S}(s_{\hat{\bar{2}}\tilde{k}}, s_{\tilde{j}k}, x_{\hat{\bar{2}}\tilde{k},\tilde{j}k}) \\
& +\mathcal{S}(s_{\hat{\bar{2}}k}, s_{jk}, x_{\hat{\bar{2}}k,jk})\Big)\Big] A_3^0(\hat{\bar{1}}, i, \hat{\bar{2}}) \; B_4^0(\hat{\bar{\bar{1}}}_q, \tilde{j}_g, \tilde{k}_g, \hat{\bar{\bar{2}}}_{\bar{q}}) \; J_2^{(2)}(p_{\tilde{j}}, p_{\tilde{k}}) \Big\}.
\end{aligned}
$$

$$(5.4.39)$$

The integrated antenna strings used in this subtraction term are given by,

$$
\begin{aligned}
\boldsymbol{J}_5^{(1)}(\hat{\bar{1}}_q, i_g, j_g, k_g, \hat{\bar{2}}_{\bar{q}}) &= \boldsymbol{J}_2^{(1)}(\hat{\bar{1}}_q, i_g) + \boldsymbol{J}_2^{(1)}(i_g, j_g) + \boldsymbol{J}_2^{(1)}(j_g, k_g) + \boldsymbol{J}_2^{(1)}(\hat{\bar{2}}_{\bar{q}}, k_g), \\
\boldsymbol{J}_D^1(\hat{\bar{1}}_q, i_g, j_g) &= \boldsymbol{J}_2^{(1)}(\hat{\bar{1}}_q, i_g) + \boldsymbol{J}_2^{(1)}(i_g, j_g) + \boldsymbol{J}_2^{(1)}(\hat{\bar{2}}_q, j_g), \\
\boldsymbol{J}_F^1(i_g, j_g, k_g) &= \boldsymbol{J}_2^{(1)}(i_g, j_g) + \boldsymbol{J}_2^{(1)}(j_g, k_g) + \boldsymbol{J}_2^{(1)}(i_g, k_g), \\
\boldsymbol{J}_D^1(\hat{\bar{2}}_q, i_g, j_g) &= \boldsymbol{J}_D^1(\hat{\bar{1}}_q, i_g, j_g), (\hat{\bar{1}} \leftrightarrow \hat{\bar{2}},\ z_1 \leftrightarrow z_2), \\
\boldsymbol{J}_{\tilde{A}}^1(\hat{\bar{1}}_q, i_g, \hat{\bar{2}}_{\bar{q}}) &= \boldsymbol{J}_2^{(1)}(\hat{\bar{1}}_q, \hat{\bar{2}}_{\bar{q}}).
\end{aligned}
\tag{5.4.40}
$$

After integration only those terms introduced at the real-virtual level are passed down to the double virtual subtraction term.

The d_3^1 antenna is derived from the decay of a neutralino to a gluino and gluons, the gluino playing the role of the quark. As with the D_4^0, we encounter a spurious divergent limit, which is removed via the $\tilde{A}_3^1$. Whilst this is not immediately an obvious requirement, we see that the A_4^0 introduced to the double real subtraction term has three parton antenna corrections that, when integrated, must appear in the real-virtual subtraction term.

In a similar manner to the double real subtraction term, a set of momenta were generated using RAMBO [109] for each divergent limit. In this configuration, the ratio of the physical matrix element to the subtraction term we compute is

$$
R = \frac{\mathrm{d}\hat{\sigma}_{NNLO}^{RV}}{\mathrm{d}\hat{\sigma}_{NNLO}^{T}}.
\tag{5.4.41}
$$

This procedure is repeated for 1000 different phase space points in each unresolved configuration, again with repeated tightening of the constraints such that the points are taken closer to the singular limit. Since the physical matrix element contains the one-loop virtual correction, we must now check limits for the pole contributions which should cancel analytically against the real-virtual subtraction term. The right hand plot in each row in Figure 5.6 illustrates the finite contribution of the single unresolved limits. The left and centre plots are the $1/\epsilon^2$ and $1/\epsilon$ contributions respectively.

Again we observe that the distribution of R peaks around unity as the limit is approached. We see from the sharp peaks at unity that there is an exact analytic
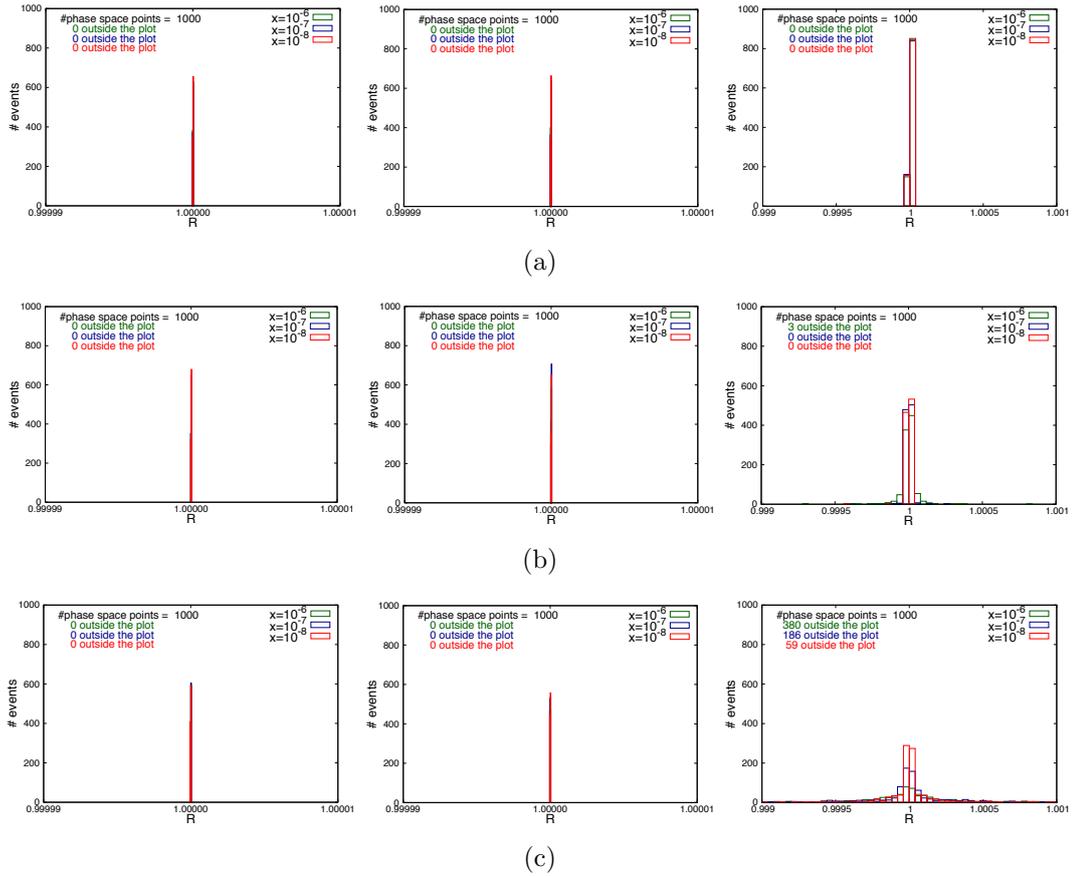
Figure 5.6: Plots displaying the convergence of the subtraction term to the real-virtual physical matrix element in various unresolved limits. The green data is furthest from the singular configuration with the blue data closer to the singular region and the red data the closest. The left plot of each row is the $1/\epsilon^2$ contribution, the centre plot the $1/\epsilon$ contribution and the right hand plot the finite contribution. (a) Final-state single soft limit for parton i such that $x = (s_{12} - s_{jk})/s_{12}$. (b) Collinear limit between final-state gluons i and j, such that $x = s_{ij}/s_{12}$. (c) Collinear limit between final-state parton i and the initial quark 1 such that $x = s_{1i}/s_{12}$.

cancellation of the pole contributions. The azimuthal corrections must also be taken into account at the real-virtual level , since we again encounter the splitting of a parent gluon into gluons or a quark-antiquark pair. The effect of including azimuthal averaging is shown in Figure 5.7 for the final-final gluon collinear limit.

The symmetry of the colour ordering is also observed in the plots, since we see similar behaviour between the quark-gluon and antiquark-gluon endpoints of the colour string in their respective collinear limits. As expected, the R distribution behaves similarly for the three gluon-gluon collinear limits, and as each gluon goes soft. The full set of finite contribution limits are contained in Appendix C.

(a)   (b)

Figure 5.7: Distributions of the finite contributions to R for the final-final collinear limit for $q\bar{q} \to ggg$ (a) without and (b) with azimuthal averaging.
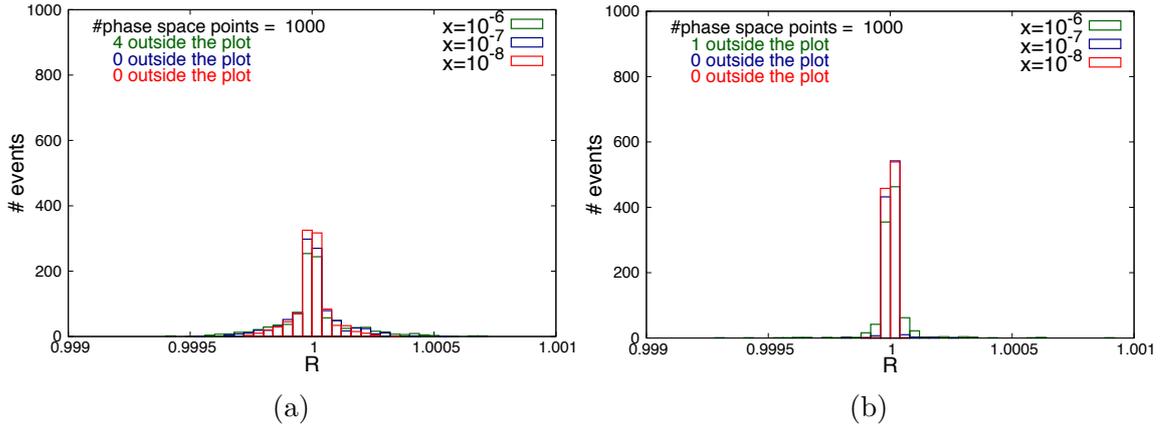
5.4.3   Double virtual subtraction term, $\mathrm{d}\hat{\sigma}^{U}_{NNLO}$

Following the discussion in Sec. 4.5.3, the double virtual subtraction term is constructed from the remaining terms inherited from the double real and the real-virtual subtraction terms, in addition to the double virtual mass factorisation contribution. The resulting double virtual subtraction term can be written in terms of single and double unresolved integrated antenna strings,

$$
\begin{aligned}
\mathrm{d}\hat{\sigma}^{U}_{q\bar{q},NNLO} = {} & -\mathcal{N}^2_{q\bar{q},4}\,\mathrm{d}\Phi_2(p_3,p_4;p_1,p_2)\int \frac{\mathrm{d}z_1}{z_1}\frac{\mathrm{d}z_2}{z_2}\frac{1}{2!}\sum_{P(i,j)} \\
& \Big\{ \; \boldsymbol{J}^{(1)}_4(\hat{\bar{1}}_q,i_g,j_g,\hat{\bar{2}}_{\bar{q}}) \left(B^1_4(\hat{\bar{1}}_q,i_g,j_g,\hat{\bar{2}}_{\bar{q}}) - \frac{b_0}{\epsilon}\,B^0_4(\hat{\bar{1}}_q,i_g,j_g,\hat{\bar{2}}_{\bar{q}}) \right) \\
& + \; \frac{1}{2}\,\boldsymbol{J}^{(1)}_4(\hat{\bar{1}}_q,i_g,j_g,\hat{\bar{2}}_{\bar{q}}) \otimes \boldsymbol{J}^{(1)}_4(\hat{\bar{1}}_q,i_g,j_g,\hat{\bar{2}}_{\bar{q}})\,B^0_4(\hat{\bar{1}}_q,i_g,j_g,\hat{\bar{2}}_{\bar{q}}) \\
& + \; \boldsymbol{J}^{(2)}_4(\hat{\bar{1}}_q,i_g,j_g,\hat{\bar{2}}_{\bar{q}})\,B^0_4(\hat{\bar{1}}_q,i_g,j_g,\hat{\bar{2}}_{\bar{q}}) \Big\}\,J^{(2)}_2(p_i,p_j). \qquad (5.4.42)
\end{aligned}
$$

The single unresolved integrated antenna string is defined in Eq. (5.2.14). The new ingredient at the double virtual level is the double unresolved integrated antenna string, $\boldsymbol{J}^{(2)}_4$, which displays the structure discussed in Sec. 4.5.3. In Eq. (5.2.14) the single unresolved integrated antenna string was written as a sum over integrated dipoles. The analogous dipole-like formula for $\boldsymbol{J}^{(2)}_4$ is given by,

$$
\boldsymbol{J}^{(2)}_4(\hat{\bar{1}}_q,i_g,j_g,\hat{\bar{2}}_{\bar{q}}) = \boldsymbol{J}^{(2)}_2(\hat{\bar{1}}_q,i_g) + \boldsymbol{J}^{(2)}_2(i_g,j_g) + \boldsymbol{J}^{(2)}_2(j_g,\hat{\bar{2}}_{\bar{q}}) - \overline{\boldsymbol{J}}^{(2)}_2(\hat{\bar{1}}_q,\hat{\bar{2}}_{\bar{q}}),
$$

$$(5.4.43)$$

where the two-parton double unresolved integrated antenna strings are given by:

$$
\begin{aligned}
\boldsymbol{J}_2^{(2)}(\hat{\bar{1}}_q, i_g) &= \frac{1}{2}\mathcal{D}_{4,q}^0(s_{\bar{1}i}) + \frac{1}{2}\mathcal{D}_{3,q}^1(s_{\bar{1}i}) + \frac{b_0}{2\epsilon}\left(\frac{|s_{\bar{1}i}|}{\mu^2}\right)^{-\epsilon}\mathcal{D}_{3,q}^0(s_{\bar{1}i}) \\
&\quad - \frac{1}{4}\big[\mathcal{D}_{3,q}^0(s_{\bar{1}i}) \otimes \mathcal{D}_{3,q}^0(s_{\bar{1}i})\big](z_1) - \overline{\Gamma}_{qq}^{(2)}(z_1)\delta(1-z_2), \quad (5.4.44) \\
\boldsymbol{J}_2^{(2)}(i_g, j_g) &= \frac{1}{4}\mathcal{F}_4^0(s_{ij}) + \frac{1}{3}\mathcal{F}_3^1(s_{ij}) + \frac{b_0}{3\epsilon}\left(\frac{s_{ij}}{\mu^2}\right)^{-\epsilon}\mathcal{F}_3^0(s_{ij}) \\
&\quad - \frac{1}{9}\big[\mathcal{F}_3^0(s_{ij}) \otimes \mathcal{F}_3^0(s_{ij})\big], \quad (5.4.45) \\
\boldsymbol{J}_2^{(2)}(i_g, \hat{\bar{2}}_{\bar{q}}) &= \boldsymbol{J}_2^{(2)}(\hat{\bar{2}}_q, i_g). \quad (5.4.46)
\end{aligned}
$$

An integrated dipole, $\boldsymbol{J}_2^{(\ell)}(i, j)$ is associated with a power of $(|s_{ij}|)^{-\ell\epsilon}$, thereby matching specific terms in the Catani representation of the one- and two-loop matrix elements. However, for the leading colour contribution to $q\bar{q} \to gg$ jets, we do not expect a singular contribution that depends on $s_{\bar{1}\bar{2}}$.

However, the D_4^0 antenna contain infrared singular limits that are not present in the matrix elements. These singularities are compensated by the $\tilde{A}_{4,q\bar{q}}^0$ contribution in $d\hat{\sigma}_{NNLO}^S$ and by the $\tilde{A}_{3,q\bar{q}}^1$ and and $\mathcal{A}_{3,q\bar{q}}^0 \times A_3^0$ terms in $d\hat{\sigma}_{NNLO}^T$. Terms of the form $(\mathcal{D}_{3,q}^0 \times A_3^0)$ and $(\mathcal{A}_{3,q\bar{q}}^0 \times d_3^0)$ which were introduced at the real-virtual level, cancel after integration. The integrated forms of these spurious contributions reappear in $d\hat{\sigma}_{NNLO}^U$ and are collected in $\overline{\boldsymbol{J}}_2^{(2)}$,

$$
\overline{\boldsymbol{J}}_2^{(2)}(\hat{\bar{1}}_q, \hat{\bar{2}}_{\bar{q}}) = \frac{1}{2}\tilde{\mathcal{A}}_{4,q\bar{q}}^0(s_{\bar{1}\bar{2}}) + \tilde{\mathcal{A}}_{3,q\bar{q}}^1(s_{\bar{1}\bar{2}}) - \frac{1}{2}\big[\mathcal{A}_{3,q\bar{q}}^0(s_{\bar{1}\bar{2}}) \otimes \mathcal{A}_{3,q\bar{q}}^0(s_{\bar{1}\bar{2}})\big](z_1, z_2),
$$

$$(5.4.47)$$

which is proportional to $(|s_{\bar{1}\bar{2}}|)^{-2\epsilon}$. At first sight, the presence of $\overline{\boldsymbol{J}}_2^{(2)}(\hat{\bar{1}}_q, \hat{\bar{2}}_{\bar{q}})$ appears to be in conflict with our earlier statement about the absence of singularities proportional to $s_{\bar{1}\bar{2}}$. However, the leading singularity in $\overline{\boldsymbol{J}}_2^{(2)}$ is $\mathcal{O}(1/\epsilon)$,

$$
\mathcal{P}oles\left(\epsilon\overline{\boldsymbol{J}}_2^{(2)}(1_q, 2_{\bar{q}})\right) = 0, \quad (5.4.48)
$$

so that, after expansion of the $(|s_{\bar{1}\bar{2}}|)^{-2\epsilon}$ factor, the singularity does not depend on

$s_{\bar{1}\bar{2}}$ while the remaining finite terms can and do depend on $\ln(s_{\bar{1}\bar{2}})$.

5.5 Gluon initiated dijet production at NNLO

The current construction of the double-real subtraction term encounters difficulties when matrix elements with both quarks and gluons have gluons in the initial state. For a matrix element of the form

$$B_n^0(m_q, \hat{1}_g, i_g, j_g, \cdots \bar{q}_m) \tag{5.5.49}$$

looks to the $D_4^0(m_q, \hat{1}_g, i_g, j_g)$ to account for the various single and double unresolved limits present at the end of the quark-gluon chain. However, the presence of the gluon in the initial state result in different mappings in the reduced-parton phase space, in the various limits. The solution to this is still under contention. This thesis turns instead to the real-virtual matrix-element, where we will see that a solution exists for a similar scenario in the three-parton D_3 antenna. Furthermore, we will see emergent structures that can be used to predict the form of the double real subtraction terms.

In this section we describe the calculation of the real-virtual subtraction term for quark-gluon scattering with two initial state gluons. For dijet production at NNLO, this involves the one-loop QCD matrix element for $gg \to gq\bar{q}$, where there are both explicit IR singularities from the one loop corrections, and also implicit single unresolved limits over the phase space integration. In Section 5.5.1 we examine the five parton real-virtual contribution to the NNLO cross section, and split it into two topologies determined by the relative position of the initial state gluons with the colour-ordered matrix element. For each of the topologies a subtraction term will be constructed.

5.5.1 Real-virtual subtraction term, $d\hat{\sigma}_{NNLO}^T$

We consider the process $gg \to gq\bar{q}$. The contribution to the cross section is given by

$$d\hat{\sigma}_{gg,NNLO}^{RV} = \mathcal{N}_{gg,5}^1 \int d\Phi_3(p_3, p_4, p_5; p_1, p_2) \frac{1}{3!} \frac{dx_1}{x_1} \frac{dx_2}{x_2} \sum_{P(\hat{1},\hat{2},i)}$$

$$\times B_5^1(j_q, \hat{\bar{1}}_g, \hat{\bar{2}}_g, i_g, k_{\bar{q}})\delta(1 - x_1)\delta(1 - x_2)J_2^{(3)}(p_i, p_j, p_k) + \mathcal{O}(\frac{1}{N^2}) \quad (5.5.50)$$

where the sum is over the set of six permutations of the gluons, including the initial states, and we just consider the leading colour contribution. We identify two topologies, defined by the relative position of the initial state gluons. Since the quarks are fixed at the end of the gluon string, the two initial gluons can either be colour connected (i.e. adjacent), or separated by the remaining final state gluon, which we label as topology $\mathbb{X}$ and $\mathbb{Y}$ respectively. In this way, (5.5.50) can be split up into

$$
\begin{aligned}
\mathrm{d}\hat{\sigma}_{gg,NNLO}^{RV,\mathbb{X}} = \quad & \mathcal{N}_{gg,5}^1 \int \mathrm{d}\Phi_3(p_3, p_4, p_5; p_1, p_2)\frac{\mathrm{d}x_1}{x_1}\frac{\mathrm{d}x_2}{x_2}\delta(1 - x_1)\delta(1 - x_2)J_2^{(3)}(p_i, p_j, p_k) \\
& \times \frac{1}{3!} \sum_{P(\hat{1},\hat{2})} \left[B_5^1(j_q, \hat{\bar{1}}_g, \hat{\bar{2}}_g, i_g, k_{\bar{q}}) + B_5^1(j_q, i_g, \hat{\bar{1}}_g, \hat{\bar{2}}_g, k_{\bar{q}}) \right] \quad (5.5.51) \\
\mathrm{d}\hat{\sigma}_{gg,NNLO}^{RV,\mathbb{Y}} = \quad & \mathcal{N}_{gg,5}^1 \int \mathrm{d}\Phi_3(p_3, p_4, p_5; p_1, p_2)\frac{\mathrm{d}x_1}{x_1}\frac{\mathrm{d}x_2}{x_2}\delta(1 - x_1)\delta(1 - x_2)J_2^{(3)}(p_i, p_j, p_k) \\
& \times \frac{1}{3!} \sum_{P(\hat{1},\hat{2})} B_5^1(j_q, \hat{\bar{1}}_g, i_g, \hat{\bar{2}}_g, k_{\bar{q}}) \quad (5.5.52)
\end{aligned}
$$

such that

$$\mathrm{d}\hat{\sigma}_{gg,NNLO}^{RV,full} = \mathrm{d}\hat{\sigma}_{gg,NNLO}^{RV,\mathbb{X}} + \mathrm{d}\hat{\sigma}_{gg,NNLO}^{RV,\mathbb{Y}}. \quad (5.5.53)$$

The full summation over the gluons is split into a block of four colour ordered matrix elements corresponding to colour-connected initial states, and two colour ordered matrix elements for those with non-adjacent initial states. Notably, the $\mathbb{Y}$ topology has a clear symmetry in the gluon ordering, which will be used to our advantage in the construction of the subtraction term. The $\mathbb{X}$ topology has a similar, although more subtle, symmetry, which can be mimicked in the subtraction term but in a less transparent fashion. Nevertheless, the aim of the next section is to construct the counter terms individually for each topology.

Subtraction term with colour connected initial states: $\mathbb{X}$ topology

The real-virtual contribution for the $\mathbb{X}$ topology is given by

$$
d\hat{\sigma}_{gg,NNLO}^{RV,\mathbb{X}} = \quad \mathcal{N}_{gg,5}^1 \int d\Phi_3(p_3,p_4,p_5;p_1,p_2)\frac{dx_1}{x_1}\frac{dx_2}{x_2}\delta(1-x_1)\delta(1-x_2)J_2^{(3)}(p_i,p_j,p_k)
$$

$$
\times \frac{1}{3!}\sum_{P(\hat{\bar{1}},\hat{\bar{2}})}\left[B_5^1(j_q,\hat{\bar{1}}_g,\hat{\bar{2}}_g,i_g,k_{\bar{q}}) + B_5^1(j_q,i_g,\hat{\bar{1}}_g,\hat{\bar{2}}_g,k_{\bar{q}})\right]. \tag{5.5.54}
$$

Whilst there are four colour orderings to consider, a unique subtraction term is required only for one, since all the orderings can be constructed via label exchange in the subtraction term.

Following this symmetry, we can write the subtraction term for the matrix element $B_5^1(j_q,\hat{\bar{1}}_g,\hat{\bar{2}}_g,i_g,k_{\bar{q}})$ as

$$
d\sigma_{NNLO}^{T,\mathbb{X}} = \mathcal{N}_{gg,5}^1 \int d\Phi_3(p_3,p_4,p_5;x_1p_1,x_2p_2)\frac{dx_1}{x_1}\frac{dx_2}{x_2} \times \Bigg\{
$$

$$
-\Big(\mathcal{D}_{3,g;gq}^0(s_{j\bar{1}}) + \mathcal{F}_{3,gg}^0(s_{\bar{1}\bar{2}}) + \frac{1}{2}\mathcal{F}_{3,g}^0(s_{i\bar{2}}) + \frac{1}{2}\mathcal{D}_3^0(s_{ik}) - \Gamma_{gg}^1(x_1)\delta(1-x_2)
$$

$$
-\Gamma_{gg}^1(x_2)\delta(1-x_1)\Big)B_5^0(j_q,\hat{1}_g,\hat{2}_g,i_g,k_{\bar{q}})J_2^{(3)}(p_j,p_i,p_k)
$$

$$
+G_3^0(\hat{\bar{2}}_g,k_{\bar{q}},j_q)\Bigg[\delta(1-x_1)\delta(1-x_2)A_4^1(\hat{\bar{2}}_g,\hat{\bar{1}}_g,i_g,\widetilde{(kj)}_g)
$$

$$
+\Big(\mathcal{F}_{3,gg}^0(s_{\bar{1}\bar{2}}) + \frac{1}{2}\mathcal{F}_{3,g}^0(s_{\bar{1}i}) + \frac{1}{3}\mathcal{F}_3^0(s_{i\widetilde{(kj)}}) + \frac{1}{2}\mathcal{F}_{3,g}^0(s_{\widetilde{(kj)}\bar{2}})
$$

$$
-\Gamma_{gg}^1(x_1)\delta(1-x_2) - \Gamma_{gg}^1(x_2)\delta(1-x_1)\Big)A_4^0(\hat{\bar{2}}_g,\hat{\bar{1}}_g,i_g,\widetilde{(kj)}_g)\Bigg]J_2^{(2)}(p_i,p_{\widetilde{(jk)}})
$$

$$
+d_{g;gq}^0(k_{\bar{q}},i_g,\hat{\bar{2}}_g)\Bigg[\delta(1-x_1)\delta(1-x_2)B_4^1(j_q,\hat{\bar{1}}_g,\hat{\bar{2}}_g,\widetilde{(ik)}_{\bar{q}})
$$

$$
+\Big(\mathcal{D}_{3,g;gq}^0(s_{j\bar{1}}) + \mathcal{F}_{3,gg}^0(s_{\bar{1}\bar{2}}) + \mathcal{D}_{3,g;gq}^0(s_{\bar{2}\widetilde{(ik)}})
$$

$$
-\Gamma_{gg}^1(x_1)\delta(1-x_2) - \Gamma_{gg}^1(x_2)\delta(1-x_1)\Big)B_4^0(j_q,\hat{\bar{1}}_g,\hat{\bar{2}}_g,\widetilde{(ik)}_{\bar{q}})\Bigg]J_2^{(2)}(p_j,p_{\widetilde{(ik)}})
$$

$$
+d_3^0(j_q,\hat{\bar{1}}_g,\hat{\bar{2}}_g)\Bigg[\delta(1-x_1)\delta(1-x_2)B_4^1(\hat{\bar{1}}_g,\hat{\bar{2}}_g,\tilde{i}_g,\tilde{k}_{\bar{q}}) + \Big(\mathcal{D}_{3,qg}^0(s_{\bar{1}\bar{2}}) + \frac{1}{2}\mathcal{F}_{3,g}^0(s_{\bar{2}\tilde{i}})
$$

$$
+\frac{1}{2}\mathcal{D}_3^0(s_{\widetilde{ik}}) - \Gamma_{gg}^1(x_1)\delta(1-x_2) - \Gamma_{gg}^1(x_2)\delta(1-x_1)
$$

$$+\Gamma^1_{qq}(x_1)\delta(1-x_2)+\Gamma^1_{qq}(x_2)\delta(1-x_1)\Big)B^1_4(\hat{\bar{\bar{1}}}_g,\hat{\bar{\bar{2}}}_g,\widetilde{i}_g,\widetilde{k}_{\bar{q}})\bigg]J^{(2)}_2(p_{\widetilde{i}},p_{\widetilde{k}})$$

$$+\bigg[G^1_3(\hat{\bar{2}}_g,k_{\bar{q}},j_q)\delta(1-x_1)\delta(1-x_2)+\Big(\mathcal{D}^0_{3,g;gq}(s_{\bar{2}j})+\mathcal{D}^0_{3,g;gq}(s_{\bar{2}k})-\mathcal{F}^0_{3,g}(s_{\bar{\bar{2}}\widetilde{(jk)}})\Big)$$

$$\times G^0_3(\hat{\bar{2}}_g,k_{\bar{q}},j_q)\bigg]A^0_4(\hat{\bar{\bar{2}}}_g,\hat{\bar{1}}_g,i_g,\widetilde{(kj)}_g)J^{(2)}_2(p_i,p_{\widetilde{(jk)}})$$

$$+\bigg[d^1_{g,gq}(k_{\bar{q}},i_g,\hat{\bar{2}}_g)\delta(1-x_1)\delta(1-x_2)+\Big(\frac{1}{2}\mathcal{D}^0_3(s_{ki})+\frac{1}{2}\mathcal{F}^0_{3,g}(s_{i\bar{2}})$$

$$+\mathcal{D}^0_{3,g;gq}(s_{k\bar{2}})-2\mathcal{D}^0_{3,g;gq}(s_{\widetilde{(ik)}\bar{\bar{2}}})\Big)d^0_{g,gq}(k_{\bar{q}},i_g,\hat{\bar{2}}_g)\bigg]B^0_4(j_q,\hat{\bar{1}}_g,\hat{\bar{\bar{2}}}_g,\widetilde{(ik)}_{\bar{q}})J^{(2)}_2(p_j,p_{\widetilde{(ik)}})$$

$$-\frac{1}{2}\bigg[\tilde{A}^1_3(j_q,i_g,k_{\bar{q}})\delta(1-x_1)\delta(1-x_2)+\Big(\mathcal{A}^0_3(s_{jk})-\mathcal{A}^0_3(s_{\widetilde{(ij)}\widetilde{(ik)}})\Big)$$

$$\times A^0_3(j_q,i_g,k_{\bar{q}})\bigg]B^0_4(\widetilde{(ij)}_q,\hat{\bar{1}}_g,\hat{\bar{\bar{2}}}_g,\widetilde{(ik)}_{\bar{q}})J^{(2)}_2(p_{\widetilde{(ij)}},p_{\widetilde{(ik)}})$$

$$+\bigg[d^1_3(j_q,\hat{\bar{1}}_g,\hat{\bar{\bar{2}}}_g)\delta(1-x_1)\delta(1-x_2)+\Big(\mathcal{D}^0_{3,g;gq}(s_{j\bar{1}})+\mathcal{F}^0_{3,gg}(s_{\bar{1}\bar{2}})$$

$$+\mathcal{D}^0_{3,g;gq}(s_{j\bar{2}})-2\mathcal{D}^0_{3,qg}(s_{\bar{\bar{1}}\bar{\bar{2}}})\Big)d^0_3(j_q,\hat{\bar{1}}_g,\hat{\bar{\bar{2}}}_g)\bigg]B^0_4(\hat{\bar{\bar{1}}}_g,\hat{\bar{\bar{2}}}_g,\widetilde{i}_g,\widetilde{k}_{\bar{q}})J^{(2)}_2(p_{\widetilde{i}},p_{\widetilde{k}})$$

$$-\bigg[\tilde{A}^1_3(j_q,\hat{\bar{1}}_g,\hat{\bar{2}})\delta(1-x_1)\delta(1-x_2)+\Big(\mathcal{A}^0_{3,q}(s_{j\bar{2}})-\mathcal{A}^0_{3,qq}(s_{\bar{1}\bar{2}})$$

$$+\Gamma^1_{qq}(x_1)\delta(1-x_2)+\Gamma^1_{qq}(x_2)\delta(1-x_1)\Big)$$

$$\times A^0_3(j_q,\hat{\bar{1}}_g,\hat{\bar{2}})\bigg]B^0_4(\hat{\bar{\bar{1}}}_q,\hat{\bar{\bar{2}}}_g,\widetilde{i}_g,\widetilde{k}_{\bar{q}})J^{(2)}_2(p_{\widetilde{i}},p_{\widetilde{k}})$$

$$+b_0\log\left(\frac{\mu^2}{|s_{2jk}|}\right)G^0_3(\hat{\bar{2}}_g,k_{\bar{q}},j_q)\delta(1-x_1)\delta(1-x_2)A^0_4(\hat{\bar{\bar{2}}}_g,\hat{\bar{1}}_g,i_g,\widetilde{(kj)}_g)J^{(2)}_2(p_{\widetilde{(jk)}},p_i)$$

$$+b_0\log\left(\frac{\mu^2}{|s_{ki2}|}\right)d^0_{g,gq}(k_{\bar{q}},i_g,\hat{\bar{2}}_g)\delta(1-x_1)\delta(1-x_2)B^0_4(j_q,\hat{\bar{1}}_g,\hat{\bar{\bar{2}}}_g,\widetilde{(ik)}_{\bar{q}})J^{(2)}_2(p_j,p_{\widetilde{(ik)}})$$

$$+b_0\log\left(\frac{\mu^2}{|s_{j12}|}\right)d^0_3(j_q,\hat{\bar{1}}_g,\hat{\bar{\bar{2}}}_g)\delta(1-x_1)\delta(1-x_2)B^0_4(\hat{\bar{\bar{1}}}_g,\hat{\bar{\bar{2}}}_g,\widetilde{i}_g,\widetilde{k}_{\bar{q}})J^{(2)}_2(p_{\widetilde{i}},p_{\widetilde{k}})$$

$$+\frac{1}{2}\bigg[\mathcal{D}^0_{3,g;gq}(s_{\widetilde{(ik)}\bar{\bar{2}}})-\mathcal{D}^0_{3,g;gq}(s_{k\bar{2}})-\mathcal{F}^0_{3,gg}(s_{\bar{\bar{2}}\bar{1}})+\mathcal{F}^0_{3,gg}(s_{\bar{2}\bar{1}})-\mathcal{A}^0_3(s_{\widetilde{(ik)}j})$$

$$+\mathcal{A}^0_3(s_{kj})+\delta(1-x_1)\delta(1-x_2)\Big(-\mathcal{S}(s_{\widetilde{(ik)}\bar{\bar{2}}},s_{kj},x_{\widetilde{(ik)}\bar{\bar{2}},kj})+\mathcal{S}(s_{k\bar{2}},s_{kj},x_{k\bar{2},kj})$$

$$+\mathcal{S}(s_{\widetilde{(ik)}j},s_{kj},x_{\widetilde{(ik)}j,kj})-\mathcal{S}(s_{kj},s_{kj},1)\Big)\Bigg]$$

$$\times d_{g,gq}^0(k_{\bar{q}},i_g,\hat{\widetilde{2}}_g)B_4^0(j_q,\hat{\widetilde{1}}_g,\hat{\widetilde{2}}_g,\widetilde{(ik)}_{\bar{q}})J_2^{(2)}(p_j,p_{\widetilde{(ik)}})$$

$$-\frac{1}{4}\Bigg[\mathcal{A}_3^0(s_{\widetilde{(ik)}\widetilde{(ij)}})-\mathcal{A}_3^0(s_{jk})-\mathcal{D}_{3,g;gq}^0(s_{\bar{2}\widetilde{(ik)}})+\mathcal{D}_{3,g;gq}^0(s_{\bar{2}k})-\mathcal{D}_{3,g;gq}^0(s_{\widetilde{(ij)}\bar{1}})$$

$$+\mathcal{D}_{3,g;gq}^0(s_{\bar{1}j})+\delta(1-x_1)\delta(1-x_2)\Big(-\mathcal{S}(s_{\widetilde{(ik)}\widetilde{(ij)}},s_{jk},x_{\widetilde{(ik)}\widetilde{(ij)},jk})+\mathcal{S}(s_{jk},s_{jk},1)$$

$$+\mathcal{S}(s_{\bar{2}\widetilde{(ik)}},s_{jk},x_{\bar{2}\widetilde{(ik)},jk})-\mathcal{S}(s_{\bar{2}k},s_{jk},x_{\bar{2}k,jk})+\mathcal{S}(s_{\widetilde{(ij)}\bar{1}},s_{jk},x_{\widetilde{(ij)}\bar{1},jk})$$

$$-\mathcal{S}(s_{\bar{1}j},s_{jk},x_{\bar{1}j,jk})\Big)\Bigg]A_3^0(j_q,i_g,k_{\bar{q}})B_4^0(\widetilde{(ij)}_q,\hat{\widetilde{1}}_g,\hat{\widetilde{2}}_g,\widetilde{(ik)}_{\bar{q}})J_2^{(2)}(p_{\widetilde{(ij)}},p_{\widetilde{(ik)}})$$

$$+\Bigg[\mathcal{D}_{3,qg}^0(s_{\bar{1}\bar{2}})-\mathcal{D}_{3,g;gq}^0(s_{j\bar{2}})-\frac{1}{2}\mathcal{F}_{3,g}^0(s_{\bar{2}\tilde{i}})+\frac{1}{2}\mathcal{F}_{3,g}^0(s_{\bar{2}i})-\mathcal{A}_{3,q}^0(s_{\bar{1}j})+\mathcal{A}_3^0(s_{jk})$$

$$+\delta(1-x_1)\delta(1-x_2)\Big(-\mathcal{S}(s_{\bar{1}\bar{2}},s_{\widetilde{ik}},x_{\bar{1}\bar{2},\widetilde{ik}})+\mathcal{S}(s_{j\bar{2}},s_{ik},x_{j\bar{2},ik})+\mathcal{S}(s_{\tilde{i}\bar{2}},s_{\widetilde{ik}},x_{\tilde{i}\bar{2},\widetilde{ik}})$$

$$-\mathcal{S}(s_{\bar{1}i},s_{ik},x_{\bar{1}i,ik})+\mathcal{S}(s_{\bar{1}\tilde{j}},s_{\widetilde{ik}},x_{\bar{1}\tilde{j},\widetilde{ik}})-\mathcal{S}(s_{jk},s_{ik},x_{jk,ik})\Big)\Bigg]$$

$$\times d_3^0(j_q,\hat{\widetilde{1}}_g,\hat{\widetilde{2}}_g)B_4^0(\hat{\widetilde{\bar{1}}}_g,\hat{\widetilde{\bar{2}}}_g,\widetilde{i}_g,\widetilde{k}_{\bar{q}})J_2^{(2)}(p_{\widetilde{i}},p_{\widetilde{k}})$$

$$-\Bigg[\mathcal{A}_{3,qq}^0(s_{\bar{1}\bar{2}})-\mathcal{A}_{3,q}^0(s_{\bar{2}j})-\mathcal{A}_{3,q}^0(s_{\bar{1}k})+\mathcal{A}_3^0(s_{jk})-\mathcal{D}_{3,g;gq}^0(s_{\tilde{i}\bar{2}})+\mathcal{D}_{3,g;gq}^0(s_{\bar{2}i})$$

$$+\delta(1-x_1)\delta(1-x_2)\Big(-\mathcal{S}(s_{\bar{1}\bar{2}},s_{\widetilde{ik}},x_{\bar{1}\bar{2},\widetilde{ik}})+\mathcal{S}(s_{\bar{2}j},s_{ik},x_{\bar{2}j,ik})+\mathcal{S}(s_{\bar{1}k},s_{\widetilde{ik}},x_{\bar{1}k,\widetilde{ik}})$$

$$-\mathcal{S}(s_{jk},s_{ik},x_{jk,ik})+\mathcal{S}(s_{\tilde{i}\bar{2}},s_{\widetilde{ik}},x_{\tilde{i}\bar{2},\widetilde{ik}})-\mathcal{S}(s_{\bar{2}i},s_{ik},x_{\bar{2}i,ik})\Big)\Bigg]$$

$$\times A_3^0(j_q,\hat{\widetilde{1}}_g,\hat{\widetilde{2}})B_4^0(\hat{\widetilde{\bar{1}}}_q,\hat{\widetilde{\bar{2}}}_g,\widetilde{i}_g,\widetilde{k}_{\bar{q}})J_2^{(2)}(p_{\widetilde{i}},p_{\widetilde{k}})$$

$$-\frac{1}{2}\Bigg[\mathcal{F}_{3,g}^0(s_{\bar{1}\bar{2}})-\mathcal{F}_{3,g}^0(s_{\bar{1}2})-\mathcal{D}_{3,g;gq}^0(s_{\bar{1}\tilde{j}})+\mathcal{D}_{3,g;gq}^0(s_{\bar{1}j})-\mathcal{D}_{3,g;gq}^0(s_{\bar{2}\tilde{k}})+\mathcal{D}_{3,g;gq}^0(s_{\bar{2}k})$$

$$+\delta(1-x_1)\delta(1-x_2)\Big(\mathcal{S}(s_{\bar{1}\bar{2}},s_{jk},x_{\bar{1}\bar{2},jk})-\mathcal{S}(s_{\bar{1}\bar{2}},s_{\widetilde{jk}},x_{\bar{1}\bar{2},\widetilde{jk}})+\mathcal{S}(s_{\bar{1}\tilde{j}},s_{jk},x_{\bar{1}\tilde{j},jk})$$

$$-\mathcal{S}(s_{\bar{1}j},s_{jk},x_{\bar{1}j,jk})+\mathcal{S}(s_{\bar{2}\tilde{k}},s_{\widetilde{jk}},x_{\bar{2}\tilde{k},\widetilde{jk}})-\mathcal{S}(s_{\bar{2}k},s_{jk},x_{\bar{2}k,jk})\Big)\Bigg]$$

$$\times F_3^0(\hat{\widetilde{1}}_g,i_g,\hat{\widetilde{2}})B_4^0(\widetilde{j}_q,\hat{\widetilde{\bar{1}}}_g,\hat{\widetilde{\bar{2}}}_g,\widetilde{k}_{\bar{q}})J_2^{(2)}(p_{\widetilde{j}},p_{\widetilde{k}})\Bigg\}. \tag{5.5.55}$$

A point of interest lies in the cancellation of the initial state collinear poles amongst the blocks of one loop matrix elements and the associated integrated an-

tennae. In a non-flavour-changing antenna such as the $d^0_{g;gq}$, the combination of integrated antennae and the mass factorisation terms form a finite block, as indicated by the square brackets. Since the flavour of the initial state remains gluonic, the initial state poles from the integrated antenna cancel against the gluonic mass factorisation terms Γ^1_{gg}.

However, this is not the case for the flavour changing antennae, which in the above subtraction terms includes the $d^1_3(j, \hat{1}_g, \hat{2}_g)$. In this instance, after remapping, the gluon $\hat{1}_g$ becomes a quark in the reduced matrix element, since the d^0_3 is a quark-gluon antenna. The j_q is effective acting as the unresolved parton in this initial-initial antenna. In order to make the block of integrated antenna and mass factorisation terms finite, we must include an extra $\Gamma_{qq}(x_1)$ into the block, to account for the fact that the mapped initial state has now become a quark. The physical matrix element is still a gluon-initiated process, and thus the $\Gamma_{qq}(x_1)$ appears to be a spurious addition.

However, this situation is remedied when incorporating the $\tilde{A}^1_3(j, \hat{1}_g, \hat{2}_g)$ antennae, introduced initially to deal with the unwanted colour connectivity of the d^1_3 as described in Section 5.4. The $\tilde{A}^1_3$ is also an initial-initial antenna and is flavour-changing in this case, since it incorporates a 'false' initial quark, such that only the $j||\hat{1}$ limit is present. Thus, the subsequent integrated antenna to cancel the poles of $\tilde{A}^1_3$ are

$$\mathcal{A}^0_{3,q}(s_{j\bar{2}}) - \mathcal{A}^0_{3,qq}(s_{\bar{1}\bar{2}}) + \Gamma^1_{qq}(x_1)\delta(1 - x_2) \tag{5.5.56}$$

where there is an over subtracted Γ^1_{qq} introduced to maintain the finiteness of the block. Since this block is coming with an opposite sign to the $d^1_3(j, \hat{1}_g, \hat{2}_g)$, and by construction is multiplied by a reduced matrix element that behaves identically in the relevant limit, then the 'spurious' Γ^1_{qq} are cancelled. In the language of the $\boldsymbol{J}^{(1)}_n$ strings, this is exactly what is taking place. The $\boldsymbol{J}^{(1)}_n$ always cancel the poles of the one loop reduced matrix elements; the mass factorisation kernels are in the definition of the $\boldsymbol{J}^{(1)}_n$ so it contains no initial-state collinear poles and matches the genuine poles of the reduced matrix element. $\bar{\boldsymbol{J}}^{(1)}_n$ does not contain any initial-state collinear poles either and it does not have any mass factorisation kernels in its definition. It contains the genuine poles of the one loop unintegrated antenna. The mass factorisation kernels

cancel the initial-state collinear poles of the integrated antennae in $\boldsymbol{J}_n^{(1)}$. In the case of identity changing configurations nothing changes: the $\boldsymbol{J}_n^{(1)}$ cancels the genuine poles of the one loop reduced matrix element and the $\bar{\boldsymbol{J}}_n^{(1)}$ cancels the genuine poles of the X_3^1. There are also the formation of identity changing $\boldsymbol{J}_n^{(1)}$s which are built from identity changing integrated antennae (like $\mathcal{G}_3^0$ and $\mathcal{E}_3^0$) inherited from the double real. The initial-state collinear poles of these are cancelled against the identity changing mass factorisation kernels to form the pole-free identity changing $\bar{\boldsymbol{J}}_n^{(1)}$s. Nevertheless, it is clear in the form of the results here exactly how the 'spurious' mass factorisation terms are cancelling. It also gives a strong indication that it is the combination of the D_3 and $\tilde{A}_3$ antennae that are the correct objects to use in the subtraction terms, since the former can never complete its job single-handedly, both in the subtraction of implicit divergences, and subsequent pole cancellation.

Subtraction term with colour connected initial states: $\mathbb{Y}$ topology

The one loop single unresolved subtraction term for the $\mathbb{Y}$ topology of Eq. (5.5.52) takes the form

$$
\begin{aligned}
d\sigma_{NNLO}^{T,\mathbb{Y}} = \mathcal{N}_{gg,5}^1 \int d\Phi_3(p_3, p_4, p_5; x_1 p_1, x_2 p_2) \frac{\mathrm{d}x_1}{x_1} \frac{\mathrm{d}x_2}{x_2} \times \Bigg\{ & \\
-\Big(\mathcal{D}_{3,g;gq}^0(s_{j\bar{1}}) + \frac{1}{2}\mathcal{F}_{3,g}^0(s_{\bar{1}i}) + \frac{1}{2}\mathcal{F}_{3,g}^0(s_{i\bar{2}}) + \mathcal{D}_{3,g;gq}^0(s_{\bar{2}k}) - \Gamma_{gg}^1(x_1)\delta(1-x_2) & \\
-\Gamma_{gg}^1(x_2)\delta(1-x_1)\Big) B_5^0(j_q, \hat{\bar{1}}_g, i_g, \hat{\bar{2}}_g, k_{\bar{q}}) J_2^{(3)}(p_j, p_i, p_k) & \\
+F_3^0(\hat{\bar{1}}_g, i_g, \hat{\bar{2}}_g)\Bigg[\delta(1-x_1)\delta(1-x_2) B_4^1(\widetilde{j}_q, \hat{\widetilde{\bar{1}}}_g, \hat{\widetilde{\bar{2}}}_g, \widetilde{k}_{\bar{q}}) + \Big(\mathcal{D}_{3,g;gq}^0(s_{\widetilde{j}\bar{1}}) + \mathcal{F}_{3,gg}^0(s_{\bar{1}\bar{2}}) & \\
+\mathcal{D}_{3,g;gq}^0(s_{\bar{2}\widetilde{k}}) - \Gamma_{gg}^1(x_1)\delta(1-x_2) - \Gamma_{gg}^1(x_2)\delta(1-x_1) \Big) B_4^0(\widetilde{j}_q, \hat{\widetilde{\bar{1}}}_g, \hat{\widetilde{\bar{2}}}_g, \widetilde{k}_{\bar{q}}) \Bigg] J_2^{(2)}(p_{\widetilde{j}}, p_{\widetilde{k}}) & \\
+A_3^0(j_q, \hat{\bar{1}}_g, \hat{\bar{2}})\Bigg[\delta(1-x_1)\delta(1-x_2) B_4^1(\hat{\widetilde{\bar{1}}}_q, \widetilde{i}_g, \hat{\widetilde{\bar{2}}}_g, \widetilde{k}_{\bar{q}}) + \Big(\frac{1}{2}\mathcal{D}_{3,q}^0(s_{\widetilde{1}\widetilde{i}}) + \frac{1}{2}\mathcal{F}_{3,g}^0(s_{\widetilde{2}i}) & \\
+\mathcal{D}_{3,g;gq}^0(s_{\bar{2}\widetilde{k}}) - \Gamma_{gg}^1(x_1)\delta(1-x_2) - \Gamma_{gg}^1(x_2)\delta(1-x_1) \Big) B_4^0(\hat{\widetilde{\bar{1}}}_q, \widetilde{i}_g, \hat{\widetilde{\bar{2}}}_g, \widetilde{k}_{\bar{q}}) \Bigg] J_2^{(2)}(p_{\widetilde{k}}, p_{\widetilde{i}}) & \\
+A_3^0(k_{\bar{q}}, \hat{\bar{2}}_g, \hat{1})\Bigg[\delta(1-x_1)\delta(1-x_2) B_4^1(\widetilde{j}_q, \hat{\widetilde{\bar{1}}}_g, \widetilde{i}_g, \hat{\widetilde{\bar{2}}}_{\bar{q}}) + \Big(\mathcal{D}_{3,g;gq}^0(s_{\widetilde{j}\bar{1}}) + \frac{1}{2}\mathcal{F}_{3,g}^0(s_{\widetilde{1}i}) &
\end{aligned}
$$

$$+\frac{1}{2}\mathcal{D}^0_{3,q}(s_{\widetilde{i}\overline{\widetilde{2}}}) - \Gamma^1_{gg}(x_1)\delta(1-x_2) - \Gamma^1_{gg}(x_2)\delta(1-x_1)\Big)B^0_4(\widetilde{j}_q,\widehat{\overline{\widetilde{1}}}_g,\widetilde{i}_g,\widehat{\overline{\widetilde{2}}}_{\bar{q}})\Bigg]J^{(2)}_2(p_{\widetilde{j}},p_{\widetilde{i}})$$

$$+G^0_3(\widehat{\overline{1}}_g,j_q,k_{\bar{q}})\Bigg[\delta(1-x_1)\delta(1-x_2)A^1_4((\widetilde{kj})_g,\widehat{\overline{\widetilde{1}}}_g,i_g,\widehat{\overline{2}}_g)$$

$$+\Big(\frac{1}{2}\mathcal{F}^0_{3,g}(s_{\widetilde{(kj)}\overline{\widetilde{1}}}) + \frac{1}{2}\mathcal{F}^0_{3,g}(s_{\overline{\widetilde{1}}i}) + \frac{1}{2}\mathcal{F}^0_{3,g}(s_{i\overline{2}}) + \frac{1}{2}\mathcal{F}^0_{3,g}(s_{\overline{2}\widetilde{(kj)}})$$

$$-\Gamma^1_{gg}(x_1)\delta(1-x_2) - \Gamma^1_{gg}(x_2)\delta(1-x_1)\Big)A^0_4((\widetilde{kj})_g,\widehat{\overline{\widetilde{1}}}_g,i_g,\widehat{\overline{2}}_g)\Bigg]J^{(2)}_2(p_{\widetilde{(kj)}},p_i)$$

$$+\Bigg[F^1_3(\widehat{\overline{1}}_g,i_g,\widehat{\overline{2}}_g)\delta(1-x_1)\delta(1-x_2) + \Big(\frac{1}{2}\mathcal{F}^0_{3,g}(s_{\overline{1}i}) + \mathcal{F}^0_{3,gg}(s_{\overline{1}\overline{2}}) + \frac{1}{2}\mathcal{F}^0_{3,g}(s_{\overline{2}i})$$

$$-2\mathcal{F}^0_{3,gg}(s_{\overline{1}\overline{2}})\Big)F^0_3(\widehat{\overline{1}}_g,i_g,\widehat{\overline{2}})\Bigg]B^0_4(\widetilde{j}_q,\widehat{\overline{\widetilde{1}}}_g,\widehat{\overline{\widetilde{2}}}_g,\widetilde{k}_{\bar{q}})J^{(2)}_2(p_{\widetilde{j}},p_{\widetilde{k}})$$

$$+\Bigg[A^1_3(j_q,\widehat{\overline{1}}_g,\widehat{\overline{2}})\delta(1-x_1)\delta(1-x_2) + \Big(\mathcal{D}^0_{3,g;gq}(s_{j\overline{1}}) + \mathcal{D}^0_{3,qg}(s_{\overline{1}\overline{2}}) - \mathcal{A}^0_{3,qq}(s_{\overline{2}\overline{1}})\Big)$$

$$\times A^0_3(j_q,\widehat{\overline{1}}_g,\widehat{\overline{2}})\Bigg]B^0_4(\widehat{\overline{\widetilde{1}}}_q,\widetilde{i}_g,\widehat{\overline{\widetilde{2}}}_g,\widetilde{k}_{\bar{q}})J^{(2)}_2(p_{\widetilde{k}},p_{\widetilde{i}})$$

$$+\Bigg[A^1_3(k_{\bar{q}},\widehat{\overline{2}}_g,\widehat{\overline{1}})\delta(1-x_1)\delta(1-x_2) + \Big(\mathcal{D}^0_{3,g;gq}(s_{\overline{2}k}) + \mathcal{D}^0_{3,qg}(s_{\overline{1}\overline{2}}) - \mathcal{A}^0_{3,qq}(s_{\overline{1}\overline{2}})\Big)$$

$$\times A^0_3(k_{\bar{q}},\widehat{\overline{2}}_g,\widehat{\overline{1}})\Bigg]B^0_4(\widetilde{j}_q,\widehat{\overline{\widetilde{1}}}_g,\widetilde{i}_g,\widehat{\overline{\widetilde{2}}}_{\bar{q}})J^{(2)}_2(p_{\widetilde{j}},p_{\widetilde{i}})$$

$$+\Bigg[G^1_3(\widehat{\overline{1}}_g,j_q,k_{\bar{q}})\delta(1-x_1)\delta(1-x_2) + \Big(\mathcal{D}^0_{3,g,gq}(s_{\overline{1}j}) + \mathcal{D}^0_{3,g,gq}(s_{\overline{1}k}) - \frac{1}{2}\mathcal{F}^0_{3,g}(s_{\overline{\widetilde{1}}\widetilde{(jk)}})\Big)$$

$$\times A^0_4((\widetilde{kj})_g,\widehat{\overline{\widetilde{1}}}_g,i_g,\widehat{\overline{2}}_g)\Bigg]J^{(2)}_2(p_{\widetilde{(kj)}},p_i)$$

$$+b_0\log\left(\frac{\mu^2}{|s_{1i2}|}\right)F^0_3(\widehat{\overline{1}}_g,i_g,\widehat{\overline{2}}_g)\delta(1-x_1)\delta(1-x_2)B^0_4(\widetilde{j}_q,\widehat{\overline{\widetilde{1}}}_g,\widehat{\overline{\widetilde{2}}}_g,\widetilde{k}_{\bar{q}})J^{(2)}_2(p_{\widetilde{j}},p_{\widetilde{k}})$$

$$+b_0\log\left(\frac{\mu^2}{|s_{12j}|}\right)A^0_3(j_q,\widehat{\overline{1}}_g,\widehat{\overline{2}})\delta(1-x_1)\delta(1-x_2)B^0_4(\widehat{\overline{\widetilde{1}}}_q,\widetilde{i}_g,\widehat{\overline{\widetilde{2}}}_g,\widetilde{k}_{\bar{q}})J^{(2)}_2(p_{\widetilde{k}},p_{\widetilde{i}})$$

$$+b_0\log\left(\frac{\mu^2}{|s_{k12}|}\right)A^0_3(k_{\bar{q}},\widehat{\overline{2}}_g,\widehat{\overline{1}})\delta(1-x_1)\delta(1-x_2)B^0_4(\widetilde{j}_q,\widehat{\overline{\widetilde{1}}}_g,\widetilde{i}_g,\widehat{\overline{\widetilde{2}}}_{\bar{q}})J^{(2)}_2(p_{\widetilde{j}},p_{\widetilde{i}})$$

$$+b_0\log\left(\frac{\mu^2}{|s_{1jk}|}\right)G^0_3(\widehat{\overline{1}}_g,j_q,k_{\bar{q}})\delta(1-x_1)\delta(1-x_2)A^0_4((\widetilde{kj})_g,\widehat{\overline{\widetilde{1}}}_g,i_g,\widehat{\overline{2}}_g)J^{(2)}_2(p_{\widetilde{(kj)}},p_i)$$

$$+\Bigg[\mathcal{F}^0_{3,g}(s_{\overline{\widetilde{1}}\overline{\widetilde{2}}}) - \mathcal{F}^0_{3,g}(s_{\overline{1}\overline{2}}) - \mathcal{D}^0_{3,g;gq}(s_{\overline{\widetilde{1}}\widetilde{j}}) + \mathcal{D}^0_{3,g;gq}(s_{\overline{1}j}) - \mathcal{D}^0_{3,g;gq}(s_{\overline{\widetilde{2}}\widetilde{k}}) + \mathcal{D}^0_{3,g;gq}(s_{\overline{2}k})$$

$$+\delta(1-x_1)\delta(1-x_2)\Big(\mathcal{S}(s_{\overline{12}},s_{jk},x_{\overline{12},jk})-\mathcal{S}(s_{\overline{12}},s_{\widetilde{jk}},x_{\overline{12},\widetilde{jk}})+\mathcal{S}(s_{\widetilde{1j}},s_{\widetilde{jk}},x_{\overline{1j},\widetilde{jk}})$$

$$-\mathcal{S}(s_{\overline{1j}},s_{jk},x_{\overline{1j},jk})+\mathcal{S}(s_{\overline{2k}},s_{\widetilde{jk}},x_{\overline{2k},\widetilde{jk}})-\mathcal{S}(s_{\overline{2k}},s_{jk},x_{\overline{2k},jk})\Big)\Bigg]$$

$$\times F_3^0(\hat{\tilde{1}}_g,i_g,\hat{\tilde{2}})B_4^0(\widetilde{j}_q,\hat{\tilde{\tilde{1}}}_g,\hat{\tilde{\tilde{2}}}_g,\widetilde{k}_{\bar{q}})J_2^{(2)}(p_{\widetilde{j}},p_{\widetilde{k}})$$

$$+\Bigg[\mathcal{A}_{3,qq}^0(s_{\overline{2}\overline{1}})-\mathcal{D}_{3,qg}^0(s_{\overline{2}\overline{1}})-\frac{1}{2}\mathcal{D}_{3,q}^0(s_{\widetilde{i1}})+\frac{1}{2}\mathcal{F}_{3,g}^0(s_{i\overline{1}})-\mathcal{A}_{3,q}^0(s_{\overline{2}\widetilde{k}})+\mathcal{A}_{3,q}^0(s_{\overline{2}k})$$

$$+\delta(1-x_1)\delta(1-x_2)\Big(\mathcal{S}(s_{\overline{12}},s_{ik},x_{\overline{12},ik})-\mathcal{S}(s_{\overline{12}},s_{\widetilde{ik}},x_{\overline{12},\widetilde{ik}})+\mathcal{S}(s_{\widetilde{1i}},s_{\widetilde{ik}},x_{\overline{1i},\widetilde{ik}})$$

$$-\mathcal{S}(s_{\overline{1i}},s_{ik},x_{\overline{1i},ik})+\mathcal{S}(s_{\overline{2}\widetilde{k}},s_{\widetilde{ik}},x_{\overline{2}\widetilde{k},\widetilde{ik}})-\mathcal{S}(s_{\overline{2k}},s_{ik},x_{\overline{2k},ik})\Big)\Bigg]$$

$$\times A_3^0(j_q,\hat{\tilde{1}}_g,\hat{\tilde{2}})B_4^0(\hat{\tilde{\tilde{1}}}_q,\widetilde{i}_g,\hat{\tilde{\tilde{2}}}_g,k_{\bar{q}})J_2^{(2)}(p_k,p_i)$$

$$+\Bigg[\mathcal{A}_{3,qq}^0(s_{\overline{2}\overline{1}})-\mathcal{D}_{3,qg}^0(s_{\overline{2}\overline{1}})-\frac{1}{2}\mathcal{D}_{3,q}^0(s_{i\widetilde{2}})+\frac{1}{2}\mathcal{F}_{3,g}^0(s_{i\overline{2}})-\mathcal{A}_{3,q}^0(s_{\widetilde{1j}})+\mathcal{A}_{3,q}^0(s_{\overline{1}j})$$

$$+\delta(1-x_1)\delta(1-x_2)\Big(\mathcal{S}(s_{\overline{12}},s_{ij},x_{\overline{12},ij})-\mathcal{S}(s_{\overline{12}},s_{\widetilde{ij}},x_{\overline{12},\widetilde{ij}})+\mathcal{S}(s_{\overline{2}\widetilde{i}},s_{\widetilde{ij}},x_{\overline{2}\widetilde{i},\widetilde{ij}})$$

$$-\mathcal{S}(s_{\overline{2}i},s_{ij},x_{\overline{2}i,ij})+\mathcal{S}(s_{\overline{1}\widetilde{j}},s_{\widetilde{ij}},x_{\overline{1}\widetilde{j},\widetilde{ij}})-\mathcal{S}(s_{\overline{1}j},s_{ij},x_{\overline{1}j,ij})\Big)\Bigg]$$

$$\times A_3^0(k_{\bar{q}},\hat{\tilde{2}}_g,\hat{\tilde{1}})B_4^0(\widetilde{j}_q,\hat{\tilde{\tilde{1}}}_g,\widetilde{i}_g,\hat{\tilde{\tilde{2}}}_{\bar{q}})J_2^{(2)}(p_{\widetilde{j}},p_{\widetilde{i}})$$

$$+\{\hat{1}_g\leftrightarrow\hat{2}_g\}\Bigg\},\tag{5.5.57}$$

with the construction of the other topologies obtained via Table 5.3.

Ordering	Subtraction term
$\mathbb{X}(j_q,\hat{\tilde{1}}_g,\hat{\tilde{2}}_g,i_g,k_{\bar{q}})$	$d\sigma_{gg,NNLO}^{T,\mathbb{X}}$
$\mathbb{X}(j_q,\hat{\tilde{2}}_g,\hat{\tilde{1}}_g,i_g,k_{\bar{q}})$	$d\sigma_{gg,NNLO}^{T,\mathbb{X}}(\hat{\tilde{1}}\leftrightarrow\hat{\tilde{2}})$
$\mathbb{X}(j_q,i_g,\hat{\tilde{1}}_g,\hat{\tilde{2}}_g,k_{\bar{q}})$	$d\sigma_{gg,NNLO}^{T,\mathbb{X}}(\hat{\tilde{1}}\leftrightarrow\hat{\tilde{2}},j\leftrightarrow k)$
$\mathbb{X}(j_q,i_g,\hat{\tilde{2}}_g,\hat{\tilde{1}}_g,k_{\bar{q}})$	$d\sigma_{gg,NNLO}^{T,\mathbb{X}}(j\leftrightarrow k)$
$\mathbb{Y}(j_q,\hat{\tilde{1}}_g,i_g,\hat{\tilde{2}}_g,k_{\bar{q}})$	$d\sigma_{gg,NNLO}^{T,\mathbb{Y}}$
$\mathbb{Y}(j_q,\hat{\tilde{2}}_g,i_g,\hat{\tilde{1}}_g,k_{\bar{q}})$	$d\sigma_{gg,NNLO}^{T,\mathbb{Y}}(\hat{\tilde{1}}\leftrightarrow\hat{\tilde{2}})$

Table 5.3: Only one unique subtraction term is required for all the $\mathbb{X}$ topology matrix elements. All others can be obtained via label exchange of either the initial state gluons or the final state quarks. The $\mathbb{Y}$ topologies behave likewise.

The subtraction term of the adjacent gluon-initiated real-virtual contribution is rendered finite in the sum of the four $\mathbb{X}$-type topologies. The A_3 antennae over-

subtract a limit in one of the terms, but this singular configuration is present in the other term. Hence, the combination of the two produces a full subtraction of the divergences. Line reversal symmetry results in identical remapped reduced matrix elements from the two configurations.

A number of interesting points arise that were not visible in the quark-initiated case. We encounter for the first time the G_3 antenna as a counterterm for the single collinear limit between the final state quark and antiquark. Constructing a subtraction term for the single quark-antiquark collinear limit for either the gluon-gluon- or quark-gluon-initiated process demands the use of the G_3^0 antenna. This contains only the limit

$$G_3^0(g, q, \bar{q}) \xrightarrow{q||\bar{q}} \frac{1}{s_{q\bar{q}}} P_{q\bar{q}\leftarrow G}(z) \tag{5.5.58}$$

with the exact form of the splitting function determined by the partonic nature of the initial state. The gluon is effectively behaving as a a spectator parton. Since the quarks appear at the end of the colour lines in the matrix elements, there is an apparent choice of gluon adjacent to the quark, to act as spectator in the antenna. The choice exits in processes where at least one of the quarks is in the final state, and without loss of generality we consider the gluon-gluon initiated process. The tree level matrix element for the $\mathbb{Y}$-type gluon colour ordering reads as

$$B_5^0(j_q, \hat{\bar{1}}_g, i_g, \hat{\bar{2}}_g, k_{\bar{q}}) \tag{5.5.59}$$

and to capture the $j_q||k_{\bar{q}}$ either

$$
\begin{aligned}
&G_3^0(\hat{\bar{1}}_g, j_q, k_{\bar{q}}) A_4^1(\widetilde{(jk)}_g, \hat{\bar{\bar{1}}}_g, i_g, \hat{\bar{2}}_g) \text{ or} \\
&G_3^0(\hat{\bar{2}}_g, k_{\bar{q}}, j_q) A_4^1(\widetilde{(jk)}_g, \hat{\bar{\bar{2}}}_g, i_g, \hat{\bar{1}}_g)
\end{aligned}
\tag{5.5.60}
$$

will capture the limit. Note that the G_3 antenna is a flavour changing antenna; the collinear quarks collapse onto a parent gluon, and the reduced matrix element is purely gluonic. The cyclic and reversal symmetry of the A_4^0 pure gluon matrix element means that the two reduced matrix elements above are identical, and will always be

for either choice of G_3 antenna. At NLO, where both the reduced matrix element and the antenna are tree level objects, two options are open for the construction of the subtraction term:

1. Pick one of the G_3^0 antennae to hold the full limit.

2. Include a sum of the two G antennae to maintain symmetry, that is

$$B_5^0(j_q, \hat{\bar{1}}_g, i_g, \hat{\bar{2}}_g, k_{\bar{q}}) \xrightarrow{j_q || k_{\bar{q}}} \quad \frac{1}{2} G_3^0(\hat{\bar{2}}_g, k_{\bar{q}}, j_q) A_4^1(\widetilde{(jk)}_g, \hat{\bar{\bar{2}}}_g, i_g, \hat{\bar{1}}_g)$$
$$+ \quad \frac{1}{2} G_3^0(\hat{\bar{1}}_g, k_{\bar{q}}, j_q) A_4^1(\widetilde{(jk)}_g, \hat{\bar{2}}_g, i_g, \hat{\bar{\bar{1}}}_g)$$

$$(5.5.61)$$

which, in the limit, have identical reduced matrix elements.

The two choices of subtraction term are identical at NLO, and can be applied to all colour orderings individually. Naïvely, one would pick that which required the fewest antenna. The game becomes more interesting at NNLO, where we must now consider the one-loop pole cancellations of both the antennae and reduced matrix elements. For a single colour ordering at RV, the implicit pole cancellation is again independent of the choice of G_3^ℓ. However, with the inclusion of the pole corrections (from both the RR dropping down and the new terms at RV), we find cancellation of integrated antennae in the $q||\bar{q}$ limit holds only in the sum of pairs of colour-ordered configurations of matrix elements, due to the flavour-changing property of the G_3^ℓ. For example, the full subtraction term for the $q||\bar{q}$ limit in $B_5^1(j_q, \hat{\bar{1}}_g, i_g, \hat{\bar{2}}_g, k_{\bar{q}})$ only behaves correctly if summed with the subtraction term for $B_5^1(j_q, \hat{\bar{2}}_g, i_g, \hat{\bar{1}}_g, k_{\bar{q}})$. Explicitly we see that, for the first ordering in the $q||\bar{q}$ limit, the block of integrated antennae

$$-\mathcal{D}_{3,g;gq}^0(s_{\bar{2}k}) + \mathcal{D}_{3,g;gq}^0(s_{\bar{1}k}) - \frac{1}{2}\mathcal{F}_{3,g}^0(s_{\widetilde{1jk}}) + \frac{1}{2}\mathcal{F}_{3,g}^0(s_{\widetilde{2jk}}) \qquad (5.5.62)$$

remain; the flavour change of the initial state results in different antenna and so no cancellation occurs. However, the same set of terms save for an opposite sign appear in the paired ordered matrix element such that a full cancellation occurs. Therefore

we see that, following choice (2) above, full cancellation naturally occurs since we include all possible pairs of colour orderings. However, it is possible to follow (1), if one is careful with the choice of gluon spectator. In doing so, we are able to reduce the number of antennae in the full summation of colour orderings by utilising the symmetry under the exchange of initial state gluon.

We also note the presence of the $d_{g;gq}$ antenna, where the gluon is now in the initial state. The full gluon-initiated $D_3^0(j_q, \hat{2}_g, i_g)$ antenna contains a soft i gluon limit, $j||\hat{2}$ and $j||i$ quark-gluon collinear limits and a $\hat{2}||i$ gluon collinear limits. The initial final quark gluon limit is an anomaly, since it changes the initial state from a gluon to a quark, whilst the other limits maintain a gluon initial state. As discussed in [24] it is possible to partition the limits into two subantennae,

$$D_3^0(j_q, \hat{2}_2, i_g) = d_{g;gq}^0(j_q, \hat{2}_g; i_g) + d_{g;qg}^0(j_q, \hat{2}_g, i_g), \tag{5.5.63}$$

where now the offending limit is contained within the first term, and all others are in the second subantenna. Unlike the final-final case discussed in Chapter 4, this partial fractioning is not symmetrical. For our results we also require the one-loop extension to this partitioning. Fortunately, we can follow a similar line of argument to the symmetric partial fractioning for the one loop antenna in section 4.3, the one loop terms proportional to the tree antenna can be attacked by replacing the full antenna with the subantennae. The finite contribution not proportional to the tree antenna is rewritten in such a way that the invariants respect the limits required. For the case of the D_3^1, the only term is $1/(s_{2i})$, which can be assigned to the second term of (5.5.63).

Again, to demonstrate its validity, the subtraction term has been tested numerically. The procedure is then repeated for 1000 different phase space points in the unresolved configuration defined by the constraints. The constraints are then tightened to force the phase space points closer to the unresolved singular point and the ratio calculated for another 1000 points. The procedure is repeated once more for a set of points even closer to the singular point and the histogram of ratios for the three sets of constraints plotted.
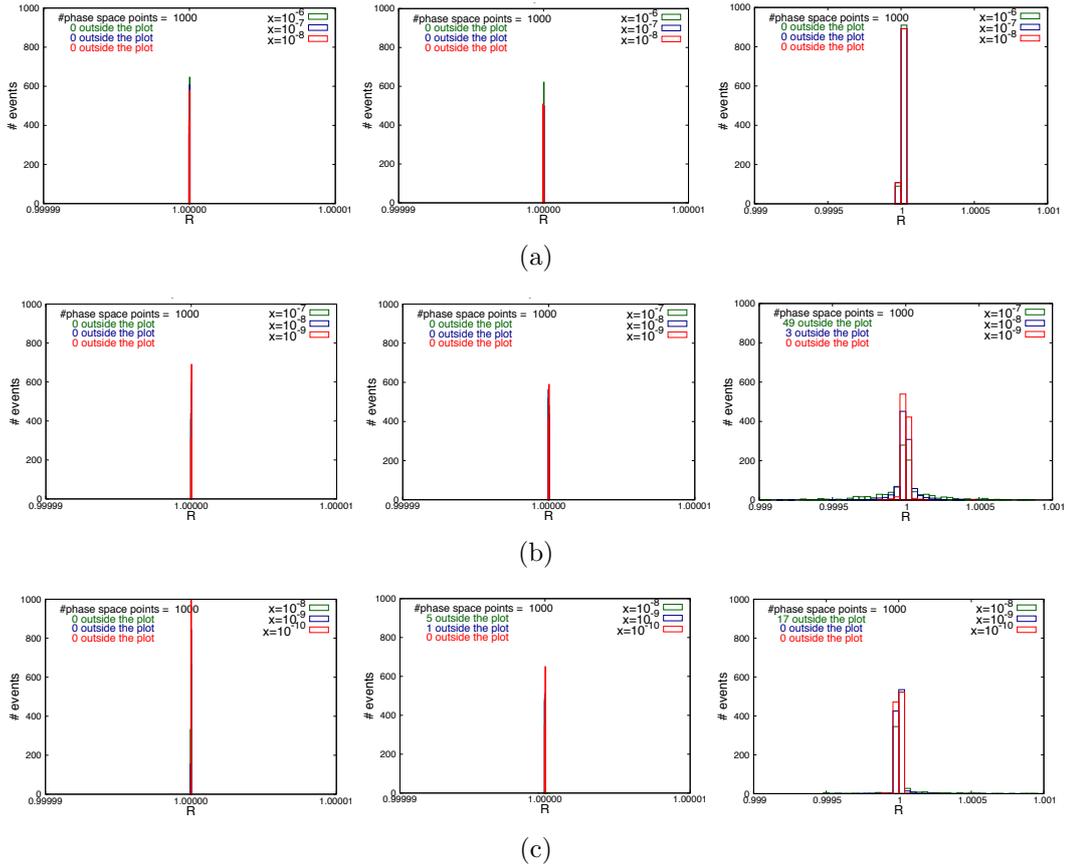
Figure 5.8: Plots displaying the convergence of the subtraction term to the real-virtual physical matrix element in various unresolved limits, for $gg \to q\bar{q}g$. The green data is furthest from the singular configuration with the blue data closer to the singular region and the red data the closest. The left plot of each row is the $1/\epsilon^2$ contribution, the centre plot the $1/\epsilon$ contribution and the right hand plot the finite contribution. (a) Final-state single soft limit for parton i such that $x = (s_{12}-s_{jk})/s_{12}$. (b) Collinear limit between final-state gluons i and j, such that $x = s_{ij}/s_{12}$. (c) Collinear limit for final state gluon i and initial state antiquark 2 such that $x = s_{2i}/s_{12}$.

A selection of plots from three different unresolved configurations is shown in Figure 5.8. Again, the right hand plot in each row in illustrates the finite contribution of the single unresolved limits. The left and centre plots are the $1/\epsilon^2$ and $1/\epsilon$ contributions respectively. In each plot we see that the distribution of R for the finite contribution becomes more sharply peaked around one as the unresolved singular limit is approached, i.e., as the parameter x gets smaller. This provides statistical evidence for the convergence of the subtraction term to the physical cross section in the IR divergent limits. The pole contributions are again cancelling analytically, as seen by the sharp peaks in the left and centre plots.

5.5.2 Double virtual subtraction term, $\mathrm{d}\hat{\sigma}^U_{NNLO}$

Following the discussion of Section 4.5.3, the double virtual subtraction term is constructed from the remaining terms dropping down from the double real and real virtual subtraction terms, as well as the double virtual mass factorisation contribution. However, since the pole structure of the two loop amplitudes is predictable via the formalism described in Chapter 2, we are able to write the subtraction term in terms of the single and double unresolved integrated antenna strings without the prerequisite of the double real and real-virtual subtraction terms. Since we are in possession of the real-virtual subtraction term however, the combination of RV and VV terms should give an indication to the structures required at the double real contribution. In terms of integrated antenna strings, the subtraction term can be written in the form of Eq. (4.5.131),

$$
\begin{aligned}
\mathrm{d}\hat{\sigma}^U_{gg,NNLO} &= -\mathcal{N}^2_{gg,4}\,\mathrm{d}\Phi_2(p_3,p_4;p_1,p_2)\int\frac{\mathrm{d}z_1}{z_1}\frac{\mathrm{d}z_2}{z_2}\frac{1}{2!}\sum_{P(\hat{1}\hat{2})}\Bigg\{ \\
&\quad \boldsymbol{J}^{(1)}_4(j_q,\hat{\bar{1}}_g,\hat{\bar{2}}_g,k_{\bar{q}})\left(B^1_4(j_q,\hat{\bar{1}}_g,\hat{\bar{2}}_g,k_{\bar{q}})-\frac{b_0}{\epsilon}\,B^0_4(j_q,\hat{\bar{1}}_g,\hat{\bar{2}}_g,k_{\bar{q}})\right) \\
&\quad +\frac{1}{2}\,\boldsymbol{J}^{(1)}_4(j_q,\hat{\bar{1}}_g,\hat{\bar{2}}_g,k_{\bar{q}})\otimes\boldsymbol{J}^{(1)}_4(j_q,\hat{\bar{1}}_g,\hat{\bar{2}}_g,k_{\bar{q}})\,B^0_4(j_q,\hat{\bar{1}}_g,\hat{\bar{2}}_g,k_{\bar{q}}) \\
&\quad +\boldsymbol{J}^{(2)}_4(j_q,\hat{\bar{1}}_g,\hat{\bar{2}}_g,k_{\bar{q}})\,B^0_4(j_q,\hat{\bar{1}}_g,\hat{\bar{2}}_g,k_{\bar{q}})\Bigg\}\,J^{(2)}_2(p_j,p_k), \quad (5.5.64)
\end{aligned}
$$

which reproduces the form of the Catani pole structure in Eq. (4.5.115). The single unresolved integrated antenna string is defined in Eq. (5.2.14), where it was written as a sum over integrated dipoles. The analogous dipole-like formula for $\boldsymbol{J}^{(2)}_4$ is given by,

$$
\boldsymbol{J}^{(2)}_4(j_q,\hat{\bar{1}}_g,\hat{\bar{2}}_g,k_{\bar{q}}) = \boldsymbol{J}^{(2)}_2(j_q,\hat{\bar{1}}_g)+\boldsymbol{J}^{(2)}_2(\hat{\bar{1}}_g,\hat{\bar{2}}_g)+\boldsymbol{J}^{(2)}_2(\hat{\bar{2}}_g,k_q)-\overline{\boldsymbol{J}}^{(2)}_2(\hat{\bar{1}}_q,\hat{\bar{2}}_{\bar{q}}),
$$

$$(5.5.65)$$

where the two-parton double unresolved integrated antenna strings are given by:

$$
\boldsymbol{J}^{(2)}_2(j_q,\hat{\bar{1}}_g) = \mathcal{D}^0_{4,g}(s_{j\bar{1}})+\mathcal{D}^1_{3,q}(s_{j\bar{1}})+\frac{b_0}{\epsilon}\left(\frac{|s_{j\bar{1}}|}{\mu^2}\right)^{-\epsilon}\mathcal{D}^0_{3,g}(s_{j\bar{1}})
$$

$$- \quad \left[\mathcal{D}_{3,g}^0(s_{j\bar{1}}) \otimes \mathcal{D}_{3,g}^0(s_{j\bar{1}})\right](z_1) - \overline{\Gamma}_{gg}^{(2)}(z_1)\delta(1-z_2), \tag{5.5.66}$$

$$\boldsymbol{J}_2^{(2)}(\hat{\bar{1}}_g, \hat{\bar{2}}_g) = 2\mathcal{F}_{4,gg}^{0,adj}(s_{\bar{1}\bar{2}}) + 2\mathcal{F}_{4,gg}^{0,n.adj}(s_{\bar{1}\bar{2}}) + \mathcal{F}_{3,gg}^{1,n.adj}(s_{\bar{1}\bar{2}}) + \frac{b_0}{\epsilon}\mathcal{F}_3^0(s_{\bar{1}\bar{2}})\left(\frac{s_{\bar{1}\bar{2}}}{\mu^2}\right)^{-\epsilon}$$

$$- \quad \Gamma_{gg}^{(2)}(z_1)\delta(1-z_2) - \Gamma_{gg}^{(2)}(z_2)\delta(1-z_1) - 2\left[\mathcal{F}_3^0(s_{\bar{1}\bar{2}}) \otimes \mathcal{F}_3^0(s_{\bar{1}\bar{2}})\right],$$

$$+ \quad \left[\Gamma_{gg}^1 \otimes \Gamma_{gg}^1\right](z_1)\delta(1-z_2) + \left[\Gamma_{gg}^1 \otimes \Gamma_{gg}^1\right](z_2)\delta(1-z_1) \tag{5.5.67}$$

$$\boldsymbol{J}_2^{(2)}(\hat{\bar{2}}_g, k_{\bar{q}}) = \boldsymbol{J}_2^{(2)}(k_{\bar{q}}, \hat{\bar{2}}_g). \tag{5.5.68}$$

5.6   Quark-gluon initiated dijet production at NNLO

5.6.1   Real-virtual subtraction term, $\mathrm{d}\hat{\sigma}_{NNLO}^T$

We consider the process $qg \to qgg$. At leading order in colour we will have the cross section

$$\mathrm{d}\hat{\sigma}_{gg,NNLO}^{RV} = \mathcal{N}_{qg,5}^1 \int \mathrm{d}\Phi_3(p_3, p_4, p_5; p_1, p_2)\frac{1}{3!}\frac{\mathrm{d}x_1}{x_1}\frac{\mathrm{d}x_2}{x_2}\sum_{P(\hat{\bar{2}},i,j)}$$

$$\times \quad B_5^1(\hat{\bar{1}}_q, \hat{\bar{2}}_g, i_g, j_g, k_{\bar{q}})\delta(1-x_1)\delta(1-x_2)J_2^{(3)}(p_i, p_j, p_k) + \mathcal{O}(\frac{1}{N^2}) \tag{5.6.69}$$

where the sum is over the set of six permutations of the gluons, including the initial states. In a similar vein to the gluon-initiated process, we identify three topologies, defined by the relative position of the initial state gluon. Since the quarks are fixed at the end of the gluon string, the initial gluon can with either be colour connected (i.e. adjacent) to the quark, sandwiched by the final state gluon or colour-connected the antiquark, which we label as $\mathbb{X}$, $\mathbb{Y}$ and $\mathbb{Z}$ respectively. In this way, the full leading colour squared matrix element can be arranged as

$$\mathrm{d}\hat{\sigma}_{qg,NNLO}^{RV,\mathbb{X}} = \mathcal{N}_{qg,5}^1 \int \mathrm{d}\Phi_3(p_3, p_4, p_5; p_1, p_2)\frac{\mathrm{d}x_1}{x_1}\frac{\mathrm{d}x_2}{x_2}\delta(1-x_1)\delta(1-x_2)J_2^{(3)}(p_i, p_j, p_k)$$

$$\times \quad \frac{1}{3!}\sum_{P(\hat{\bar{1}},\hat{\bar{2}})} B_5^1(j_q, \hat{\bar{1}}_g, \hat{\bar{2}}_g, i_g, k_{\bar{q}}) \tag{5.6.70}$$

$$\mathrm{d}\hat{\sigma}_{qg,NNLO}^{RV,\mathbb{Y}} = \mathcal{N}_{qg,5}^1 \int \mathrm{d}\Phi_3(p_3, p_4, p_5; p_1, p_2)\frac{\mathrm{d}x_1}{x_1}\frac{\mathrm{d}x_2}{x_2}\delta(1-x_1)\delta(1-x_2)J_2^{(3)}(p_i, p_j, p_k)$$

$$\times \quad \frac{1}{3!} \sum_{P(\hat{\bar{1}},\hat{\bar{2}})} B_5^1(\hat{\bar{1}}_q, i_g, \hat{\bar{2}}_g, j_g, k_{\bar{q}}) \tag{5.6.71}$$

$$d\hat{\sigma}_{qg,NNLO}^{RV,\mathbb{Z}} = \mathcal{N}_{qg,5}^1 \int d\Phi_3(p_3, p_4, p_5; p_1, p_2) \frac{dx_1}{x_1} \frac{dx_2}{x_2} \delta(1-x_1)\delta(1-x_2) J_2^{(3)}(p_i, p_j, p_k)$$

$$\times \quad \frac{1}{3!} \sum_{P(\hat{\bar{1}},\hat{\bar{2}})} B_5^1(\hat{\bar{1}}_q, i_g, j_g, \hat{\bar{2}}_g, k_{\bar{q}}) \tag{5.6.72}$$

such that

$$d\hat{\sigma}_{qg,NNLO}^{RV,full} = d\hat{\sigma}_{qg,NNLO}^{RV,\mathbb{X}} + d\hat{\sigma}_{qg,NNLO}^{RV,\mathbb{Y}} + d\hat{\sigma}_{qg,NNLO}^{RV,\mathbb{Z}}. \tag{5.6.73}$$

Subtraction term with colour connected initial states: $\mathbb{X}$ topology

The real-virtual contribution for the $\mathbb{X}$ topology is given by

$$d\hat{\sigma}_{qg,NNLO}^{RV,\mathbb{X}} = \mathcal{N}_{qg,5}^1 \int d\Phi_3(p_3, p_4, p_5; p_1, p_2) \frac{dx_1}{x_1} \frac{dx_2}{x_2} \delta(1-x_1)\delta(1-x_2) J_2^{(3)}(p_i, p_j, p_k)$$

$$\times \quad \frac{1}{3!} \sum_{P(\hat{\bar{1}},\hat{\bar{2}})} B_5^1(j_q, \hat{\bar{1}}_g, \hat{\bar{2}}_g, i_g, k_{\bar{q}}) \tag{5.6.74}$$

The sum over the initial states can be achieved by a simple label exchange, such that we only need to the subtraction term for the single ordering: it has the form

$$d\hat{\sigma}_{NNLO}^{T,\mathbb{X}} = \mathcal{N}_{qg,5}^1 \sum_{P(i,j)} \int d\Phi_3(p_3, p_4, p_5; x_1 p_1, x_2 p_2) \frac{1}{2!} \frac{dx_1}{x_1} \frac{dx_2}{x_2} \times \Bigg\{$$

$$-\Big(\frac{1}{2}\mathcal{F}_{3,g}^0(s_{\bar{2}i}) + \frac{1}{3}\mathcal{F}_3^0(s_{ij}) + \frac{1}{2}\mathcal{D}_3^0(s_{jk}) + \mathcal{D}_{3,qg}^0(s_{\bar{1}\bar{2}})$$

$$-\Gamma_{qq}^1(x_1)\delta(1-x_2) - \Gamma_{gg}^1(x_2)\delta(1-x_1)\Big) B_5^0(\hat{\bar{1}}_q, \hat{\bar{2}}_g, i_g, j_g, k_{\bar{q}}) J_2^{(3)}(p_i, p_j, p_k)$$

$$+f_3^0(\hat{\bar{2}}_g, i_g, j_g)\Bigg[\delta(1-x_1)\delta(1-x_2) B_4^1(\hat{\bar{1}}_q, \hat{\bar{2}}_g, \widetilde{(ij)}_g, k_{\bar{q}})$$

$$+\Big(\mathcal{D}_{3,qg}^0(s_{\bar{1}\bar{2}}) + \frac{1}{2}\mathcal{F}_{3,g}^0(s_{\bar{2}\widetilde{(ij)}}) + \frac{1}{2}\mathcal{D}_3^0(s_{\widetilde{(ij)}k}) - \Gamma_{qq}^1(x_1)\delta(1-x_2)$$

$$-\Gamma_{gg}^1(x_2)\delta(1-x_1)\Big) B_4^0(\hat{\bar{1}}_q, \hat{\bar{2}}_g, \widetilde{(ij)}_g, k_{\bar{q}})\Bigg] J_2^{(2)}(p_{\widetilde{(ij)}}, p_k)$$

$$+d_3^0(k_{\bar{q}}, j_g, i_g)\Bigg[\delta(1-x_1)\delta(1-x_2) B_4^1(\hat{\bar{1}}_q, \hat{\bar{2}}_g, \widetilde{(ij)}_g, \widetilde{(jk)}_{\bar{q}}) + \Big(\mathcal{D}_{3,qg}^0(s_{\bar{1}\bar{2}})$$

$$+\frac{1}{2}\mathcal{F}^0_{3,g}(s_{\bar{\widetilde{2}(ij)}}) + \frac{1}{2}\mathcal{D}^0_3(s_{\widetilde{(ij)}\widetilde{(jk)}}) - \Gamma^1_{qq}(x_1)\delta(1-x_2)$$

$$-\Gamma^1_{gg}(x_2)\delta(1-x_1)\Big)B^0_4(\hat{\bar{1}}_q,\hat{\bar{2}}_g,\widetilde{(ij)}_g,\widetilde{(jk)}_{\bar{q}})\bigg]J^{(2)}_2(p_{\widetilde{(ij)}},p_{\widetilde{(jk)}})$$

$$+G^0_3(\hat{\bar{2}}_g,\hat{\bar{1}}_q,k_{\bar{q}})\bigg[\delta(1-x_1)\delta(1-x_2)A^1_4(\hat{\bar{2}}_g,\widetilde{i}_g,\widetilde{j}_g,\hat{\bar{1}}_g) + \Big(\frac{1}{2}\mathcal{F}^0_{3,g}(s_{\bar{\widetilde{2}i}}) + \frac{1}{3}\mathcal{F}^0_3(s_{\widetilde{ij}})$$

$$+\frac{1}{2}\mathcal{F}^0_{3,g}(s_{\widetilde{j\bar{1}}}) + \mathcal{F}^0_{3,gg}(s_{\bar{\bar{12}}}) - \Gamma^1_{qq}(x_1)\delta(1-x_2) - \Gamma^1_{gg}(x_2)\delta(1-x_1)\Big)$$

$$\times A^0_4(\hat{\bar{2}}_g,\widetilde{i}_g,\widetilde{j}_g,\hat{\bar{1}}_g)\bigg]J^{(2)}_2(p_{\widetilde{i}},p_{\widetilde{j}})$$

$$+\bigg[f^1_3(\hat{\bar{2}}_g,i_g,j_g)\delta(1-x_1)\delta(1-x_2) + \Big(\frac{1}{2}\mathcal{F}^0_{3,g}(s_{\bar{2}j}) + \frac{1}{3}\mathcal{F}^0_3(s_{ji}) + \frac{1}{2}\mathcal{F}^0_{3,g}(s_{\bar{2}i})$$

$$-\mathcal{F}^0_{3,g}(s_{\bar{\widetilde{2}(ji)}})\Big)f^0_3(\hat{\bar{2}}_g,i_g,j_g)\bigg]B^0_4(\hat{\bar{1}}_q,\hat{\bar{\bar{2}}}_g,\widetilde{(ij)}_g,k_{\bar{q}})J^{(2)}_2(p_{\widetilde{(ij)}},p_k)$$

$$+\bigg[d^1_3(k_{\bar{q}},j_g,i_g)\delta(1-x_1)\delta(1-x_2) + \Big(\frac{1}{2}\mathcal{D}^0_3(s_{ki}) + \frac{1}{3}\mathcal{F}^0_3(s_{ij}) + \frac{1}{2}\mathcal{D}^0_3(s_{kj})$$

$$-\mathcal{D}^0_3(s_{\widetilde{(ki)(ij)}})\Big)d^0_3(k_{\bar{q}},j_g,i_g)\bigg]B^0_4(\hat{\bar{1}}_q,\hat{\bar{2}}_g,\widetilde{(ij)}_g,\widetilde{(jk)}_{\bar{q}})J^{(2)}_2(p_{\widetilde{(ij)}},p_{\widetilde{(jk)}})$$

$$+\bigg[G^1_3(\hat{\bar{2}}_g,\hat{\bar{1}}_q,k_{\bar{q}})\delta(1-x_1)\delta(1-x_2) + \Big(\mathcal{D}^0_{3,qg}(s_{\bar{2}\bar{1}}) + \mathcal{D}^0_{3,g;gq}(s_{\bar{2}k}) - 2\mathcal{F}^0_{3,gg}(s_{\bar{\bar{12}}})\Big)$$

$$\times G^0_3(\hat{\bar{2}}_g,\hat{\bar{1}}_q,k_{\bar{q}})\bigg]A^1_4(\hat{\bar{2}}_g,\widetilde{i}_g,\widetilde{j}_g,\hat{\bar{1}}_g)J^{(2)}_2(p_i,p_{\widetilde{jk}})$$

$$-\bigg[\tilde{A}^1_3(\hat{\bar{1}}_q,j_g,k_{\bar{q}})\delta(1-x_1)\delta(1-x_2) + \Big(\mathcal{A}^0_{3,q}(s_{\bar{1}k}) - \mathcal{A}^0_{3,q}(s_{\bar{\bar{1}}\widetilde{(jk)}})\Big)$$

$$\times A^0_3(\hat{\bar{1}}_q,j_g,k_{\bar{q}})\bigg]B^0_4(\hat{\bar{\bar{1}}}_q,\hat{\bar{2}}_g,i_g,\widetilde{(jk)}_{\bar{q}})J^{(2)}_2(p_{\widetilde{(jk)}},p_i)$$

$$+b_0\log\left(\frac{\mu^2}{|s_{2ij}|}\right)f^0_3(\hat{\bar{2}}_g,i_g,j_g)\delta(1-x_1)\delta(1-x_2)B^0_4(\hat{\bar{1}}_q,,\hat{\bar{\bar{2}}}_g,\widetilde{(ij)}_g,k_{\bar{q}})J^{(2)}_2(p_{\widetilde{ij}},p_k)$$

$$+b_0\log\left(\frac{\mu^2}{|s_{kji}|}\right)d^0_3(k_{\bar{q}},j_g,i_g)\delta(1-x_1)\delta(1-x_2)B^0_4(\hat{\bar{1}}_q,\hat{\bar{2}}_g,\widetilde{(ij)}_g,\widetilde{(jk)}_{\bar{q}})J^{(2)}_2(p_{\widetilde{ij}},p_{\widetilde{jk}})$$

$$+b_0\log\left(\frac{\mu^2}{|s_{12k}|}\right)G^0_3(\hat{\bar{2}}_g,\hat{\bar{1}}_q,k_{\bar{q}})\delta(1-x_1)\delta(1-x_2)A^0_4(\hat{\bar{2}}_g,\widetilde{i}_g,\widetilde{j}_g,\hat{\bar{1}}_g)J^{(2)}_2(p_i,p_{\widetilde{jk}})$$

$$+\frac{1}{2}\bigg[\frac{1}{2}\mathcal{F}^0_{3,g}(s_{\bar{\widetilde{2}(ij)}}) - \frac{1}{2}\mathcal{F}^0_{3,g}(s_{\bar{2}j}) - \mathcal{D}^0_{3,qg}(s_{\bar{1}\bar{2}}) + \mathcal{D}^0_{3,qg}(s_{\bar{1}\bar{2}}) - \frac{1}{2}\mathcal{D}^0_3(s_{k\widetilde{(ij)}})$$

$$+\frac{1}{2}\mathcal{D}^0_3(s_{kj}) + \delta(1-x_1)\delta(1-x_2)\Big(\mathcal{S}(s_{\bar{2}j},s_{jk},x_{\bar{2}j,jk}) - \mathcal{S}(s_{\bar{\widetilde{2}(ij)}},s_{jk},x_{\bar{\widetilde{2}(ij)},jk})\Big)$$

$$+\mathcal{S}(s_{k\widetilde{(ij)}}, s_{jk}, x_{k\widetilde{(ij)},jk}) - \mathcal{S}(s_{jk}, s_{jk}, 1)\Big)\Bigg]$$

$$\times f_3^0(\hat{\tilde{2}}_g, i_g, j_g) B_4^0(\hat{\tilde{1}}_q, , \hat{\tilde{\tilde{2}}}_g, \widetilde{(ij)}_g, k_{\bar{q}}) J_2^{(2)}(p_{\widetilde{(ij)}}, p_k)$$

$$+\frac{1}{2}\Bigg[\frac{1}{2}\mathcal{D}_3^0(s_{\widetilde{(ij)}\widetilde{(jk)}}) - \frac{1}{2}\mathcal{D}_3^0(s_{ik}) - \frac{1}{2}\mathcal{F}_{3,g}^0(s_{\hat{2}\widetilde{(ij)}}) + \frac{1}{2}\mathcal{F}_{3,g}^0(s_{\hat{2}i})$$

$$-\mathcal{A}_{3,q}^0(s_{\hat{1}\widetilde{(jk)}}) + \mathcal{A}_{3,q}^0(s_{\hat{1}k}) + \delta(1-x_1)\delta(1-x_2)\Big(\mathcal{S}(s_{ik}, s_{ik}, 1)$$

$$-\mathcal{S}(s_{\widetilde{(ij)}\widetilde{(jk)}}, s_{ik}, x_{\widetilde{(ij)}\widetilde{(jk)},ik}) + \mathcal{S}(s_{\hat{2}\widetilde{(ij)}}, s_{ik}, x_{\hat{2}\widetilde{(ij)},ik}) - \mathcal{S}(s_{\hat{2}i}, s_{ik}, x_{\hat{2}i,ik})\Big)\Bigg]$$

$$\times d_3^0(k_{\bar{q}}, j_g, i_g) B_4^0(\hat{\tilde{1}}_q, \hat{\tilde{2}}_g, \widetilde{(ij)}_g, \widetilde{(jk)}_{\bar{q}}) J_2^{(2)}(p_{\widetilde{(ij)}}, p_{\widetilde{(jk)}})$$

$$-\frac{1}{2}\Bigg[\mathcal{A}_{3,q}^0(s_{\hat{1}k}) - \mathcal{A}_{3,q}^0(s_{\hat{\bar{1}}\widetilde{(jk)}}) - \frac{1}{2}\mathcal{D}_3^0(s_{ik}) + \frac{1}{2}\mathcal{D}_3^0(s_{i\widetilde{(jk)}}) - \mathcal{D}_{3,qg}^0(s_{\hat{1}\hat{2}})$$

$$+\mathcal{D}_{3,qg}^0(s_{\hat{\bar{1}}\hat{2}}) + \delta(1-x_1)\delta(1-x_2)\Big(\mathcal{S}(s_{ik}, s_{ik}, 1) - \mathcal{S}(s_{i\widetilde{(jk)}}, s_{ik}, x_{i\widetilde{(jk)},ik})$$

$$+\mathcal{S}(s_{\hat{\bar{1}}\widetilde{(jk)}}, s_{ik}, x_{\hat{\bar{1}}\widetilde{(jk)},ik}) - \mathcal{S}(s_{\hat{1}k}, s_{ik}, x_{\hat{1}k,ik})\Big)\Bigg]$$

$$\times A_3^0(\hat{\tilde{1}}_q, j_g, k_{\bar{q}}) B_4^0(\hat{\tilde{\tilde{1}}}_q, \hat{\tilde{2}}_g, i_g, \widetilde{(jk)}_{\bar{q}}) J_2^{(2)}(p_{\widetilde{(jk)}}, p_i)\Bigg\}. \tag{5.6.75}$$

Subtraction term with colour connected initial states: $\mathbb{Y}$ topology

The real-virtual contribution for the $\mathbb{Y}$ topology is given by

$$
\begin{aligned}
\mathrm{d}\hat{\sigma}_{qg,NNLO}^{RV,\mathbb{Y}} &= \mathcal{N}_{qg,5}^1 \int \mathrm{d}\Phi_3(p_3, p_4, p_5; p_1, p_2)\frac{\mathrm{d}x_1}{x_1}\frac{\mathrm{d}x_2}{x_2}\delta(1-x_1)\delta(1-x_2)J_2^{(3)}(p_i, p_j, p_k) \\
&\times \frac{1}{3!}\sum_{P(\hat{1},\hat{2})} B_5^1(\hat{\tilde{1}}_q, j_g, \hat{\tilde{2}}_g, i_g, k_{\bar{q}}).
\end{aligned} \tag{5.6.76}
$$

The sum over the initial states can be achieved by a simple label exchange, such that we only need the subtraction term for a single ordering: it has the form

$$
\begin{aligned}
\mathrm{d}\hat{\sigma}_{qg,NNLO}^{T,\mathbb{Y}} &= \mathcal{N}_{qg,5}^1 \sum_{P(i,j)}\int d\Phi_3(p_3, p_4, p_5; x_1 p_1, x_2 p_2)\frac{1}{2!}\frac{\mathrm{d}x_1}{x_1}\frac{\mathrm{d}x_2}{x_2} \times \Bigg\{ \\
&-\Big(\frac{1}{2}\mathcal{D}_{3,q}^0(s_{\hat{1}i}) + \frac{1}{2}\mathcal{F}_{3,g}^0(s_{i\hat{2}}) + \frac{1}{2}\mathcal{F}_{3,g}^0(s_{\hat{2}j}) + \frac{1}{2}\mathcal{D}_3^0(s_{jk}) - \Gamma_{qq}^1(x_1)\delta(1-x_2) \\
&-\Gamma_{gg}^1(x_2)\delta(1-x_1)\Big)B_5^0(\hat{1}_q, i_g, \hat{2}_g, j_g, k_{\bar{q}}) J_2^{(3)}(p_i, p_j, p_k)
\end{aligned}
$$

$$+D_3^0(\hat{\bar{1}}_q, i_g, \hat{\bar{2}}_g)\Bigg[\delta(1-x_1)\delta(1-x_2)B_4^1(\hat{\bar{1}}_q, \hat{\bar{2}}_g, \widetilde{j}_g, \widetilde{k}_{\bar{q}}) + \Big(\mathcal{D}_{3,qg}^0(s_{\bar{1}\bar{2}}) + \frac{1}{2}\mathcal{F}_{3,g}^0(s_{\bar{2}\widetilde{j}})$$

$$+\frac{1}{2}\mathcal{D}_3^0(s_{\widetilde{kj}}) - \Gamma_{qq}^1(x_1)\delta(1-x_2) - \Gamma_{gg}^1(x_2)\delta(1-x_1)\Big)B_4^0(\hat{\bar{1}}_q, \hat{\bar{2}}_g, \widetilde{j}_g, \widetilde{k}_{\bar{q}})\Bigg]J_2^{(2)}(p_{\widetilde{j}}, p_{\widetilde{k}})$$

$$+d_{g;gq}^0(k_{\bar{q}}, j_g, \hat{\bar{2}}_g)\Bigg[\delta(1-x_1)\delta(1-x_2)B_4^1(\hat{\bar{1}}_q, i_g, \hat{\bar{2}}_g, \widetilde{(jk)}_{\bar{q}})$$

$$+\Big(\frac{1}{2}\mathcal{D}_{3,q}^0(s_{\bar{1}i}) + \frac{1}{2}\mathcal{F}_{3,g}^0(s_{\bar{2}i}) + \mathcal{D}_{3,g;gq}^0(s_{\bar{2}\widetilde{(jk)}}) - \Gamma_{qq}^1(x_1)\delta(1-x_2)$$

$$-\Gamma_{gg}^1(x_2)\delta(1-x_1)\Big)B_4^0(\hat{\bar{1}}_q, i_g, \hat{\bar{2}}_g, \widetilde{(jk)}_{\bar{q}})\Bigg]J_2^{(2)}(p_i, p_{\widetilde{(jk)}})$$

$$+G_3^0(j_g, \hat{\bar{1}}_q, k_{\bar{q}})\Bigg[\delta(1-x_1)\delta(1-x_2)A_4^1(\hat{\bar{1}}_g, i_g, \hat{\bar{2}}_g, \widetilde{(jk)}_g)$$

$$+\Big(\frac{1}{2}\mathcal{F}_{3,g}^0(s_{\bar{1}i}) + \frac{1}{2}\mathcal{F}_{3,g}^0(s_{\bar{2}i}) + \frac{1}{2}\mathcal{F}_{3,g}^0(s_{\bar{2}\widetilde{(jk)}}) + \frac{1}{2}\mathcal{F}_{3,g}^0(s_{\bar{1}\widetilde{(jk)}})$$

$$-\Gamma_{qq}^1(x_1)\delta(1-x_2) - \Gamma_{gg}^1(x_2)\delta(1-x_1)\Big)A_4^0(\hat{\bar{1}}_g, i_g, \hat{\bar{2}}_g, \widetilde{(jk)}_g)\Bigg]J_2^{(2)}(p_i, p_{\widetilde{(jk)}})$$

$$+\Bigg[D_3^1(\hat{\bar{1}}_q, i_g, \hat{\bar{2}}_g)\delta(1-x_1)\delta(1-x_2) + \Big(\frac{1}{2}\mathcal{D}_{3,q}^0(s_{\bar{1}i}) + \frac{1}{2}\mathcal{F}_{3,g}^0(s_{i\bar{2}}) + \mathcal{D}_{3,qg}^0(s_{\bar{1}\bar{2}})$$

$$-2\mathcal{D}_{3,qg}^0(s_{\bar{\bar{1}}\bar{\bar{2}}})\Big)D_3^0(\hat{\bar{1}}_q, i_g, \hat{\bar{2}}_g)\Bigg]B_4^0(\hat{\bar{1}}_q, \hat{\bar{2}}_g, \widetilde{j}_g, \widetilde{k}_{\bar{q}})J_2^{(2)}(p_{\widetilde{j}}, p_{\widetilde{k}})$$

$$+\Bigg[d_{g;gq}^1(k_{\bar{q}}, j_g, \hat{\bar{2}}_g)\delta(1-x_1)\delta(1-x_2) + \Big(\frac{1}{2}\mathcal{D}_3^0(s_{kj}) + \frac{1}{2}\mathcal{F}_{3,g}^0(s_{j\bar{2}}) + \mathcal{D}_{3,g;gq}^0(s_{k\bar{2}})$$

$$-2\mathcal{D}_{3,g;gq}^0(s_{\widetilde{(kj)}\bar{\bar{2}}})\Big)d_{g;gq}^0(k_{\bar{q}}, j_g, \hat{\bar{2}}_g)\Bigg]B_4^0(\hat{\bar{1}}_q, i_g, \hat{\bar{2}}_g, \widetilde{(jk)}_{\bar{q}})J_2^{(2)}(p_i, p_{\widetilde{(jk)}})$$

$$+\Bigg[G_3^1(j_g, \hat{\bar{1}}_q, k_{\bar{q}})\delta(1-x_1)\delta(1-x_2) + \Big(\frac{1}{2}\mathcal{D}_3^0(s_{jk}) + \frac{1}{2}\mathcal{D}_{3,q}^0(s_{j\bar{1}}) - \mathcal{F}_{3,g}^0(s_{\widetilde{(jk)}\bar{\bar{1}}})\Big)$$

$$\times G_3^0(j_g, \hat{\bar{1}}_q, k_{\bar{q}})\Bigg]A_4^0(\hat{\bar{1}}_g, i_g, \hat{\bar{2}}_g, \widetilde{(jk)}_g)J_2^{(2)}(p_i, p_{\widetilde{(jk)}})$$

$$+b_0\log\left(\frac{\mu^2}{|s_{1i2}|}\right)D_3^0(\hat{\bar{1}}_q, i_g, \hat{\bar{2}}_g)\delta(1-x_1)\delta(1-x_2)B_4^0(\hat{\bar{1}}_q, \hat{\bar{2}}_g, \widetilde{j}_g, \widetilde{k}_{\bar{q}})J_2^{(2)}(p_{\widetilde{j}}, p_{\widetilde{k}})$$

$$+b_0\log\left(\frac{\mu^2}{|s_{kj2}|}\right)d_{g;gq}^0(k_{\bar{q}}, j_g, \hat{\bar{2}}_g)\delta(1-x_1)\delta(1-x_2)B_4^0(\hat{\bar{1}}_q, i_g, \hat{\bar{2}}_g, \widetilde{(jk)}_{\bar{q}})J_2^{(2)}(p_i, p_{\widetilde{(jk)}})$$

$$+b_0\log\left(\frac{\mu^2}{|s_{jk1}|}\right)G_3^0(j_g, \hat{\bar{1}}_q, k_{\bar{q}})\delta(1-x_1)\delta(1-x_2)A_4^0(\hat{\bar{1}}_g, i_g, \hat{\bar{2}}_g, \widetilde{(jk)}_g)J_2^{(2)}(p_i, p_{\widetilde{(jk)}})$$

$$
+\frac{1}{2}\left[\mathcal{D}^0_{3,qg}(s_{\bar{\bar{1}}\bar{2}}) - \mathcal{D}^0_{3,qg}(s_{\bar{1}\bar{2}}) - \frac{1}{2}\mathcal{F}^0_{3,g}(s_{\bar{2}\widetilde{j}}) + \frac{1}{2}\mathcal{F}^0_{3,g}(s_{\bar{2}j}) - \mathcal{A}^0_{3,q}(s_{\bar{1}\widetilde{k}}) + \mathcal{A}^0_{3,q}(s_{\bar{1}k})\right.
$$

$$
+\delta(1-x_1)\delta(1-x_2)\Big(\mathcal{S}(s_{\bar{1}\bar{2}}, s_{jk}, x_{\bar{1}\bar{2},jk}) - \mathcal{S}(s_{\bar{1}\bar{2}}, s_{\widetilde{jk}}, x_{\bar{1}\bar{2},\widetilde{jk}}) - \mathcal{S}(s_{\bar{2}j}, s_{jk}, x_{\bar{2}j,jk})
$$

$$
+\mathcal{S}(s_{\bar{\bar{2}}\widetilde{j}}, s_{\widetilde{jk}}, x_{\bar{\bar{2}}\widetilde{j},\widetilde{jk}}) - \mathcal{S}(s_{\bar{1}k}, s_{jk}, x_{\bar{1}k,jk}) + \mathcal{S}(s_{\bar{\bar{1}}\widetilde{k}}, s_{\widetilde{jk}}, x_{\bar{\bar{1}}\widetilde{k},\widetilde{jk}})\Big)\bigg]
$$

$$
\times D^0_3(\hat{\bar{1}}_q, i_g, \hat{\bar{2}}_g) B^0_4(\hat{\bar{\bar{1}}}_q, \hat{\bar{\bar{2}}}_g, \widetilde{j}_g, \widetilde{k}_{\bar{q}}) J^{(2)}_2(p_{\widetilde{j}}, p_{\widetilde{k}})
$$

$$
+\frac{1}{2}\left[\mathcal{D}^0_{3,g;gq}(s_{\bar{\bar{2}}\widetilde{(jk)}}) - \mathcal{D}^0_{3,g;gq}(s_{\bar{2}k}) - \frac{1}{2}\mathcal{F}^0_{3,g}(s_{\bar{2}i}) + \frac{1}{2}\mathcal{F}^0_{3,g}(s_{\bar{2}i})\right.
$$

$$
-\mathcal{A}^0_{3,q}(s_{\widetilde{(jk)}\bar{1}}) + \mathcal{A}^0_{3,q}(s_{k\bar{1}}) + \delta(1-x_1)\delta(1-x_2)\Big(\mathcal{S}(s_{\bar{2}k}, s_{ik}, x_{\bar{2}k,ik})
$$

$$
-\mathcal{S}(s_{\bar{\bar{2}}\widetilde{(jk)}}, s_{ik}, x_{\bar{\bar{2}}\widetilde{(jk)},ik}) + \mathcal{S}(s_{\widetilde{(jk)}\bar{1}}, s_{ik}, x_{\widetilde{(jk)}\bar{1},ik}) - \mathcal{S}(s_{k\bar{1}}, s_{ik}, x_{k\bar{1},ik})\Big)\bigg]
$$

$$
\times d^0_{q;gq}(k_{\bar{q}}, j_g, \hat{\bar{2}}_g) B^0_4(\hat{\bar{1}}_q, i_g, \hat{\bar{\bar{2}}}_g, \widetilde{(jk)}_{\bar{q}}) J^{(2)}_2(p_i, p_{\widetilde{(jk)}})\bigg\}. \tag{5.6.77}
$$

Subtraction term with colour connected initial states: $\mathbb{Z}$ topology

The real-virtual contribution for the $\mathbb{Z}$ topology is given by

$$
d\hat{\sigma}^{RV,\mathbb{Z}}_{qg,NNLO} = \quad \mathcal{N}^1_{qg,5} \int d\Phi_3(p_3, p_4, p_5; p_1, p_2) \frac{dx_1}{x_1}\frac{dx_2}{x_2}\delta(1-x_1)\delta(1-x_2) J^{(3)}_2(p_i, p_j, p_k)
$$

$$
\times\frac{1}{3!}\sum_{P(\hat{1},\hat{2})} B^1_5(\hat{\bar{1}}_q, i_g, j_g, \hat{\bar{2}}_g, k_{\bar{q}}). \tag{5.6.78}
$$

The sum over the initial states can be achieved by a simple label exchange, such that we only need to the subtraction term for the single ordering: it has the form

$$
d\hat{\sigma}^{T,\mathbb{Z}}_{qg,NNLO} = \mathcal{N}^1_{qg,5}\sum_{P(i,j)}\int d\Phi_3(p_3, p_4, p_5; x_1 p_1, x_2 p_2)\frac{1}{2!}\frac{dx_1}{x_1}\frac{dx_2}{x_2}\times\Bigg\{
$$

$$
-\left(\frac{1}{2}\mathcal{D}^0_{3,q}(s_{\bar{1}i}) + \frac{1}{3}\mathcal{F}^0_3(s_{ij}) + \frac{1}{2}\mathcal{F}^0_{3,g}(s_{j\bar{2}}) + \mathcal{D}^0_{3,g;gq}(s_{\bar{2}k})\right.
$$

$$
-\Gamma^1_{qq}(x_1)\delta(1-x_2) - \Gamma^1_{gg}(x_2)\delta(1-x_1)\Big) B^0_5(\hat{1}_q, i_g, j_g, \hat{2}_g, k_{\bar{q}}) J^{(3)}_2(p_i, p_j, p_k)
$$

$$
d^0_3(\hat{\bar{1}}_q, i_g, j_g)\left[\delta(1-x_1)\delta(1-x_2) B^1_4(\hat{\bar{\bar{1}}}_q, \widetilde{(ij)}_g, \hat{\bar{2}}_g, k_{\bar{q}}) + \left(\frac{1}{2}\mathcal{D}^0_{3,q}(s_{\bar{1}\widetilde{(ij)}})\right.\right.
$$

$$
+\frac{1}{2}\mathcal{F}^0_{3,g}(s_{\widetilde{(ij)}\bar{2}}) + \mathcal{D}^0_{3,g;gq}(s_{\bar{2}k}) - \Gamma^1_{qq}(x_1)\delta(1-x_2) - \Gamma^1_{gg}(x_2)\delta(1-x_1)\Big)
$$

$$\times B_4^0(\hat{\bar{\tilde{1}}}_q, \widetilde{(ij)}_g, \hat{\bar{\tilde{2}}}_g, k_{\bar{q}}) \Bigg] J_2^{(2)}(p_{\widetilde{(ij)}}, p_k)$$

$$+ f_3^0(\hat{\bar{\tilde{2}}}_g, j_g, i_g) \Bigg[\delta(1-x_1)\delta(1-x_2) B_4^1(\hat{\bar{\tilde{1}}}_q, \widetilde{(ij)}_g, \hat{\bar{\tilde{2}}}_g, k_{\bar{q}}) + \Big(\frac{1}{2}\mathcal{D}_{3,q}^0(s_{\bar{1}\widetilde{(ij)}})$$

$$+ \frac{1}{2}\mathcal{F}_{3,g}^0(s_{\widetilde{(ij)}\bar{2}}) + \mathcal{D}_{3,g;gq}^0(s_{\bar{2}k}) - \Gamma_{qq}^1(x_1)\delta(1-x_2) - \Gamma_{gg}^1(x_2)\delta(1-x_1) \Big)$$

$$\times B_4^0(\hat{\bar{\tilde{1}}}_q, \widetilde{(ij)}_g, \hat{\bar{\tilde{2}}}_g, k_{\bar{q}}) \Bigg] J_2^{(2)}(p_{\widetilde{(ij)}}, p_k)$$

$$+ A_3^0(\hat{\bar{1}}_q, \hat{\bar{2}}_g, k_{\bar{q}}) \Bigg[\delta(1-x_1)\delta(1-x_2) B_4^1(\hat{\bar{\tilde{1}}}_q, \tilde{i}_g, \tilde{j}_g, \hat{\bar{\tilde{2}}}_{\bar{q}}) + \Big(\frac{1}{2}\mathcal{D}_{3,q}^0(s_{\bar{1}\tilde{i}})$$

$$+ \frac{1}{3}\mathcal{F}_3^0(s_{\widetilde{ij}}) + \frac{1}{2}\mathcal{D}_{3,q}^0(s_{\tilde{j}\bar{2}}) - \Gamma_{qq}^1(x_1)\delta(1-x_2) - \Gamma_{qq}^1(x_2)\delta(1-x_1) \Big)$$

$$\times B_4^0(\hat{\bar{\tilde{1}}}_q, \tilde{i}_g, \tilde{j}_g, \hat{\bar{\tilde{2}}}_{\bar{q}}) \Bigg] J_2^{(2)}(p_{\tilde{i}}, p_{\tilde{j}})$$

$$+ G_3^0(i_g, \hat{\bar{1}}_q, k_{\bar{q}}) \Bigg[\delta(1-x_1)\delta(1-x_2) A_4^1(\hat{\bar{\tilde{1}}}_g, \widetilde{(ik)}_g, j_g, \hat{\bar{2}}_g) + \Big(\frac{1}{2}\mathcal{F}_{3,g}^0(s_{\bar{1}\widetilde{(ik)}})$$

$$+ \frac{1}{3}\mathcal{F}_3^0(s_{\widetilde{(ik)}j}) + \frac{1}{2}\mathcal{F}_{3,g}^0(s_{j\bar{2}}) + \mathcal{F}_{3,gg}^0(s_{\bar{1}\bar{2}}) - \Gamma_{qq}^1(x_1)\delta(1-x_2) - \Gamma_{gg}^1(x_2)\delta(1-x_1) \Big)$$

$$\times A_4^0(\hat{\bar{\tilde{1}}}_g, \widetilde{(ik)}_g, j_g, \hat{\bar{2}}_g) \Bigg] J_2^{(2)}(p_{\widetilde{(ik)}}, p_j)$$

$$+ \Bigg[d_3^1(\hat{\bar{1}}_q, i_g, j_g)\delta(1-x_1)\delta(1-x_2) + \Big(\frac{1}{2}\mathcal{D}_{3,q}^0(s_{\bar{1}i}) + \frac{1}{3}\mathcal{F}_3^0(s_{ij}) + \frac{1}{2}\mathcal{D}_{3,q}^0(s_{\bar{1}j})$$

$$- \mathcal{D}_{3,q}^0(s_{\bar{\bar{1}}\widetilde{(ij)}}) \Big) d_3^0(\hat{\bar{1}}_q, i_g, j_g) \Bigg] B_4^0(\hat{\bar{\tilde{1}}}_q, \widetilde{(ij)}_g, \hat{\bar{2}}_g, k_{\bar{q}}) J_2^{(2)}(p_{\widetilde{(ij)}}, p_k)$$

$$- \Bigg[\tilde{A}_3^1(\hat{\bar{1}}_q, i_g, k_{\bar{q}})\delta(1-x_1)\delta(1-x_2) + \Big(\mathcal{A}_{3,q}^0(s_{\hat{\bar{1}}k}) - \mathcal{A}_{3,q}^0(s_{\hat{\bar{1}}\widetilde{(ik)}}) \Big)$$

$$\times A_3^0(\hat{\bar{1}}_q, i_g, k_{\bar{q}}) \Bigg] B_4^0(\hat{\bar{\tilde{1}}}_q, j_g, \hat{\bar{2}}_g, \widetilde{(ik)}_{\bar{q}}) J_2^{(2)}(p_{\widetilde{(ik)}}, p_j)$$

$$+ \Bigg[f_3^1(\hat{\bar{2}}_g, j_g, i_g)\delta(1-x_1)\delta(1-x_2) + \Big(\frac{1}{2}\mathcal{F}_{3,g}^0(s_{\bar{2}j}) + \frac{1}{3}\mathcal{F}_3^0(s_{ji}) + \frac{1}{2}\mathcal{F}_{3,g}^0(s_{\bar{2}i})$$

$$- \mathcal{F}_{3,g}^0(s_{\bar{\bar{2}}\widetilde{(ji)}}) \Big) f_3^0(\hat{\bar{2}}_g, j_g, i_g) \Bigg] B_4^0(\hat{\bar{1}}_q, \widetilde{(ij)}_g, \hat{\bar{\tilde{2}}}_g, k_{\bar{q}}) J_2^{(2)}(p_{\widetilde{ij}}, p_k)$$

$$+ \Bigg[A_3^1(\hat{\bar{1}}_q, \hat{\bar{2}}_g, k_{\bar{q}})\delta(1-x_1)\delta(1-x_2) + \Big(\mathcal{D}_{3,qg}^0(s_{\bar{1}\bar{2}}) + \mathcal{D}_{3,g;gq}^0(s_{\bar{2}k}) - \mathcal{A}_{3,qq}^0(s_{\bar{\bar{1}}\bar{2}}) \Big)$$

$$\times A_3^0(\hat{\bar{1}}_q, \hat{\bar{2}}_g, k_{\bar{q}})\Bigg] B_4^0(\hat{\bar{\bar{1}}}_q, \widetilde{i}_g, \widetilde{j}_g, \hat{\bar{\bar{2}}}_{\bar{q}}) J_2^{(2)}(p_{\widetilde{i}}, p_{\widetilde{j}})$$

$$+\Bigg[G_3^1(i_g, \hat{\bar{1}}_q, k_{\bar{q}})\delta(1-x_1)\delta(1-x_2) + \Big(\frac{1}{2}\mathcal{D}_{3,q}^0(s_{\bar{1}i}) + \frac{1}{2}\mathcal{D}_3^0(s_{ki}) - \mathcal{F}_{3,g}^0(s_{\widetilde{(ik)}\bar{1}})\Big)$$

$$\times G_3^0(i_g, \hat{\bar{1}}_q, k_{\bar{q}})\Bigg] A_4^0(\hat{\bar{\bar{1}}}_g, \widetilde{(ik)}_g, j_g, \hat{\bar{2}}_g)\Bigg] J_2^{(2)}(p_{\widetilde{(ik)}}, p_j)$$

$$+b_0\log\left(\frac{\mu^2}{|s_{1ij}|}\right) d_3^0(\hat{\bar{1}}_q, i_g, j_g)\delta(1-x_1)\delta(1-x_2) B_4^0(\hat{\bar{\bar{1}}}_q, \widetilde{(ij)}_g, \hat{\bar{2}}_g, k_{\bar{q}}) J_2^{(2)}(p_{\widetilde{(ij)}}, p_k)$$

$$+b_0\log\left(\frac{\mu^2}{|s_{2ji}|}\right) f_3^0(\hat{\bar{2}}_g, j_g, i_g)\delta(1-x_1)\delta(1-x_2) B_4^0(\hat{\bar{1}}_q, \widetilde{(ij)}_g, \hat{\bar{\bar{2}}}_g, k_{\bar{q}}) J_2^{(2)}(p_{\widetilde{(ij)}}, p_k)$$

$$+b_0\log\left(\frac{\mu^2}{|s_{12k}|}\right) A_3^0(\hat{\bar{1}}_q, \hat{\bar{2}}_g, k_{\bar{q}})\delta(1-x_1)\delta(1-x_2) B_4^0(\hat{\bar{\bar{1}}}_q, \widetilde{i}_g, \widetilde{j}_g, \hat{\bar{\bar{2}}}_{\bar{q}}) J_2^{(2)}(p_{\widetilde{i}}, p_{\widetilde{j}})$$

$$+b_0\log\left(\frac{\mu^2}{|s_{1ik}|}\right) G_3^0(i_g, \hat{\bar{1}}_q, k_{\bar{q}})\delta(1-x_1)\delta(1-x_2) A_4^0(\hat{\bar{\bar{1}}}_g, \widetilde{(ik)}_g, j_g, \hat{\bar{2}}_g) J_2^{(2)}(p_{\widetilde{(ik)}}, p_j)$$

$$+\frac{1}{2}\Bigg[\frac{1}{2}\mathcal{D}_{3,q}^0(s_{\bar{1}\widetilde{(ij)}}) - \frac{1}{2}\mathcal{D}_{3,q}^0(s_{\bar{1}j}) - \frac{1}{2}\mathcal{F}_{3,g}^0(s_{\widetilde{(ij)}\bar{2}}) + \frac{1}{2}\mathcal{F}_{3,g}^0(s_{\bar{2}j})$$

$$+\mathcal{A}_{3,q}^0(s_{\bar{1}k}) - \mathcal{A}_{3,q}^0(s_{\bar{1}k})\delta(1-x_1)\delta(1-x_2)\Big(\mathcal{S}(s_{\bar{1}j}, s_{jk}, x_{\bar{1}j,jk})$$

$$-\mathcal{S}(s_{\bar{1}\widetilde{(ij)}}, s_{jk}, x_{\bar{1}\widetilde{(ij)},jk}) - \mathcal{S}(s_{\bar{2}j}, s_{jk}, x_{\bar{2}j,jk}) + \mathcal{S}(s_{\bar{2}\widetilde{(ij)}}, s_{jk}, x_{\bar{2}\widetilde{(ij)},jk})\Big)\Bigg]$$

$$\times d_3^0(\hat{\bar{1}}_q, i_g, j_g) B_4^0(\hat{\bar{\bar{1}}}_q, \widetilde{(ij)}_g, \hat{\bar{2}}_g, k_{\bar{q}}) J_2^{(2)}(p_{\widetilde{(ij)}}, p_k)$$

$$+\frac{1}{2}\Bigg[\frac{1}{2}\mathcal{F}_{3,g}^0(s_{\bar{2}\widetilde{(ij)}}) - \frac{1}{2}\mathcal{F}_{3,g}^0(s_{\bar{2}i}) - \frac{1}{2}\mathcal{D}_{3,q}^0(s_{\bar{1}\widetilde{(ij)}}) + \frac{1}{2}\mathcal{D}_{3,q}^0(s_{\bar{1}i})$$

$$-\frac{1}{2}\mathcal{D}_{3,g;gq}^0(s_{\bar{2}k}) + \frac{1}{2}\mathcal{D}_{3,g;gq}^0(s_{\bar{2}k}) + \delta(1-x_1)\delta(1-x_2)\Big(\mathcal{S}(s_{\bar{2}i}, s_{ik}, x_{\bar{2}i,ik})$$

$$-\mathcal{S}(s_{\bar{2}\widetilde{(ij)}}, s_{ik}, x_{\bar{2}\widetilde{(ij)},ik}) + \mathcal{S}(s_{\bar{1}\widetilde{(ij)}}, s_{ik}, x_{\bar{1}\widetilde{(ij)},ik}) - \mathcal{S}(s_{\bar{1}i}, s_{ik}, x_{\bar{1}i,ik})\Big)\Bigg]$$

$$\times f_3^0(\hat{\bar{2}}_g, j_g, i_g) B_4^0(\hat{\bar{1}}_q, \widetilde{(ij)}_g, \hat{\bar{\bar{2}}}_g, k_{\bar{q}}) J_2^{(2)}(p_{\widetilde{(ij)}}, p_k)$$

$$+\Bigg[\mathcal{A}_{3,qq}^0(s_{\bar{1}\bar{2}}) - \mathcal{D}_{3,qg}^0(s_{\bar{1}\bar{2}}) - \frac{1}{2}\mathcal{D}_{3,q}^0(s_{\bar{1}i}) + \frac{1}{2}\mathcal{D}_{3,q}^0(s_{\bar{1}i}) - \frac{1}{2}\mathcal{D}_{3,q}^0(s_{\bar{2}j}) + \frac{1}{2}\mathcal{F}_{3,g}^0(s_{\bar{2}j})$$

$$+\delta(1-x_1)\delta(1-x_2)\Big(\mathcal{S}(s_{\bar{1}\bar{2}}, s_{ij}, x_{\bar{1}\bar{2},ij}) - \mathcal{S}(s_{\bar{1}\bar{2}}, s_{\widetilde{ij}}, x_{\bar{1}\bar{2},\widetilde{ij}}) - \mathcal{S}(s_{\bar{1}i}, s_{ij}, x_{\bar{1}i,ij})$$

$$+\mathcal{S}(s_{\bar{1}i}, s_{\widetilde{ij}}, x_{\bar{1}i,\widetilde{ij}}) - \mathcal{S}(s_{\bar{2}j}, s_{ij}, x_{\bar{2}j,ij}) + \mathcal{S}(s_{\bar{2}j}, s_{\widetilde{ij}}, x_{\bar{2}j,\widetilde{ij}})\Big)\Bigg]$$

$$\times A_3^0(\hat{\bar{1}}_q, \hat{\bar{2}}_g, k_{\bar{q}}) B_4^0(\hat{\bar{\bar{1}}}_q, \widetilde{i}_g, \widetilde{j}_g, \hat{\bar{\bar{2}}}_{\bar{q}}) J_2^{(2)}(p_{\widetilde{i}}, p_{\widetilde{j}})$$

$$-\frac{1}{2}\Bigg[\mathcal{A}^0_{3,q}(s_{\bar{1}k}) - \mathcal{A}^0_{3,q}(s_{\bar{\bar{1}}\widetilde{(ik)}}) - \mathcal{D}^0_{3,q}(s_{\bar{1}j}) + \mathcal{D}^0_{3,q}(s_{\bar{1}j}) - \mathcal{D}^0_{3,g;gq}(s_{\widetilde{(ik)}\bar{2}})$$

$$+\mathcal{D}^0_{3,g;gq}(s_{\bar{2}k}) + \delta(1-x_1)\delta(1-x_2)\Big(-\mathcal{S}(s_{\widetilde{(ik)}\widetilde{(ij)}}, s_{jk}, x_{\widetilde{(ik)}\widetilde{(ij)},jk}) + \mathcal{S}(s_{jk}, s_{jk}, 1)$$

$$+\mathcal{S}(s_{\bar{2}\widetilde{(ik)}}, s_{jk}, x_{\bar{2}\widetilde{(ik)},jk}) - \mathcal{S}(s_{\bar{2}k}, s_{jk}, x_{\bar{2}k,jk}) + \mathcal{S}(s_{\widetilde{(ij)}\bar{1}}, s_{jk}, x_{\widetilde{(ij)}\bar{1},jk})$$

$$-\mathcal{S}(s_{\bar{1}j}, s_{jk}, x_{\bar{1}j,jk})\Big)\Bigg] A^0_3(\hat{\bar{1}}_q, i_g, k_{\bar{q}}) B^0_4(\hat{\bar{\bar{1}}}_q, j_g, \hat{\bar{2}}_g, \widetilde{(ik)}_{\bar{q}}) J^{(2)}_2(p_{\widetilde{(ik)}}, p_j)\Bigg\}. \qquad (5.6.79)$$

In a similar scenario to the gluon-gluon initiated process, it is only in the summation of the topologies that we see a full cancellation of singularities. Whilst the antenna functions introduced to compensate for the unresolved limits are not shared amongst topologies, the finite contributions of integrated antennae from $\int \mathrm{d}\hat{\sigma}^{S,a}$ and the corrections to the one loop structures do not cancel until the sum is performed.

Once more, the subtraction term has been tested numerically. The procedure is then repeated for 1000 different phase space points in the unresolved configuration defined by the constraints. The constraints are then tightened to force the phase space points closer to the unresolved singular point and the ratio calculated for another 1000 points. The procedure is repeated once more for a set of points even closer to the singular point and the histogram of ratios for the three sets of constraints plotted.

A selection of plots from three different unresolved configurations is shown in Figure 5.9, for both pole and finite contributions. Again, we see that the distribution of R becomes more sharply peaked around one as the unresolved singular limit is approached, i.e., as the parameter x gets smaller. This provides statistical evidence for the convergence of the subtraction term to the physical cross section in the IR divergent limits.

An important feature of these subtraction terms is the highly predictive nature of the real-virtual subtraction term, which in the case of the quark-gluon and gluon-gluon initiated process, has been constructed without explicit knowledge of the terms dropping down from the double real subtraction term. Given the pole structure of $\mathrm{d}\hat{\sigma}^{RV}_{NNLO}$ which has universal structure via the Catani formalism, the integrated block $\int \mathrm{d}\hat{\sigma}^{s,a}$ can be constructed to cancel the explicit pole structure. The colour ordering of the reduced matrix elements and antennae illuminates the single unresolved limits, and thus indicates the new three parton antennae required. These in turn have their own
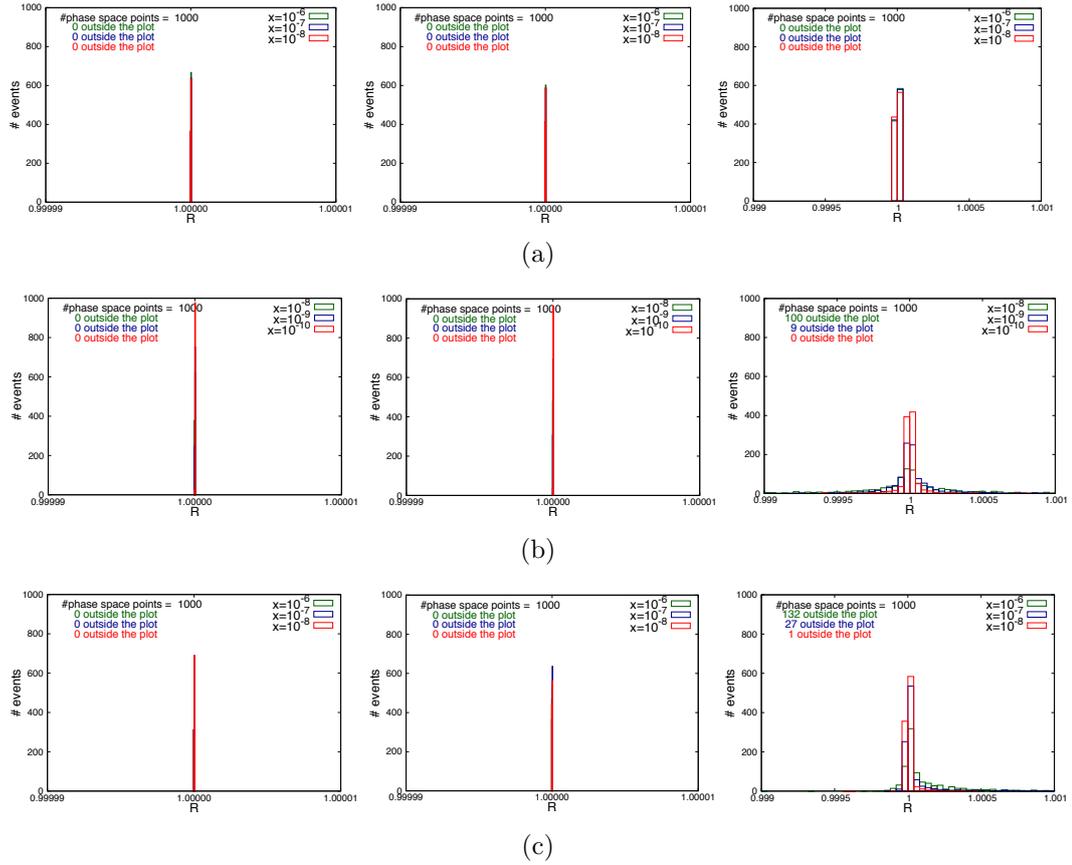
Figure 5.9: Plots displaying the convergence of the subtraction term to the real-virtual physical matrix element in various unresolved limits, for $qg \to qgg$. The green data is furthest from the singular configuration with the blue data closer to the singular region and the red data the closest. The left plot of each row is the $1/\epsilon^2$ contribution, the centre plot the $1/\epsilon$ contribution and the right hand plot the finite contribution. (a) Final-state single soft limit for parton i such that $x = (s_{12}-s_{jk})/s_{12}$. (b) Collinear limit between final-state gluons i and j, such that $x = s_{ij}/s_{12}$. (c) Collinear limit between final-state parton i and the initial quark 1 such that $x = s_{1i}/s_{12}$.

colour structure that is well understood, and the integrated antenna corrections are established. The infrared structure discussed in this thesis give a clear indication of which antenna are new at real-virtual, and which have dropped down from the double real subtraction term.

Crucially, analytic checks of the real-virtual subtraction term in the various limits can also predict the presence of the integrated terms $\int \mathrm{d}\hat{\sigma}^{b,c}$, again without prior knowledge of their existence at the double real level. A failure to cancel the finite contributions of the integrated antenna in the single unresolved limits put stringent requirements on the presence of additional integrated antennae to cancel those correc-

tions to the reduced matrix elements. The inclusion of these $\mathcal{X}_3^0$ antennae, appearing as blocks of the form given in (5.5.62), necessitates a block of integrated large angle soft terms in order to complete the $1/\epsilon$ pole cancellation. The presence of the large angle soft terms can be inferred heuristically by considering the $\widetilde{X}_4^0$ present at the double real level, appealing to Table 4.7. However, this algorithm not only requires no input knowledge from the double real and real-virtual contributions, but also gives a strong indication of what terms should be expected at these levels of the calculations.

5.6.2 Double virtual subtraction term, $d\hat{\sigma}_{NNLO}^U$

The double virtual subtraction term is constructed from the remaining terms dropping down from the double real and real virtual subtraction terms, as well as the double virtual mass factorisation contribution. Since the pole structure of the two loop amplitudes is predictable via the formalism described in Chapter 2, we write the subtraction term in terms of the single and double unresolved integrated antenna strings without the prerequisite of the double real and real-virtual subtraction terms.

Since there is a sum over the permuations of gluons, there are two distinct topologies, where the initial gluon is either adjacent ($\mathbb{X}$ topology) or non-adjacent ($\mathbb{Y}$ topology) to the initial state quark, in a similar vein to the RV terms. Unique integrated antennae string are present in each, so both topologies are presented. The VV pole structure for the $\mathbb{X}$ topology reads,

$$
\begin{aligned}
d\hat{\sigma}_{qg,NNLO}^{U,\mathbb{X}} \;=\; & -\mathcal{N}_{qg,4}^2 \, d\Phi_2(p_3,p_4;p_1,p_2) \int \frac{dz_1}{z_1}\frac{dz_2}{z_2} \times \Bigg\{ \\
& \boldsymbol{J}_4^{(1)}(\hat{\bar{1}}_q,\hat{\bar{2}}_g,i_g,j_{\bar{q}}) \left(B_4^1(\hat{\bar{1}}_q,\hat{\bar{2}}_g,i_g,j_{\bar{q}}) - \frac{b_0}{\epsilon} \, B_4^0(\hat{\bar{1}}_q,\hat{\bar{2}}_g,i_g,j_{\bar{q}}) \right) \\
& + \; \frac{1}{2} \, \boldsymbol{J}_4^{(1)}(\hat{\bar{1}}_q,\hat{\bar{2}}_g,i_g,j_{\bar{q}}) \otimes \boldsymbol{J}_4^{(1)}(\hat{\bar{1}}_q,\hat{\bar{2}}_g,i_g,j_{\bar{q}}) \, B_4^0(\hat{\bar{1}}_q,\hat{\bar{2}}_g,i_g,j_{\bar{q}}) \\
& + \; \boldsymbol{J}_4^{(2)}(\hat{\bar{1}}_q,\hat{\bar{2}}_g,i_g,j_{\bar{q}}) \, B_4^0(\hat{\bar{1}}_q,\hat{\bar{2}}_g,i_g,j_{\bar{q}}) \Bigg\} \, J_2^{(2)}(p_i,p_j).
\end{aligned}
\tag{5.6.80}
$$

The single unresolved integrated antenna string is defined in Eq. (5.2.14). In Eq. (5.2.14) the single unresolved integrated antenna string was written as a sum over integrated

dipoles. The analogous dipole-like formula for $\boldsymbol{J}_4^{(2)}$ is given by,

$$\boldsymbol{J}_4^{(2)}(\hat{\bar{1}}_q, \hat{\bar{2}}_g, i_g, j_{\bar{q}}) = \boldsymbol{J}_2^{(2)}(\hat{\bar{1}}_q, \hat{\bar{2}}_g) + \boldsymbol{J}_2^{(2)}(\hat{\bar{2}}_g, i_g) + \boldsymbol{J}_2^{(2)}(i_g, j_q) - \overline{\boldsymbol{J}}_2^{(2)}(\hat{\bar{1}}_q, j_{\bar{q}}), \quad (5.6.81)$$

where the two-parton double unresolved integrated antenna strings are given by:

$$\begin{aligned}
\boldsymbol{J}_2^{(2)}(\hat{\bar{1}}_q, \hat{\bar{2}}_g) &= 2\mathcal{D}_{4,qg}^{0,adj}(s_{\bar{1}\bar{2}}) + 2\mathcal{D}_{4,qg}^{0,n.adj}(s_{\bar{1}\bar{2}}) + \mathcal{D}_{3,qg}^1(s_{\bar{1}\bar{2}}) + \frac{b_0}{\epsilon}\left(\frac{|s_{\bar{1}\bar{2}}|}{\mu^2}\right)^{-\epsilon}\mathcal{D}_{3,qg}^0(s_{\bar{1}\bar{2}}) \\
&\quad - \Gamma_{qq}^{(2)}(z_1)\delta(1-z_2) - \Gamma_{gg}^{(2)}(z_2)\delta(1-z_1) - \left[\mathcal{D}_{3,qg}^0(s_{\bar{1}\bar{2}}) \otimes \mathcal{D}_{3,qg}^0(s_{\bar{1}\bar{2}})\right] \\
&\quad + \left[\Gamma_{qq}^1 \otimes \Gamma_{qq}^1\right](z_1)\delta(1-z_2) + \left[\Gamma_{gg}^1 \otimes \Gamma_{gg}^1\right](z_2)\delta(1-z_1), \quad (5.6.82) \\
\boldsymbol{J}_2^{(2)}(\hat{\bar{2}}_g, i_g) &= \mathcal{F}_{4,g}^{0,adj}(s_{\bar{2}i}) + \mathcal{F}_{4,g}^{0,n.adj}(s_{\bar{2}i}) + \frac{1}{2}\mathcal{F}_{3,g}^{1,n.adj}(s_{\bar{2}i}) + \frac{b_0}{2\epsilon}\mathcal{F}_3^0(s_{\bar{2}i})\left(\frac{|s_{\bar{2}i}|}{\mu^2}\right)^{-\epsilon} \\
&\quad - \frac{1}{4}\left[\mathcal{F}_{3,g}^0(s_{\bar{2}i}) \otimes \mathcal{F}_{3,g}^0(s_{\bar{2}i})\right](z_2) - \overline{\Gamma}_{gg}^{(2)}(z_2)\delta(1-z_1), \quad (5.6.83) \\
\boldsymbol{J}_2^{(2)}(i_g, j_{\bar{q}}) &= \mathcal{D}_{4,a}^0(s_{ij}) + \mathcal{D}_{4,c}^0(s_{ij}) + \frac{1}{2}\mathcal{D}_3^1(s_{ij}) + \frac{b_0}{2\epsilon}\mathcal{D}_3^0(s_{ij})\left(\frac{|s_{ij}|}{\mu^2}\right)^{-\epsilon} \\
&\quad - \frac{1}{4}\left[\mathcal{D}_3^0(s_{ij}) \otimes \mathcal{D}_3^0(s_{ij})\right] \quad (5.6.84)
\end{aligned}$$

The double virtual contribution for the $\mathbb{Y}$ topology can be written in the form of Eq. (4.5.131),

$$\begin{aligned}
\mathrm{d}\hat{\sigma}_{qg,NNLO}^{U,\mathbb{Y}} &= -\mathcal{N}_{qg,4}^2\,\mathrm{d}\Phi_2(p_3, p_4; p_1, p_2)\int\frac{\mathrm{d}z_1}{z_1}\frac{\mathrm{d}z_2}{z_2} \times \left\{ \vphantom{\frac{1}{2}} \right. \\
&\quad \boldsymbol{J}_4^{(1)}(\hat{\bar{1}}_q, i_g, \hat{\bar{2}}_g, j_{\bar{q}})\left(B_4^1(\hat{\bar{1}}_q, i_g, \hat{\bar{2}}_g, j_{\bar{q}}) - \frac{b_0}{\epsilon}B_4^0(\hat{\bar{1}}_q, i_g, \hat{\bar{2}}_g, j_{\bar{q}})\right) \\
&\quad + \frac{1}{2}\,\boldsymbol{J}_4^{(1)}(\hat{\bar{1}}_q, i_g, \hat{\bar{2}}_g, j_{\bar{q}}) \otimes \boldsymbol{J}_4^{(1)}(\hat{\bar{1}}_q, i_g, \hat{\bar{2}}_g, j_{\bar{q}})\,B_4^0(\hat{\bar{1}}_q, i_g, \hat{\bar{2}}_g, j_{\bar{q}}) \\
&\quad \left. + \boldsymbol{J}_4^{(2)}(\hat{\bar{1}}_q, i_g, \hat{\bar{2}}_g, j_{\bar{q}})\,B_4^0(\hat{\bar{1}}_q, i_g, \hat{\bar{2}}_g, j_{\bar{q}})\right\}\,J_2^{(2)}(p_i, p_j), \quad (5.6.85)
\end{aligned}$$

which reproduces the form of the Catani pole structure in Eq. (4.5.115). The single unresolved integrated antenna string is defined in Eq. (5.2.14). In Eq. (5.2.14) the single unresolved integrated antenna string was written as a sum over integrated dipoles. The analogous dipole-like formula for $\boldsymbol{J}_4^{(2)}$ is given by,

$$\boldsymbol{J}_4^{(2)}(\hat{\bar{1}}_q, i_g, \hat{\bar{2}}_g, j_{\bar{q}}) = \boldsymbol{J}_2^{(2)}(\hat{\bar{1}}_q, i_g) + \boldsymbol{J}_2^{(2)}(i_g, \hat{\bar{2}}_g) + \boldsymbol{J}_2^{(2)}(\hat{\bar{2}}_g, j_q) - \overline{\boldsymbol{J}}_2^{(2)}(\hat{\bar{1}}_q, j_{\bar{q}}).$$

$$(5.6.86)$$

The expressions for $\boldsymbol{J}_2^{(2)}(\hat{\bar{1}}_q, i_g), \boldsymbol{J}_2^{(2)}(i_g, \hat{\bar{2}}_g)$ and $\boldsymbol{J}_2^{(2)}(\hat{\bar{2}}_g, j_q)$ can be obtained from (5.4.44), (5.6.83) and (5.5.67) respectively.

$$*$$

In this chapter we have constructed the full subtraction term for quark-initiated contribution to dijet production, and shown that they correctly mimic the physical matrix elements in all divergent limits.

The real-virtual and double virtual subtraction terms have also been completed, the former again successfully tested in all single unresolved limits. Chapter 6 will illustrate the application of the antenna subtraction formalism to the real-vitual contributions involving two pairs of non-identical quarks.

Chapter 6

Dijet Production from Four-Quark Processes

The previous chapter saw the real-virtual subtraction terms constructed for all required crossings for quark-gluon scattering contributing to dijet production at the LHC. We now extend the analysis to the processes involving two quark pairs. This can include scenarios in which the quark pairs are identical, although here we only consider the non-identical quark case. These are the leading colour contributions since the identical quark terms are suppressed by a factor of $1/N$ relative to the non-identical quark pairs.

In this chapter we again focus on the real-virtual subtraction term, which involves two quark pairs and a single gluon. Importantly, we see that the real-virtual subtraction terms are constructed without prior knowledge of the double real subtraction terms. Due to the higher complexity of the latter, having the real-virtual term in place, and of course with the pole structure at double virtual known for some time [110], we have a powerful tool for asserting the terms expected for the double real subtraction term. The purpose of this chapter is to not only establish the matrix elements and antennae that will be required for the subtraction terms dealing with processes with multiple quark pairs, but show that the antenna formalism is successful in dealing with all the associated limits.

In order to construct a subtraction term for hadronic interactions, we must send two partons into the initial state. For four-quark, single gluon scattering, we must

consider all available processes, given that each interacting hadron can contain any one of the five partons. For non-identical quark pairs we find that there are twenty processes possible, remembering that the initial state labels are important: $q(x_1)Q(x_2)$ $\neq q(x_2)Q(x_1)$. However, we can use charge conjugation operations and the exchanging of initial state labels to reduce this number down to six independent processes. We have

$$\bar{q}(p_1)Q(p_2) \quad \rightarrow \quad \bar{q}(p_3)Q(p_4)g(p_5), \tag{6.0.1}$$

$$q(p_1)\bar{q}(p_2) \quad \rightarrow \quad Q(p_3)\bar{Q}(p_4)g(p_5), \tag{6.0.2}$$

$$q(p_1)g(p_2) \quad \rightarrow \quad Q(p_3)\bar{Q}(p_4)g(p_5), \tag{6.0.3}$$

$$q(p_1)Q(p_2) \quad \rightarrow \quad q(p_3)Q(p_4)g(p_5), \tag{6.0.4}$$

$$Q(p_1)g(p_2) \quad \rightarrow \quad Q(p_3)q(p_4)\bar{q}(p_5), \tag{6.0.5}$$

$$Q(p_1)\bar{Q}(p_2) \quad \rightarrow \quad q(p_3)\bar{q}(p_4)g(p_5). \tag{6.0.6}$$

For this thesis we shall construct the subtraction term for the case where a quark and antiquark are in the initial state as in (6.0.1).

6.1 Notation and amplitudes

The four parton amplitude with two non-identical quark pairs at tree level reads

$$\mathcal{C}_4^0 = 2g^2 \left(\delta_{q\bar{Q}}\delta_{Q\bar{q}} - \frac{1}{N}\delta_{q\bar{q}}\delta_{Q\bar{Q}} \right) \mathcal{C}_4^0(q, Q, \bar{q}, \bar{Q}), \tag{6.1.7}$$

where the only colour structures are naturally the quark colour lines. The one loop amplitude has a similar colour structure, however the introduction of loop diagrams result in richer colour connectivity; the subamplitudes with colour connectivity between like and different quark-antiquark pairs are no longer identical and thus the amplitude cannot be factorised as at tree level. We have

$$\mathcal{C}_4^0 = 2g^2 \left(\frac{g^2 N C(\epsilon)}{2} \right) \times \left\{ \delta_{q\bar{Q}}\delta_{Q\bar{q}} \mathcal{C}_4^{1,l}(q, Q, \bar{q}, \bar{Q}) - \frac{1}{N}\delta_{q\bar{q}}\delta_{Q\bar{Q}} \mathcal{C}_4^{1,s}(q, Q, \bar{q}, \bar{Q}) \right\} \tag{6.1.8}$$

In increasing the multiplicity for the real-virtual contribution to dijet production at NNLO we allow for an additional external gluon. The tree level and one loop amplitude with two quark-antiquark pairs of different flavour and one gluon has the form

$$
\begin{aligned}
\mathcal{C}_5^\ell(\{p_i, \lambda_i, a_i\}) \;=\; & 2^{3/2} g^3 \left(\frac{g^2 N C(\epsilon)}{2} \right)^\ell \times \Bigg\{ \\
& \sum_{(q_1 \neq q_2) \in \{q, Q\}} (T^g)_{q_1 \bar{q}_2} \delta_{q_2 \bar{q}_1} \mathcal{C}_5^\ell(q_1, g, \bar{q}_2; q_2, \bar{q}_1) \\
& - \sum_{(q_1 \neq q_2) \in \{q, Q\}} \frac{1}{N} (T^g)_{q_1 \bar{q}_1} \delta_{q_2 \bar{q}_2} \mathcal{C}_5^\ell(q_1, g, \bar{q}_1, q_2, \bar{q}_2) \Bigg\}
\end{aligned}
\tag{6.1.9}
$$

for $\ell = 0, 1$. The one loop amplitude must be treated with care before it is squared. The functions $\mathcal{C}_5^1$ present in the one-loop decomposition are not independent of the number of colours or flavours. Whilst the structure in (6.1.9) elucidates the explicit pole structure, for a full expansion in N we must further decompose these partial amplitudes into more primitive ones. We thus redefine the partial amplitudes as linear combinations of structures proportional to N and N_F:

$$
\mathcal{C}_5^1(\{q_i\}) = N \mathcal{C}_5^{1,l}(\{q_i\}) + \frac{1}{N} \mathcal{C}_5^{1,s}(\{q_i\}) + N_F \mathcal{C}_5^{1,F}(\{q_i\}).
\tag{6.1.10}
$$

It is then possible to write the amplitude in terms of these primitive amplitudes which are completely independent of colour or flavour factors. The amplitude, excluding N_F terms, thus becomes

$$
\begin{aligned}
\mathcal{C}_5^1(\bar{q}, \bar{Q}, Q, q, g) \;=\; & 2^{3/2} g^3 \left(\frac{g^2 N C(\epsilon)}{2} \right)^\ell \times \Bigg\{ \\
& N \Big((T^g)_{q\bar{Q}} \delta_{Q\bar{q}} \mathcal{C}_5^l(q, g, \bar{Q}; Q, \bar{q}) + (T^g)_{Q\bar{q}} \delta_{q\bar{Q}} \mathcal{C}_5^l(Q, g, \bar{q}; q, \bar{Q}) \Big) \\
& + \frac{1}{N} \Big((T^g)_{q\bar{Q}} \delta_{Q\bar{q}} \mathcal{C}_5^s(q, g, \bar{Q}; Q, \bar{q}) + (T^g)_{Q\bar{q}} \delta_{q\bar{Q}} \mathcal{C}_5^s(Q, g, \bar{q}; q, \bar{Q}) \Big) \\
& - \Big((T^g)_{q\bar{q}} \delta_{Q\bar{Q}} \mathcal{C}_5^l(q, g, \bar{q}; Q, \bar{Q}) + (T^g)_{Q\bar{Q}} \delta_{q\bar{q}} \mathcal{C}_5^l(Q, g, \bar{Q}; q, \bar{q}) \Big) \\
& - \frac{1}{N^2} \Big((T^g)_{q\bar{q}} \delta_{Q\bar{Q}} \mathcal{C}_5^s(q, g, \bar{q}; Q, \bar{Q}) + (T^g)_{Q\bar{Q}} \delta_{q\bar{q}} \mathcal{C}_5^s(Q, g, \bar{Q}; q, \bar{q}) \Big) \Bigg\}
\end{aligned}
\tag{6.1.11}
$$

The full amplitude can be found in [111], from which we construct the colour decomposition numerically to be incorporated in the NNLOJET program.

6.2 Matrix elements for four and five partons

6.2.1 Four-parton matrix elements

The tree level, Born cross section can be colour-decomposed as follows:

$$\mathrm{d}\hat{\sigma}_{LO} = \mathcal{N}_{qQ,LO} \int \mathrm{d}\Phi_2(p_3, p_4; p_1, p_2)\, C_4^0(q, \bar{Q}; Q, \bar{q})\, J_2^{(2)}(\{p\}_2) \tag{6.2.12}$$

where for four quark scattering,

$$\mathcal{N}_{qQ,LO} = \frac{1}{2s}\frac{1}{4N^2}(g^2)^2(N^2 - 1). \tag{6.2.13}$$

We note that the squared tree level matrix element is the only structure present due to the symmetry of the quarks in the colour structure.

The full colour decomposition of the one loop squared matrix element can also be constructed. Omitting flavour contributions, it takes the form

$$\begin{aligned}
\mathrm{d}\hat{\sigma}_{NLO}^V &= \mathcal{N}_4^1 \int \mathrm{d}\Phi_3(p_3, p_4, p_5; p_1, p_2)\frac{\mathrm{d}x_1}{x_1}\frac{\mathrm{d}x_2}{x_2}\delta(1 - x_1)\delta(1 - x_2) \\
&\times \left\{ C_4^{1,l}(q, \bar{Q}; Q, \bar{q}) - \frac{1}{N^2}C_4^{1,s}(q, \bar{q}; Q, \bar{Q}) \right\} J_2^{(2)}(\{p\}_2),
\end{aligned} \tag{6.2.14}$$

where

$$\mathcal{N}_4^1 = \mathcal{N}_{qQ,LO}\left(\frac{\alpha_s N}{2\pi}\right)\bar{C}(\epsilon). \tag{6.2.15}$$

The pole structure is derived in Appendix B; expressed in terms of singularity operators,

$$\mathcal{P}oles\left[C_4^{1,l}(q, \bar{Q}; Q, \bar{q})\right] = -2(\mathbf{I}_{q\bar{q}}^{(1)}(\epsilon, s_{q\bar{Q}}) + \mathbf{I}_{q\bar{q}}^{(1)}(\epsilon, s_{Q\bar{q}}))C_4^0(q, \bar{Q}; Q, \bar{q}), \tag{6.2.16}$$

$$\mathcal{P}oles\left[C_4^{1,s}(q, \bar{q}; Q, \bar{Q})\right] = -2(\mathbf{I}_{q\bar{q}}^{(1)}(\epsilon, s_{q\bar{q}}) + \mathbf{I}_{q\bar{q}}^{(1)}(\epsilon, s_{Q\bar{Q}}))C_4^0(q, \bar{q}; Q, \bar{Q}). \tag{6.2.17}$$

6.2.2   Five-parton matrix elements

The five-parton one-loop cross section contains the colour-ordered matrix elements that we must construct the real-virtual subtraction term for at NNLO in our dijet calculations. At tree level, the real emission to the N_F independent NLO cross section is

$$
\begin{aligned}
\mathrm{d}\hat{\sigma}_{NLO}^{R} \;=\; & \mathcal{N}_{qQ,5}^{0} \int \mathrm{d}\Phi_3(p_3, p_4, p_5; p_1, p_2) \times \Big\{ C_5^0(Q, g, \bar{q}; q, \bar{Q}) + C_5^0(q, g, \bar{Q}; Q, \bar{q}) \\
& + \frac{1}{N^2}(C_5^0(Q, g, \bar{Q}; q, \bar{q}) + C_5^0(q, g, \bar{q}; Q, \bar{Q})) - 2\,\tilde{C}_5^0(Q, \bar{Q}, q, \bar{q}, g)) \Big\} J_2^{(3)}(\{p\}_2),
\end{aligned}
$$

(6.2.18)

where

$$
\begin{aligned}
\tilde{C}_5^0(Q, \bar{Q}, q, \bar{q}, g) \;=\; & (C_5^0(Q, g, \bar{q}; q, \bar{Q}) + C_5^0(q, g, \bar{Q}; Q, \bar{q}))^\dagger \\
& \times \; (C_5^0(Q, g, \bar{q}; q, \bar{Q}) + C_5^0(q, g, \bar{Q}; Q, \bar{q})) \\
\;=\; & (C^0(Q, g, \bar{Q}; q, \bar{q}) + C^0(q, g, \bar{q}; Q, \bar{Q}))^\dagger \\
& \times \; (C^0(Q, g, \bar{Q}; q, \bar{q}) + C^0(q, g, \bar{q}; Q, \bar{Q})).
\end{aligned}
$$

(6.2.19)

Here we have used the fact that

$$
C_5^0(Q, g, \bar{q}; q, \bar{Q}) + C_5^0(q, g, \bar{Q}; Q, \bar{q}) = C_5^0(Q, g, \bar{Q}; q, \bar{q}) + C_5^0(q, g, \bar{q}; Q, \bar{Q})
$$

(6.2.20)

to write the squared matrix element as a sum of complete squares. The ordering of the quarks is important. At leading colour, the colour flow has the gluon sandwiched between quarks of differing flavour, whereas the first two terms in (6.2.18) proportional to $1/N^2$ have the gluon between the same flavour quark and antiquark.

The real-virtual contribution is given by

$$
\begin{aligned}
\mathrm{d}\hat{\sigma}_{NNLO}^{RV} \;=\; & \mathcal{N}_{qQ,5}^{1} \int \mathrm{d}\Phi_3(p_3, p_4, p_5; p_1, p_2) \frac{\mathrm{d}x_1}{x_1} \frac{\mathrm{d}x_2}{x_2} \delta(1 - x_1)\delta(1 - x_2) \times \Bigg\{ \\
& \Big(C_5^{1,l}(Q, g, \bar{q}; q, \bar{Q}) + C_5^{1,l}(q, g, \bar{Q}; Q, \bar{q}) \Big)
\end{aligned}
$$

$$
\begin{aligned}
+ \quad & \frac{1}{N^2}\left(C_5^{1,s}(Q,g,\bar{q};q,\bar{Q}) + C_5^{1,s}(q,g,\bar{Q};Q,\bar{q}) + C_5^{1,l}(q,g,\bar{q};Q,\bar{Q})\right. \\
+ \quad & \left. C_5^{1,l}(Q,g,\bar{Q};q,\bar{q}) - \frac{1}{2}\tilde{C}_5^{1,l}(Q,\bar{Q},q,\bar{q},g)\right) \\
+ \quad & \frac{1}{N^4}\left.\left(C_5^{1,s}(q,g,\bar{q};Q,\bar{Q}) + C_5^{1,s}(Q,g,\bar{Q};q,\bar{q}) - \frac{1}{2}\tilde{C}_5^{1,s}(Q,\bar{Q},q,\bar{q},g)\right)\right\},
\end{aligned}
$$

$$(6.2.21)$$

where

$$
\begin{aligned}
\tilde{\mathcal{C}}^{1,x}(Q,\bar{Q},q,\bar{q},g) \;=\; & \mathcal{C}^{1,x}(Q,g,\bar{q};Q,\bar{q}) + \mathcal{C}^{1,x}(q,g,\bar{Q};q,\bar{Q}) \\
& + \; \mathcal{C}^{1,x}(Q,g,\bar{Q};q,\bar{q}) + \mathcal{C}^{1,x}(q,g,\bar{q};Q,\bar{Q}).
\end{aligned}
$$

$$(6.2.22)$$

and

$$
\mathcal{N}^1_{qQ,5} = \mathcal{N}_{qQ,LO}\left(\frac{\alpha_s N}{2\pi}\right)^2 \frac{\bar{C}(\epsilon)}{C(\epsilon)}.
$$

$$(6.2.23)$$

The pole structure of the squared matrix element is derived in Appendix B. For the purposes of this thesis we are considering the leading colour squared matrix element: the pole structure reads

$$
\begin{aligned}
\mathcal{P}oles\left[C_5^{1,l}(q,g,\bar{Q};Q,\bar{q})\right] \;=\; & -2(\mathbf{I}^{(1)}_{qg}(\epsilon,s_{qg}) + \mathbf{I}^{(1)}_{qg}(\epsilon,s_{\bar{Q}g}) + \mathbf{I}^{(1)}_{q\bar{q}}(\epsilon,s_{Q\bar{q}})) \\
& \times \; C_5^0(q,g,\bar{Q};Q,\bar{q}),
\end{aligned}
$$

$$(6.2.24)$$

with a similar expression for the pole structure of $C_5^{1,l}(q,g,\bar{Q};Q,\bar{q})$ obtained by $q \leftrightarrow Q, \bar{q} \leftrightarrow \bar{Q}$. As with the quark-gluon scattering, we test the colour decomposition of the matrix elements against Njet [105]. The calculations are carried out in CDR, $\mu = \sqrt{s} = 1000$ GeV, and we compute the ratio given in (5.2.27). The results for four and five parton matrix elements are given in Tables 6.1 and 6.2 respectively.

Note that we naturally expect a small numerical discrepancy in the leading colour cases. The leading colour matrix elements that we have constructed are colour-decomposed explicitly, whereas the leading colour values for Njet are obtained by sending N large. The subleading contributions are small but nevertheless still contributing.

		$\bar{q}Q \to \bar{q}Q$		
		$1/\epsilon^2$	$1/\epsilon$	$1/\epsilon^0$
PS #1	NNLOJET	-12.0000000000	28357.1792325814	-102347.563633429
	Njet	-11.99999866666	28357.1759731143	-102347.563345437
PS #2	NNLOJET	-12.0000000000	31247.6971786493	-112788.616101719
	Njet	-11.99999866666	31247.6927521201	-112788.611484261

Table 6.1: Comparison of NNLOJET and Njet [105] matrix element values for $\bar{q}Q \to \bar{q}Q$ at leading colour.

		$\bar{q}Q \to \bar{q}Qg$		
		$1/\epsilon^2$	$1/\epsilon$	$1/\epsilon^0$
PS #1	NNLOJET	-16.66666666666	8.49560865414164	-82.1207823942190
	Njet	-16.66666666666	8.49560856413850	-82.1207815386345
PS #2	NNLOJET	-16.66666666666	-1.30752347948607	-16.2855124538146
	Njet	-16.66666666666	-1.30752399291760	-16.2855128287786

Table 6.2: Comparison of NNLOJET and Njet [105] matrix element values for $\bar{q}Q \to \bar{q}Qg$ to all orders in colour.

6.3 $\bar{q}Q$ initiated dijet production at NNLO

6.3.1 Real-virtual subtraction term, $d\hat{\sigma}_{NNLO}^T$

This section will focus on the leading colour NNLO subtraction term for the process in which a quark and antiquark of different flavour are in the initial state. There are two colour orderings at leading colour, corresponding to the quark-antiquark pair that is colour connected to the gluon.

We consider the case of non-identical quarks where $\bar{q}$ and Q are in the initial state, that is

$$
\begin{aligned}
d\hat{\sigma}_{NNLO}^{RV} &= \mathcal{N}_{qQ,5}^1 \int d\Phi_3(p_3, p_4, p_5; x_1 p_1, x_2 p_2) \frac{1}{S_3} \frac{dx_1}{x_1} \frac{dx_2}{x_2} \times \Big\{ \\
&\quad C_5^1(3_Q, 5_g, 4_{\bar{q}}; \hat{1}_q, \hat{2}_{\bar{Q}}) + C_5^1(\hat{1}_q, 5_g, \hat{2}_{\bar{Q}}; 3_{\bar{q}}, 4_Q) \Big\} J_2^{(3)}(p_3, p_4, p_5),
\end{aligned}
$$

$$(6.3.25)$$

where the initial states partons are labelled $\hat{1}$ and $\hat{2}$. A subtraction term is required for each of the two squared matrix elements, and will be written out separately for transparency.

The first term in (6.3.25) requires the subtraction term $\mathrm{d}\hat{\sigma}_{NNLO}^{T_1}$,

$$
\mathrm{d}\hat{\sigma}_{NNLO}^{T_1} = \mathcal{N}_{qQ,5}^1 \int d\Phi_3(p_3,p_4,p_5;x_1p_1,x_2p_2)\frac{1}{S_3}\frac{\mathrm{d}x_1}{x_1}\frac{\mathrm{d}x_2}{x_2} \times \Bigg\{
$$

$$
-\Big(\frac{1}{2}\mathcal{D}_3^0(s_{35}) + \frac{1}{2}\mathcal{D}_3^0(s_{45}) + \mathcal{A}_{3,qq}^0(s_{\bar{1}\bar{2}})
$$

$$
-\Gamma_{qq}^1(x_1)\delta(1-x_2) - \Gamma_{qq}^1(x_2)\delta(1-x_1)\Big)C_5^0(3_Q,5_g,4_{\bar{q}};\hat{1}_q,\hat{2}_{\bar{Q}})J_2^{(3)}(p_3,p_4,p_5)
$$

$$
+A_3^0(3_Q,5_g,4_{\bar{q}})\Bigg[\delta(1-x_1)\delta(1-x_2)C_4^1(\widetilde{(35)}_Q,\widetilde{(45)}_{\bar{q}};\hat{\tilde{1}}_q,\hat{\tilde{2}}_{\bar{Q}}) + \Bigg(\mathcal{A}_3^0(s_{\widetilde{(35)}\widetilde{(45)}})
$$

$$
+\mathcal{A}_{3,qq}^0(s_{\bar{1}\bar{2}}) - \Gamma_{qq}^1(x_1)\delta(1-x_2) - \Gamma_{qq}^1(x_2)\delta(1-x_1)\Bigg)
$$

$$
\times C_4^0(\widetilde{(35)}_Q,\widetilde{(45)}_{\bar{q}};\hat{\tilde{1}}_q,\hat{\tilde{2}}_{\bar{Q}})\Bigg]J_2^{(2)}(p_{\widetilde{(45)}},p_{\widetilde{(35)}})
$$

$$
+E_3^0(\hat{1}_q,\hat{2}_{\bar{Q}},3_Q)\Bigg[\delta(1-x_1)\delta(1-x_2)B_4^1(\hat{\bar{\tilde{1}}}_q,\hat{\bar{\tilde{2}}}_g,\widetilde{5}_g,\widetilde{4}_{\bar{q}}) + \Bigg(\mathcal{D}_{3,qg}^0(s_{\bar{\bar{1}}\bar{\bar{2}}}) + \frac{1}{2}\mathcal{F}_{3,g}^0(s_{\bar{\bar{2}}\widetilde{5}})
$$

$$
+\frac{1}{2}\mathcal{D}_3^0(s_{\widetilde{4}\widetilde{5}}) - \Gamma_{qq}^1(x_1)\delta(1-x_2) - \Gamma_{qq}^1(x_2)\delta(1-x_1)\Bigg)B_4^0(\hat{\bar{\tilde{1}}}_q,\hat{\bar{\tilde{2}}}_g,\widetilde{5}_g,\widetilde{4}_{\bar{q}})\Bigg]J_2^{(2)}(p_{\widetilde{4}},p_{\widetilde{5}})
$$

$$
+E_3^0(\hat{2}_{\bar{Q}},\hat{1}_q,4_{\bar{q}})\Bigg[\delta(1-x_1)\delta(1-x_2)B_4^1(\widetilde{3}_Q,\widetilde{5}_g,\hat{\bar{\tilde{1}}}_g,\hat{\bar{\tilde{2}}}_{\bar{Q}}) + \Bigg(\frac{1}{2}\mathcal{D}_3^0(s_{\widetilde{3}\widetilde{5}}) + \frac{1}{2}\mathcal{F}_{3,g}^0(s_{\widetilde{5}\bar{\bar{1}}})
$$

$$
+\mathcal{D}_{3,qg}^0(s_{\bar{\bar{2}}\bar{\bar{1}}}) - \Gamma_{qq}^1(x_1)\delta(1-x_2) - \Gamma_{qq}^1(x_2)\delta(1-x_1)\Bigg)B_4^0(\widetilde{3}_Q,\widetilde{5}_g,\hat{\bar{\tilde{1}}}_g,\hat{\bar{\tilde{2}}}_{\bar{Q}})\Bigg]J_2^{(2)}(p_{\widetilde{3}},p_{\widetilde{5}})
$$

$$
+\Bigg[A_3^1(3_Q,5_g,4_{\bar{q}})\delta(1-x_1)\delta(1-x_2) + \Bigg(\frac{1}{2}\mathcal{D}_3^0(s_{35}) + \frac{1}{2}\mathcal{D}_3^0(s_{45}) - \mathcal{A}_3^0(s_{\widetilde{(35)}\widetilde{(45)}})\Bigg)
$$

$$
\times A_3^0(3_Q,5_g,4_{\bar{q}})\Bigg]C_4^0(\widetilde{(35)}_Q,\widetilde{(45)}_{\bar{q}};\hat{1}_q,\hat{2}_{\bar{Q}})J_2^{(2)}(p_{\widetilde{(45)}},p_{\widetilde{(35)}})
$$

$$
+\Bigg[E_3^1(\hat{1}_q,\hat{2}_{\bar{Q}},3_Q)\delta(1-x_1)\delta(1-x_2) + \Bigg(\mathcal{A}_{3,qq}^0(s_{\bar{1}\bar{2}}) + \mathcal{A}_{3,q}^0(s_{\bar{1}3}) - 2\mathcal{D}_{3,q}^0(s_{\bar{1}\bar{2}})\Bigg)
$$

$$
\times E_3^0(\hat{1}_q,\hat{2}_{\bar{Q}},3_Q)\Bigg]B_4^0(\hat{\bar{\tilde{1}}}_q,\hat{\bar{\tilde{2}}}_g,\widetilde{5}_g,\widetilde{4}_{\bar{q}})J_2^{(2)}(p_{\widetilde{4}},p_{\widetilde{5}})
$$

$$
+\Bigg[E_3^1(\hat{2}_{\bar{Q}},\hat{1}_q,4_{\bar{q}})\delta(1-x_1)\delta(1-x_2) + \Bigg(\mathcal{A}_{3,qq}^0(s_{\bar{2}\bar{1}}) + \mathcal{A}_{3,q}^0(s_{\bar{2}4}) - 2\mathcal{D}_{3,gq}^0(s_{\bar{1}\bar{2}})\Bigg)
$$

$$\times E_3^0(\hat{2}_{\bar{Q}}, \hat{1}_q, 4_{\bar{q}})\Bigg] B_4^0(\widetilde{3}_Q, \widetilde{5}_g, \tilde{\hat{\bar{1}}}_g, \tilde{\hat{\bar{2}}}_{\bar{Q}}) J_2^{(2)}(p_{\widetilde{3}}, p_{\widetilde{5}})$$

$$+b_0 \log\left(\frac{\mu^2}{|s_{354}|}\right) A_3^0(3_Q, 5_g, 4_{\bar{q}})\delta(1-x_1)\delta(1-x_2) C_4^0(\widetilde{(35)}_Q, \widetilde{(45)}_{\bar{q}}; \hat{\bar{1}}_q, \hat{\bar{2}}_{\bar{Q}}) J_2^{(2)}(p_{\widetilde{(45)}}, p_{\widetilde{(35)}})$$

$$+b_0 \log\left(\frac{\mu^2}{|s_{123}|}\right) E_3^0(\hat{1}_q, \hat{2}_{\bar{Q}}, 3_Q)\delta(1-x_1)\delta(1-x_2) B_4^0(\tilde{\hat{\bar{1}}}_q, \tilde{\hat{\bar{2}}}_g, \widetilde{5}_g, \widetilde{4}_{\bar{q}}) J_2^{(2)}(p_{\widetilde{4}}, p_{\widetilde{5}})$$

$$+b_0 \log\left(\frac{\mu^2}{|s_{543}|}\right) E_3^0(\hat{2}_{\bar{Q}}, \hat{1}_q, 4_{\bar{q}})\delta(1-x_1)\delta(1-x_2) B_4^0(\widetilde{3}_Q, \widetilde{5}_g, \tilde{\hat{\bar{1}}}_g, \tilde{\hat{\bar{2}}}_{\bar{Q}})\Bigg] J_2^{(2)}(p_{\widetilde{3}}, p_{\widetilde{5}})$$

$$+\frac{1}{2}\Bigg[\mathcal{D}_{3,qg}^0(s_{\bar{1}\bar{2}}) - \mathcal{A}_{3,q}^0(s_{3\bar{1}}) + \frac{1}{2}\mathcal{D}_3^0(s_{53}) - \frac{1}{2}\mathcal{F}_{3,g}^0(s_{\widetilde{5}\widetilde{2}}) + \mathcal{A}_{3,q}^0(s_{\bar{1}4}) - \mathcal{A}_{3,q}^0(s_{\widetilde{4}\bar{1}})$$

$$+\delta(1-x_1)\delta(1-x_2)\Big(\mathcal{S}(s_{3\bar{1}}, s_{45}, x_{3\bar{1},45}) - \mathcal{S}(s_{\bar{1}\bar{2}}, s_{\widetilde{4}\widetilde{5}}, x_{\bar{1}\bar{2},\widetilde{4}\widetilde{5}}) + \mathcal{S}(s_{\widetilde{5}\widetilde{2}}, s_{\widetilde{4}\widetilde{5}}, x_{\widetilde{5}\widetilde{2},\widetilde{4}\widetilde{5}})$$

$$-\mathcal{S}(s_{53}, s_{45}, x_{53,45}) + \mathcal{S}(s_{\widetilde{4}\bar{1}}, s_{\widetilde{4}\widetilde{5}}, x_{\widetilde{4}\bar{1},\widetilde{4}\widetilde{5}}) - \mathcal{S}(s_{4\bar{1}}, s_{45}, x_{4\bar{1},45})\Big)\Bigg]$$

$$\times E_3^0(\hat{1}_q, \hat{2}_{\bar{Q}}, 3_Q) B_4^0(\tilde{\hat{\bar{1}}}_q, \tilde{\hat{\bar{2}}}_g, \widetilde{5}_g, \widetilde{4}_{\bar{q}}) J_2^{(2)}(p_{\widetilde{4}}, p_{\widetilde{5}})$$

$$+\frac{1}{2}\Bigg[\mathcal{D}_{3,qg}^0(s_{\bar{1}\bar{2}}) - \mathcal{A}_{3,q}^0(s_{4\bar{2}}) + \frac{1}{2}\mathcal{D}_3^0(s_{54}) - \frac{1}{2}\mathcal{F}_{3,g}^0(s_{\widetilde{5}\bar{1}}) + \mathcal{A}_{3,q}^0(s_{23}) - \mathcal{A}_{3,q}^0(s_{\widetilde{4}\bar{2}})$$

$$+\delta(1-x_1)\delta(1-x_2)\Big(\mathcal{S}(s_{4\bar{2}}, s_{45}, x_{4\bar{2},45}) - \mathcal{S}(s_{\bar{1}\bar{2}}, s_{\widetilde{4}\widetilde{5}}, x_{\bar{1}\bar{2},\widetilde{4}\widetilde{5}}) + \mathcal{S}(s_{\widetilde{5}\bar{1}}, s_{\widetilde{4}\widetilde{5}}, x_{\widetilde{5}\bar{1},\widetilde{4}\widetilde{5}})$$

$$-\mathcal{S}(s_{54}, s_{45}, x_{54,45}) + \mathcal{S}(s_{\widetilde{4}\bar{2}}, s_{\widetilde{4}\widetilde{5}}, x_{\widetilde{4}\bar{2},\widetilde{4}\widetilde{5}}) - \mathcal{S}(s_{2\bar{2}}, s_{45}, x_{2\bar{2},45})\Big)\Bigg]$$

$$\times E_3^0(\hat{2}_{\bar{Q}}, \hat{1}_q, 4_{\bar{q}}) B_4^0(\widetilde{3}_Q, \widetilde{5}_g, \tilde{\hat{\bar{1}}}_g, \tilde{\hat{\bar{2}}}_{\bar{Q}})\Bigg] J_2^{(2)}(p_{\widetilde{3}}, p_{\widetilde{5}})\Bigg\}, \tag{6.3.26}$$

whilst the second term in (6.3.25) requires a subtraction term $d\hat{\sigma}_{NNLO}^{T_2}$ of the form

$$d\hat{\sigma}_{NNLO}^{T_2} = \mathcal{N}_{qQ,5}^1 \int d\Phi_3(p_3, p_4, p_5; x_1 p_1, x_2 p_2)\frac{1}{S_3}\frac{dx_1}{x_1}\frac{dx_2}{x_2} \times \Bigg\{$$

$$-\Big(\frac{1}{2}\mathcal{D}_{3,q}^0(s_{\bar{1}5}) + \frac{1}{2}\mathcal{D}_{3,q}^0(s_{\bar{2}5}) + \mathcal{A}_3^0(s_{34})$$

$$-\Gamma_{qq}^1(x_1)\delta(1-x_2) - \Gamma_{qq}^1(x_2)\delta(1-x_1)\Big) C_5^0(\hat{1}_q, 5_g, \hat{2}_{\bar{Q}}; 3_Q, 4_{\bar{q}}) J_2^{(3)}(p_3, p_4, p_5)$$

$$+A_3^0(\hat{1}_q, 5_g, \hat{2}_{\bar{Q}})\Bigg[\delta(1-x_1)\delta(1-x_2) C_4^1(\widetilde{3}_Q, \widetilde{4}_{\bar{q}}; \tilde{\hat{\bar{1}}}_q, \tilde{\hat{\bar{2}}}_{\bar{Q}}) + \Big(\mathcal{A}_3^0(s_{\widetilde{3}\widetilde{4}}) + \mathcal{A}_{3,qq}^0(s_{\bar{1}\bar{2}})$$

$$-\Gamma^1_{qq}(x_1)\delta(1-x_2) - \Gamma^1_{qq}(x_2)\delta(1-x_1)\Bigg) C^0_4(\widetilde{3}_Q,\widetilde{4}_{\bar{q}};\hat{\bar{\tilde{1}}}_q,\hat{\bar{\tilde{2}}}_{\bar{Q}})\Bigg] J^{(2)}_2(p_{\widetilde{3}},p_{\widetilde{4}})$$

$$+E^0_3(4_{\bar{q}},3_Q,\hat{2}_{\bar{Q}})\Bigg[\delta(1-x_1)\delta(1-x_2)B^1_4(\hat{\tilde{1}}_q,5_g,\hat{\bar{\tilde{2}}}_g,\widetilde{(34)}_{\bar{q}}) + \bigg(\frac{1}{2}\mathcal{D}^0_{3,q}(s_{\bar{1}5})$$

$$+\frac{1}{2}\mathcal{F}^0_{3,g}(s_{\bar{2}5}) + \mathcal{D}^0_{3,g}(s_{\bar{2}\widetilde{(34)}}) - \Gamma^1_{qq}(x_1)\delta(1-x_2) - \Gamma^1_{qq}(x_2)\delta(1-x_1)\bigg)$$

$$\times B^0_4(\hat{\tilde{1}}_q,5_g,\hat{\bar{\tilde{2}}}_g,\widetilde{(34)}_{\bar{q}})\Bigg] J^{(2)}_2(p_{\widetilde{(34)}},p_5)$$

$$+E^0_3(3_Q,4_{\bar{q}},\hat{1}_q)\Bigg[\delta(1-x_1)\delta(1-x_2)B^1_4(\widetilde{(34)}_Q,\hat{\bar{\tilde{1}}}_g,5_g,\hat{\bar{\tilde{2}}}_{\bar{Q}}) + \bigg(\mathcal{D}^0_{3,g}(s_{\widetilde{(34)}\bar{1}})$$

$$+\frac{1}{2}\mathcal{F}^0_{3,g}(s_{5\bar{1}}) + \frac{1}{2}\mathcal{D}^0_{3,q}(s_{5\bar{2}}) - \Gamma^1_{qq}(x_1)\delta(1-x_2) - \Gamma^1_{qq}(x_2)\delta(1-x_1)\bigg)$$

$$\times B^0_4(\widetilde{(34)}_Q,\hat{\bar{\tilde{1}}}_g,5_g,\hat{\bar{\tilde{2}}}_{\bar{Q}})\Bigg] J^{(2)}_2(p_{\widetilde{(34)}},p_5)$$

$$+\Bigg[A^1_3(\hat{1}_q,5_g,\hat{2}_{\bar{Q}})\delta(1-x_1)\delta(1-x_2) + \bigg(\frac{1}{2}\mathcal{D}^0_{3,q}(s_{\bar{1}5}) + \frac{1}{2}\mathcal{D}^0_{3,q}(s_{\bar{2}5}) - \mathcal{A}^0_{3,qq}(s_{\bar{1}\bar{2}})\bigg)$$

$$\times A^0_3(\hat{1}_q,5_g,\hat{2}_{\bar{Q}})\Bigg] C^0_4(\widetilde{3}_Q,\widetilde{4}_{\bar{q}};\hat{\bar{\tilde{1}}}_q,\hat{\bar{\tilde{2}}}_{\bar{Q}}) J^{(2)}_2(p_{\widetilde{3}},p_{\widetilde{4}})$$

$$+\Bigg[E^1_3(4_{\bar{q}},3_Q,\hat{2}_{\bar{Q}})\delta(1-x_1)\delta(1-x_2) + \bigg(\mathcal{A}^0_3(s_{34}) + \mathcal{A}^0_{3,q}(s_{\bar{2}4}) - 2\mathcal{D}^0_{3,g;gq}(s_{\widetilde{(34)}\bar{2}})\bigg)$$

$$\times E^0_3(4_{\bar{q}},3_Q,\hat{2}_{\bar{Q}})\Bigg] B^0_4(\hat{\tilde{1}}_q,5_g,\hat{\bar{\tilde{2}}}_g,\widetilde{(34)}_{\bar{q}}) J^{(2)}_2(p_{\widetilde{(34)}},p_5)$$

$$+\Bigg[E^0_3(3_Q,4_{\bar{q}},\hat{1}_q)\delta(1-x_1)\delta(1-x_2) + \bigg(\mathcal{A}^0_3(s_{34}) + \mathcal{A}^0_{3,q}(s_{\bar{1}3}) - 2\mathcal{D}^0_{3,g;gq}(s_{\widetilde{(34)}\bar{1}})\bigg)$$

$$\times E^0_3(3_Q,4_{\bar{q}},\hat{1}_q)\Bigg] B^0_4(\widetilde{(34)}_Q,\hat{\bar{\tilde{1}}}_g,5_g,\hat{\bar{\tilde{2}}}_{\bar{Q}}) J^{(2)}_2(p_{\widetilde{(34)}},p_5)$$

$$+b_0 \log\left(\frac{\mu^2}{|s_{152}|}\right) A^0_3(\hat{1}_q,5_g,\hat{2}_{\bar{Q}})\delta(1-x_1)\delta(1-x_2)C^0_4(\widetilde{3}_Q,\widetilde{4}_{\bar{q}};\hat{\bar{\tilde{1}}}_q,\hat{\bar{\tilde{2}}}_{\bar{Q}}) J^{(2)}_2(p_{\widetilde{3}},p_{\widetilde{4}})$$

$$+b_0 \log\left(\frac{\mu^2}{|s_{234}|}\right) E^0_3(4_{\bar{q}},3_Q,\hat{2}_{\bar{Q}})\delta(1-x_1)\delta(1-x_2)B^0_4(\hat{\tilde{1}}_q,5_g,\hat{\bar{\tilde{2}}}_g,\widetilde{(34)}_{\bar{q}}) J^{(2)}_2(p_{\widetilde{(34)}},p_5)$$

$$+b_0 \log\left(\frac{\mu^2}{|s_{143}|}\right) E^0_3(3_Q,4_{\bar{q}},\hat{1}_q)\delta(1-x_1)\delta(1-x_2)B^0_4(\widetilde{(34)}_Q,\hat{\bar{\tilde{1}}}_g,5_g,\hat{\bar{\tilde{2}}}_{\bar{Q}}) J^{(2)}_2(p_{\widetilde{(34)}},p_5)$$

$$
+\frac{1}{2}\Bigg[\mathcal{D}_{3,g}^0(s_{\bar{\tilde{2}}\widetilde{(34)}}) - \mathcal{A}_{3,q}^0(s_{4\bar{2}}) + \frac{1}{2}\mathcal{D}_{3,q}^0(s_{\bar{2}5}) - \frac{1}{2}\mathcal{F}_{3,g}^0(s_{5\bar{2}}) + \mathcal{A}_{3,q}^0(s_{\bar{1}4}) - \mathcal{A}_{3,q}^0(s_{\widetilde{(34)}\bar{1}})
$$

$$
+\delta(1-x_1)\delta(1-x_2)\Big(\mathcal{S}(s_{4\bar{1}}, s_{45}, x_{4\bar{1},45}) - \mathcal{S}(s_{\bar{\tilde{2}}\widetilde{(34)}}, s_{45}, x_{\bar{\tilde{2}}\widetilde{(34)},45})
$$

$$
+\mathcal{S}(s_{5\bar{2}}, s_{45}, x_{5\bar{2},45}) - \mathcal{S}(s_{\bar{2}5}, s_{45}, x_{\bar{2}5,45}) + \mathcal{S}(s_{\widetilde{(34)}\bar{1}}, s_{45}, x_{\widetilde{(34)}\bar{1},45})
$$

$$
-\mathcal{S}(s_{\bar{1}4}, s_{45}, x_{\bar{1}4,45})\Big)\Bigg]E_3^0(4_{\bar{q}}, 3_Q, \hat{2}_{\bar{Q}})B_4^0(\hat{\bar{1}}_q, 5_g, \hat{\bar{\tilde{2}}}_g, \widetilde{(34)}_{\bar{q}})J_2^{(2)}(p_{\widetilde{(34)}}, p_5)
$$

$$
+\frac{1}{2}\Bigg[\mathcal{D}_{3,g}^0(s_{\bar{\tilde{1}}\widetilde{(34)}}) - \mathcal{A}_{3,q}^0(s_{3\bar{1}}) + \frac{1}{2}\mathcal{D}_{3,q}^0(s_{5\bar{1}}) - \frac{1}{2}\mathcal{F}_{3,g}^0(s_{5\bar{1}}) + \mathcal{A}_{3,q}^0(s_{\bar{2}3}) - \mathcal{A}_{3,q}^0(s_{\widetilde{(34)}\bar{2}})
$$

$$
+\delta(1-x_1)\delta(1-x_2)\Big(\mathcal{S}(s_{3\bar{1}}, s_{35}, x_{3\bar{1},35}) - \mathcal{S}(s_{\bar{\tilde{1}}\widetilde{(34)}}, s_{35}, x_{\bar{\tilde{1}}\widetilde{(34)},35})
$$

$$
+\mathcal{S}(s_{5\bar{1}}, s_{35}, x_{5\bar{1},35}) - \mathcal{S}(s_{5\bar{1}}, s_{35}, x_{5\bar{1},35}) + \mathcal{S}(s_{\widetilde{(34)}\bar{2}}, s_{35}, x_{\widetilde{(34)}\bar{2},35})
$$

$$
-\mathcal{S}(s_{\bar{2}3}, s_{35}, x_{\bar{2}3,35})\Big)\Bigg]E_3^0(3_Q, 4_{\bar{q}}, \hat{1}_q)B_4^0(\widetilde{(34)}_Q, \hat{\bar{\tilde{1}}}_g, 5_g, \hat{2}_{\bar{Q}})J_2^{(2)}(p_{\widetilde{(34)}}, p_5)\Bigg\}. \quad (6.3.27)
$$

Only the sum of the two terms will produce a full cancellation in all the limits.

We see that there are large angle soft terms proportional to the two E_3^0 antennae but not for A_3^0. This can be justified given the arguments in Chapter 4. The channel presented here contains the maximal number of terms required for a single channel at leading colour. All other channels either have a structure akin to the subtraction terms in (6.3.26) and (6.3.27), or will have fewer E_3^ℓ antennae if a quark-antiquark pair of the same flavour are in the initial state; for the squared matrix element

$$
C_5^1(\hat{\bar{1}}_q, 5_g, 3_{\bar{Q}}; 4_Q, \hat{\bar{2}}_{\bar{q}}) \quad (6.3.28)
$$

we observe no $q||\bar{q}$ collinear limit. If the gluon appears in the initial state, the matrix element will contain no soft limits.

The $q||\bar{q}$ and $Q||\bar{Q}$ collinear limits that exist across colour structures have been constructed in the real-virtual subtraction term through the use of $E_3(Q, q, \bar{q})$, where the Q acts as a spectator parton. It is possible therefore, to use the $G_3(g, q, \bar{q})$ to cancel this limit, as again the gluon is not involved in the limit.
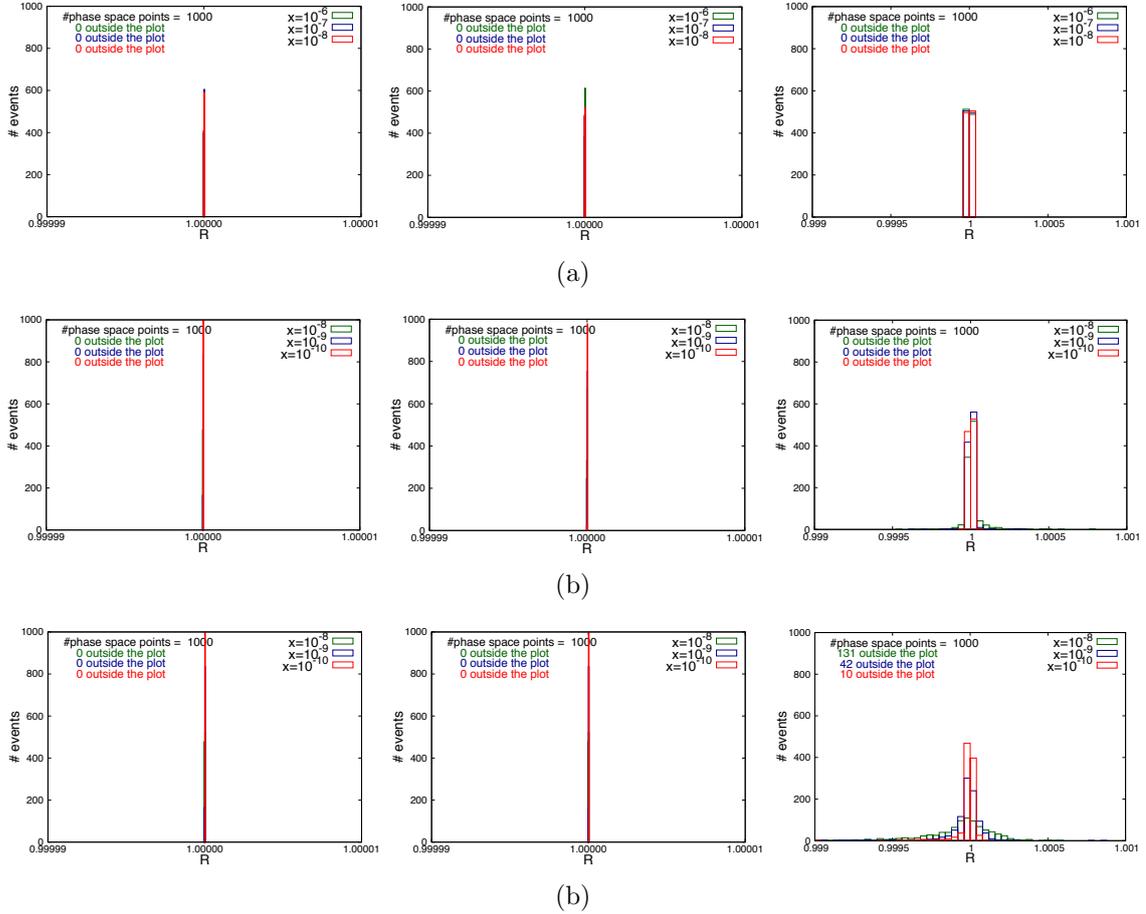
Figure 6.1: Plots displaying the convergence of the subtraction term to the real-virtual physical matrix element in various unresolved limits for $\bar{q}Q \to \bar{q}Qg$. The green data is furthest from the singular configuration with the blue data closer to the singular region and the red data the closest. The left plot of each row is the $1/\epsilon^2$ contribution, the centre plot the $1/\epsilon$ contribution and the right hand plot the finite contribution. (a) Final-state single soft limit for the gluon 5_g such that $x = (s_{12} - s_{34})/s_{12}$. (b) Collinear limit between initial state quark 1_q and final state gluon 5_g, such that $x = s_{15}/s_{12}$. (c) Collinear limit for final state quark 3_Q and initial state antiquark $2_{\bar{Q}}$ such that $x = s_{23}/s_{12}$.
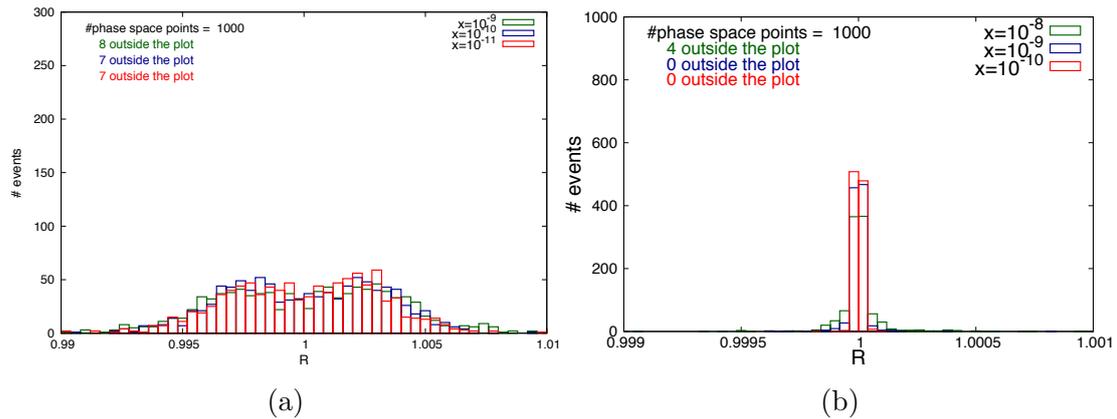
Figure 6.2: Distributions of R displaying the effect of azimuthal angular rotations for single collinear limits: final-final collinear limit for $\bar{q}Q \to \bar{q}Qg$ (a) without corrections and (b) with corrections turned on. Note the enlarged scale in (a) to make the data visible.

However, we find that, if the subtraction term is to be self-contained as above, the E_3 is enforced at the stage of cancelling the integrated antenna dropping down from the double real subtraction term and those dealing with the explicit poles in the one-loop reduced matrix element and antennae. The integrated antennae required to cancel the G_3^1 pole structure do not cancel against the remaining $\mathcal{X}_3^0$ not involved in the limit. It is not yet clear whether this is an artefact of just considering a single channel independently. Since the singularity operators used to describe G_3^1 are of the flavour type, $\mathbf{I}_{q\bar{q},F}^{(1)}(\epsilon, s)$, it may be necessary to employ these over the E_3^1 for the subtraction term contributing to the flavour dependent squared matrix element.

For each IR divergent limit, we again generate momenta with `RAMBO` to enforce the unresolved configuration, and compute the ratio given in (5.2.27). As in the previous chapter, three constraints are chosen, forcing the phase space points closer to the limits. This provides statistical evidence for the convergence of the subtraction term to the physical cross section in the various IR limits. A selection of plots are given in Figure 6.1.

Again we see the R distribution become more sharply peaked as we approach the limit. There are no divergent limits for the soft quarks, nor any collinear divergences between different flavour quarks, as expected. The R ratio for all the finite contributions to the singular limits is collected in Appendix C. We also test the azimuthal

corrections for the cases where a gluon in the Born process can split into a quark antiquark pair. The scenario is different from the colour-connected gluon terms in the previous chapter, since here we have collinear limits between quark pairs spanning two colour structures. It is more akin to the $q||\bar{q}$ collinear limit in the quark-gluon scattering, although subtly different since there the quarks were still in the same colour string. Nevertheless, Figure 6.2 shows that the rotation of phase space is functioning well in accounting for the azimuthal corrections. Indeed, in its absence we see no matching of the matrix element and subtraction term in the single unresolved limits.

6.3.2 Double virtual subtraction term, $\mathrm{d}\hat{\sigma}^U_{NNLO}$

The double virtual subtraction term is constructed from the remaining terms dropping down from the double real and real virtual subtraction terms, as well as the double virtual mass factorisation contribution. However, since the pole structure of the two loop amplitudes is predictable via the formalism described in Chapter 2, we are able to write the subtraction term in terms of the single and double unresolved integrated antenna strings without the prerequisite of the double real and real-virtual subtraction terms. Since we are in possession of the real virtual subtraction term however, the combination of RV and VV terms should give an indication to the structures required at the double real contribution. In terms of integrated antenna strings, the subtraction term can be written in the form of Eq. (4.5.131),

$$
\begin{aligned}
\mathrm{d}\hat{\sigma}^U_{q\bar{Q},NNLO} \;=\; & -\mathcal{N}^2_{qQ,4}\,\mathrm{d}\Phi_2(p_3,p_4;p_1,p_2)\int\frac{\mathrm{d}z_1}{z_1}\frac{\mathrm{d}z_2}{z_2}\times\Bigg\{ \\
& \boldsymbol{J}^{(1)}_4(\hat{\bar{1}}_q,\hat{\bar{2}}_{\bar{Q}};3_Q,4_{\bar{q}})\left(C^1_4(\hat{\bar{1}}_q,\hat{\bar{2}}_{\bar{Q}};3_Q,4_{\bar{q}})-\frac{b_0}{\epsilon}\,C^0_4(\hat{\bar{1}}_q,\hat{\bar{2}}_{\bar{Q}};3_Q,4_{\bar{q}})\right) \\
& +\;\frac{1}{2}\,\boldsymbol{J}^{(1)}_4(\hat{\bar{1}}_q,\hat{\bar{2}}_{\bar{Q}};3_Q,4_{\bar{q}})\otimes\boldsymbol{J}^{(1)}_4(\hat{\bar{1}}_q,\hat{\bar{2}}_{\bar{Q}};3_Q,4_{\bar{q}})\,C^0_4(\hat{\bar{1}}_q,\hat{\bar{2}}_{\bar{Q}};3_Q,4_{\bar{q}}) \\
& +\;\boldsymbol{J}^{(2)}_4(\hat{\bar{1}}_q,\hat{\bar{2}}_{\bar{Q}};3_Q,4_{\bar{q}})\,C^0_4(\hat{\bar{1}}_q,\hat{\bar{2}}_{\bar{Q}};3_Q,4_{\bar{q}})\Bigg\}\,J^{(2)}_2(p_3,p_4), \qquad (6.3.29)
\end{aligned}
$$

which reproduces the form of the Catani pole structure in Eq. (4.5.115). The single unresolved integrated antenna string is defined in Eq. (5.2.14). In Eq. (5.2.14) the single unresolved integrated antenna string was written as a sum over integrated

dipoles. The analogous dipole-like formula for $\boldsymbol{J}_4^{(2)}$ is given by,

$$\boldsymbol{J}_4^{(2)}(\hat{\bar{1}}_q, \hat{\bar{2}}_{\bar{Q}}; 3_Q, 4_{\bar{q}}) \;=\; \boldsymbol{J}_2^{(2)}(\hat{\bar{1}}_q, \hat{\bar{2}}_{\bar{Q}}) + \boldsymbol{J}_2^{(2)}(3_Q, 4_{\bar{q}}) \tag{6.3.30}$$

where the two-parton double unresolved integrated antenna strings are given by:

$$
\begin{aligned}
\boldsymbol{J}_2^{(2)}(\hat{\bar{1}}_q, \hat{\bar{2}}_{\bar{Q}}) \;=\;& \mathcal{A}_{4,q\bar{q}}^0(s_{\bar{1}\bar{2}}) + \mathcal{A}_{3,q\bar{q}}^1(s_{\bar{1}\bar{2}}) + \frac{b_0}{\epsilon}\mathcal{A}_{q\bar{q},3}^0(s_{\bar{1}\bar{2}})\left(\frac{|s_{\bar{1}\bar{2}}|}{\mu^2}\right)^{-\epsilon} \\
&- \Gamma_{qq}^{(2)}(z_1)\delta(1-z_2) - \Gamma_{qq}^{(2)}(z_2)\delta(1-z_1) - \frac{1}{2}\left[\mathcal{A}_{3,q\bar{q}}^0(s_{\bar{1}\bar{2}}) \otimes \mathcal{A}_{3,q\bar{q}}^0(s_{\bar{1}\bar{2}})\right] \\
&+ \frac{1}{2}\left[\Gamma_{qq}^1 \otimes \Gamma_{qq}^1\right](z_1)\delta(1-z_2) + \frac{1}{2}\left[\Gamma_{qq}^1 \otimes \Gamma_{qq}^1\right](z_2)\delta(1-z_1) \tag{6.3.31} \\
\boldsymbol{J}_2^{(2)}(3_Q, 4_{\bar{q}}) \;=\;& \mathcal{A}_4^0(s_{34}) + \mathcal{A}_3^1(s_{34}) \\
&+ \frac{b_0}{\epsilon}\mathcal{A}_3^0(s_{34})\left(\frac{|s_{34}|}{\mu^2}\right)^{-\epsilon} - 2\left[\mathcal{A}_3^0(s_{34}) \otimes \mathcal{A}_3^0(s_{34})\right]. \tag{6.3.32}
\end{aligned}
$$

$$*$$

In this chapter we have constructed the leading colour real-virtual and double virtual subtraction terms for the dijet subprocess involving two unlike-quark pairs, for the Born channel $\bar{q}Q \to \bar{q}Q$. It is the channel requiring the maximal number of antenna, and we have shown numerically that the subtraction term and the physical cross section converge successfully in the various unresolved limits.

Chapter 7

Conclusions

The research discussed in this thesis was twofold. Firstly, to explore the underlying structure of NNLO calculations that are manifest in the antenna subtraction scheme, and secondly to apply the antenna subtraction formalism directly to processes involving hadronic initial states relevant for dijet production at the Large Hadron Collider.

Such are the spectacular levels of precision in data collected from the LHC since its first successful run in 2010, that the experimental measurements are sensitive to NNLO effects. Theoretical perturbative calculations must now incorporate two loop corrections to the Born process, as well as up to two real unresolved emissions of on-shell particles. The matrix elements relevant for dijet production at NNLO are well known; the bottleneck for systematic predictions is defining a procedure to cancel the infrared divergences emanating from the explicit pole structure of the loop amplitude along with the soft and collinear dynamic poles manifest during the integration over phase space.

Ideally, this occurs in a numerically robust fashion, applicable to arbitrary production channels. The antenna subtraction formalism provides a general method by which the rich divergent behaviour of physical matrix elements can be extracted and cancelled by utilising the universal infrared behaviour of colour-ordered matrix elements. At NLO, the antenna subtraction method is straightforward and well understood. There is a simple, direct link between the real and virtual singular structures, reflected concisely in the subtraction terms. In this thesis we made the same connections - albeit now more complex - between the various structures present at NNLO,

and begin to implement them in a physical setting.

The first goal of this research was to gain control of the infrared structure existing in double-virtual, real virtual and double-real subtraction terms constructed with the antenna formalism. Whilst the general formalism is in place for constructing individual subtraction terms, we discussed the implementation of the integrated antenna strings as a bridge between the well-known Catani factorisation formula for loop amplitudes and the integrated antennae. The integrated antenna strings combine the mass factorisation terms and integrated antennae into blocks of terms free of explicit poles that not only match up with the Catani singularity operators but form structured-blocks in correspondence with the underlying colour ordering.

The divergent behaviour is far richer at NNLO than NLO; we now encounter doubly unresolved configurations associated with two additional final state partons contributing to the same underlying Born process. Different subtraction terms will be required for the variety of limits that exist, dictated by the colour-connectivity of the matrix elements. Real-virtual corrections contain both singly unresolved limits and explicit poles from one-loop effects. The double virtual contribution, although containing no dynamic divergences, involves the interference of two-loop amplitudes with the tree level Born process and one-loop self-interferences, which hold explicit poles up to $\mathcal{O}(\epsilon^{-4})$. We present in this thesis a 'roadmap' tracking the various structures between the double-real, real-virtual and double-virtual subtraction terms. It is now feasible to follow explicitly the role of each block of subtraction terms - introduced at the double-real and real-virtual level to mimic implicit divergences of unresolved partons - as they are returned after integration over the unresolved phase space. Having such an understanding over the flow of terms introduces a level of predictive power that can greatly simplify calculations. The double-real subtraction term is the most complex to construct due to the multitude of unresolved configurations. Yet we have a link, through the $\boldsymbol{J}_n^{(l)}$ operators, between the blocks of unintegrated antennae and the pole structure of the real-virtual and double-real matrix elements, the latter being already well understood. With the divergent structure under control, it is possible to attack physical processes in a systematic fashion.

The second goal of this thesis was to apply the antenna formalism to processes rel-

evant to LHC analysis, namely dijet production from hadronic initial states. Chapters 5 and 6 discussed the construction of the double-real, real-virtual and double-virtual subtraction terms for the necessary partonic channels. Chapter 5 focussed primarily on gluon production with a quark-antiquark pair initial state, constructing all three subtraction terms at leading colour and introducing the integrated antenna strings. For the double real emission of two unresolved gluons at NNLO, we required final-final, initial-final and initial-initial antennae functions. The real-virtual subtraction term incorporated one-loop antenna, again for all three combinations of initial states within the antennae. We found it possible - and greatly advantageous - to deconstruct the one-loop three parton antennae into sub antennae via partial fractioning as with the tree-level case. In doing so, the D_3^1 was still seen to require an $\widetilde{A}_3^1$ to cancel the over subtracted poles present due to the supersymmetric construction of the d_3^1. The integrated antennae required to cancel the explicit poles of $\widetilde{A}_3^1$ are traced back to the terms in the double real subtraction term, a further predictive link between the terms despite these antenna existing to perform unphysical cancellations.

From Catani's factorisation formula, the double-virtual subtraction term was recast in terms of integrated antenna strings. The double real and real-virtual have now been subject to numerical checks in all single and double unresolved limits, and tested for complete pole cancellation such that the combination of subtraction term and physical matrix element is rendered finite over all phase space. We found that in all singular limits, the real-virtual and double-real subtraction terms correctly mimicked the matrix partonic matrix elements. With the subtraction terms successfully tested here, a similar treatment to [101] can be carried out and preliminary predictions for observables made to accompany the pure gluon analysis.

The natural progression was to construct subtraction terms for the remaining channels, namely where gluons can appear in the initial state of quark-gluon scattering processes. Here the double-real terms are not known, due to the as yet unresolved subtlety with the four-parton flavour-changing antenna. Nevertheless, the strong predictive structure allows the real-virtual and double-virtual terms to be constructed without knowledge from the double-real terms. Crucially, we propose that in addition to the one-loop matrix element and antenna corrections built from integrated

antenna strings, the integrated terms returned at real-virtual that dealt with the large-angle soft corrections at double-real are also entirely predictive, even without prior knowledge of the presence of $\widetilde{X}_4^0$. The combination of a) requiring the finite contributions from the integrated antennae cancel in the various unresolved limits, and b) the well-defined block structure of the subtraction terms, can be used to predict the integrated antennae that dropped down from the double-real terms. We are in a powerful position: the double-virtual and real-virtual subtraction terms can be used to reconstruct the more complex double-real subtraction terms from the integrated antenna strings. Numerical checks illustrated the success of the real-virtual subtraction term in mimicking all single unresolved limits of the physical matrix element whilst removing all explicit poles. The subtraction terms with gluonic initial states utilised the initial-initial three parton antenna with false partonic entries. For the parton string $(\cdots, j_q, \hat{1}_g, i_g, \cdots \hat{2}_g, \cdots)$ the $A(j_q, \hat{1}_g, \hat{2}_g)$ is preferred over the $D(j_q, \hat{1}_g, i_g)$ since the ambiguity over the remapped initial states is avoided, and the single $j_q||\hat{1}_g$ limit is isolated.

In a similar way, we have applied the antenna formalism to construct the real-virtual and double virtual subtraction terms for processes involving two pairs of non-identical quarks at leading colour, where again numerical tests illustrated the successful cancellation of both explicit and implicit divergences of the matrix elements. The channels for the real-virtual four quark, one gluon scattering process have not dissimilar subtraction terms. This channel contains the maximum number of antenna that would be required for any of the leading colour contributions, since the choice of initial states does not nullify any of the quark-antiquark collinear limits.

Born Process	$d\hat{\sigma}_{NNLO}^S$	$d\hat{\sigma}_{NNLO}^T$	$d\hat{\sigma}_{NNLO}^U$
$gg \to gg$	✔ [79]	✔ [15]	✔ [80]
$q\bar{q} \to gg$	✔ (5.2.31)	✔ (5.4.39)	✔ (5.4.42)
$gg \to q\bar{q}$	✘	✔ (5.5.55),(5.5.57)	✔ (5.5.64)
$qg \to qg$	✘	✔ (5.6.75),(5.6.77),(5.6.79)	✔ (5.6.80), (5.6.85)
$\bar{q}Q \to \bar{q}Q$	✘	✔ (6.3.26),(6.3.27)	✔ (6.3.29)

Table 7.1: Checklist for leading colour subtraction terms relevant for quark-gluon scattering at NNLO.

Table 7.1 indicates the current level of completion of leading colour subtraction terms.

The progression from the work in this thesis is clear. The remaining dijet production channels must be addressed, both at leading and subleading colour. Work has begun also on the V+jet and H+jet computations. With a firm grasp of the underlying infrared structure of NNLO calculations within the antenna framework, and clear evidence of the robustness and generality of the antenna subtraction method, we are in a commanding position to produce concrete predictions for LHC processes at NNLO accuracy.

Bibliography

[1] G. Herten, *The First Year of the Large Hadron Collider: A Brief Review,* Mod. Phys. Lett. A **26**, 843 (2011) [`1104.4205`].

[2] O. W. Greenberg, *Spin and Unitary Spin Independence in a Paraquark Model of Baryons and Mesons,* Phys. Rev. Lett. **13**, 598 (1964).

[3] G. Dissertori, I. G. Knowles and M. Schmelling, *Quantum chromodynamics: high energy experiments and theory,* Oxford University Press, 2003.

[4] R. Ellis, W. Stirling and B. Webber, *QCD and collider physics,* Camb. Monogr. Part. Phys. Nucl. Phys. Cosmol., 1996.

[5] M. E. Peskin and D. V. Schroeder, *An Introduction to Quantum Field Theory,* Advanced Book Program. Westview Press, 1995.

[6] W. Greiner and A. Schafer, *Quantum Chromodynamics,* Springer London Limited, 1997.

[7] J.C. Collins, *Renormalization: An Introduction to Renormalization, the Renormalization Group and the Operator-Product Expansion,* Camb. Monogr. Math. Phys. Cambridge University Press, 1996.

[8] P. Pascual and R. Tarrach, *QCD: Renormalization for the Practitioner*, Springer-Verlag, 1984

[9] G. 't Hooft and M. J. G. Veltman, *Regularization and Renormalization of Gauge Fields,* Nucl. Phys. B **44**, 189 (1972).

[10] M. L. Mangano and S. J. Parke, *Multiparton amplitudes in gauge theories,* Phys. Rept. **200**, 301 (1991) [`hep-th/0509223`].

[11] M. L. Mangano and S. J. Parke, *Quark - Gluon Amplitudes in the Dual Expansion,* Nucl. Phys. B **299**, 673 (1988).

[12] P. Cvitanovic, *Group Theory for Feynman Diagrams in Nonabelian Gauge Theories,* SLAC-PUB-1663.

[13] J. C. Collins, D. E. Soper and G. F. Sterman, *Factorization of Hard Processes in QCD,* Adv. Ser. Direct. High Energy Phys. **5**, 1 (1988) [`hep-ph/0409313`].

[14] R. K. Ellis, H. Georgi, M. Machacek, H. D. Politzer and G. G. Ross, *Factorization and the Parton Model in QCD,* Phys. Lett. B **78**, 281 (1978).

[15] A. Gehrmann-De Ridder, E. W. N. Glover and J. Pires, *Real-Virtual corrections for gluon scattering at NNLO,* JHEP **1202**, 141 (2012) [`1112.3613`].

[16] G. Altarelli and G. Parisi, *Asymptotic Freedom in Parton Language,* Nucl. Phys. B **126**, 298 (1977).

[17] Y. L. Dokshitzer, *Calculation of the Structure Functions for Deep Inelastic Scattering and e^+e^- Annihilation by Perturbation Theory in Quantum Chromodynamics,* Sov. Phys. JETP **46**, 641 (1977) [Zh. Eksp. Teor. Fiz. **73**, 1216 (1977)].

[18] V. N. Gribov and L. N. Lipatov, e^+e^- *pair annihilation and deep inelastic e p scattering in perturbation theory* Sov. J. Nucl. Phys. **15**, 675 (1972) [Yad. Fiz. **15**, 1218 (1972)].

[19] S. Catani, S. Dittmaier and Z. Trocsanyi, *One loop singular behavior of QCD and SUSY QCD amplitudes with massive partons,* Phys. Lett. B **500**, 149 (2001) [`hep-ph/0011222`].

[20] S. Catani, *The Singular behavior of QCD amplitudes at two loop order,* Phys. Lett. B **427**, 161 (1998) [`hep-ph/9802439`].

[21] S. Catani and M. H. Seymour, *A General algorithm for calculating jet cross-sections in NLO QCD,* Nucl. Phys. B **485**, 291 (1997) [Erratum-ibid. B **510**, 503 (1998)] [`hep-ph/9605323`].

[22] A. Gehrmann-De Ridder, T. Gehrmann and E. W. N. Glover, *Antenna subtraction at NNLO,* JHEP **0509**, 056 (2005) [`hep-ph/0505111`].

[23] R. K. Ellis, G. Marchesini and B. R. Webber, *Soft Radiation in Parton Parton Scattering,* Nucl. Phys. B **286** (1987) 643 [Erratum-ibid. B **294** (1987) 1180].

[24] A. Daleo, T. Gehrmann and D. Maitre, *Antenna subtraction with hadronic initial states,* JHEP **0704**, 016 (2007) [`hep-ph/0612257`].

[25] Z. Bern, V. Del Duca and C. R. Schmidt, *The Infrared behavior of one loop gluon amplitudes at next-to-next-to-leading order,* Phys. Lett. B **445**, 168 (1998) [`hep-ph/9810409`].

[26] Z. Bern, V. Del Duca, W. B. Kilgore and C. R. Schmidt, *The Infrared behavior of one loop QCD amplitudes at next-to-next-to leading order,* Phys. Rev. D **60**, 116001 (1999) [`hep-ph/9903516`].

[27] Z. Bern, L. J. Dixon, D. C. Dunbar and D. A. Kosower, *One loop n point gauge theory amplitudes, unitarity and collinear limits,* Nucl. Phys. B **425**, 217 (1994) [`hep-ph/9403226`].

[28] S. Catani and M. Grazzini, *Infrared factorization of tree level QCD amplitudes at the next-to-next-to-leading order and beyond,* Nucl. Phys. B **570**, 287 (2000) [`hep-ph/9908523`].

[29] S. Catani and M. Grazzini, *Collinear factorization and splitting functions for next-to-next-to-leading order QCD calculations,* Phys. Lett. B **446**, 143 (1999) [`hep-ph/9810389`].

[30] F. A. Berends and W. T. Giele, *Multiple Soft Gluon Radiation in Parton Processes,* Nucl. Phys. B **313**, 595 (1989).

[31] J. M. Campbell and E. W. N. Glover, *Double unresolved approximations to multiparton scattering amplitudes,* Nucl. Phys. B **527**, 264 (1998) [`hep-ph/9710255`].

[32] F. Bloch and A. Nordsieck, *Note on the Radiation Field of the electron,* Phys. Rev. **52**, 54 (1937).

[33] T. Kinoshita, *Mass singularities of Feynman amplitudes,* J. Math. Phys. **3**, 650 (1962).

[34] T. D. Lee and M. Nauenberg, *Degenerate Systems and Mass Singularities,* Phys. Rev. **133**, B1549 (1964).

[35] A. Gehrmann-De Ridder, T. Gehrmann, E. W. N. Glover and G. Heinrich, *Infrared structure of $e^+e^- \to 3$ jets at NNLO,* JHEP **0711**, 058 (2007) [`0710.0346`].

[36] Y. I. Azimov, Y. L. Dokshitzer, V. A. Khoze and S. I. Troyan, *Similarity of Parton and Hadron Spectra in QCD Jets,* Z. Phys. C **27**, 65 (1985).

[37] G. P. Salam, *Towards Jetography,* Eur. Phys. J. C **67**, 637 (2010) [`0906.1833`].

[38] M. H. Seymour, *Jet phenomenology,* In *La Thuile 1997, Results and perspectives in particle physics* 475-491 [`hep-ph/9707349`].

[39] S. D. Ellis and D. E. Soper, *Successive combination jet algorithm for hadron collisions,* Phys. Rev. D **48**, 3160 (1993) [`hep-ph/9305266`].

[40] M. Cacciari, G. P. Salam and G. Soyez, *The Anti-k(t) jet clustering algorithm,* JHEP **0804**, 063 (2008) [`0802.1189`].

[41] Y. L. Dokshitzer, G. D. Leder, S. Moretti and B. R. Webber, *Better jet clustering algorithms,* JHEP **9708**, 001 (1997) [`hep-ph/9707323`].

[42] M. Cacciari and G. P. Salam, *Dispelling the N^3 myth for the k_t jet-finder,* Phys. Lett. B **641**, 57 (2006) [`hep-ph/0512210`].

[43] J. M. Butterworth, J. P. Couchman, B. E. Cox and B. M. Waugh, *KtJet: A `C++` implementation of the K-perpendicular clustering algorithm,* Comput. Phys. Commun. **153**, 85 (2003) [hep-ph/0210022].

[44] G. P. Salam and G. Soyez, *A Practical Seedless Infrared-Safe Cone jet algorithm,* JHEP **0705**, 086 (2007) [`0704.0292`].

[45] G. Aad *et al.* [ATLAS Collaboration], *Search for Quark Contact Interactions in Dijet Angular Distributions in pp Collisions at $\sqrt{s} = 7$ TeV Measured with the ATLAS Detector,* Phys. Lett. B **694**, 327 (2011) [`1009.5069`].

[46] S. Moch, J. A. M. Vermaseren and A. Vogt, *The Three loop splitting functions in QCD: The Nonsinglet case,* Nucl. Phys. B **688**, 101 (2004) [`hep-ph/0403192`].

[47] G. Aad *et al.* [ATLAS Collaboration], *Measurement of the inclusive jet cross section in pp collisions at sqrt(s)=2.76 TeV and comparison to the inclusive jet cross section at sqrt(s)=7 TeV using the ATLAS detector,* [`1304.4739`]

[48] H. Abramowicz *et al.* [ZEUS Collaboration], *Inclusive-jet photoproduction at HERA and determination of alphas,* Nucl. Phys. B **864**, 1 (2012) [`1205.6153`].

[49] G. Dissertori, A. Gehrmann-De Ridder, T. Gehrmann, E. W. N. Glover, G. Heinrich and H. Stenzel, *First determination of the strong coupling constant using NNLO predictions for hadronic event shapes in e^+e^- annihilations,* JHEP **0802**, 040 (2008) [`0712.0327`].

[50] C. Anastasiou, E. W. N. Glover, C. Oleari and M. E. Tejeda-Yeomans, *Two loop QCD corrections to massless quark gluon scattering,* Nucl. Phys. B **605**, 486 (2001) [`hep-ph/0101304`].

[51] C. Anastasiou, L. J. Dixon, K. Melnikov and F. Petriello, *High precision QCD at hadron colliders: Electroweak gauge boson rapidity distributions at NNLO,* Phys. Rev. D **69**, 094008 (2004) [`hep-ph/0312266`].

[52] E. W. N. Glover, *Progress in NNLO calculations for scattering processes,* Nucl. Phys. Proc. Suppl. **116**, 3 (2003) [`hep-ph/0211412`].

[53] E. B. Zijlstra and W. L. van Neerven, *Order α_s^2 QCD corrections to the deep inelastic proton structure functions F2 and F(L),* Nucl. Phys. B **383**, 525 (1992).

[54] A. D. Martin, W. J. Stirling, R. S. Thorne and G. Watt, *Parton distributions for the LHC,* Eur. Phys. J. C **63**, 189 (2009) [`0901.0002`].

[55] W. T. Giele, E. W. N. Glover and D. A. Kosower, *Higher order corrections to jet cross-sections in hadron colliders,* Nucl. Phys. B **403**, 633 (1993) [`hep-ph/9302225`].

[56] W. T. Giele and E. W. N. Glover, *Higher order corrections to jet cross-sections in e^+e^- annihilation,* Phys. Rev. D **46**, 1980 (1992).

[57] G. Heinrich, *Sector Decomposition,* Int. J. Mod. Phys. A **23**, 1457 (2008) [`0803.4177`].

[58] T. Binoth and G. Heinrich, *An Automatized algorithm to compute infrared divergent multiloop integrals,* Nucl. Phys. B **585**, 741 (2000) [`hep-ph/0004013`].

[59] G. Heinrich, *A Numerical method for NNLO calculations,* Nucl. Phys. Proc. Suppl. **116**, 368 (2003) [hep-ph/0211144].

[60] C. Anastasiou, F. Herzog and A. Lazopoulos, *On the factorization of overlapping singularities at NNLO,* JHEP **1103**, 038 (2011) [1011.4867].

[61] K. Melnikov and F. Petriello, *Electroweak gauge boson production at hadron colliders through $O(\alpha(s)^2)$,* Phys. Rev. D **74**, 114017 (2006) [hep-ph/0609070].

[62] C. Anastasiou, F. Herzog and A. Lazopoulos, *The Fully differential decay rate of a Higgs boson to bottom-quarks at NNLO in QCD,* JHEP **1203**, 035 (2012) [1110.2368].

[63] S. Frixione, Z. Kunszt and A. Signer, *Three jet cross-sections to next-to-leading order,* Nucl. Phys. B **467**, 399 (1996) [hep-ph/9512328].

[64] S. Catani and M. H. Seymour, *A General algorithm for calculating jet cross-sections in NLO QCD,* Nucl. Phys. B **485**, 291 (1997) [Erratum-ibid. B **510**, 503 (1998)] [hep-ph/9605323].

[65] R. Frederix, S. Frixione, F. Maltoni and T. Stelzer, *Automation of next-to-leading order computations in QCD: The FKS subtraction,'* JHEP **0910**, 003 (2009) [0908.4272].

[66] T. Gleisberg and F. Krauss, Eur. Phys. J. C **53**, 501 (2008) [0709.2881].

[67] S. Catani and M. Grazzini, *An NNLO subtraction formalism in hadron collisions and its application to Higgs boson production at the LHC,* Phys. Rev. Lett. **98**, 222002 (2007) [hep-ph/0703012].

[68] M. Grazzini, *NNLO predictions for the Higgs boson signal in the $H \to WW \to l\nu l\nu$ and $H \to ZZ \to 4l$ decay channels,* JHEP **0802**, 043 (2008) [0801.3232].

[69] S. Catani, L. Cieri, D. de Florian, G. Ferrera and M. Grazzini, *Diphoton production at hadron colliders: a fully-differential QCD calculation at NNLO,* Phys. Rev. Lett. **108**, 072001 (2012) [1110.2375].

[70] M. Czakon, *A novel subtraction scheme for double-real radiation at NNLO,* Phys. Lett. B **693**, 259 (2010) [1005.0274].

[71] M. Czakon and A. Mitov, *NNLO corrections to top pair production at hadron colliders: the quark-gluon reaction,* JHEP **1301**, 080 (2013) [1210.6832].

[72] M. Czakon and A. Mitov, *NNLO corrections to top-pair production at hadron colliders: the all-fermionic scattering channels,* JHEP **1212**, 054 (2012) [1207.0236].

[73] R. Boughezal, F. Caola, K. Melnikov, F. Petriello and M. Schulze, *Higgs boson production in association with a jet at next-to-next-to-leading order in perturbative QCD,* JHEP **1306**, 072 (2013) [1302.6216].

[74] S. Weinzierl, *NNLO corrections to 3-jet observables in electron-positron annihilation,* Phys. Rev. Lett. **101**, 162001 (2008) [0807.324].

[75] S. Weinzierl, *The Infrared structure of $e^+e^- \to$ 3 jets at NNLO reloaded,* JHEP **0907**, 009 (2009) [0904.1145].

[76] A. Gehrmann-De Ridder, T. Gehrmann, E. W. N. Glover and G. Heinrich, *NNLO corrections to event shapes in $e^+ e^-$ annihilation,* JHEP **0712**, 094 (2007) [0711.4711].

[77] S. Weinzierl, *Event shapes and jet rates in electron-positron annihilation at NNLO,* JHEP **0906**, 041 (2009) [0904.1077].

[78] S. Weinzierl, *Moments of event shapes in electron-positron annihilation at NNLO,* Phys. Rev. D **80**, 094018 (2009) [0909.5056].

[79] E. W. Nigel Glover and J. Pires, *Antenna subtraction for gluon scattering at NNLO,* JHEP **1006**, 096 (2010) [1003.2824].

[80] A. Gehrmann-De Ridder, T. Gehrmann, E. W. N. Glover and J. Pires, *Double Virtual corrections for gluon scattering at NNLO,* JHEP **1302**, 026 (2013) [1211.2710].

[81] G. Abelof and A. Gehrmann-De Ridder, *Antenna subtraction for the production of heavy particles at hadron colliders,* JHEP **1104**, 063 (2011) [1102.2443].

[82] G. Abelof and A. Gehrmann-De Ridder, *Double real radiation corrections to $t\bar{t}$ production at the LHC: the all-fermion processes,* JHEP **1204**, 076 (2012) [1112.4736].

[83] D. A. Kosower, *Multiple singular emission in gauge theories,* Phys. Rev. D **67**, 116003 (2003) [hep-ph/0212097].

[84] D. A. Kosower, *Antenna factorization of gauge theory amplitudes,* Phys. Rev. D **57**, 5410 (1998) [`hep-ph/9710213`].

[85] A. Gehrmann-De Ridder, T. Gehrmann and E. W. N. Glover, *Infrared structure of* $e^+e^- \to 2$ *jets at NNLO,* Nucl. Phys. B **691**, 195 (2004) [`hep-ph/0403057`].

[86] A. Gehrmann-De Ridder, T. Gehrmann and E. W. N. Glover, *Quark-gluon antenna functions from neutralino decay,* Phys. Lett. B **612**, 36 (2005) [`hep-ph/0501291`].

[87] A. Gehrmann-De Ridder, T. Gehrmann and E. W. N. Glover, *Gluon-gluon antenna functions from Higgs boson decay,* Phys. Lett. B **612**, 49 (2005) [`hep-ph/0502110`].

[88] A. Daleo, A. Gehrmann-De Ridder, T. Gehrmann and G. Luisoni, *Antenna subtraction at NNLO with hadronic initial states: initial-final configurations,* JHEP **1001**, 118 (2010) [`0912.0374`].

[89] R. Boughezal, A. Gehrmann-De Ridder and M. Ritzmann, *Antenna subtraction at NNLO with hadronic initial states: double real radiation for initial-initial configurations with two quark flavours,* JHEP **1102**, 098 (2011) [`1011.663`].

[90] T. Gehrmann and P. F. Monni, *Antenna subtraction at NNLO with hadronic initial states: real-virtual initial-initial configurations,* JHEP **1112**, 049 (2011) [`1107.4037`].

[91] A. Gehrmann-De Ridder, T. Gehrmann and M. Ritzmann, *Antenna subtraction at NNLO with hadronic initial states: double real initial-initial configurations,* JHEP **1210**, 047 (2012) [`1207.5779`].

[92] V.A. Smirnov, *Evaluating Feynman Integrals*, Springer, 2004.

[93] A. G. Grozin, *Integration by parts: An Introduction,* Int. J. Mod. Phys. A **26**, 2807 (2011) [`1104.3993`].

[94] A. Gehrmann-De Ridder, T. Gehrmann and G. Heinrich, *Four particle phase space integrals in massless QCD,* Nucl. Phys. B **682**, 265 (2004) [`hep-ph/0311276`].

[95] T. Binoth, J. P. .Guillet, G. Heinrich, E. Pilon and C. Schubert, *An Algebraic/numerical formalism for one-loop multi-leg amplitudes,* JHEP **0510**, 015 (2005) [`hep-ph/0504267`].

[96] G. F. Sterman and M. E. Tejeda-Yeomans, *Multiloop amplitudes and resummation,* Phys. Lett. B **552**, 48 (2003) [`hep-ph/0210130`].

[97] J. Currie, E. W. N. Glover and S. Wells, *Infrared Structure at NNLO Using Antenna Subtraction,* JHEP **1304**, 066 (2013) [`1301.4693`].

[98] V. Del Duca, G. Somogyi and Z. Trocsanyi, *Integration of collinear-type doubly unresolved counterterms in NNLO jet cross sections,* JHEP **1306**, 079 (2013) [`1301.3504`].

[99] G. Somogyi, *A subtraction scheme for computing QCD jet cross sections at NNLO: integrating the doubly unresolved subtraction terms,* JHEP **1304**, 010 (2013) [`1301.3919`].

[100] S. Weinzierl, *Does one need the $O(\epsilon)$- and $O(\epsilon^2)$-terms of one-loop amplitudes in an NNLO calculation?* Phys. Rev. D **84**, 074007 (2011) [`1107.5131`].

[101] A. G. -D. Ridder, T. Gehrmann, E. W. N. Glover and J. Pires, *Second order QCD corrections to jet production at hadron colliders: the all-gluon contribution,* Phys. Rev. Lett. **110**, 162003 (2013) [`1301.7310`].

[102] A. D. Martin, W. J. Stirling, R. S. Thorne and G. Watt, *Parton distributions for the LHC,* Eur. Phys. J. C **63**, 189 (2009) [`0901.0002`].

[103] CMS Collaboration, *Measurement of the double-differential inclusive jet cross section at $\sqrt{s} = 8\,TeV$ with the CMS detector,* CMS-PAS-SMP-12-012 (2013)

[104] Z. Bern, L. J. Dixon and D. A. Kosower, *One loop corrections to two quark three gluon amplitudes,* Nucl. Phys. B **437**, 259 (1995) [`hep-ph/9409393`].

[105] S. Badger, B. Biedermann, P. Uwer and V. Yundin, *Numerical evaluation of virtual corrections to multi-jet production in massless QCD,* Comput. Phys. Commun. **184**, 1981 (2013) [`1209.0100`].

[106] A. Signer, *Helicity Method for next-to-leading order corrections in QCD,* unpublished doctoral thesis, ETH Zürich, 1994.

[107] Z. Kunszt, A. Signer and Z. Trocsanyi, *One loop helicity amplitudes for all $2 \to 2$ processes in QCD and $N = 1$ supersymmetric Yang-Mills theory,* Nucl. Phys. B **411**, 397 (1994) [`hep-ph/9305239`].

[108] J. Pires and E. W. N. Glover, *Double real radiation corrections to gluon scattering at NNLO,* Nucl. Phys. Proc. Suppl. **205-206**, 176 (2010) [`1006.1849`].

[109] R. Kleiss, W. J. Stirling and S. D. Ellis, *A New Monte Carlo Treatment Of Multi-particle Phase Space At High-energies,* Comput. Phys. Commun. **40**, 359 (1986).

[110] E. W. N. Glover, *Two loop QCD helicity amplitudes for massless quark quark scattering,* JHEP **0404**, 021 (2004) [`hep-ph/0401119`].

[111] Z. Kunszt, A. Signer and Z. Trocsanyi, *One loop radiative corrections to the helicity amplitudes of QCD processes involving four quarks and one gluon,* Phys. Lett. B **336**, 529 (1994) [`hep-ph/9405386`].

[112] F. A. Berends, R. Kleiss, P. De Causmaecker, R. Gastmans and T. T. Wu, *Single Bremsstrahlung Processes in Gauge Theories,* Phys. Lett. B **103**, 124 (1981).

[113] P. De Causmaecker, R. Gastmans, W. Troost and T. T. Wu, *Multiple Bremsstrahlung in Gauge Theories at High-Energies. 1. General Formalism for Quantum Electrodynamics,* Nucl. Phys. B **206**, 53 (1982).

[114] R. Kleiss and W. J. Stirling, *Spinor Techniques for Calculating p anti-p $\to W^{\pm}/Z^0 +$ Jets,* Nucl. Phys. B **262**, 235 (1985).

[115] Z. Xu, D. -H. Zhang and L. Chang, *Helicity Amplitudes for Multiple Bremsstrahlung in Massless Nonabelian Gauge Theories,* Nucl. Phys. B **291**, 392 (1987).

[116] S. J. Parke and T. R. Taylor, *An Amplitude for n Gluon Scattering,* Phys. Rev. Lett. **56**, 2459 (1986).

[117] F. A. Berends and W. T. Giele, *Recursive Calculations for Processes with n Gluons,* Nucl. Phys. B **306**, 759 (1988).

[118] R. K. Ellis and J. C. Sexton, *QCD Radiative Corrections to Parton Parton Scattering,* Nucl. Phys. B **269**, 445 (1986).

[119] Z. Kunszt, A. Signer and Z. Trocsanyi, *Collinear limits of one loop helicity amplitudes in QCD,* Heavy Ion Phys. **1**, 43 (1995).

Appendix A

QCD Matrix Elements for Quark-Gluon Scattering

A.1 Tree level $q\bar{q}gg \to 0$

The squared matrix element for the leading order contribution to the process

$$q(p_1) + \bar{q}(p_2) + g(p_3) + g(p_4) \to 0 \tag{A.1.1}$$

can be constructed in a highly compact form using the helicity formalism [112–115] and utilising rules for MHV [116] amplitudes. For two quark, two gluon scattering, there are two colour orderings and four non-vanishing helicity amplitudes, due to analysis in [117], and conservation of helicity along quark lines constraining the quark and antiquark always to have opposite helicities. The helicity amplitudes are given by

$$\mathcal{B}_4^0(q, g_3, g_4, \bar{q}) = i\frac{\langle qi\rangle^3\langle\bar{q}i\rangle}{\langle q3\rangle\langle34\rangle\langle4\bar{q}\rangle\langle q\bar{q}\rangle} \tag{A.1.2}$$

where q has negative helicity and i is the negative helicity gluon. The amplitudes with positive helicity q are obtained by charge conjugation. Summing over helicities,

the leading colour squared matrix element is given by

$$|\mathbf{B}_4^0|^2 = g^4 NV \left(\sum_i s_{qi} s_{\bar{q}i}^3 + s_{qi}^3 s_{\bar{q}i} \right) \times \sum_{\{3,4\}} \frac{1}{s_{q3} s_{34} s_{4\bar{q}} s_{q\bar{q}}} + \mathcal{O}(N^{-2}). \qquad (A.1.3)$$

These are the colour ordered matrix elements used in the subtraction terms in Chapters 5 and 6.

A.2   One loop $q\bar{q}gg \to 0$ pole structure

The squared matrix element taking into account the higher order loop corrections to the process

$$q(p_1) + \bar{q}(p_2) + g(p_3) + g(p_4) \to 0 \qquad (A.2.4)$$

is constructed by the interference of the loop amplitude with its tree level counterpart,

$$|\mathbf{B}_4^1|^2 = \langle \mathcal{B}_4^0 | \mathcal{B}_4^{1,\dagger} \rangle + \langle \mathcal{B}_4^1 | \mathcal{B}_4^{0,\dagger} \rangle. \qquad (A.2.5)$$

The full expressions for the squared matrix element are well-known, and can be found in [107, 118].

The pole structure of the various matrix elements can be constructed by utilising the formalism of Chapter 2, and requires no knowledge of the explicit form of the amplitudes. Decomposing the tree amplitude $|\mathcal{B}_4^{(0)}\rangle$ and unrenormalised one-loop amplitude $|\mathcal{B}_4^{(1,un)}\rangle$ in terms of the $SU(N)$ generators T^a results in

$$|\mathcal{B}_4^{(0)}\rangle = \sum_{P(i,j)} (T^{a_i} T^{a_j})_{ij} \mathcal{B}_4^0(1_q, i_g, j_g, 2_{\bar{q}}) \qquad (A.2.6)$$

for the tree level contribution, and

$$\begin{aligned} |\mathcal{B}_4^{(1,un)}\rangle &= N \sum_{P(i,j)} (T^{a_i} T^{a_j})_{ij} \mathcal{B}_{4,a}^1(1_q, i_g, j_g, 2_{\bar{q}}) \\ &+ N_F \Big[\sum_{P(i,j)} (T^{a_i} T^{a_j})_{ij} - \frac{2}{N} \mathrm{Tr}(T^{a_3} T^{a_4}) \delta_{ij} \Big] \mathcal{B}_{4,f}^1(1_q, i_g, j_g, 2_{\bar{q}}) \end{aligned}$$

$$+ \quad \text{Tr}(T^{a_3}T^{a_4})\delta_{ij}\mathcal{B}^1_{4,b}(1_q, 3_g, 4_g, 2_{\bar{q}}) \tag{A.2.7}$$

for the one loop amplitude. The sum is over the two permutations of the gluons, whereas those amplitudes without a summation are invariant under an exchange of the gluon. The tree level amplitudes enjoy reflection symmetry. To proceed, by setting $N_F = 0$, the amplitudes are expressed as vectors in colour space,

$$|\mathcal{B}_4^{(0)}\rangle = (\mathcal{T}_1, \mathcal{T}_2, 0)^T, \tag{A.2.8}$$

$$|\mathcal{B}_4^{(1,un)}\rangle = (\mathcal{L}_1, \mathcal{L}_2, \mathcal{L}_3)^T. \tag{A.2.9}$$

with the projection of $|\mathcal{B}_4^{(0)}\rangle$ and $|\mathcal{B}_4^{(1,un)}\rangle$ in each direction of colour space given by $\mathcal{T}_i$ and $\mathcal{L}_i$ respectively. They are obtained from the colour subamplitudes $\mathcal{B}_4^0$ and $\mathcal{B}_4^1$, although for the extraction of the pole structure, only the squared tree level matrix elements are necessary. The colour space is spanned by the basis constructed from the colour structures present in the full loop amplitude, namely

$$\mathcal{K}_1 = (T^{a_3}T^{a_4})_{ij},$$

$$\mathcal{K}_2 = (T^{a_4}T^{a_3})_{ij},$$

$$\mathcal{K}_3 = \text{Tr}(T^{a_3}T^{a_4})\delta_{ij}. \tag{A.2.10}$$

In this colour basis, it is possible to construct the infra-red singularity operator $\mathbf{I}^{(1)}(\epsilon)$, having the form

$$\mathbf{I}^{(1)}(\epsilon) = \frac{e^{\epsilon\gamma}}{\Gamma(1-\epsilon)} \times \begin{pmatrix} \mathbf{X}(s,t,u,\epsilon) & 0 & \mathbf{Y}(u,t,s,\epsilon) \\ 0 & \mathbf{X}(s,u,t,\epsilon) & \mathbf{Y}(t,u,s,\epsilon) \\ \mathbf{Y}(s,t,u,\epsilon) & \mathbf{Y}(s,u,t,\epsilon) & \mathbf{Z}(s,\epsilon) \end{pmatrix}, \tag{A.2.11}$$

where the elements are defined by

$$\mathbf{X}(s,t,u,\epsilon) = -\frac{1}{2}\left(\frac{1}{\epsilon^2} + \frac{3}{2\epsilon}\right)\left[N(2\mathcal{U} + \mathcal{S}) - \frac{1}{N}\mathcal{S}\right], \tag{A.2.12}$$

$$\mathbf{Y}(s,t,u,\epsilon) = \left(\frac{1}{\epsilon^2} + \frac{3}{4\epsilon} + \frac{\beta_0}{2N\epsilon}\right)[\mathcal{T} + \mathcal{S}], \tag{A.2.13}$$

$$\mathbf{Z}(s,\epsilon) \;=\; -\frac{1}{2}\left[\left(\frac{2}{\epsilon^2} + \frac{3}{2\epsilon} + \frac{\beta_0}{N\epsilon}\right)N\mathcal{S} - \left(\frac{1}{\epsilon^2} + \frac{3}{2\epsilon}\right)\frac{1}{N}\mathcal{S}\right], \quad (\text{A.2.14})$$

and

$$\mathcal{S} = \left(-\frac{\mu^2}{s}\right)^{\epsilon}, \qquad \mathcal{T} = \left(-\frac{\mu^2}{t}\right)^{\epsilon}, \qquad \mathcal{U} = \left(-\frac{\mu^2}{u}\right)^{\epsilon}, \qquad (\text{A.2.15})$$

with s, t and u being the standard Mandelstaam variables. Acting with the matrix $\mathbf{I}^{(1)}(\epsilon)$ upon the state vector $|\mathcal{B}_4^{(0)}\rangle$ produces a new vector $|\mathcal{M}\rangle$ that contains the pole structure of $|\mathcal{B}_4^{(1,un)}\rangle$. Since we are after the interference of the tree and the loop amplitudes, all that remains is the contraction of $|\mathcal{M}\rangle$ with the tree level amplitude in colour space, which can be expressed by summing over spins and colours as

$$\langle\mathcal{B}_4^{(0)}|\mathcal{M}\rangle = \sum_{\text{spins}} \sum_{\text{colours}} \sum_{i,j=1}^{3} \mathcal{T}_i^* \mathcal{M}_j \mathcal{K}_i^* \mathcal{K}_j. \qquad (\text{A.2.16})$$

The factors for the sum over colours are obtained via the elements of the matrix $\mathcal{K}_{\mathcal{M}}$, where $(\mathcal{K}_{\mathcal{M}})_{ij} = \mathcal{K}_i^* \mathcal{K}_j$, which is given by

$$\mathcal{K}_{\mathcal{M}} = \frac{V}{4N}\begin{pmatrix} V & -1 & N \\ -1 & V & N \\ N & N & N^2 \end{pmatrix}, \qquad (\text{A.2.17})$$

and the interference of the tree level amplitudes $\mathcal{T}_{\mathcal{M}}$, with $(\mathcal{T}_{\mathcal{M}})_{ij} = \mathcal{T}_i^* \mathcal{M}_j$, is expressed in matrix form as

$$\mathcal{T}_{\mathcal{M}} = \frac{8(1-\epsilon)(u^2 + t^2 - \epsilon s^2)}{s^2 tu}\begin{pmatrix} t^2 & ut & 0 \\ ut & u^2 & 0 \\ 0 & 0 & 0 \end{pmatrix}. \qquad (\text{A.2.18})$$

The evaluation of the interference term, and subsequent decomposition according to powers of N, result in the isolation of the pole structures of the one-loop matrix elements.

A.3 One loop $q\bar{q}ggg \to 0$ pole structure

We now consider the squared matrix element with three gluons and a single quark pair,

$$q(p_1) + \bar{q}(p_2) + g(p_3) + g(p_4) + g(p_5) \to 0. \tag{A.3.19}$$

Examining the form of the amplitude in (5.2.22), we can set up the basis spanning the colour space to be

$$
\begin{aligned}
\mathcal{K}_1 &= (T^{a_3}T^{a_4}T^{a_5})_{ij} \\
\mathcal{K}_2 &= (T^{a_3}T^{a_5}T^{a_4})_{ij} \\
\mathcal{K}_3 &= (T^{a_4}T^{a_5}T^{a_3})_{ij} \\
\mathcal{K}_4 &= (T^{a_4}T^{a_3}T^{a_5})_{ij} \\
\mathcal{K}_5 &= (T^{a_5}T^{a_3}T^{a_4})_{ij} \\
\mathcal{K}_6 &= (T^{a_5}T^{a_4}T^{a_3})_{ij} \\
\mathcal{K}_7 &= (T^{a_3})_{ij}Tr(T^{a_4}T^{a_5}) \\
\mathcal{K}_8 &= (T^{a_4})_{ij}Tr(T^{a_5}T^{a_3}) \\
\mathcal{K}_9 &= (T^{a_5})_{ij}Tr(T^{a_3}T^{a_4}) \\
\mathcal{K}_{10} &= \delta_{ij}Tr(T^{a_3}T^{a_4}T^{a_5}) \\
\mathcal{K}_{11} &= \delta_{ij}Tr(T^{a_3}T^{a_5}T^{a_4})
\end{aligned}
$$

such that the tree level one-loop amplitudes can be written as an eleven dimensional vector in colour space:

$$|\mathcal{M}^{(0)}\rangle = (\mathcal{T}_1, \ldots, \mathcal{T}_6, 0 \ldots 0)^T, \tag{A.3.20}$$

$$|\mathcal{M}^{(1,un)}\rangle = (\mathcal{L}_1, \mathcal{L}_2, \ldots \mathcal{L}_{11})^T, \tag{A.3.21}$$

Using this basis and applying Catani's formula we find that

$$\boldsymbol{I}^{(1)}(\epsilon) = \frac{1}{2}\frac{e^{\epsilon\gamma}}{\Gamma(1-\epsilon)} \times \begin{pmatrix}
\mathbf{A}_1 & 0 & 0 & 0 & 0 & 0 & \mathbf{B}_1 & 0 & \mathbf{C}_1 & \mathbf{D}_1 & 0 \\
0 & \mathbf{A}_2 & 0 & 0 & 0 & 0 & \mathbf{B}_2 & \mathbf{C}_2 & 0 & 0 & \mathbf{D}_2 \\
0 & 0 & \mathbf{A}_3 & 0 & 0 & 0 & 0 & \mathbf{B}_3 & \mathbf{C}_3 & 0 & \mathbf{D}_3 \\
0 & 0 & 0 & \mathbf{A}_4 & 0 & 0 & \mathbf{C}_4 & \mathbf{B}_4 & 0 & \mathbf{D}_4 & 0 \\
0 & 0 & 0 & 0 & \mathbf{A}_5 & 0 & 0 & \mathbf{C}_5 & \mathbf{B}_5 & \mathbf{D}_5 & 0 \\
0 & 0 & 0 & 0 & 0 & \mathbf{A}_6 & \mathbf{C}_6 & 0 & \mathbf{B}_6 & 0 & \mathbf{D}_6 \\
\mathbf{B}_1 & \mathbf{B}_2 & 0 & \mathbf{C}_4 & 0 & \mathbf{C}_6 & \mathbf{E}_1 & 0 & 0 & 0 & 0 \\
0 & \mathbf{C}_2 & \mathbf{B}_3 & \mathbf{B}_4 & \mathbf{C}_5 & 0 & 0 & \mathbf{E}_4 & 0 & 0 & 0 \\
\mathbf{C}_1 & 0 & \mathbf{C}_3 & 0 & \mathbf{B}_5 & \mathbf{B}_6 & 0 & 0 & \mathbf{E}_6 & 0 & 0 \\
\mathbf{D}_1 & 0 & 0 & \mathbf{D}_4 & \mathbf{D}_5 & 0 & 0 & 0 & 0 & \mathbf{F}_1 & 0 \\
0 & \mathbf{D}_2 & \mathbf{D}_3 & 0 & 0 & \mathbf{D}_6 & 0 & 0 & 0 & 0 & \mathbf{F}_1
\end{pmatrix}$$

where the elements are given as

$$\mathbf{A}_n = -N\left[\frac{1}{\epsilon^2} + \frac{\beta_0}{N\epsilon}\right]\left(\frac{\mathcal{S}_{1i}}{2} + \frac{\mathcal{S}_{2k}}{2} + \mathcal{S}_{ij} + \mathcal{S}_{jk}\right) + N\left[\frac{1}{\epsilon^2} + \frac{3}{2\epsilon}\right]\left(\frac{\mathcal{S}_{12}}{N^2} - \frac{\mathcal{S}_{1i}}{2} - \frac{\mathcal{S}_{2k}}{2}\right)$$

$$\mathbf{B}_n = \left[\frac{1}{\epsilon^2} + \frac{\beta_0}{N\epsilon}\right](\mathcal{S}_{ik} - \mathcal{S}_{2i} - \mathcal{S}_{jk} + \mathcal{S}_{2j}) + \left[\frac{\beta_0}{2N\epsilon} - \frac{3}{4\epsilon}\right](\mathcal{S}_{2i} - \mathcal{S}_{2j})$$

$$\mathbf{C}_n = \left[\frac{1}{\epsilon^2} + \frac{\beta_0}{N\epsilon}\right](\mathcal{S}_{1j} - \mathcal{S}_{1k} - \mathcal{S}_{ij} + \mathcal{S}_{ik}) + \left[\frac{\beta_0}{2N\epsilon} - \frac{3}{4\epsilon}\right](\mathcal{S}_{1k} - \mathcal{S}_{1j})$$

$$\mathbf{D}_n = \left[\frac{1}{\epsilon^2} + \frac{\beta_0}{N\epsilon}\right]\left(\frac{\mathcal{S}_{1k}}{2} + \frac{\mathcal{S}_{2i}}{2} - \mathcal{S}_{ik}\right) + \left[\frac{1}{\epsilon^2} + \frac{3}{2\epsilon}\right]\left(\frac{\mathcal{S}_{1k}}{2} + \frac{\mathcal{S}_{2i}}{2} - \mathcal{S}_{12}\right)$$

$$\mathbf{E}_n = N\left[\frac{1}{\epsilon^2} + \frac{\beta_0}{N\epsilon}\right]\left(-\frac{\mathcal{S}_{1i}}{2} - \frac{\mathcal{S}_{2i}}{2} - 2\mathcal{S}_{jk}\right) + N\left[\frac{1}{\epsilon^2} + \frac{3}{2\epsilon}\right]\left(\frac{\mathcal{S}_{12}}{N^2} - \frac{\mathcal{S}_{1i}}{2} - \frac{\mathcal{S}_{2i}}{2}\right)$$

$$\mathbf{F}_n = \left[-\frac{1}{\epsilon^2} - \frac{\beta_0}{\epsilon}\right](\mathcal{S}_{ij} + \mathcal{S}_{ik} + \mathcal{S}_{jk}) - \left[\frac{1}{\epsilon^2} + \frac{3}{2\epsilon}\right](2C_F\mathcal{S}_{12})$$

and

$$\mathcal{S}_{ij} = \left(\frac{-\mu^2}{2p_i \cdot p_j}\right)^{\epsilon}. \tag{A.3.22}$$

The functions $\mathbf{B}_n$ and $\mathbf{C}_n$ are related under quark exchange but are kept as separate functions to maintain quark ordering. The subscripts of these function relate to the

colour ordering of the gluons as defined by the colour basis in (A.3.20). Thus for $\mathbf{M}_n$, where $\mathbf{M} \in \{\mathbf{A} \cdots \mathbf{F}\}$, the arguments i, j, k are given by the nth triplet in the ordered set $\{i, j, k\} \in \{\{2,3,4\}, \{2,4,3\}, \{3,2,4\}, \{3,4,2\}, \{4,2,3\}, \{4,3,2\}\}$.

Note that the elements $\mathbf{E}$, and $\mathbf{F}$ are not required for the one loop pole construction, since they will always be hitting onto a colour basis direction that vanishes at the tree level case.

Acting with the matrix $\mathbf{I}^{(1)}(\epsilon)$ upon the state vector $|\mathcal{B}_5^{(0)}\rangle$ produces a new vector $|\mathcal{M}\rangle$ that contains the pole structure of $|\mathcal{B}_5^{(1,un)}\rangle$. Since we are after the interference of the tree and the loop amplitudes, all that remains is the contraction of $|\mathcal{M}\rangle$ with the tree level amplitude in colour space, which can be expressed by summing over spins and colours as

$$\langle \mathcal{B}_5^{(0)}|\mathcal{M}\rangle = \sum_{\text{spins}} \sum_{\text{colours}} \sum_{i,j=1}^{3} \mathcal{T}_i^* \mathcal{M}_j \mathcal{K}_i^* \mathcal{K}_j. \tag{A.3.23}$$

The factors for the sum over colours are obtained via the elements of the matrix $\mathcal{K}_{\mathcal{M}}$, where $(\mathcal{K}_{\mathcal{M}})_{ij} = \mathcal{K}_i^* \mathcal{K}_j$, and is given by (A.3.24).

The $\mathbf{A}_i$ immediately can be used to construct the pole structure of the leading colour squared matrix element due to the diagonal 6×6 block of (A.3.22). These correspond to the tree-type colour structures. Converted into integrated antenna strings multiplying tree level squared matrix elements they take the form given in (5.2.26). Again, the pole structure could be ascertained without knowledge of the explicit form of the one-loop amplitudes. Nevertheless, the finite contributions are of course necessary for a full calculation, which were obtained from [106]. The amplitudes were colour decomposed according to (5.2.22).

$$\mathcal{K}_{\mathcal{M}} = \frac{V}{8N^2}
\begin{pmatrix}
V^2 & -V & -V & 1 & 1 & N^2+1 & VN & -N & NV & NV-N & -2N \\
-V & V^2 & 1 & N^2+1 & -V & 1 & NV & NV & -N & -2N & NV-N \\
-V & 1 & V^2 & -V & N^2+1 & 1 & -N & NV & NV & NV-N & -2N \\
1 & N^2+1 & -V & V^2 & 1 & -V & NV & NV & -N & NV-N & -2N \\
1 & -V & N^2+1 & 1 & V^2 & -V & -N & NV & NV & NV-N & -2N \\
N^2+1 & 1 & 1 & -V & -V & V^2 & NV & -N & NV & -2N & NV-N \\
NV & NV & -N & NV & -N & NV & N^2V & N^2 & N^2 & 0 & 0 \\
-N & NV & NV & NV & NV & -N & N^2 & N^2V & N^2 & 0 & 0 \\
NV & -N & NV & -N & NV & NV & N^2 & N^2 & N^2V & 0 & 0 \\
NV-N & -2N & NV-N & NV-N & NV-N & -2N & 0 & 0 & 0 & VN^2-N^2 & -2N^2 \\
-2N & NV-N & -2N & -2N & -2N & NV-N & 0 & 0 & 0 & -2N^2 & VN^2-N^2
\end{pmatrix}
\qquad (\text{A.3.24})$$

Appendix B

QCD Matrix Elements for Scattering of Two Non-Identical Quark Pairs

B.1 Tree level $\bar{q}\bar{Q}Qq \to 0$

The squared matrix element for the leading order contribution to the process

$$\bar{q}(p_1) + \bar{Q}(p_2) + Q(p_3) + q(p_4) \to 0, \tag{B.1.1}$$

can again be constructed in a highly compact form using the helicity formalism. Summing over helicities, the squared matrix element is given by

$$|\mathbf{C}_4^0|^2 = g^4(N^2 - 1)\left(\frac{s^2 + u^2}{t^2} - \epsilon\right) \tag{B.1.2}$$

These are the colour ordered matrix elements used in the subtraction terms in Chapter 6.

B.2 One loop $\bar{q}\bar{Q}Qq \to 0$ pole structure

The squared matrix element taking into account the higher order loop corrections to the process

$$\bar{q}(p_1) + \bar{Q}(p_2) + Q(p_3) + q(p_4) \to 0 \tag{B.2.3}$$

are well-known, and can be found in [107, 118].

The pole structure of the various matrix elements can be constructed by utilising the formalism of Chapter 2, and requires no knowledge of the explicit form of the amplitudes. Decomposing the tree amplitude $|\mathcal{C}_4^{(0)}\rangle$ and unrenormalised one-loop amplitude $|\mathcal{C}_4^{(1,un)}\rangle$ in terms of the $SU(N)$ generators T^a for the tree level and one loop contribution, and results in (6.1.11). We express $|\mathcal{C}_4^{(1)}\rangle$ as a four dimensional vector in colour space:

$$|\mathcal{C}_4^{(1)}\rangle = (\mathcal{L}_1, \mathcal{L}_2)^T, \tag{B.2.4}$$

where the colour space is spanned by the basis

$$\mathcal{K}_1 = \delta_{Q\bar{q}}\delta_{q\bar{Q}}$$
$$\mathcal{K}_2 = \delta_{q\bar{q}}\delta_{Q\bar{Q}}$$

We find Catani's formula given by

$$\boldsymbol{I}^{(1)}(\epsilon) = \frac{1}{2}\frac{e^{\epsilon\gamma}}{\Gamma(1-\epsilon)} \times \begin{pmatrix} \mathbf{A} & \mathbf{B} \\ \mathbf{B'} & \mathbf{A'} \end{pmatrix}$$

where

$$\mathbf{A} = \frac{1}{N}\left[\frac{1}{\epsilon^2} + \frac{3}{2\epsilon}\right]((N^2-1)\mathcal{S}_{q\bar{Q}} + \mathcal{S}_{qQ} - \mathcal{S}_{q\bar{q}}) \tag{B.2.5}$$

$$\mathbf{B} = N\left[\frac{1}{\epsilon^2} + \frac{3}{2\epsilon}\right](\mathcal{S}_{q\bar{Q}} - \mathcal{S}_{qQ}) \tag{B.2.6}$$

whereby $\mathbf{A'}$ and $\mathbf{B'}$ are obtained from $\mathbf{A}$ and $\mathbf{B}$ respectively via exchange of antiquark

labels, that is

$$\mathbf{A}' = \mathbf{A}(\bar{q} \leftrightarrow \bar{Q}). \tag{B.2.7}$$

Acting the matrix $\mathbf{I}^{(1)}(\epsilon)$ upon the state vector $|\mathcal{C}_4^{(0)}\rangle$ produces a new vector $|\mathcal{M}\rangle$ equivalent to the pole structure of $|\mathcal{C}_4^{(1,un)}\rangle$. Since we are after the interference of the tree and the loop amplitudes, all that remains is the contraction of $|\mathcal{M}\rangle$ with the tree level amplitude in colour space, which can be expressed by summing over spins and colours as

$$\langle \mathcal{C}_4^{(0)}|\mathcal{M}\rangle = \sum_{\text{spins}} \sum_{\text{colours}} \sum_{i,j=1}^{3} \mathcal{T}_i^* \mathcal{M}_j \mathcal{K}_i^* \mathcal{K}_j \tag{B.2.8}$$

The factors for the sum over colours are obtained via the elements of the matrix $\mathcal{K}_{\mathcal{M}}$, where again $(\mathcal{K}_{\mathcal{M}})_{ij} = \mathcal{K}_i^* \mathcal{K}_j$:

$$\mathcal{K}_{\mathcal{M}} = \begin{pmatrix} N^2 & N \\ N & N^2 \end{pmatrix}, \tag{B.2.9}$$

and the interference of the tree level amplitudes $\mathcal{T}_{\mathcal{M}}$, with $(\mathcal{T}_{\mathcal{M}})_{ij} = \mathcal{T}_i^* \mathcal{M}_j$, is

$$\mathcal{T}_{\mathcal{M}} = 2\left(\frac{t^2 + u^2}{s^2} - e\right)\begin{pmatrix} 1 & -1/N \\ -1/N & 1/N^2 \end{pmatrix}. \tag{B.2.10}$$

The evaluation of the interference term, and subsequent decomposition according to powers of N, result in the isolation of the pole structures of the one-loop matrix elements.

B.3 One loop $\bar{q}\bar{Q}Qqg \to 0$ pole structure

The squared matrix element taking into account the higher order loop corrections to the process

$$\bar{q}(p_1) + \bar{Q}(p_2) + q(p_3) + q(p_4) + g(p_5) \to 0 \tag{B.3.11}$$

are well-known, and can be found in [111, 119].

The pole structure of the various matrix elements can be constructed by utilising the formalism of Chapter 2, and requires no knowledge of the explicit form of the amplitudes. Decomposing the tree amplitude $|\mathcal{C}_5^{(0)}\rangle$ and unrenormalised one-loop amplitude $|\mathcal{C}_5^{(1,un)}\rangle$ in terms of the $SU(N)$ generators T^a for the tree level and one loop contribution, and results in (6.1.11). We express $|\mathcal{C}_5^{(1)}\rangle$ as a four dimensional vector in colour space:

$$|\mathcal{M}_4^{(1)}\rangle = (\mathcal{L}_1, \mathcal{L}_2, \mathcal{L}_3, \mathcal{L}_4)^T, \tag{B.3.12}$$

where the colour space is spanned by the basis

$$\begin{aligned}
\mathcal{K}_1 &= (T^a)_{Q\bar{q}}\delta_{Q\bar{q}} \\
\mathcal{K}_2 &= (T^a)_{q\bar{Q}}\delta_{q\bar{Q}} \\
\mathcal{K}_3 &= (T^a)_{q\bar{q}}\delta_{Q\bar{Q}} \\
\mathcal{K}_4 &= (T^a)_{Q\bar{Q}}\delta_{q\bar{q}}
\end{aligned}$$

We find Catani's formula given by

$$\boldsymbol{I}^{(1)}(\epsilon) = \frac{1}{2}\frac{e^{\epsilon\gamma}}{\Gamma(1-\epsilon)} \times \begin{pmatrix} \mathbf{A} & 0 & \mathbf{B} & \mathbf{C} \\ 0 & \mathbf{D} & \mathbf{E} & \mathbf{F} \\ \mathbf{F'} & \mathbf{E'} & \mathbf{D'} & 0 \\ \mathbf{C'} & \mathbf{B'} & 0 & \mathbf{A'} \end{pmatrix}$$

where

$$\begin{aligned}
\mathbf{A} &= \left[\frac{1}{\epsilon^2} + \frac{\beta_0}{2N\epsilon} + \frac{3}{4\epsilon}\right]\left(-2C_F\mathcal{S}_{13} + \frac{1}{N}(\mathcal{S}_{14} - \mathcal{S}_{12} + \mathcal{S}_{23} + \mathcal{S}_{24} - \mathcal{S}_{34})\right. \\
&\quad \left. -N(\mathcal{S}_{25} + \mathcal{S}_{45})\right) + \frac{1}{N}\left[\frac{\beta_0}{2N\epsilon} - \frac{3}{4\epsilon}\right](\mathcal{S}_{23} + \mathcal{S}_{24} - \mathcal{S}_{34}), \\
\mathbf{B} &= \left[\frac{1}{\epsilon^2} + \frac{\beta_0}{2N\epsilon} + \frac{3}{4\epsilon}\right](\mathcal{S}_{12} - \mathcal{S}_{15} - \mathcal{S}_{23} + \mathcal{S}_{35}) + \left[\frac{\beta_0}{2N\epsilon} - \frac{3}{4\epsilon}\right](\mathcal{S}_{15} - \mathcal{S}_{23}), \\
\mathbf{C} &= \left[\frac{1}{\epsilon^2} + \frac{\beta_0}{2N\epsilon} + \frac{3}{4\epsilon}\right](\mathcal{S}_{15} - \mathcal{S}_{35} - \mathcal{S}_{14} + \mathcal{S}_{34}) + \left[\frac{\beta_0}{2N\epsilon} - \frac{3}{4\epsilon}\right](\mathcal{S}_{34} - \mathcal{S}_{15}), \\
\mathbf{D} &= \left[\frac{1}{\epsilon^2} + \frac{\beta_0}{2N\epsilon} + \frac{3}{4\epsilon}\right]\left(-2C_F\mathcal{S}_{24} - N(\mathcal{S}_{15} + \mathcal{S}_{35}) + \frac{1}{N}(\mathcal{S}_{13} - \mathcal{S}_{12} + \mathcal{S}_{14}\right.
\end{aligned}$$

$$+S_{23} - S_{34}\bigg) + \left[\frac{\beta_0}{2N\epsilon} - \frac{3}{4\epsilon}\right]\left(NS_{15} + \frac{1}{N}(S_{23} - S_{34})\right)$$

$$\mathbf{E} = \left[\frac{1}{\epsilon^2} + \frac{\beta_0}{2N\epsilon}\right](S_{25} - S_{23} + S_{34} - S_{45}) + \left[\frac{3}{4\epsilon} - \frac{\beta_0}{2N\epsilon}\right](S_{25} - S_{45})$$

$$\mathbf{F} = \left[\frac{1}{\epsilon^2} + \frac{\beta_0}{2N\epsilon} + \frac{3}{4\epsilon}\right](S_{12} - S_{14} - S_{25} + S_{45})$$

$$\text{(B.3.13)}$$

The primed functions are related via $(3 \leftrightarrow 4)$ exchange, i.e.,

$$\mathbf{X}'(\bar{q}, \bar{Q}, Q, q, g) = \mathbf{X}(\bar{q}, \bar{Q}, q, Q, g). \tag{B.3.14}$$

Acting the matrix $\mathbf{I}^{(1)}(\epsilon)$ upon the state vector $|\mathcal{C}_5^{(0)}\rangle$ produces a new vector $|\mathcal{M}\rangle$ equivalent to the pole structure of $|\mathcal{C}_5^{(1,un)}\rangle$. Since we are after the interference of the tree and the loop amplitudes, all that remains is the contraction of $|\mathcal{M}\rangle$ with the tree level amplitude in colour space, which can be expressed by summing over spins and colours as

$$\langle \mathcal{C}_5^{(0)}|\mathcal{M}\rangle = \sum_{\text{spins}} \sum_{\text{colours}} \sum_{i,j=1}^{3} \mathcal{T}_i^* \mathcal{M}_j \mathcal{K}_i^* \mathcal{K}_j. \tag{B.3.15}$$

The factors for the sum over colours are obtained via the elements of the matrix $\mathcal{K}_{\mathcal{M}}$,

$$\mathcal{K}_{\mathcal{M}} = \frac{V}{2}\begin{pmatrix} N & 0 & 1 & 1 \\ 0 & N & 1 & 1 \\ 1 & 1 & N & 0 \\ 1 & 1 & 0 & N \end{pmatrix}. \tag{B.3.16}$$

The $\mathbf{A}_i$ can be used to construct the pole structure of the leading colour squared matrix element, given in (6.2.24) Again, the pole structure could be ascertained without knowledge of the explicit form of the one-loop amplitudes. Nevertheless, the finite contributions are of course necessary for a full calculation, which were obtained from [106]. The amplitudes were colour decomposed according to (6.1.11).

Appendix C

Full Numerical Results

In this appendix we collate the full set of plots illustrating the success of the real-virtual subtraction terms in the matching of the finite contribution of full matrix elements to the subtraction term in all single unresolved limits. The poles are reproduced exactly: all plots for $1/\epsilon$ and $1/\epsilon^2$ contributions are identical to those given in Figures 5.6, 5.8, 5.9 and 6.1, and are not repeated here. We includes all real-virtual contributions to the real-virtual five parton quark gluon scattering and the non-identical quark-antiquark initiated contribution to the five parton process with two non-identical quark pairs. The plots follow an identical form to those presented in previous sections, namely they represent the ratio

$$ R = \left. \frac{d\hat{\sigma}_{NNLO}^{RV}}{d\hat{\sigma}_{NNLO}^{T}} \right|_{finite} . $$

For each divergent configuration, a set of phase space points are generated with `RAMBO` [109], and the ratio calculated within the singular region defined by constraints that are tightened to force the phase space points closer to the singular point. The green data is furthest from the singular point, the blue closer and the red closest.

C.1   Finite real-virtual subtraction for $q\bar{q} \rightarrow ggg$

Here we consider the case of the real-virtual contribution to the two quark, two gluon Born process, that of the leading colour five parton one loop squared matrix element,

which allows for a single unresolved parton. Both quarks are in the initial state. The cross section reads

$$d\hat{\sigma}_{NNLO}^{RV} = \mathcal{N}_{q\bar{q},5}^1 \int d\Phi_3 \frac{1}{3!} \frac{dx_1}{x_1} \frac{dx_2}{x_2} \sum_{P(i,j,k)} B_5^0(\hat{1}_q, i_g, j_g, k_g, \hat{2}_{\bar{q}}) J_2^{(3)}(p_3, p_4, p_5), \ \text{(C.1.1)}$$

where the sum runs over the permutations of the gluons. The subtraction term for this contribution is given in (5.4.39). In the sum over the six gluon permutations we will encounter soft limits of each gluon. There are collinear limits between all possible pairing of gluons, and also between each gluon and each of the quark and antiquark. Since both quarks are in the initial state, there is no $q||\bar{q}$ collinear limit.
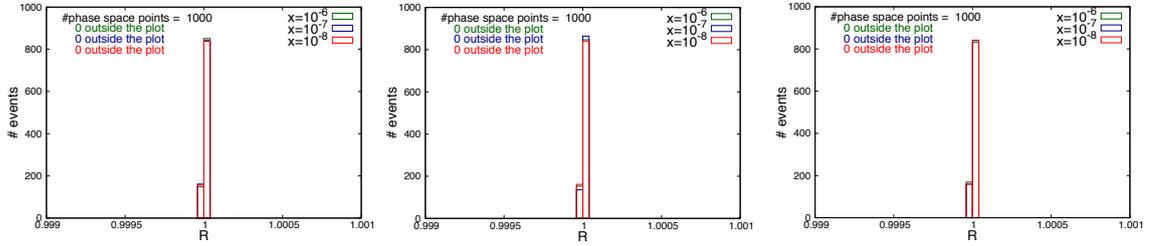
Figure C.1: Final soft limits for i_g(left), j_g (centre) and k_g(right).
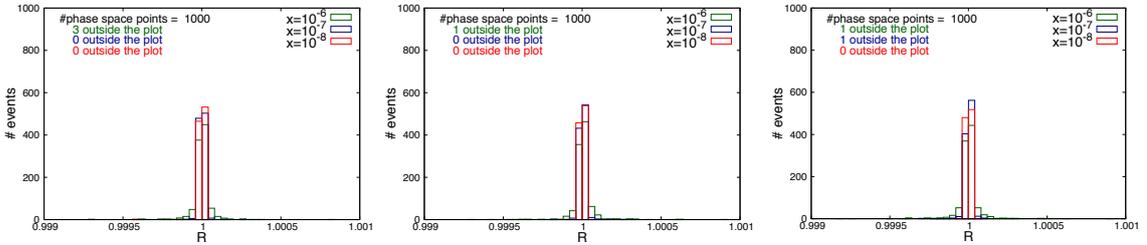
Figure C.2: Final-final collinear limits for $i_g||j_g$(left), $i_g||k_g$ (centre) and $j_g||k_g$(right).
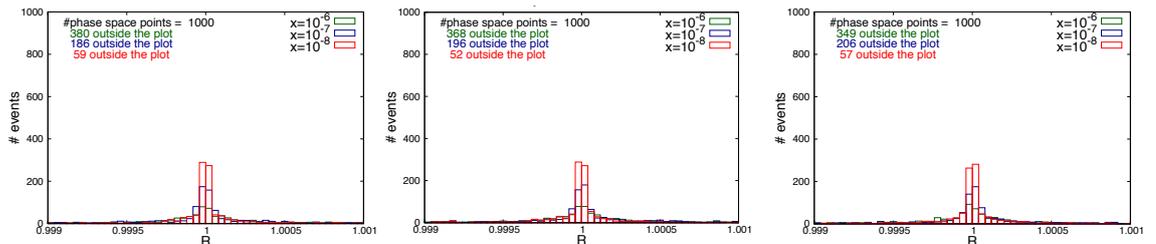
Figure C.3: Initial-final collinear limits for $\hat{1}_q||i_g$(left), $\hat{1}_q||j_g$ (centre) and $\hat{1}_q||k_g$(right).
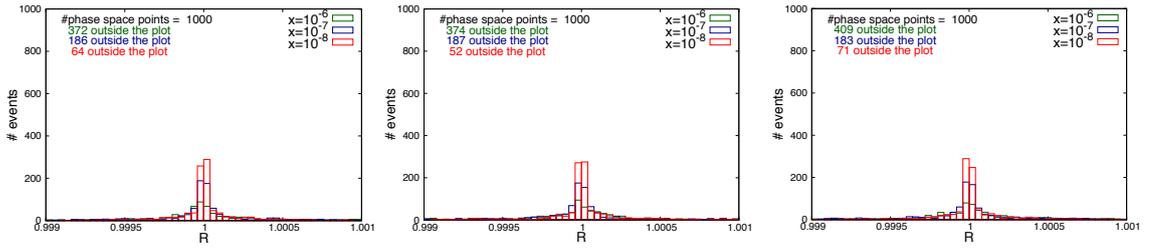
Figure C.4: Initial-final collinear limits for $\hat{2}_q||i_g$(left), $\hat{2}_q||j_g$ (centre) and $\hat{2}_q||k_g$(right).

C.2   Finite real-virtual subtraction for $gg \to q\bar{q}g$

Here we consider the case of the real-virtual contribution to the two quark, two gluon Born process, that of the leading colour five parton one loop squared matrix element, which allows for a single unresolved parton. Two gluons are in the initial state. The cross section reads

$$d\hat{\sigma}^{RV}_{NNLO} = \mathcal{N}^1_{gg,5} \int d\Phi_3 \frac{1}{3!} \frac{dx_1}{x_1} \frac{dx_2}{x_2} \sum_{P(\hat{1},\hat{2},i)} B^0_5(j_q, \hat{1}_g, \hat{2}_g, i_g, k_{\bar{q}}) J^{(3)}_2(p_3, p_4, p_5), \quad \text{(C.2.2)}$$

where the sum runs over the permutations of the gluons. The independent subtraction terms for this contribution are given in (5.5.55) and (5.5.57), with the terms for the remaining four permutations obtained via Table 5.3. In the sum over the six gluon permutations only the single final state gluon can go soft. We therefore observe no spike in Figure C.5 (right and centre), since these correspond to the final state quarks which cannot by current conservation go singly unresolved. There are collinear limits between all possible pairing of gluons, and also between each gluon and each of the quark and antiquark. We observe similar behaviour in the R ratio for the pairs of collinear limits where $(\hat{1} \leftrightarrow \hat{2})$ occurs. This is to be expected naïvely due to the symmetry of the physical matrix element.
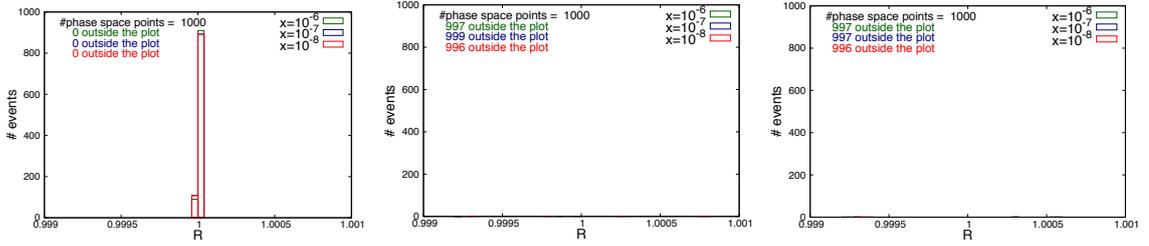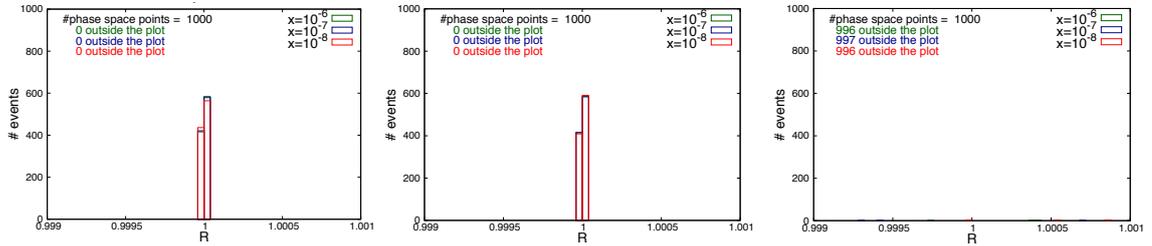
Figure C.5: Final soft limits for i_g(left), j_q (centre) and $k_{\bar{q}}$(right).
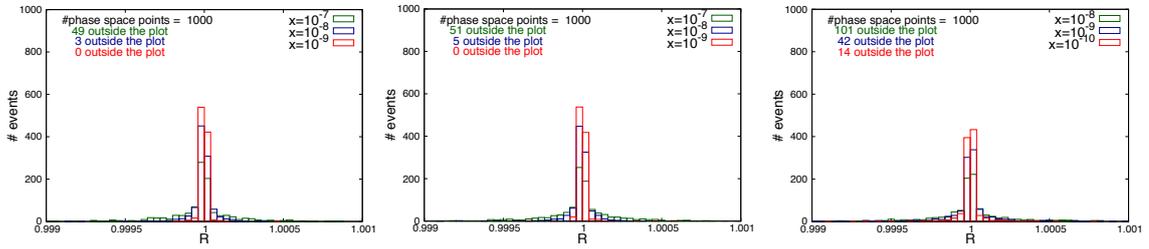
Figure C.6: Final-final collinear limits for $i_g||j_q$(left), $i_g||k_{\bar{q}}$ (centre) and $j_q||k_{\bar{q}}$(right).
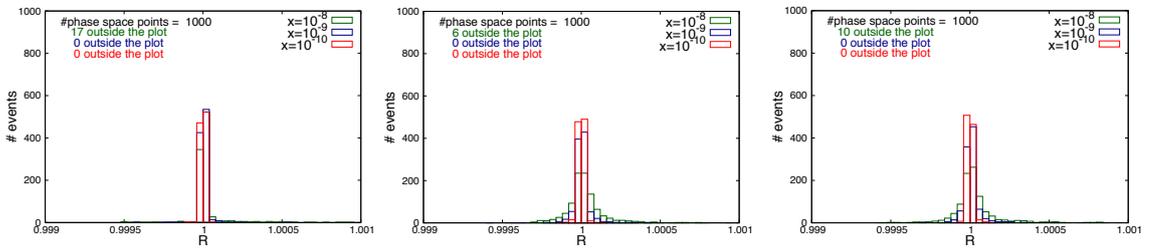
Figure C.7: Initial-final collinear limits for $\hat{1}_g||i_g$(left), $\hat{1}_g||j_q$ (centre) and $\hat{1}_g||k_{\bar{q}}$(right).
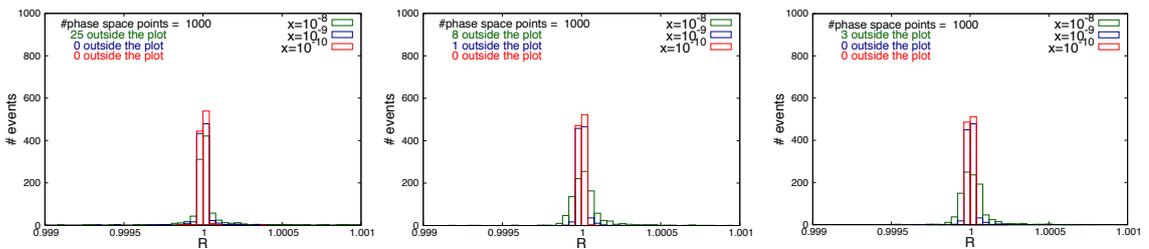
Figure C.8: Initial-final collinear limits for $\hat{2}_g||i_g$(left), $\hat{2}_g||j_q$ (centre) and $\hat{2}_g||k_{\bar{q}}$(right).

C.3 Finite real-virtual subtraction for $qg \to qgg$

For the last case of the real-virtual contribution to the two quark, two gluon Born process, we consider a quark and a gluon in the initial state. The cross section reads

$$d\hat{\sigma}_{NNLO}^{RV} = \mathcal{N}_{qg,5}^1 \int d\Phi_3 \frac{1}{3!} \frac{dx_1}{x_1} \frac{dx_2}{x_2} \sum_{P(\hat{1},i,j)} B_5^0(\hat{1}_q, \hat{2}_g, i_g, j_g, k_{\bar{q}}) J_2^{(3)}(p_3, p_4, p_5), \quad \text{(C.3.3)}$$

where the sum runs over the permutations of the gluons. The subtraction terms of this contribution are given in (5.6.75), (5.6.77) and (5.6.79). There is no soft $k_{\bar{q}}$ limit due to current conservation. All other limits between partons are present in the summation. Recall that the subtraction terms only hold in the sum over all orderings. Unlike the gluon-gluon initiated process, we no longer have symmetry in plots for quark-gluon collieanr limits, since one of them is now in the initial state. The right hand plot in Figure C.9 is empty since this corresponds to the soft limit of the final state quark, which does not exist.

Figure C.9: Final soft limits for i_g(left), j_g (centre) and $k_{\bar{q}}$(right).
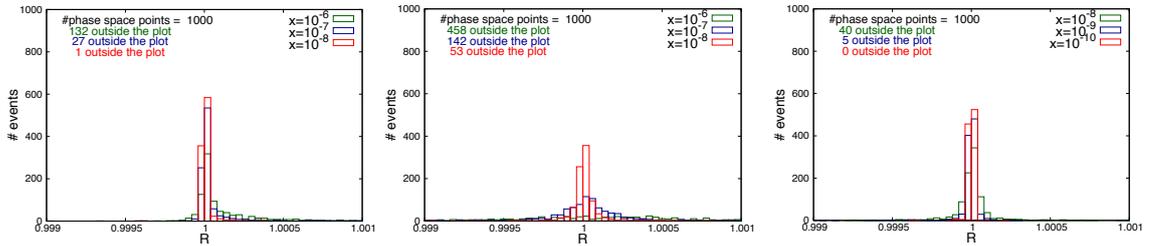
Figure C.10: Final-final collinear limits for $i_g||j_g$(left), $i_g||k_{\bar{q}}$ (centre) and $j_g||k_{\bar{q}}$(right).
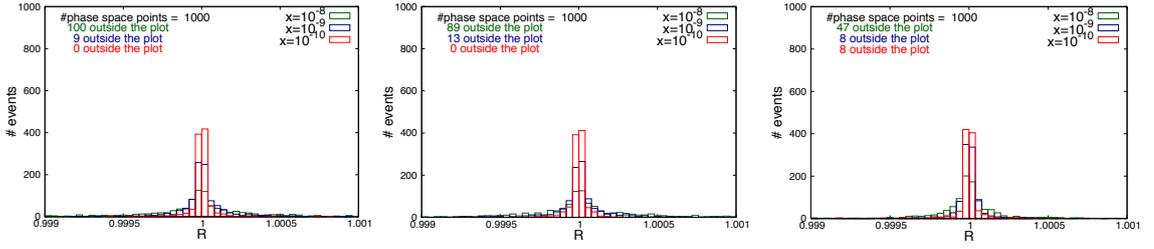
Figure C.11: Initial-final collinear limits for $\hat{1}_q||i_g$(left), $\hat{1}_q||j_g$ (centre) and $\hat{1}_q||k_{\bar{q}}$(right).

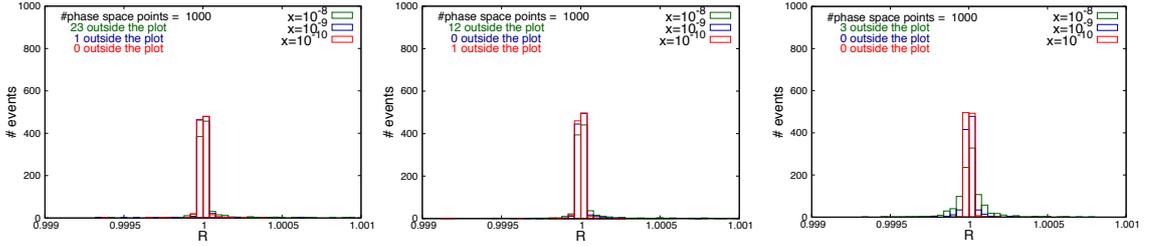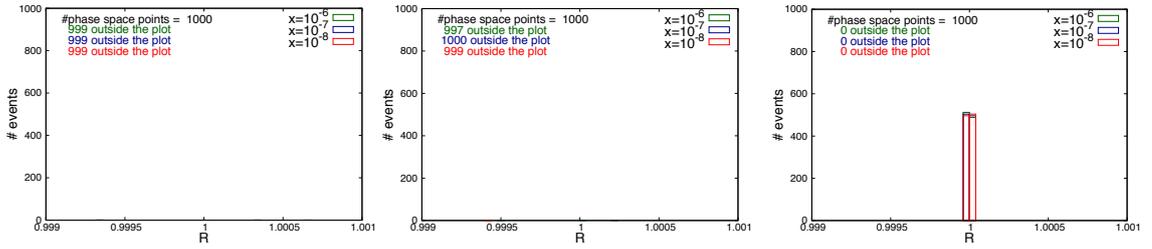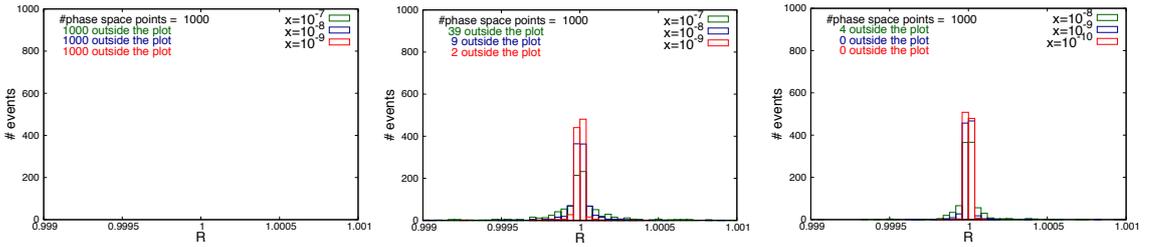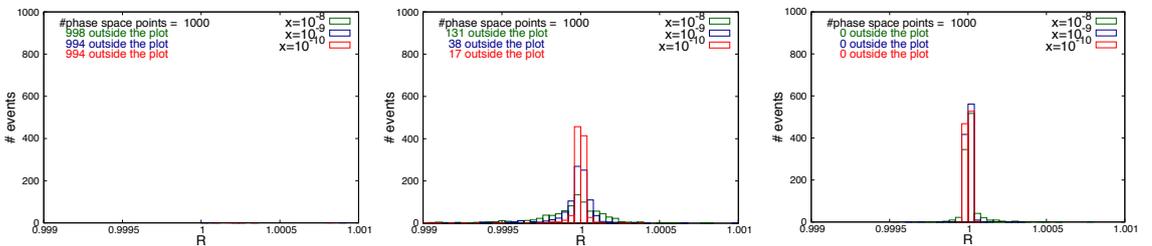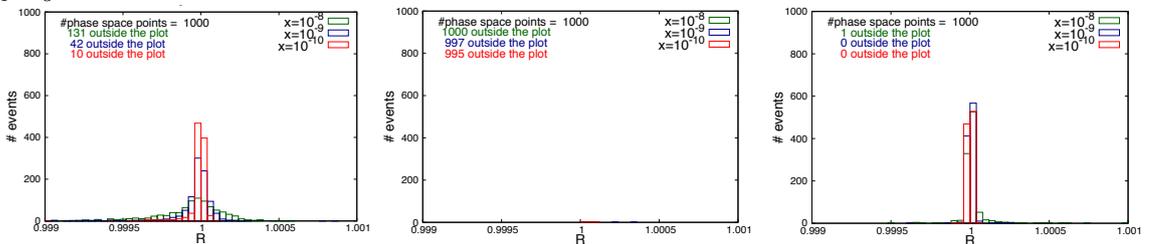Figure C.12: Initial-final collinear limits for $\hat{2}_g||i_g$(left), $\hat{2}_g||j_g$ (centre) and $\hat{2}_g||k_{\bar{q}}$(right).

C.4   Finite real-virtual subtraction for $\bar{q}Q \to \bar{q}Qg$

Finally, we present the case of the real-virtual five parton process with two different quark pairs and a single gluon. A quark and antiquark of different flavour are in the initial state. The cross section reads

$$
\begin{aligned}
d\sigma_{RV} &= \mathcal{N}_{qQ,5}^1 \int d\Phi_3(p_3, p_4, p_5; x_1 p_1, x_2 p_2) \frac{1}{S_3} \frac{dx_1}{x_1} \frac{dx_2}{x_2} \times \Big[\\
&\quad C_5^1(3_Q, 5_g, 4_{\bar{q}}; \hat{1}_q, \hat{2}_{\bar{Q}}) + C_5^1(\hat{1}_q, 5_g, \hat{2}_{\bar{Q}}; 3_Q, 4_{\bar{q}}) \Big] J_2^{(3)}(p_3, p_4, p_5) \quad \text{(C.4.4)}
\end{aligned}
$$

The subtraction terms for this contribution are given in (6.3.26) and (6.3.26). There are no soft quark limits limit due to current conservation, and now we observe from Figures C.14, C.15 (left) and C.16 (centre) that no collinear limits exist between quark/antiquarks of different flavour, as expected. Note the symmetry of like-quark collinear limits $q||\bar{q}$ and $Q||\bar{Q}$, which is again expected due to invariance of the matrix element under exchange of quark pairs.

Figure C.13: Final soft limits for 3_Q(left), $4_{\bar{q}}$ (centre) and 5_g(right).

Figure C.14: Final-final collinear limits for $3_Q||4_{\bar{q}}$(left), $3_Q||5_g$ (centre) and $4_{\bar{q}}||5_g$(right).

Figure C.15: Initial-final collinear limits for $\hat{1}_q||3_Q$(left), $\hat{1}_q||4_{\bar{q}}$ (centre) and $\hat{1}_q||5_g$(right).

Figure C.16: Initial-final collinear limits for $\hat{2}_{\bar{Q}}||3_Q$(left), $\hat{2}_{\bar{Q}}||4_{\bar{q}}$ (centre) and $\hat{2}_{\bar{Q}}||5_g$(right).